Hydrocarbon Oxidations Using Metal-Containing Polypropylene-imine Dendrimers

by
Derik Wilbers

Dissertation presented for the degree of
Doctor of Philosophy in the Faculty of Chemistry and Polymer Science at Stellenbosch University

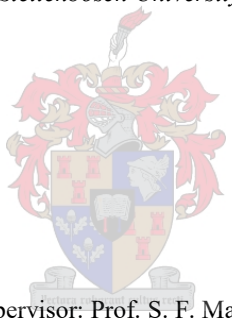

Supervisor: Prof. S. F. Mapolie

Co-supervisor: Dr. R. C. Luckay

December 2019

Declaration

By submitting this thesis electronically, I declare that the entirety of the work contained therein is my own, original work and that all sources I have used or quoted have been acknowledged by means of complete references.

December 2019

D. Wilbers

Acknowledgements

An undertaking such as this project is not possible without the guidance and support of an exceptional supervisor. First and foremost, I would like to thank my supervisor Prof S.F. Mapolie for providing guidance and mentorship during this project. This encompasses everything from work related queries, financial support and to expressing interest in my general well-being.

Secondly, to my parents without whom this project would also have been impossible. I will never be able to repay you for supporting me during this degree. I wish to thank you for your financial support, positivity and unconditional love.

I would like to thank my wife, Carli Wilbers, who undertook this journey with me. We started our relationship at the same time as this project. You were there during both the good and the bad times. During this project you have acted in many roles including bank manager, psychiatrist, editor as well as loving wife- to name but a few. You selflessly supported us financially without complaining. Again, I shall never be able to repay you for your help.

I wish to thank my friends Luke and Leon for their amazing friendship over the past 8 years. Almost daily chats, coffee and a shared beer or two kept me sane during this project.

Lastly, I would like to thank all the members of the Organometallic group, past and present, at Stellenbosch University. Your friendship and input during group meetings and while working in the lab was absolutely invaluable. As a new member of the Organometallic research group, I would like to extend my thanks to Wessel Horak for his help with the kinetic studies.

Financial assistance provided by the NRF and c*change centre for excellence in catalysis is greatly appreciated.

Conference Contributions

Poster Presentations

D. Wilbers, R.C. Luckay and S.F. Mapolie

The Synthesis and Application of Novel Metallodendrimers as Catalyst Precursors for the Oxidation of Alkanes. CATSA annual Conference 2014 at Saint George Hotel, Pretoria.

D. Wilbers, R.C. Luckay and S.F. Mapolie

Novel Iron Metallodendrimers as Catalyst Precursors for the Oxidation of Alkanes. CATSA annual Conference 2015 at Arabella Country Estate, Kleinmond.

D. Wilbers, R.C. Luckay and S.F. Mapolie

The Application of Novel Metallodendrimers as Catalyst Precursors for the Oxidation of Hydrocarbons. CATSA annual Conference 2016 at Champagne Sports Resort, Central Drakensberg.

D. Wilbers and S.F. Mapolie

The Application of Novel Metallodendrimers as Catalyst Precursors for the Oxidation of Hydrocarbons. CATSA annual Conference 2017 at Kwa Maritane Bush Lodge, Pilansberg.

Oral

D. Wilbers and S.F. Mapolie

The Application of Novel Metallodendrimers as Catalyst Precursors for the Oxidation of Cyclic Hydrocarbons. SASOL University Symposium at SASOL place Sandton, 2017.

Abstract

The production of oxygenates from hydrocarbon feedstocks is an important industrial process. However, this process suffers from various weaknesses such as poor catalytic activity, chemoselectivity, and often requires the use of harsh reaction conditions. In this thesis attempts to address these shortcomings are described.

The synthesis and characterization of a number of transition metal complexes, many of which are novel, as well as their application in the oxidation of hydrocarbons (both unsaturated and saturated) are described. The complexes include both iron metallodendrimers as well as iron mononuclear complexes (model complexes) based on pyridine-imine ligands. In addition to the iron complexes, a number of cobalt salicylaldimine complexes (metallodendrimers and model complexes) as well as cobalt thioether-amine complexes were synthesized.

The complexes were then employed as catalyst precursors in the catalytic oxidation of cyclohexene. Both the cobalt model complexes **C1** and **C2** as well as their dendritic counterparts (**MD1** and **MD2**) performed poorly as catalyst precursors in the oxidation of cyclohexene when using H_2O_2 as oxidant. The poor performance of the model complexes was attributed to the disproportionation of the oxidant, a process catalyzed by the model cobalt complexes **C1** and **C2**. When H_2O_2 was replaced by TBHP as oxidant, virtually no disproportionation of this oxidant was observed and an improvement in catalytic activity was obtained, however, turnover numbers (20 mol product/ mol catalyst) remain relatively low. The cobalt complexes exhibited poor activity in the oxidation of n-octane obtaining product yields of around 2% under the optimized conditions (2 mmol cyclohexene, 1 mol% catalyst, 4 mmol TBHP, 40°C, MeCN).

The iron complexes were more active for catalytic cyclohexene oxidation than the cobalt complexes. **C4** and **MD5** (iron pyridine-imine complexes) gave cyclohexene conversions of around 50% with turnover numbers around 60. In all cases high

selectivity towards the allylic oxidation product 2-cyclohexen-1-one was obtained. The iron complexes were also more active than the cobalt complexes in n-octane oxidation achieving product yields of around 7% (2 mmol octane, 0.5 mol% iron, 4 mmol TBHP, 60°C, MeCN).

The kinetics of the reaction of selected complexes with peroxide-based oxidants were investigated in an attempt to rationalize the observed differences in catalytic activity for these systems. It was found that the cobalt salicylaldimine complex **MD1** has a significantly higher activation energy than the iron complex **MD5** which might serve as a possible explanation for the observed differences in catalytic activity of the two catalyst systems.

Further investigations attempted to ascertain the most likely mechanism by which hydrocarbon oxidation, catalyzed by these complexes, is achieved. It was found that these complexes are likely to operate via a free radical-centered mechanism.

Uittreksel

Die produksie van suurstofbevattende produkte vanuit koolwaterstowwe is ‘n belangrike industriële proses. Hierdie proses het egter verskeie nadele, soos onder andere, lae katalitiese aktiwiteit, swak produkselektiwiteit, asook die gebruik van energie-intensiewe reaksie toestande. In hierdie tesis word pogings om die voorgenoemde tekortkominge en nadele aan te spreek, beskryf.

Die sintese en karakterisering van verskeie oorgangsmetaal-komplekse asook hul gebruik as katalisators in die oksidasie van verskeie koolwaterstowwe (beide versadigde sowel as onversadigde) word hier beskryf. Hierdie komplekse sluit in beide yster metallodendrimere sowel as mononukleêre yster modelkomplekse van piridien-imien ligande. Benewens die ysterkomplekse is ‘n reeks kobaltsalisielaldemien komplekse (metallodendrimere en modelkomplekse) sowel as kopertioeter-amien komplekse gesintetiseer.

Die komplekse is getoets as katalisators in die oksidasie van siklohekseen. Beide die kobalt metallodendrimere en die kobalt modelkomplekse het lae katalitiese aktiwiteit vir hierdie transformasie getoon in reaksies waar waterstofperoksied gebruik is as oksideermiddel. Die swak katalitiese aktiwiteit is toe geskryf aan die disproporsionering van waterstofperoksied na water en suurstof. As die H_2O_2 oksideermiddel met TBHP vervang word, is feitlik geen disproporsionering waargeneem nie. In hierdie geval is die katalitiese aktiwiteit hoër, maar omset getalle (20 mol produk/ mol katalis) is steeds relatief laag. Hierdie kobalt komplekse toon uiters lae aktiwiteit in die katalitiese oksidasie van oktaan waar omsette van slegs 2% onder optimale kondisies verkry is (2 mmol oktaan, 1 mol% kobalt, 4 mmol TBHP, 60°C).

Die ysterkomplekse was relatief meer aktief in die oksidasie van siklohekseen as die kobaltkomplekse. Komplekse **C4** en **MD5**, beide piridienimien-komplekse, kon omsette van ongeveer 50% behaal, met TON waardes bo 60. In alle gevalle is hoë selektiwiteit na die produkte, 2-sikloheksen-1-oon asook 2-sikloheksen-1-ol verkry.

Die ysterkomplekse was veel meer aktief as die kobaltkomplekse in die oksidasie van oktaan en omsette van 7% is verkry. (2 mmol oktaan, 0.5 mol% yster, 4 mmol TBHP 4 ure, 60°C in MeCN).

Die kinetika van die reaksies van geselekteerde komplekse met waterstofperoksied as oksideermiddel is ondersoek in ‘n poging om die waargenome verskille in katalitiese aktiwiteit vir hierdie sisteme te rasionaliseer. Daar is gevind dat die kobaltsalisielaldemien kompleks **MD1**, ‘n beduidend hoër aktiveringsenergie as die yster kompleks **MD5** het. Dit mag ‘n moontlike verduideliking wees vir die waargenome verskille in katalitiese aktiwiteit van die twee katalisatorsisteme.

In verdere ondersoeke is daar gepoog om vas te stel wat die mees waarskynlike meganisme is waarvolgens oksidasie reaksies, gekataliseer deur hierdie komplekse, plaasvind. Daar is gevind dat hierdie komplekse waarskynlik oksidasie bewerkstellig via ‘n vrye radikaalgesentreerde meganisme.

Table of Contents

Chapter 2: The Synthesis and Characterization of Ligands and Complexes

Chapter 4: Catalytic Oxidation of Hydrocarbons by Iron, Cobalt and Copper Complexes

Chapter 5: Kinetic and Mechanistic Studies of Dendritic Iron and Cobalt Catalysed Decomposition of H_2O_2

Chapter 6: Chapter Summaries, Conclusions and Future Work

List of Figures

Chapter 1

Chapter 2

Chapter 3

Chapter 4

Chapter 5

List of Schemes

Chapter 1

Chapter 2

Chapter 3

Chapter 4

Chapter 5

Chapter 6

List of Tables

Chapter 1

Chapter 2

Chapter 3

Chapter 4

Chapter 5

List of Abbreviations

µm	Micrometer
Atm	Atmosphere
ATR	Attenuated total reflectance
A:K	Alcohol to ketone ratio
BDE	Bond dissociation energy
Br	Broad (broad signal in NMR spectroscopy)
BM	Bohr Magneton
Calc.	Calculated
CYP450	Cytochrome P450
d	Doublet (in NMR spectroscopy)
DAB	Diaminobutane
DCM	Dichloromethane
dec.	Decomposition
DENs	Dendrimer-encapsulated nanoparticles
DMF	Dimethyl formamide
DMSO	Dimethyl sulfoxide
E.A.	Elemental analysis
EPR	Electron paramagnetic resonance
ESI	Electrospray ionization
EtOAc	Ethyl acetate
FT-IR	Fourier transform infrared (spectroscopy)
Fc	Ferrocene

G_x	Dendrimer Generation, where x= 0,1,2,3…
GC	Gas chromatography
Glu	Glutamine
HPLC	High-performance liquid chromatography
Hpca	Pyrazinecarboxylic acid
His	Histidine
Hz	Hertz
L	Ligand
m/z	Mass to charge ratio
m.p.	Melting point
MeCN	Acetonitrile
MeOH	Methanol
MEP	N,N-dimethyl-N,N-bis(2-pyridylmethyl)- ethane-1,2-diamine
MHz	Megahertz
nm	nanometer
NMR	Nuclear magnetic resonance
PAMAM	Poly(amidoamine)
PPI	poly(propylene imine)
ppm	Parts per million
q	Quartet (In NMR spectroscopy)
s	Singlet (In NMR spectroscopy))
t	Triplet (in NMR spectroscopy)
TBHP	*tert*-butyl hydroperoxide (*t*BuOOH)
TEMPO	(2,2,6,6-Tetramethylpiperidin-1-yl)oxyl
TFA	Trifluoroacetic acid

TfOH	Trifluoromethanesulfonic acid
TGA	Thermogravimetric analysis
THF	Tetrahydrofuran
TLC	Thin layer chromatography
TOF	Turnover frequency
TON	Turnover number
TPA	tris(2-pyridylmethyl)amine
UV-Vis	Ultraviolet–visible spectroscopy

Chapter 1: An Overview of the Current State of Catalytic Oxidation of Hydrocarbons

1.1 Introduction to oxidative transformation processes applied to hydrocarbons

Hydrocarbons, both saturated and unsaturated, are ubiquitous in both life processes and chemical industry. Industrially hydrocarbons are obtained from crude oil. Typically, crude oil consists of around 80% carbon and up to 15% hydrogen (mass %) while various other elements are also present in smaller quantities. During the refining process of crude oil, different fractions are obtained which can be used as feedstocks in downstream processes.[1, 2] As such the fuel pool consists mostly of hydrocarbons; however, hydrocarbons also find application as solvents and in the synthesis of fine chemicals.[1, 2]

Here we review the various oxidation processes that have been developed in the last fifteen years to address the challenges faced in hydrocarbon oxidation in the fields of homogeneous, heterogeneous and hybrid catalytic systems.

1.2 Oxidation of hydrocarbons

1.2.1 Oxidation of alkanes

Alkanes are used industrially to generate energy through combustion[3–5] or subjected to cracking[6, 7] to generate unsaturated hydrocarbons for further functionalization. However, despite the large body of work that has been done in this field, the oxidation of alkanes to more valuable oxygenates (under mild reaction conditions with high selectivity) remains both an academic and an industrial challenge.[8–11]

Alkane oxidation processes have traditionally suffered from various weaknesses such as poor chemoselectivity and the use of harsh reaction conditions. Typically, a range of different oxygenate products are formed such as alcohols, aldehydes ketones and

carboxylic acids. The economic importance of an oxidative method that addresses these problems cannot be overstated.

1.2.2 The nature of the C-H bond

In principle, for oxidation of an alkane substrate to occur a C-H bond must be cleaved either homolytically or heterolytically. Table 1 shows the bond dissociation energy (BDE) of various bonds in a number of different organic compounds.[12]

Table 1: Bond dissociation energies of selected organic compounds[12]

Entry	Compound	Type of Bond	BDE (kJ/ mol)
1	H-CH_3	C-H	439
2	H-CH_2OH	C-H	393
3	H-CH_2CH_3	C-H	423
4	H-CH_2CO_2H	C-H	406
5	H-C_6H_5	C-H	464
6	H-$CH=CH_2$	C-H	435
7	$HC=CHCH_2$-H	C-H	372
8	H-CH_2-C_6H_5	C-H	368
9	$H_2C=CH_2$	C=C	728

It is observed that the C-H bond dissociation energy is extremely high for the aliphatic alkanes (Entries 1, 3) and to a slightly lesser extent, the alkenes. A process in which C-H bonds of alkanes and alkenes are cleaved would have to overcome this thermodynamic burden. The longer the aliphatic chain the lower the bond dissociation energy (longer alkyl chain results in a more stable radical upon C-H bond cleavage).[12] The alkenes have high C-H bond dissociation energies (Entry 6) while benzylic and allylic C-H bonds are comparatively activated and have much lower BDEs (Entries 7, 8). The above-mentioned observations can have serious implications for selectivity in hydrocarbon oxidation reactions.

Furthermore, it is observed that the C-H BDE of methane (Table 1, entry 1) is much higher than that of methanol (entry 2). In addition, the C-O bond (BDE 385.3 kJ/mol) is much weaker than the C-H bond of methanol.[12] These observations are of important consequence when designing new catalytic systems for hydrocarbon oxidation processes, since the potential products of the process could have weaker C-H bonds than that of the alkane substrate. This can have a serious detrimental effect on the selectivity of such a process. Often the product of such a reaction is more prone to oxidation than the alkane substrate which leads to over oxidation and a decreased yield of the target products (as observed for many of the catalytic systems reviewed in Section 1.3).

In theory, these potential obstacles can be overcome by employing a suitable catalyst to lower the energetic burden of this process and to impart some selectivity. Such work was pioneered in the early 1960s by Shilov and co-workers, employing Pt(II) complexes.[13]

1.2.3 Alkene oxidation and epoxidation

In addition to the oxidation of saturated hydrocarbons the oxidation of partially unsaturated molecules is also of particular economic interest. The oxidation of alkenes to more valuable oxygenates has been the subject of many studies, and has been reviewed on numerous occasions.[14–16]

Epoxides are valuable products, as selectivity in alkene oxidation reactions are often hard to achieve. Epoxidation of the C=C bond is in competition with the oxidation of C-H bonds. The C=C BDE is very high compared to the C-H BDE in ethene (Table 1, Entries 6 and 9). Furthermore, comparison of these BDE values with the allylic or benzylic C-H bonds present in propene and toluene (respectively) suggests that oxidation at the allylic/ benzylic position is often much more facile (Table 1 entries 6-9). In addition, the C-H BDE increases with increasing hybridization of the carbon centre ($sp > sp^2 > sp^3$).[12] This can also influence the product selectivity in alkene oxidation reactions. The mechanism of such oxidation reactions is of great significance and influences the selectivity as well as the activity of the oxidation process. Alkene

and alkane oxidation reactions typically occur via similar reaction mechanisms as reviewed below.

1.2.4 General hydrocarbon oxidation mechanisms

In the literature various mechanisms have been reported and reviewed for catalytic hydrocarbon oxidation.[11] These mechanisms will be discussed in more detail in Chapters 3 and 4, however, a basic understanding of these mechanisms is important when reviewing catalyst systems reported in the literature. Typically, three main reaction mechanisms are reported in the literature.

The first mechanism is shown in Scheme 1. In this scheme the catalytically active metal centre is denoted with the letter M. This mechanism is often referred to as the true organometallic mechanism and involves the activation of the C-H bond by the formation of metal carbon (M-C) σ-bonds.[17] Activated M-C bonds can be further functionalized depending on reaction conditions and reagents present. Oxidants such as O_2 and H_2O_2 eventually yield the oxygen-containing product as shown in Scheme 1. Catalyst systems that operate under this mechanism often exhibit selectivity to the oxidation of primary carbons because the oxidative addition of the C-H bond across the metal centre occurs in such a way as to minimize steric strain of the resulting organometallic complex.[18]

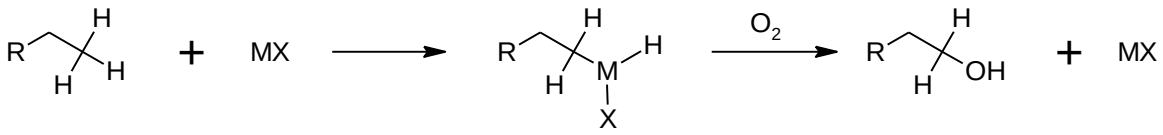

Scheme 1: C-H activation via the so-called organometallic mechanism

Such a mechanism is thought to be operative in the well-known Shilov catalyst system.[19] Subsequent to Shilov's discovery a myriad of catalyst systems which operate via an organometallic -type mechanism have been demonstrated.[10,18,19]

Alternatively, a catalytically active metal centre reacts with the oxidant. This results in either homolytic or heterolytic cleavage of the oxidant.

In the case of homolytic bond cleavage (Scheme 2), free radicals are produced which can subsequently abstract a proton from the alkane, forming highly reactive alkyl radicals. These radicals can undergo further reaction, for example reaction with the oxidant or O_2 to produce the oxidized product. Typically, catalyst precursors susceptible to the free radical mechanism tend to suffer from poor product selectivity. The use of iron salts along with oxidants such as H_2O_2 to generate strongly oxidizing hydroxyl radicals, a process referred to as Fenton chemistry, has been extensively studied.[20, 21]

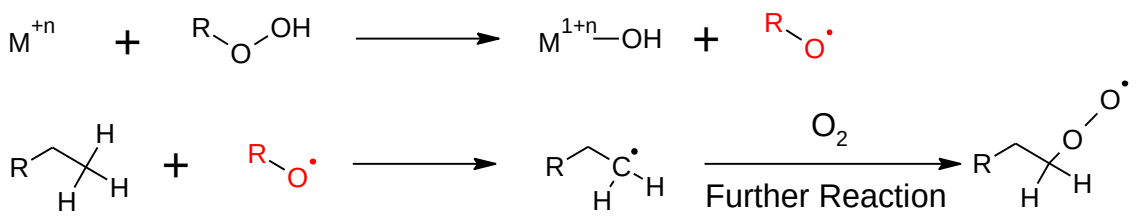

Scheme 2: Metal-mediated generation of free radicals

A third possible mechanism for hydrocarbon oxidation involves the catalyst mediating heterolytic bond cleavage of the oxidant (Scheme 3).[22, 23] This leads to the formation of a highly electrophilic metal-oxo species that acts as a metal-based oxidant. This mechanism, called the rebound mechanism, has been reported for hydrocarbon oxidation processes mediated by various enzymes such as cytochrome P450.[24, 25] Catalysts systems operating via the rebound mechanism are often highly selective.

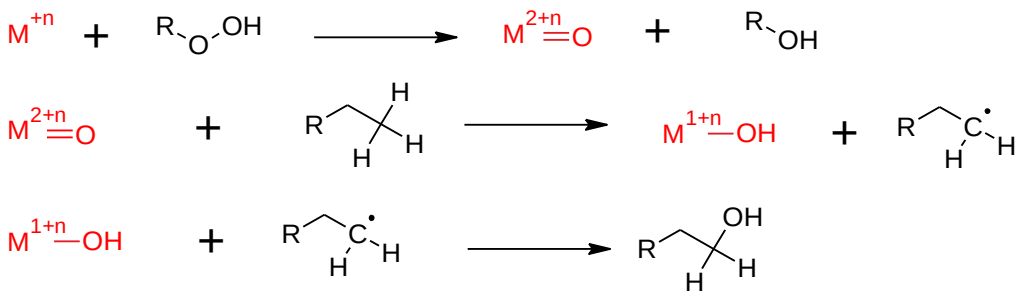

Scheme 3: Metal based oxidant rebound mechanism[22]

1.2.5 Historical perspectives

Towards the end of the 1960s several research groups across the world embarked on an intensive study of alkane and alkene activation by transition metal complexes, most notably the group of A.E. Shilov. The first breakthrough came when Shilov's group observed that the so-called Garnet systems[26] consisting of $K_2PtCl_4/CH_3OH/H_2O$ (originally used to catalyse an H/D exchange reaction in aromatic hydrocarbons) could in fact catalyse the hydrogen-deuterium exchange in saturated substrates, such as methane and ethane (as shown in Scheme 4), which the authors could follow by mass spectrometry.[13, 19]

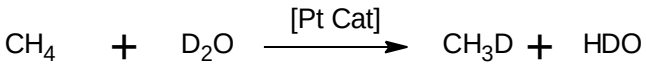

Scheme 4: Shilov's H/D exchange

This reaction proceeded under mild conditions in the presence of the platinum (II) catalyst. However, in the absence of catalyst the H/D exchange reaction would only occur at temperatures above 600°C, a stark reminder of the low reactivity of the C-H bond in this particular system.

With these first positive results in hand, interest in hydrocarbon activation increased exponentially.

1.3 Recent developments in catalytic hydrocarbon oxidation

1.3.1 Biological and enzymatic hydrocarbon oxidation

Nature has managed to find interesting ways of incorporating oxygen functionalities into saturated hydrocarbons (albeit with a couple million years head start) by employing various enzymes. As such a good starting point would be to look to nature when designing new catalyst systems. An example of such an enzymatic system is methane monooxygenase (MMO). MMO catalyses the conversion of methane to methanol. Two forms of methane monooxygenase are known. These are soluble methane monooxygenase (sMMO) and particulate methane monooxygenase

(pMMO).[27] It is believed that the sMMO has a Fe-O-Fe active site (Figure 1) while pMMO has a Cu active site, though these systems are still poorly understood.[27] Some variance in the exact structure of the enzyme is observed between different organisms and in different states (active vs resting).[28]

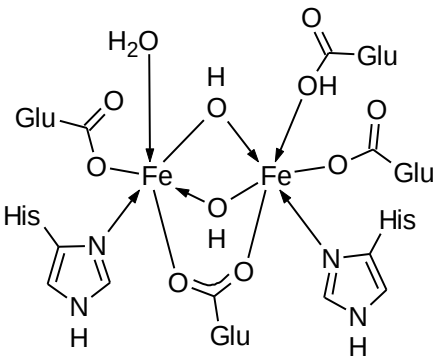

1

Figure 1: Soluble methane monooxygenase (active form)[28]

Another such oxidative enzymatic system is the heme containing cytochrome P450. This enzymatic system typically oxidizes primary methyl groups (from a variety of substrates) to alcohols. The heme co-factor of this catalyst system consists of a low spin iron metal centre complexed to a porphyrin ring. Various axial ligands are also often present such as sulphur-containing histidine (His) residues.[29]

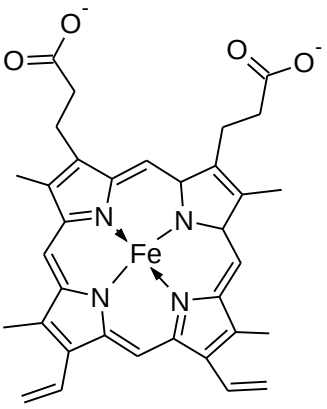

2

Figure 2: Fe-Porphyrin subunit of heme[29]

The identification and characterization of these active sites has sparked intensive research into the use of first row transition metals like Fe, Cu, and Co for hydrocarbon oxidation.

1.3.2 Modern developments in hydrocarbon oxidation

Drawing inspiration from the structural features of the enzymes described above, Fernandes et al. synthesized new macrocyclic ligands that include the N_2S_2 donor set as shown in Figure 3.[30] Two ligands were synthesized viz. a 14 membered N_2S_2 macrocycle and a nine membered S_2N macrocycle with a pyridine pendant arm.

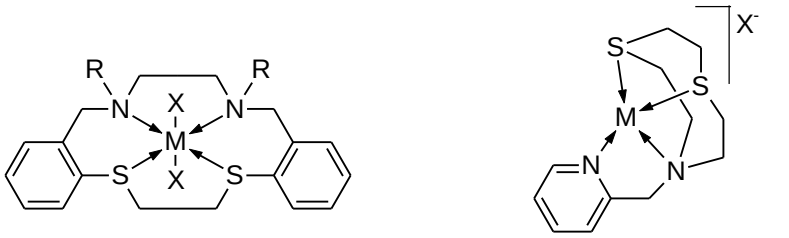

3: M= Fe, X= Cl, R=H

4: M=Cu, X= Otf, R=H

5: M=Cu, X= Otf, R=Me

6: M= Fe, X= Cl,

7: M=Cu, X= Otf

Figure 3: Macrocyclic complexes as catalysts for alkane oxidation[30]

The complexes were applied in two model oxidation studies namely i) the oxidation of cyclohexane and ii) solvent free oxidation of 1-phenylethanol to acetophenone with *tert*-butyl hydroperoxide (TBHP) under microwave irradiation. It was found that in general the Fe(II) complexes were much more active than the corresponding Cu(II) complexes (Table 2).

Table 2: Catalytic oxidation of cyclohexane by Fernandes et al.[30]

Additive	Total yield %				
	3	**4**	**5**	**6**	**7**
none	2.5	8.3	10.3	12.2	8.6
Hpca	17.5	0.4	0.2	15.9	0.2
HNO_3	19.2	5.8	7.3	15.8	4.5
TfOH	21.3	6.1	6.0	18.0	4.8
TFA	20.0	6.0	6.1	16.7	4.1

Typical reaction conditions: CH_3CN (3.0 mL), cyclohexane (5.0 mmol), catalyst precursor (0.2 mol% relative to substrate), H_2O_2 (7.0 mmol), acid promotors [Hpca (50 µmol), HNO_3, TfOH or TFA (200 µmol)], 6 h reaction time, 25 °C.

Complexes **3** and **6** (both Fe(II) complexes) yielded relatively high turnover numbers (TON) values. **3** is the 14 membered S_2N_2 catalyst while **6** is of the second type shown (Figure 3). Reactions performed with *tert*-butylhydroperoxide (TBHP) yielded significantly worse results than reactions utilizing H_2O_2 as the oxidant. However, the authors do not elaborate further on this observation. It was found that in cyclohexane oxidation reactions, the major product is cyclohexanol peroxide, which can be converted to cyclohexanol with PPh_3 via the so called Shul'pin method.[31]

A range of additives were also tested along with the catalyst precursors. It was found that acid additives enhanced the activity of the Fe(II) complexes, however a decrease in activity was observed for the Cu(II) complexes using the same acid additives. The authors state that the role of the acid promotor is not fully understood but speculated that the acid promotor may be involved in proton transfer steps to yield the active catalyst for example to protonate the secondary or tertiary amines of the ligand, thereby decreasing the electron density around the iron centre. It may also enhance the oxidizing properties of the metal intermediates or the peroxide itself.[30]

The introduction of a radical trap into the reaction setup, leads to a dramatic drop in activity for these systems. This provided some evidence that the system likely follows a free radical-mediated mechanism.[30]

Silva et al. synthesized a range of novel salicylaldimine as well as pyridyl-imine transition metal complexes of the metal cations V(IV), Mn(III), Fe(III), Fe(II) Co(III) and Cu(II).[32]

These complexes were tested as catalyst precursors in the catalytic oxidation of cyclooctane, cyclohexane and n-hexane. The Fe(III) complex with the N_2O_2 donor set (**11**) was the best performing catalyst, achieving a TON of up to 45 for cyclohexane and 97 for n-hexane. However poor selectivity is observed for complex **11** most probably due to the fact that non-selective hydroxyl radicals are involved. Much better selectivity, albeit at lower catalytic activity, is observed for **13** an Fe(II) complex. The authors suggest that **13** might follow the metal-based oxidant pathway (rebound mechanism) as described in Section 1.2.4. Such a mechanism is unlikely for **11** which would need to form a (presumably) highly unstable Fe(V) centre while **13** would form a (relatively) more stable Fe(IV) centre.

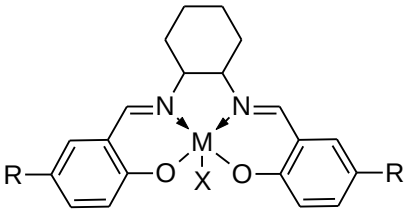

8: M= Cu(II) X= N/A, R=H

9: M=Co(III), X= Cl, R=H

10: M=V, X=O, R=H

11: M=Fe, X=Cl, R=H

12: M=Fe, X=Cl, R=Me

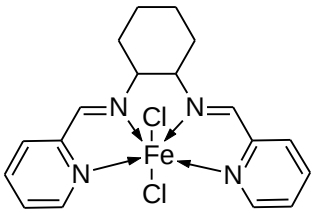

13

Figure 4: Biomimetic transition metal complexes prepared by Silva et al.[32]

Tang et al. reported an exceptionally active cyclohexane oxidation catalyst system. The catalyst is generated *in situ* by combining $Fe(BF_4)_2$ and the ligand 6-bis, [1-(2-methylanisoleimino)ethyl] pyridine] in acetonitrile to produce a purple homogeneous solution.[33] To this solution is added the alkane substrate and oxidants. While no crystal structure for this compound is available the authors reported that in related compounds coordination to the metal centre is typically observed through the pyridine and imine

groups while the methoxy groups interact but do not formally coordinate to the Fe(II) centre.[34] On this basis, Tang et al. postulated that the complex formed in-situ could be represented by **15** (Figure 5).

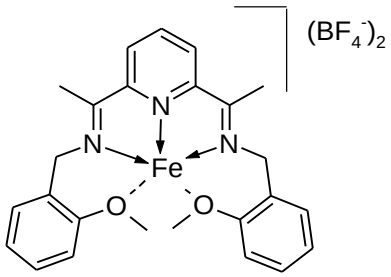

15

Figure 5: Proposed structure of in situ generated catalyst reported by Tang et al.[33]

Tang et al. observed high conversion of the substrate, cyclohexane, achieving 100% conversion in as little as 7 hours (Table 3 entries 1 and 2). The alcohol to ketone ratio (denoted A: K) were found to be around 1 for these reactions leading the researchers to speculate that a free radical process might be at work.

The authors proposed that cyclohexanone is not generated from the overoxidation of cyclohexanol. This is because the relative ratio of cyclohexanol to cyclohexanone does not change much over time (Table 3, entries 1 and 2). This lead them to believe that the Hermans auto-oxidation (auto-oxidation of cyclohexanol to cyclohexanone) is not the main oxidation route to cyclohexanone.[35] The formation of cyclohexanone could thus be generated by a different mechanism than via the oxidation of cyclohexanol. The proposed auto-oxidation mechanism involves a cyclohexylperoxyl radical which is generated by reaction of a cyclohexyl radical and oxygen when the reaction is performed aerobically.[35]

Table 3: Oxidation of alkane substrates by Fe(II) in situ catalyst[33]

Entry	Substrate	Solvent	Time (h)	Conversion (%)	A: K
1	Cyclohexane	MeCN	12	100	1.00
2[a]	Cyclohexane	MeCN	7	100	1.11
3	Cyclohexane	MeCN + DMSO	9	55	1.32
4[b]	Cyclohexane	MeCN	3	100	0.35
5	Cyclohexane	Acetone	30	0	0.38
6	Cyclohexane	MeCN	20	100	2.22
7	Cyclooctene	MeCN	22	30	n/a
8	n-Heptane	MeCN	54	82	n/a

Typical reaction conditions: 8 mg (0.02 mmol) of Ligand, 2ml MeCN, 6.8 mg (0.02 mmol) of $Fe(BF_4)_2 \cdot 6H_2O$ were added. 2.00 mmol of substrate and 3.00 mmol of H_2O_2 (30% in H_2O_2). Reactions were stirred at 50°C. [a] Reaction under argon. [b] 10 equivalents H_2O_2

The authors tested their hypothesis by performing the oxidation reaction under argon to exclude oxygen (Table 3, entry 2). They found that under argon (excluding any role the O_2 might play and supressing the formation of cyclohexylperoxyl radical) the reaction activity was actually enhanced (complete conversion achieved in 7 hours) while the product distribution did not change appreciably, and a comparable yield of ketone was obtained. Interestingly when the reaction is performed with a large excess of oxidant (entry 4, 10 equivalents) more ketone is produced. This could likely be ascribed to overoxidation of the alcohol product.

To probe the mechanism of the oxidation reaction, DMSO was added to the aerobic reaction mixture. DMSO is known to be a scavenger of hydroxyl radicals.[36, 37] Indeed, a significant retardation of the formation of oxidation products is observed in the presence of DMSO (Table 3, entry 3). The authors note however that in the presence of DMSO a colour change is observed indicating that a different active species might be formed in the presence of DMSO. Furthermore, after about 30 minutes the catalytic activity is no longer inhibited, possibly due to the formation of a new catalytically active species. Acetone is also a radical scavenger. When acetone was used as solvent no oxidation products were isolated (Entry 5). The oxidation chemistry of this *in situ* generated catalyst was further studied using cyclohexene (Scheme 5) as substrate and mechanistic probe.

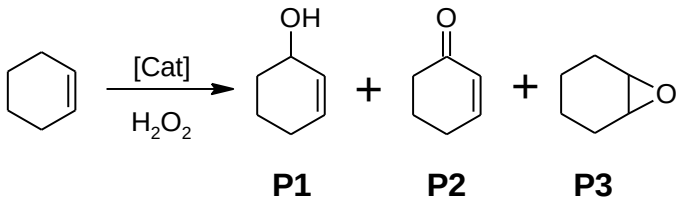

Scheme 5: Cyclohexene oxidation performed by Tang et al.[33]

The catalyst was also fairly active in cyclohexene oxidation, obtaining 100% substrate conversion after 20 hours (Table 4 entry 1).

Interestingly no epoxidation products were detected in these experiments. The major products obtained are the allylic oxidation products namely 2-cyclohexen-1-ol and 2-cyclohexen-1-one. Typically, these products are produced in free-radical mediated reactions while the metal-based oxidants (described previously, rebound mechanism) have high selectivity towards epoxides.[38] A reaction was also performed under an argon atmosphere (Table 4, entry 2). When no oxygen is present in the system a substantially reduced yield is observed in contrast to the results obtained for cyclohexane. Additionally, the system is less selective towards the ketone product which indicates that oxygen might play a role as co-oxidant to oxidize 2-cyclohexen-1-ol to 2-cyclohexen-1-one.

These observations lead the authors to postulate that two different mechanisms might be operative simultaneously. The main oxidation pathway likely involves the formation of hydroxyl radicals however a different metal-centered mechanism might be operative and even enhanced, under very specific reaction conditions.

Table 4: Oxidation of cyclohexene performed by Tang et al.[33]

Entry	Temp (°C)	Time (h)	Conversion (%)	Products
1	50	20	100	P1(49.4), P2(49.3)
2[a]	25	150	27	P1(17.5), P2(7.9)
3	50	31	86	P1(23.3), P2(51.4)

Typical reaction conditions: 8 mg (0.02 mmol) of Ligand, 2 ml MeCN, 6.8 mg (0.02 mmol) of $Fe(BF_4)_2{\cdot}6H_2O$ were added. 2.00 mmol of substrate and 3.00 mmol of H_2O_2 (30% in H_2O_2). [a] Reaction under argon

Tordin et al. reported four novel metal complexes of Cu(II), Ni(II), Co(II) based on two different ligands, an alkylamine ligand and a pyridylamine ligand as shown in Figure 6.[39] The complexes were tested in the oxidation of cyclohexane and adamantane. Complex **16**, a Co(II) catalyst, displayed significant catalytic activity in the oxidation of cyclohexane, with a TON of 237 and with an alcohol to ketone ratio (A: K) of 2.9 obtained. Catalytic test reactions were performed in mixed solvent systems either MeCN:DCM (1:3, v/v) or (3:1, v/v). When the more polar (MeCN: DCM, 3:1) solvent system is used, high TONs (237) are observed for **16**. The authors demonstrated the importance of the solvent system in this reaction by observing that when the less polar solvent system is used the TON of **16** decreased significantly to 68, however, the alcohol to ketone ratio increased to 10.3: 1 showing a significant increase in selectivity to cyclohexanol. Complex **18** exhibited no catalytic activity under any of the tested conditions which is something the authors do not elaborate on any further. However, it was found that compound **19** is highly unstable under the catalytic conditions and decomposes without catalysing the reaction.

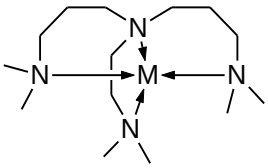

16: M= Co(II)
17: M= Ni(II)
18: M= Cu(II)

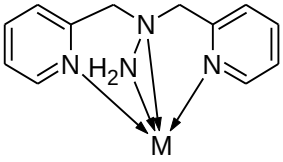

19: M= Ni(II)

Figure 6: Aliphaticamine and pyridylamine metal complexes synthesized by Tordin et al.[39]

A large body of work has been reported on the catalyst precursor Fe(TPA) shown in Figure 7 below reported by the group of Lawrence Que Jr.[40]

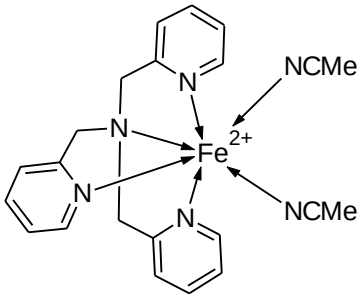

20

Figure 7: Highly active Fe(TPA) 20 catalyst precursor[40]

The mechanism of this catalytic system has generated a great deal of debate. Initially, the aforementioned authors favoured a metal-based oxidant as the catalytically active species and proposed either a metal-peroxide or a high-valent iron-oxo compound. This was based on the observation that the catalytic system is inhibited by the addition of DMSO (potentially coordinating with the iron centre), and the fact that replacing the TPA ligand with a similar polypyridine ligand greatly affected the selectivity of the reaction.

Arends et al. however claimed that *tert*-BuO radicals generated *in situ* are solely responsible for the observed oxidation.[41] They reasoned that complexes of Fe^{3+} and the TPA ligand would according to the so called rebound mechanism (discussed in Section **1.2.2**) have to be oxidized from Fe(III) to the high valent Fe(V)=O centre, which would be expected to be highly unstable. Furthermore, the observation that the alcohol to ketone ratios obtained during the oxidation of cyclohexane were typically close to 1/1 also piqued their interest (typical of free radical processes).

Arends et al. postulated an alternative radical-mediated route to explain the cyclohexanol and cyclohexanone formation. Cyclohexylperoxy radicals formed during the reaction could undergo so-called Russel termination steps as shown in Scheme 6.[42] This would yield cyclohexanol and cyclohexanone in roughly equal amounts (as shown in Scheme 6 A) or a slight excess of ketone (B).

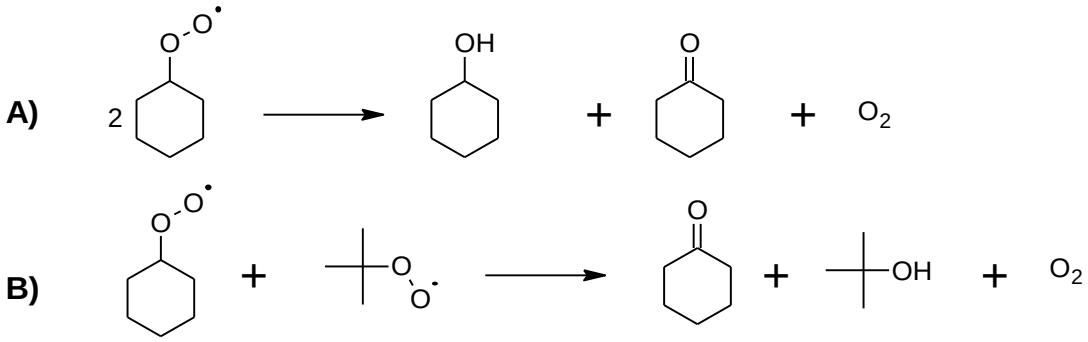

Scheme 6: Production of cyclohexanol and cyclohexanone via Russel termination[42]

The cyclohexylperoxy radicals necessary for the above reaction to occur could be formed by the well-known Haber-Weiss decomposition of the oxidant by the Fe(TPA) complex (Scheme 7).

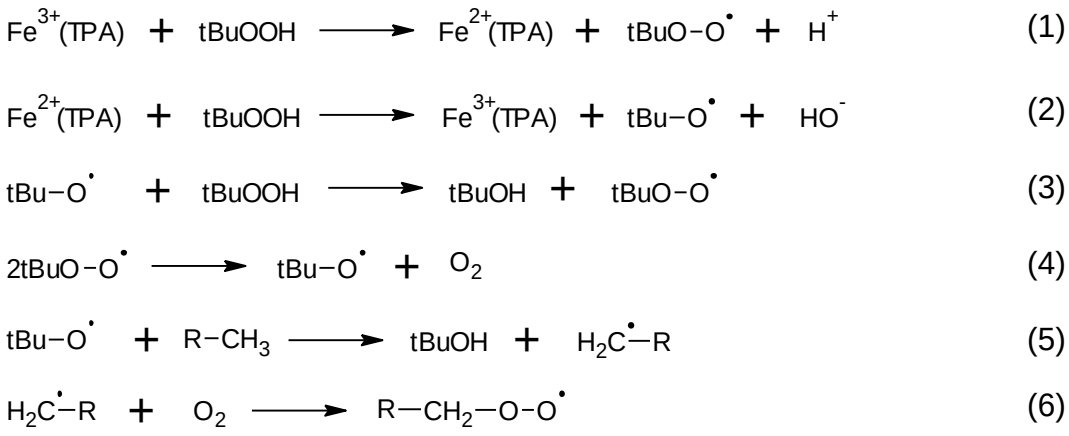

Scheme 7: Generation of free radical species from TBHP reported by Arends et al.[41] reproduced from Kim et al.[43]

Arends et al. also questioned the validity of using the well-known radical inhibitor 2,6 di-*tert*-butyl-4-methylphenol (BHT) (used by Que Jr.'s group) to test for the presence of *tert*-BuO radicals. By measuring the rate constants of hydrogen atom abstraction by *tert*-BuO radicals from BHT as well as cyclohexane, they found that hydrogen abstraction from cyclohexane to be roughly 3 times faster. The influence of a radical trap in this system is therefore expected to be small.

Furthermore, when the reaction vessel was purged with argon prior to and during the reaction, significantly reduced yields of alcohols and ketones are obtained, thus, indicating the importance of atmospheric oxygen as co-oxidant in the system.

In a follow-up paper Que Jr. and co-workers re-evaluated their initial findings and addressed the criticisms of Arends et al.[43] They concluded that two competing mechanistic pathways are operative in these reactions. The radical mechanism is likely to operate when a large excess of oxidant is present. However, when a small excess of oxidant is present, selectivity of the reaction shifts toward the formation of alcohols and the rebound mechanism is likely operative. Mention is made of the (fleeting) intense blue colour observed when the oxidant is added to a solution of the catalyst precursor. It was speculated that this could be due to the formation of a high valent iron transition state; an observation which has inspired subsequent research initiatives. [44]

White et al. reported an iron-based catalytic system that is very similar in structure to the complexes reported by Tordin et al. and Que Jr et al. (described above).[45] A number of different iron complexes based on the MEP (N,N-dimethyl- N,N-bis(2-pyridylmethyl)-ethane-1,2-diamine) ligand were previously reported.[46] These complexes were screened as oxidation catalysts in the oxidation of cyclohexane. Only low turnover numbers (2-5) were observed.[47] However due to the possibility of the complexes operating under a metal-based oxidant mechanism, White et al. speculated that these complexes could be useful in the oxidation of alkenes to selectively form the corresponding epoxides as typically various oxygenated products (such as alcohols, aldehydes) are also formed when the reaction occurs via the free radical mechanism.

Initial test reactions in the oxidation of 1-decene by Fe(II)(MEP)$(MeCN)_2(ClO_4)_2$ in the presence of H_2O_2 (Scheme 8) produced the epoxide in 40% yield along with a variety of overoxidized products.

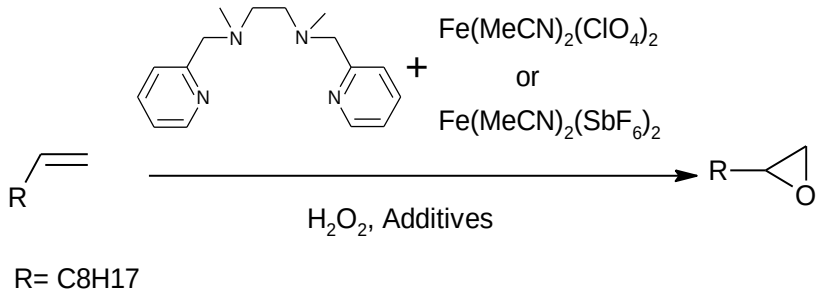

Scheme 8: Alkene epoxidation with iron(MEP) catalysts performed by White et al.[45]

The authors found that exchanging the perchlorate anion for SbF_6 dramatically improved the selectivity to 71%. However, the authors offer little explanation for the dramatic effect or the role of the counterions. A comment is made that 4 equivalents of H_2O_2 was needed for the complete conversion of alkene when the perchlorate anion is present while only 1.5 equivalents are necessary when the SbF_6 anion is present. Degradation of the oxidant might play a role and is clearly different for the two iron catalyst precursors. It appears quite possible that in the presence of the perchlorate system, Fenton-type chemistry could be occurring where the formation of free hydroxyl radicals leads to the formation of various other oxygenated products.

A number of additives were screened in an attempt to improve the selectivity of the SbF_6 system even further. It was found that 1 equivalent of acetic acid substantially increased the selectivity towards epoxide formation (82% yield). The pronounced effect of acetic acid on the catalyst system was further investigated. Crystallization of the catalyst precursor from solutions containing acetic acid (to form single crystals) and subsequent x-ray crystal structure determination revealed that in the presence of acetic acid a μ-oxo carboxylate bridged diiron(III) complex is formed. UV-Vis spectroscopy of this material matched that of the reaction mixture during catalysis, thus providing evidence that the dimeric structure is maintained in solution. Given the close resemblance of the crystal structure isolated by White et al. to that of the diiron cored enzymes discussed previously (Section **1.2.4.1**) it should come as no surprise that after fully optimizing the catalyst system various aliphatic alkenes could be oxidized to the corresponding epoxides (60-90% yield) in as little as 5 minutes.

Al-hunaiti et al. reported a simple catalyst system consisting of $FeCl_3$ and thymine-1-acetate (THA).[48] The catalyst can be generated in situ by combining 1 equivalent of $FeCl_3$ and 2 equivalents of THA as shown in Scheme 9.

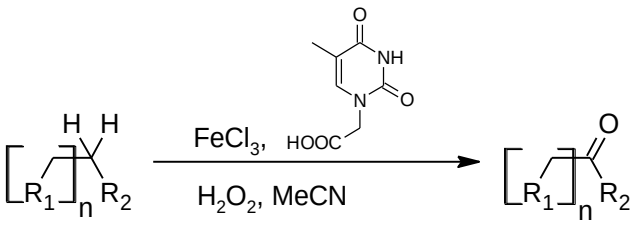

Scheme 9: General in situ catalysis reaction performed with $FeCl_3$ and thymine-1-acetate[48]

The authors could also isolate the metal complex as a yellow solid but never fully characterized the material. FTIR analysis concluded that coordination of the thymine acetate to the Fe(III) centre occurs in a monodentate fashion through the carboxylate oxygen. Additionally, coordination also occurs through the pyrimidine nitrogen donor. The authors suggested that the structure of the complex has two thymine-1-acetate ligands (based on mass spectrometry) complexed to the Fe(III) centre.

A variety of cyclic alkanes are oxidized to the corresponding ketones in very good yields. When octane was used as substrate, ketone products were observed in the ratio C_3:C_2:C_4 (8:5:1) indicating that the C_2 and C_3 carbons are more reactive. The system proved to be highly active in oxidizing octane, leading to combined product yields of 62-68% (12 hours, H_2O_2, 80°C, Cat: H_2O_2: substrate 5: 360: 100).

The selectivity of the catalytic system was further probed by careful choice of substrate. Various cycloalkanes containing 1°, 2° and 3° carbon atoms were investigated as potential substrates as shown in Table 5.

Table 5:Aliphatic alkane substrates used for selectivity studies by Al-hunaiti et al.[48]

Entry	Substrate	Products		
1	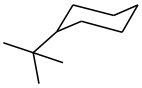	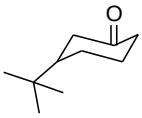 22%	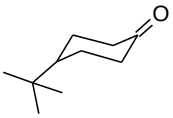 11%	
2	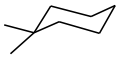	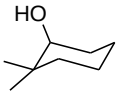 8%	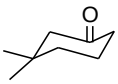 10%	 18%
3	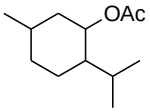	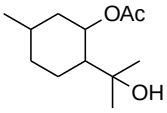 10%	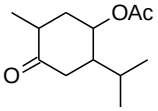 33%	

Reaction conditions: substrate 2.0 mmol, $FeCl_3$ 5 mol% relative to substrate, THA 10 mol% relative to substrate, H_2O_2 6.5 mmol, MeCN 1 ml, temperature 60°C.

Interestingly the catalytic system showed preference for activating the 2° carbon C-H bond compared to the more sterically hindered 3° carbon C-H (Table 5 entry 1) and the less sterically hindered 1° carbon. In the oxidation of dimethylcyclohexane no oxidation at the 1° carbons are observed. Curiously, when adamantane is used as substrate, a high selectivity is observed for the oxidation of 3° carbon C-H bonds. No explanation for these observations is offered by the authors.

Okuno et al. reported on the synthesis and catalytic properties of two μ-oxo bridged iron(III) complexes prepared from the ligands TPA and MEP shown below.[47]

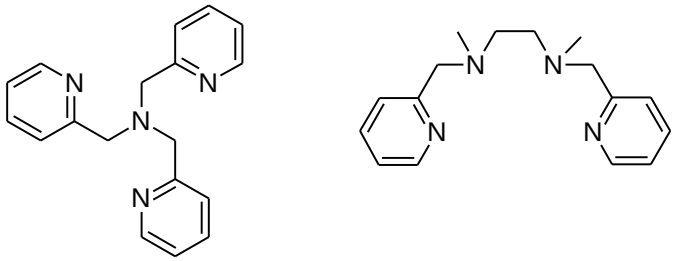

21: tpa **22**: mep

Figure 8: Ligands used in the synthesis of μ-oxo Iron(III) dimers[47]

The two complexes $[Fe_2O(CH_3CO_2)(MEP)_2]^{3+}$ and $[Fe_2O(CH_3CO_2)(TPA)_2]^{3+}$ both show some activity for the oxidation of cyclohexane. However, the authors found that the $[Fe_2O(CH_3CO_2)(MEP)_2]^{3+}$ complex showed vastly superior catalytic activity in the oxidation of cyclohexane, compared to $[Fe_2O(CH_3CO_2)(TPA)_2]^{3+}$. The authors observed gas evolution upon addition of the oxidant to the catalytic test reactions and postulated that the difference in catalytic activity might be due to disproportionation of the oxidant. This was tested by measuring oxygen evolution over the course of the reaction. Interestingly the $[Fe_2O(CH_3CO_2)(TPA)_2]^{3+}$ complex decomposed virtually all of the H_2O_2 within the first 5 minutes of the reaction, while the $[Fe_2O(CH_3CO_2)(MEP)_2]^{3+}$ complex showed almost no appreciable catalase-like activity over this time period.

The authors suggested that the nature of the active species formed from the two complexes differ in solution. If the Fe-O-Fe bond is linear (Figure 9, Case 1) the iron-hydroperoxy moiety is highly electrophilic and catalyses the oxidation of hydrocarbons readily. The authors postulated that the bent doubly bridged structure (Figure 9, Case 2) is in fact the intermediate responsible for the catalase-like decomposition of hydrogen peroxide to H_2O and O_2 and low hydrocarbon oxidation activity.

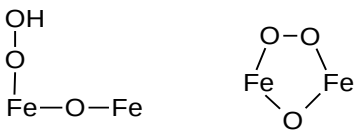

Case 1 Case 2

Figure 9: Active species for alkane oxidation and H_2O_2 decomposition

This theory is further supported by the different solution-state UV-Vis spectra, especially spectra recorded in the presence H_2O_2. Additional evidence is provided by crystal structures of analogous peroxodiiron(III) compounds (that also display significant disproportionation of the oxidant) such as those reported by Kim et al. and Dong et al.[49, 50]

Wang et al. reported on a related μ-oxo diiron complexes of the ligand 2,6-bis(N-methylbenzimidazol-2-yl)pyridine denoted as L.[38] Two complexes were reported viz. the oxo bridged complex $[Fe_2O(L)_2(NO_3)_2(CH_3OH)_2](NO_3)_2$ (denoted as **23**) as well as the mononuclear complex $Fe(L)Cl_3$ denoted (**24**) . Interestingly the mononuclear iron complex is almost completely inactive in the catalytic oxidation of cyclohexane while the dimeric species easily catalyses the oxidation of various alkanes and alkenes. When complex **23** is used as catalyst in the oxidation of styrene the epoxide product is formed in a remarkable 99.2% yield. Similarly, cyclohexene oxide is formed with a selectivity of 97.5% in the oxidation of cyclohexene. The authors attribute this remarkable difference in catalytic activity to the presence of an exchangeable coordination site in complex **23**. The ligands MeOH and NO_3^- are labile and can be readily replaced by coordinating H_2O_2, while in the case of **24** the chloride ligands are less labile and less likely to be replaced by H_2O_2.

Interestingly low selectivity is observed in the catalytic oxidation of cyclohexane by **23** with alcohol to ketone ratios of 1.2 (TBHP oxidant) and 1.1 (H_2O_2 oxidant). This suggests that the reaction mechanism likely involves the formation of free radicals. However, complex **23** catalyses the oxidation of alkenes with extremely high selectivity towards epoxide products which likely suggests a metal-based oxidant is involved. The authors suggest that both the metal-based oxidant as well as the free radical mechanism could be operative simultaneously. However, it is not understood how the substrate influences which mechanism dominates the reaction.

Drawing inspiration from the porphyrin and heme type systems, Sorokin and co-workers have published extensively on the use of iron phthalocyanines (denoted Pc) for the oxidation of alkanes. In particular the group of Sorokin found that bridged diiron phthalocyanines are highly active catalysts for the oxidation of light alkanes such as methane and ethane.

Sorokin et al. reported the use of the catalyst precursor $(FePC)_2N$ which consists of two phthalocyanine macrocyclic rings each coordinated to iron (with formal +3.5 oxidation state) bridged by a single nitrogen atom (Figure 10, **25**).[51] Initial attempts to use **25** as a catalyst precursor were plagued by difficulties, due to problems encountered in the purification of the metal complex, and its low solubility. The $(FePc)_2N$ system was found to be insoluble in all organic solvents surveyed. The ligand was then modified by the introduction of *tert*-butyl groups (to yield **26**) to improve the solubility of the compound in organic solvents.

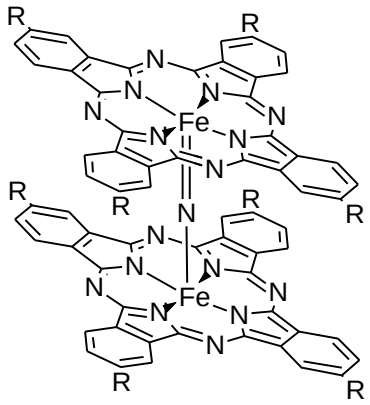

25: R= H

26: R= *t*-Bu

Figure 10: μ-Nitrido iron phthalocyanine catalyst precursor[51]

Sorokin and co-workers then proceeded to thoroughly investigate the reaction of **26** with H_2O_2. When H_2O_2 is introduced to a solution of **26** significant changes in its UV-Vis and EPR spectra are observed. The EPR spectrum of **26** initially shows a signal at g= 1.99, typical for low spin Fe(III) centers with 1 unpaired electron. When H_2O_2 is added additional signals are observed (g= 8.16, 4.25, 2.07) that are in good agreement with the g-values reported for iron peroxo species.

Furthermore, the authors found that the bridged structure stays intact after reaction with H_2O_2. ESI mass spectrometry was employed to characterize the products formed during the reaction of H_2O_2 with catalyst. The authors observed a signal at m/z = 1615.9 which could be assigned as O-$(FePc\text{-}t Bu_4)_2N$. When the reaction was performed with isotopically labelled $H_2{}^{18}O_2$.a signal at m/z 1617.9 was observed

corresponding to ^{18}O-(FePc-*t*Bu$_4$)$_2$N. Furthermore, no mononuclear FePc complexes were observed under ESI-MS conditions.

The nitrido bridged complex was further supported on silica and tested in the catalytic oxidation of methane. Catalytic reactions were performed using methane at a pressure of 32 Bar and employing the silica supported catalyst precursor in water as solvent and hydrogen peroxide as oxidant. The catalytic system gave a total turnover number (TON) of 39.0 when operated at a temperature of 25°C over 48 hours. The major product of this reaction was formic acid. The total TON could be increased by increasing the temperature of the reaction. At 50°C a TON of 84.4 was obtained. Formic acid and formaldehyde formed as products in the ratio 2:1, however the formation of methanol and CO_2 were not observed. The authors probed this observation further by testing if methanol could be converted under these conditions to formic acid. Under the reaction conditions tested, 80% of the methanol was converted to formic acid after 1 hour.

Sorokin et al. theorized that according to the so-called rebound mechanism (as discussed previously) the heterolytic cleavage of the peroxo moiety in Fe^{IV}NFe^{III}OOH should be enhanced in the presence of acid due to protonation of the peroxo oxygen atom. The authors tested this hypothesis by performing the catalytic reaction in 0.1M H_2SO_4. Under acidic conditions the reaction was greatly enhanced achieving a very high total TON of 436.8.

The (FePc-*t*Bu$_4$)$_2$N complexes were also tested as catalyst precursors in the oxidation of ethane.[52] Heterogeneous catalyst precursors were prepared by the physical absorption of (FePc^{t}Bu$_4$)$_2$N onto various supports namely silica Aerosil 200, Graphite HSAG 300 and Nafion SAC-13. Total product yields as high as 65% were obtained with acetic acid and formic acid formed as major products, while traces of ethanol and acetaldehyde were also detected. Formic acid would have to form via the cleavage of a C-C bond in ethane. The source of the formic acid was established when acetic acid was used as substrate under similar reaction conditions. Within 20 hours the acetic acid was quantitatively converted to formic acid. No CO_2 evolution was, however, observed. It was also found that acidic conditions increased the selectivity of the reaction to formic acid.

Połtowicz et al. reported on immobilized metalloporphyrin catalyst precursors for hydrocarbon oxidation.[53] Manganese porphyrin complexes were immobilized on Si,Al-mesoporous molecular sieves. Both the immobilized as well as the unsupported complexes were tested in the oxidation of cyclohexene. The unsupported metalloporphyrin gave cyclohexene conversions around 30% using PhIO as oxidant. In this case high selectivity towards cyclohexene oxide as the major product is observed. The immobilized catalysts were in general more active than the unsupported catalyst (depending on support material), however, when using the supported catalyst precursors high selectivity towards the allylic oxidation products were obtained. The authors proposed that due to the relatively small pore size of the immobilized catalyst, the formation of a highvalent metal-oxo species and its subsequent reaction with the substrate is unfavourable. Thus, oxidation catalysed by the immobilized catalysts occurs primarily through the generation of free radicals. The use of support materials with larger pore sizes resulted in increased epoxide yields, providing some proof for this hypothesis.[53]

Similar observations were made in a follow-up study conducted by Serwicka et al.[54] Iron, cobalt and manganese metalloporphyrins were immobilized on various silica supports. Both the iron as well as the manganese porphyrin complexes were active for the oxidation of cyclohexene, while the cobalt porphyrin complexes (both supported and unsupported) were highly inactive for the transformation. It was found that pore-size as well as location of the catalytically active metal complex, (inside pore or on the outside) played a significant role in allylic oxidation selectivity.[54]

Goberna-Ferron et al. reported a Cu(II) proline catalyst precursor (**27**) capable of oxidizing both alkanes and alkenes.[55] The catalyst was prepared in a single step from Cu(II) hydroxide in water and L-proline to yield a crystalline material with two chelating proline ligands. The complex has an N_2O_2 coordinating environment (as shown in Figure 11) and is soluble in water but insoluble in most organic solvents.

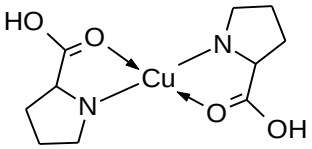

27

Figure 11: Cu(II)proline catalyst precursor reported by Goberna-Ferron et al.[55]

Catalysis reactions were performed in a water-acetonitrile mixture due to the low solubility of the catalyst precursor in organic media. When only organic solvents were used no conversion is observed due to the low solubility of the catalyst.

The catalyst was fairly active in the oxidation of cyclohexane. Turnover numbers up to a maximum of 150 were achieved while very low selectivity was observed (55:45, alcohol to ketone). The oxidation of n-hexane was also attempted. The authors observed around 12% conversion of the n-hexane after 48 hours and recorded a TON of 46. No clear preference was observed for the position of activation (1-hexanol vs 2-hexanol) or for the alcohol vs ketone selectivity. However, the activity of this complex remains unusually high for a Cu(II) complex.

The authors speculate that the mechanism of oxidation might involve the formation of non-selective radicals. The role of the metal species would then be to generate and stabilize the produced OH radicals. This seemingly explains the poor selectivity observed during catalytic reactions.

The Cu(II) catalyst precursor was also tested in the oxidation of cyclohexene. In the presence of cyclohexanecarboxaldehyde and oxygen, cyclohexene could be converted with fairly high turnovers to the corresponding epoxide with high selectivity (95%). The mechanism proposed for this reaction is however unusual.

According to the mechanism (evoked by Goberna-Ferron et al.) proposed by Komiya et al., the aldehyde first reacts with oxygen to form a peroxy acid (Scheme 10, reaction 1).[56] Reaction of the peroxy acid with Cu(II) then forms a Cu(III) centred radical (Scheme10, reaction 2). This metal centred radical is then responsible for further oxidation.

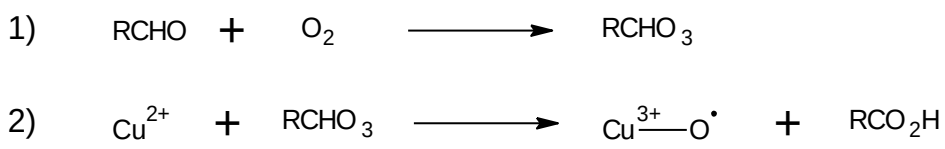

Scheme 10: Mechanism of Cu catalysed oxidation in the presence of aldehydes[56]

However, evidence for this mechanism is limited. It should be noted that no Cu(III) intermediates were isolated in either of the Komiya et al or Goberna-Ferron et al. studies. Furthermore, Goberna-Ferron et al. reports that around 30% conversion (24 hours) of the substrate is achieved when no copper catalyst is present (O_2 and cyclohexanecarboxaldehyde still present). In this case the formed peracid on its own is capable of this oxidation process (when the copper catalyst is added enhancement of the rate of reaction is observed). Additionally, it is thought that the formation of a Cu(III) species is expected to be energetically unfavourable.

1.3.3 Second and third row transition metals for hydrocarbon oxidation

Shul'pin and co-workers have recently shown that simple osmium metal salts such as $OsCl_3$ could catalyse the oxidation of alkanes.[57] Due to this encouraging result significant research efforts have gone into the testing of a variety of osmium metal complexes as potential catalyst for hydrocarbon oxidation.

Vinogradov et al. showed that osmium *p*-cymene ligands are relatively active in the oxidation of cyclohexane, methylcyclohexane and n-octane amongst others.[58] These complexes along with the co-catalyst pyridine catalysed the oxidation of cyclohexane at extremely low catalyst loading (1:9200 catalyst to substrate ratio) yielding some of the highest TON's yet reported (to the best of our knowledge).

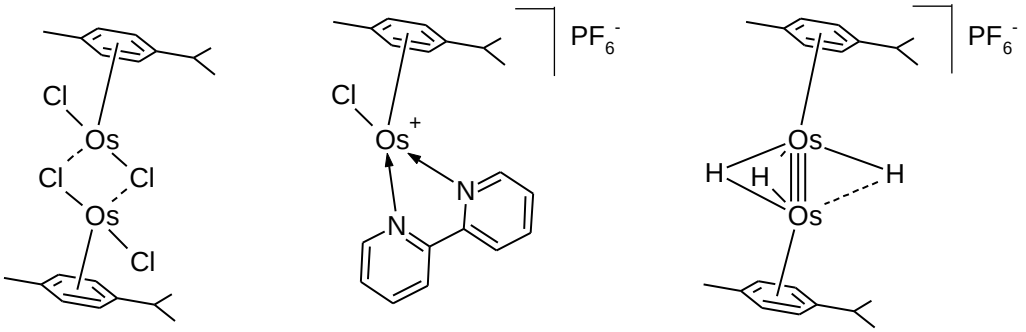

28 **29** **30**

Figure 12: Osmium *p*-cymene catalyst precursors reported by Vinogradov et al.[58]

Pyridine, however, is required to achieve these high reaction rates. A very thorough study of the kinetics of complex **28** (Figure 12) was undertaken and based on these results, the authors postulate that the active catalyst is in fact not the dimeric form as pictured, but rather a mononuclear osmium species.

Therefore, the added pyridine could facilitate the formation of the monomeric species. Pyridine could also act as ligand and coordinate to the osmium centre after the cleavage of the bridged compound to the mononuclear complex. However, it is quite strange that **29**, the mononuclear complex, showed the lowest catalytic activity of the three complexes. This is something the authors did not elaborate on further. One could speculate that the bidentate nature of the 2,2-bypiridine ligand inhibits the coordination of substrate when compared to complexes containing monopyridine. It would have been interesting to see whether the addition of 2,2-bypiridine instead of pyridine as co-catalyst inhibits the reaction.

Lau and co-workers reported that the complex $[Os(IV)N(Cl_4)]^-$ is a highly active catalyst precursor for the oxidation of cyclohexane.[59] In an attempt to improve on this result Chen et al. reported the synthesis and use of (salen)Os(IV) nitrido type complexes as catalyst precursors.[60] Chen employed the salen ligands and their derivatives as these have traditionally been used to successfully stabilize metals in high oxidation states.[61, 62] High valent metal centres are important intermediates during the alkane oxidation mechanism as discussed above.

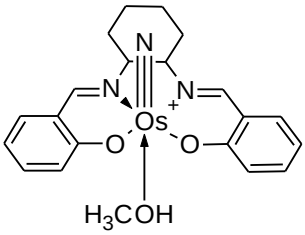

31

Figure 13: Highly active Os(IV) salen derivative by Chen et al.[60]

Initial experiments showed that a 75% conversion of cyclohexane could be achieved in 3 hours at room temperature. This corresponds to a TON of 60. Chen et al. theorized that the oxidant, H_2O_2, could possibly be decomposed by the metal complex. By slowly adding the oxidant via a syringe pump and therefore keeping the oxidant concentration low in the reaction mixture the TON could be improved to 2230. In all cases selectivity towards the formation of cyclohexanol is observed with alcohol to ketone ratios of around 5:1 typically observed.

1.4 Concluding remarks

Hydrocarbon oxidation remains one of the great challenges faced by modern chemists. This is due to the extremely unreactive nature of the C-H bond as we have discussed in Section 1.2.2. Furthermore, the C-H bonds of potential products of these oxidation reactions such as alcohols and ketones are far more labile than that of the starting alkane. This is particularly problematic when trying to achieve selectivity in terms of product distribution.

We have briefly discussed the most prominent hydrocarbon oxidation mechanisms reported in the literature, namely the so-called organometallic activation, oxidation by free radicals and the metal oxidant based rebound mechanism. Throughout the review of the literature, we have noted the difficulty in following and assigning these mechanisms unambiguously.

Reviewing the catalytic results, it is observed that turnover numbers for the oxidation of alkanes are typically low. Only recently have TON's in the thousands been reported by Shul'pin and co-workers for their osmium-based catalysts.

Thus, there remains great scope for improving both the catalytic activity and selectivity of these reactions. Furthermore, investigation into the mechanisms of these reactions remains an active research field.

In this chapter we have broadly reviewed a number of active catalysts for the oxidation of various hydrocarbons. Interestingly, many of these systems incorporate Schiff base and pyridine moieties.

However, many of these catalyst precursors still suffer from one of the biggest problems facing homogeneous catalysts in industry namely, removal of the catalyst from the product stream and recycling of the catalyst.

1.5 Aims and objectives of this study

In this chapter we have highlighted a number of difficulties usually encountered in current hydrocarbon oxidation processes, including poor activity, selectivity and in the case of homogeneous catalyst systems, removal of the catalyst material from the product stream. With this in mind, the aims of this study (firstly) were to synthesize and characterize novel ligands by drawing inspiration from enzymatic systems and other promising catalysts reported in the literature. Such ligands are based on the moieties commonly present in the systems reviewed in this chapter, including Schiff base and pyridine derivatives. A second aim was to synthesize and characterize a range of metal complexes based on some of these ligands. An additional aim was to attempt to synthesize large multinuclear transition metal complexes such as metallodendrimers that can potentially be removed from the product stream by ultrafiltration. Removal of the spent catalyst from the product stream would represent an improvement on traditional homogeneous processes. The final aim was to evaluate these metal complexes as catalyst precursors in the catalytic oxidation of various hydrocarbons. This includes a preliminary exploration to gain insight into the mechanism of these catalytic oxidation reactions.

1.6 Overview of thesis by chapter

Chapter 1: An overview of the current state of catalytic oxidation of hydrocarbons

Chapter 2: The synthesis and characterization of ligands and complexes

Chapter 3: The effect of cobalt salicylaldimine and iron pyridine-imine complexes on oxidant decomposition, mechanistic and kinetic aspects

Chapter 4: Catalytic oxidation of hydrocarbons by iron, cobalt and copper complexes

Chapter 5: Kinetic and mechanistic studies of dendritic iron and cobalt catalysed decomposition of H_2O_2

Chapter 6: Chapter summaries, conclusions and future work

1.7 References

1 Y. Ishii, S. Sakaguchi and T. Iwahama, *Adv. Synth. Catal.*, 2001, **343**, 393–427.

2 P. Dagaut, *Phys. Chem. Chem. Phys.*, 2002, **4**, 2079–2094.

3 D. L. Trimm, *Appl. Catal.*, 1983, **7**, 249–282.

4 T. V. Choudhary, S. Banerjee and V. R. Choudhary, *Appl. Catal. A Gen.*, 2002, **234**, 1–23.

5 C. K. Westbrook, W. J. Pitz, O. Herbinet, H. J. Curran and E. J. Silke, *Combust. Flame*, 2009, **156**, 181–199.

6 N. Rahimi and R. Karimzadeh, *Appl. Catal. A Gen.*, 2011, **398**, 1–17.

7 Y. V Kissin, *Catal. Rev.*, 2001, **43**, 85–146.

8 R. A. Periana, G. Bhalla, W. J. Tenn, K. J. H. Young, X. Y. Liu, O. Mironov, C. Jones and V. R. Ziatdinov, *J. Mol. Catal. A Chem.*, 2004, **220**, 7–25.

9 J. A. Labinger, *J. Mol. Catal. A Chem.*, 2004, **220**, 27–35.

10 M. Lersch and M. Tilset, *Chem. Rev.*, 2005, **105**, 2471–2526.

11 G. Shul'pin, *Catalysts*, 2016, **6**, 1–40.

12 S. J. Blanksby and G. B. Ellison, *Acc. Chem. Res.*, 2003, **36**, 255–263.

13 A. A. Gol'dshleger, N. F.; Tyabin, M. B.; Shilov, A. E.; Shteinman, *Zhurnal Fiz. Khimii*, 1969, **43**, 2174–2175.

14 K. A. Jorgensen, *Chem. Rev.*, 1989, **89**, 431–458.

15 B. S. Lane and K. Burgess, *Chem. Rev.*, 2003, **103**, 2457–2473.

16 E. M. McGarrigle and D. G. Gilheany, *Chem. Rev.*, 2005, **105**, 1563–1602.

17 X. Xu, J. Kua, R. A. Periana and W. A. Goddard, *Organometallics*, 2003, **22**, 2057–2068.

18 R. H. Crabtree, *J. Organomet. Chem.*, 2004, **689**, 4083–4091.

19 A. A. Shteinman, *J. Organomet. Chem.*, 2015, **793**, 34–40.

20 E. Neyens and J. Baeyens, *J. Hazard. Mater.*, 2003, **98**, 33–50.

21 S. Goldstein, D. Meyerstein and G. Czapski, *Free Radic. Biol. Med.*, 1993, **15**, 435–445.

22 J. T. Groves, *J. Chem. Educ.*, 1985, **52**, 928–931.

23 F. Ogliaro, N. Harris, S. Cohen, M. Filatov, S. P. De Visser and S. Shaik, *J. Am. Chem. Soc.*, 2000, **122**, 8977–8989.

24 J. T. Groves, *J. Chem. Educ.*, 1985, **62**, 928.

25 S. Shaik, M. Filatov, D. Schröder and H. Schwarz, *Chem. - A Eur. J.*, 1998, **4**, 193–199.

26 R. J. Hodges and J. L. Garnett, *J. Phys. Chem.*, 1968, **72**, 1673–1682.

27 B. E. R. Snyder, P. Vanelderen, M. L. Bols, S. D. Hallaert, L. H. Böttger, L. Ungur, K. Pierloot, R. A. Schoonheydt, B. F. Sels and E. I. Solomon, *Nature*, 2016, **536**, 317–321.

28 M. Merkx, D. a. Kopp, M. H. Sazinsky, J. L. Blazyk, J. Muandller and S. J. Lippard, *Angew. Chemie - Int. Ed.*, 2001, **40**, 2782–2807.

29 T. L. Poulos, *Chem. Rev.*, 2014, **114**, 3919–3962.

30 R. R. Fernandes, J. Lasri, A. M. Kirillov, M. F. C. Guedes da Silva, J. A. L. da Silva, J. J. R. Fraústo da Silva and A. J. L. Pombeiro, *Eur. J. Inorg. Chem.*, 2011, 3781–3790.

31 G. B. Shul'pin, *J. Mol. Catal. A Chem.*, 2002, **189**, 39–66.

32 A. R. Silva, T. Mourão and J. Rocha, *Catal. Today*, 2013, **203**, 81–86.

33 J. Tang, P. Gamez and J. Reedijk, *Dalton Trans.*, 2007, 4644–4646.

34 S. Taktak, W. Ye, A. M. Herrera and E. V. Rybak-Akimova, *Inorg. Chem.*, 2007, **46**, 2929–2942.

35 I. Hermans, P. Jacobs and J. Peeters, *Chem. - A Eur. J.*, 2007, **13**, 754–761.

36 M. J. Ashwood-Smith, *Ann. N. Y. Acad. Sci.*, 1975, **243**, 246–256.

37 R. V Panganamala, H. M. Sharma, R. E. Heikkila, J. C. Geer and D. G. Cornwell, *Prostaglandins*, 1976, **11**, 599–607.

38 X. Wang, S. Wang, L. Li, E. B. Sundberg and G. P. Gachot, *Inorg. Chem.*, 2003, **42**, 7799–7808.

39 E. Tordin, M. List, U. Monkowius, S. Schindler and G. Knör, *Inorganica Chim. Acta*, 2013, **402**, 90–96.

40 R. A. Leising, J. Kim, M. A. Pérez and L. Que Jr., *J. Am. Chem. Soc.*, 1993, **115**, 9524–9530.

41 I. W. C. E. Arends, K. U. Ingold and D. D. M. Wayner, *J. Am. Chem. Soc.*, 1995, **117**, 4710–4711.

42 G. A. Russell, *J. Am. Chem. Soc.*, 1957, **79**, 3871–3877.

43 J. Kim, R. G. Harrison, C. Kim and L. Que, *J. Am. Chem. Soc.*, 1996, **2**, 4373–4379.

44 A. R. McDonald and L. Que, *Coord. Chem. Rev.*, 2013, **257**, 414–428.

45 M. C. White, A. G. Doyle and E. N. Jacobsen, *J. Am. Chem. Soc.*, 2001, **123**, 7194–7195.

46 H. Toftlund, E. Pederson and S. Yde-Andersen, *Acta Chem. Scand.*, 1984, **38**, 693–697.

47 T. Okuno, S. Ito, S. Ohba and Y. Nishida, *J. Chem. Soc. Dalton Trans.*, 1997, 3547–3551.

48 A. Al-hunaiti, M. Räisänen and T. Repo, *Chem. Commun.*, 2016, **52**, 2043–2046.

49 K. Kim and S. J. Lippard, *J. Am. Chem. Soc.*, 1996, **118**, 4914–4915.

50 Y. Dong, S. Yan, V. G. Young Jr. and L. Que Jr., *Angew. Chemie Int. Ed.*, 1996, **35**, 618–620.

51 A. B. Sorokin, E. V Kudrik and D. Bouchu, *Chem. Commun.*, 2008, 2562–2564.

52 L. X. Alvarez and A. B. Sorokin, *J. Organomet. Chem.*, 2015, **793**, 139–144.

53 J. Połtowicz, E. . Serwicka, E. Bastardo-Gonzalez, W. Jones and R. Mokaya, *Appl. Catal. A Gen.*, 2001, **218**, 211–217.

54 E. M. Serwicka, J. Połtowicz, K. Bahranowski, Z. Olejniczak and W. Jones, *Appl. Catal. A Gen.*, 2004, **275**, 9–14.

55 S. Goberna-Ferrón, V. Lillo and J. R. Galán-Mascarós, *Catal. Commun.*, 2012, **23**, 30–33.

56 N. Komiya, T. Naota, Y. Oda and S. I. Murahashi, *J. Mol. Catal. A Chem.*, 1997, **117**, 21–37.

57 G. B. Shul'pin, G. Süss-Fink and L. S. Shul'pina, *Chem. Commun.*, 2000, 1131–1132.

58 M. M. Vinogradov, Y. N. Kozlov, D. S. Nesterov, L. S. Shul'pina, A. J. L. Pombeiro and G. B. Shul'pin, *Catal. Sci. Technol.*, 2014, **4**, 3214–3226.

59 S. M. Yiu, W. L. Man and T. C. Lau, *J. Am. Chem. Soc.*, 2008, **130**, 10821–10827.

60 M. Chen, Y. Pan, H.-K. Kwong, R. J. Zeng, K.-C. Lau and T.-C. Lau, *Chem. Commun.*, 2015, **51**, 13686–13689.

61 K. Srinivasan and J. K. Kochi, *J. Am. Chem. Soc.*, 1985, **107**, 7606–7617.

62 K. Srinivasan, P. Michaud and J. K. Kochi, *J. Am. Chem. Soc.*, 1986, **108**, 2309–2320.

Chapter 2: The Synthesis and Characterization of Ligands and Complexes

2.1 Introduction: the rational design of ligands

A number of highly active oxidation catalyst systems were discussed in Chapter 1. Considering the structures of the transition metal complexes described in Chapter 1, it can be seen that certain moieties are quite prevalent in the ligand structure of successful oxidation catalyst precursors. As can be expected similar moieties are also present in the active sites of several enzymatic systems.

The design of new transition metal complexes and their corresponding ligands described in this thesis draws inspiration from enzymatic systems such as cytochrome P450 and methane monooxygenase, which are well known for their utility in different oxidation processes.[1]

One of many problems associated with homogeneous catalysis (as discussed in Chapter 1) is that of catalyst separation from the product stream and the inability of recycling of the often-expensive catalysts. One way of overcoming this problem is to immobilize the catalyst species on either organic or inorganic supports. Dendrimers have previously been employed[2] and in this thesis we aim to expand the scope of dendritic catalysis.

2.2 Introduction to dendrimers

2.2.1 Overview of dendrimers

Dendrimers are branched macromolecules that display three important structural features. These include (1) an interior core unit, (2) branching points (that give rise to different generations of dendrimers depending on degree of branching) and (3) peripheral functional groups as shown in Figure 1.[3]

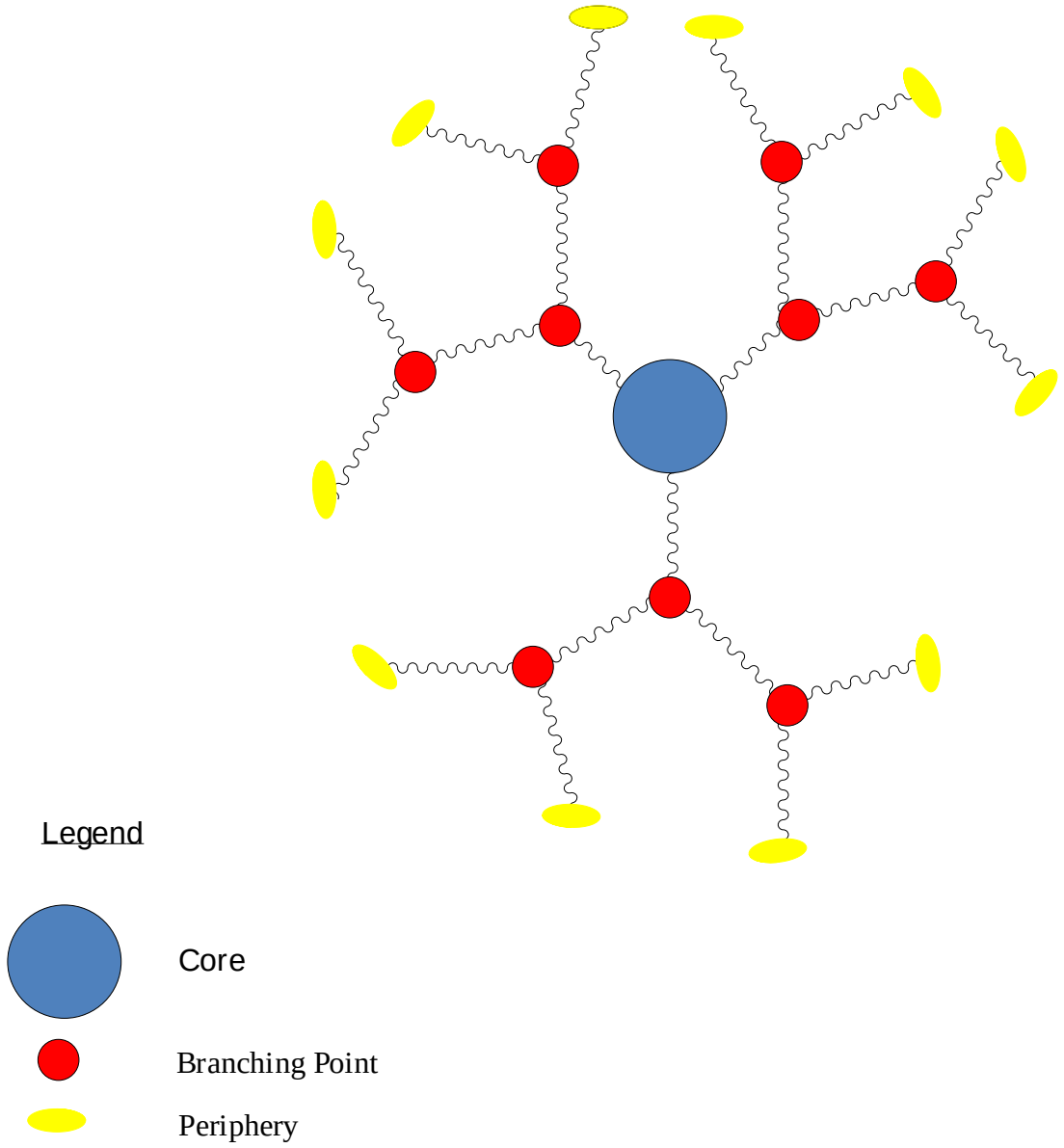

Figure 1: General structure of a dendrimer

The dendrimer architecture (that of repetitive branching) was conceptualized by Flory in 1941, however the first successful synthesis was reported in 1978 by Buhleier et al. who synthesized highly branched low molecular weight amines to create what the authors named cascade molecules.[4] Tomalia et al. were the first to coin the term “dendrimer” for these highly branched molecules in their article describing the synthesis of branched poly(amidoamines).[5] The term dendrimer has been adopted widely by the scientific community, while synonyms such as “arborol” and “cascade molecule” are rarely used.

2.2.2 Dendrimer synthesis: convergent versus divergent routes

Dendrimers can be synthesized by two different synthetic methods the so-called divergent and convergent methods respectively. The groups of Vögtle and Tomalia pioneered the divergent dendrimer synthesis.[3, 5] The divergent synthesis begins at the interior dendrimer core. Dendrimer branches are then attached at reactive functional groups onto the dendrimer core (Scheme 1, Step 1). Further branching may then occur on these dendrimer arms as the molecule is grown outward (Scheme 1 Step 2) towards the dendrimer peripheries (Scheme 1 Step 3). Increasing the extent of branching in Steps 2 and 3 increases the generation of the dendrimer.

While the divergent synthesis starts at the dendrimer core, the convergent synthesis on the other hand, starts at the periphery. During the convergent dendrimer growth, (introduced by the group of Fréchet) the synthesis of a dendron is first completed.[6] The dendron is then coupled to the branching monomer at an appropriate functional group before finally being attached to the dendrimer core. This method has the advantage that intermediate products can be purified by common lab techniques such as recrystallization or column chromatography before the next reaction in the dendrimer growth sequence is performed (this is usually not possible during the divergent synthesis).

A major disadvantage of the divergent method is the lack of control when the dendrimer generation is increased. Incomplete dendrimer growth as well as any potential side reactions that occur are difficult to control. This disadvantage complicates product separation and purification as incomplete/ imperfect dendrimers are difficult to separate from the target product, potentially lowering the obtained yield and purity.

Thus, the convergent approach can often lead to a higher purity of the final product when compared to the divergent method.

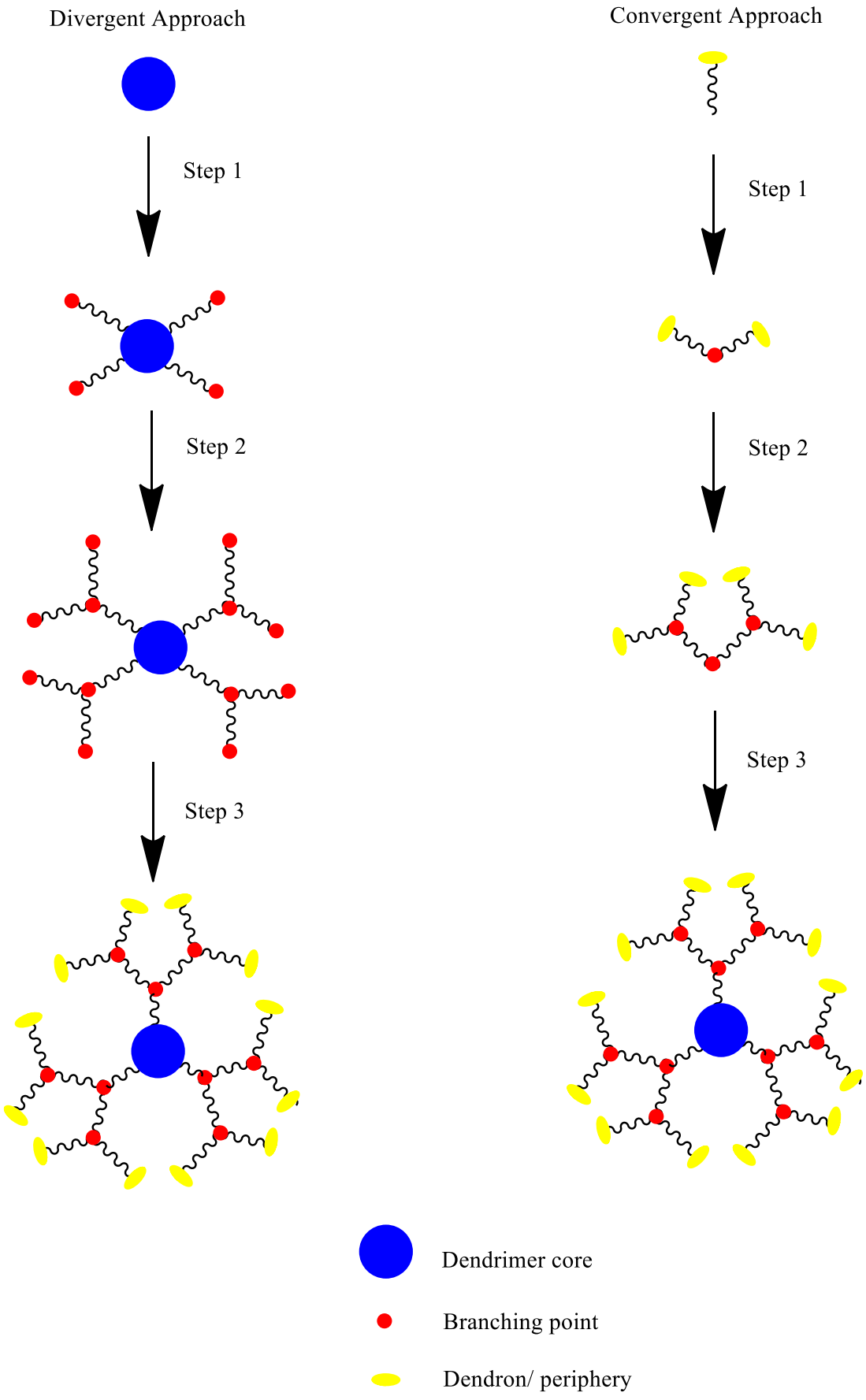

Scheme 1: Convergent and divergent dendrimer growth

2.2.3 Metallodendrimers and their advantages

Dendrimers, due to their unique architecture and structure, have several applications such as drug delivery agents[7], extractants for the removal of pollutants (such as transition metals) from aqueous waste streams[8, 9] and as stabilizers for metal nanoparticles.[10] Dendrimers can also act as ligands to form transition metal complexes known as metallodendrimers. Furthermore, transition metals can be incorporated at various positions of the dendrimer architecture including at the dendrimer core, dendrimer branching points or at the periphery.

Metallodendrimers are of particular interest in the field of catalysis.[2] Due to the typically large molecular weight of metallodendrimers these complexes can sometimes be removed from the product stream by ultrafiltration and recycled.[8] Removal and/or recycling of the metal catalyst represents a significant improvement over traditional homogeneous catalysis by reducing the amount of downstream processing necessary to purify reaction products.

Metallodendrimers often exhibit unique properties that are not present in the non-metallated dendrimer nor in the model dendrimer subunits. These properties can give rise to so called positive and negative dendritic effects. Dendritic effects can influence, for example, the catalytic activity[11], selectivity and stability of these metallodendrimers when compared to the non metallodendrimer analogues.[12]

The branching architecture of dendrimers has been found to have interesting effects on both activity and selectivity in catalytic systems. For example Francavilla et al.[11] observed greatly enhanced catalytic performance (per mole active centre) when the generation of their dendrimer catalysts were increased while Kleij[13] et al. observed a marked decrease in catalytic activity for their nickel metallodendrimers in the Kharasch addition reaction of CCl_4 to MMA.

2.3 Synthesis and characterization of ligands and complexes

Here we describe the synthesis and characterization of both ligands and complexes. The synthesis of these materials draw inspiration from the structures of the enzymatic systems as well as other catalysts precursors reported in the literature (as reviewed in

Chapter 1). To this end, iron, copper and cobalt transition metals and moieties such as salicylaldimine (N_2O_2) as well as pyridine-imine (N_4) and thioether amine (N_2S_2 donor groups) groups were included in the design of the new catalyst precursors. Given the potential advantages of dendrimers as discussed above, we thus report the synthesis and characterization of various dendrimer ligands as well as metallodendrimers that incorporate the above moieties.

2.3.1 Synthesis and characterization of N_2O_2 salicylaldimine type ligands and transition metal complexes

Schiff base ligands such as salen and salophen have long been valued by coordination chemists due to the ease of synthesis and their ability to stabilize transition metals in various oxidation states.[14] In addition Silva et al.[15] and Tang et al.[16] have shown that transition metal complexes of salicyladimine ligands are highly active catalyst precursors in various oxidation reactions (as reviewed in Chapter 1). Due to these advantages, we envisaged the design and preparation of several salicylaldimine ligands that could later be complexed to various transition metals.

Salicylaldimine ligands, **L1** and **L2** were obtained by refluxing propylamine along with the appropriate salicylaldehyde derivative in ethanol (Scheme 2) as was previously described in the literature.[17, 18]

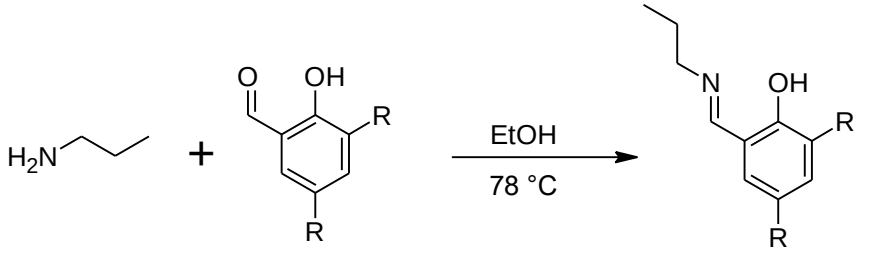

L1: R= H
L2: R= *tert*-Bu

Scheme 2: Synthesis of salicylaldimine model compounds[18]

The Schiff base ligands obtained were stable in air and exhibited solubility in most organic solvents with the exception of diethyl ether and highly non-polar solvents such as unsaturated alkanes. Characterization data obtained for **L1** and **L2** closely matched

those previously reported.[19, 20] With these model compounds in hand we turned our attention to the synthesis of their dendritic analogues.

The immobilization of salicylaldimine moieties on the peripheries of dendritic molecules was undertaken by modifying the method reported by van Martinovic et al.[21]

Reaction of the appropriate salicylaldehyde derivative with the primary amine groups of the commercially available diaminobutane-cored polypropylenimine tetramine dendrimer (DAB-PPI generation 1 dendrimer) in a Schiff base condensation reaction yielded the corresponding dendritic ligands as shown in Scheme 3. The compounds were isolated as yellow powders.

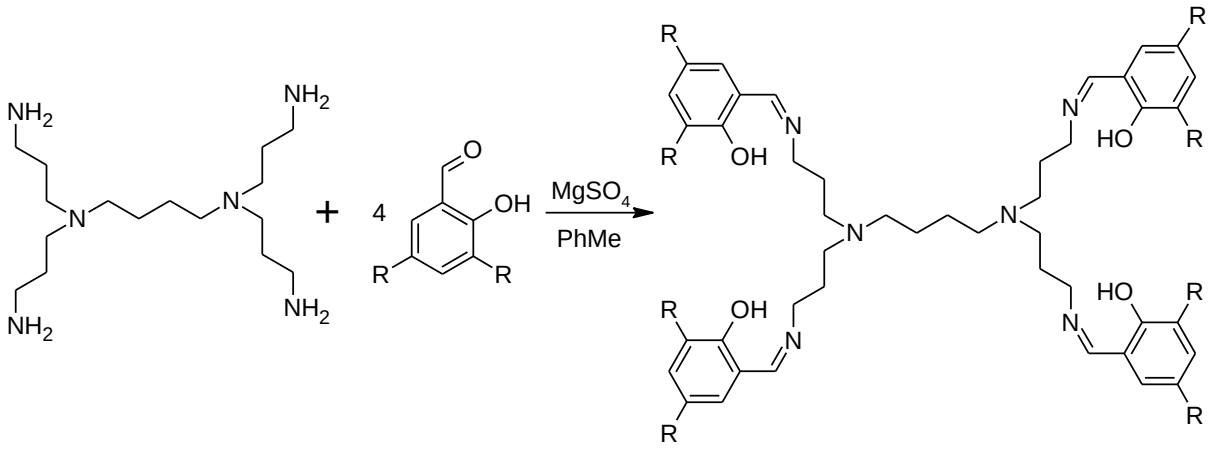

D1: R = H

D2: R= *tert*-Butyl

Scheme 3: Synthesis of salicylaldimine dendrimers[21]

Similar to the model ligands **L1** and **L2** the dendritic compounds are fairly stable and can be safely stored in air at ambient conditions. The dendrimers are soluble in a variety of organic solvents such as methylene chloride (DCM), chloroform, toluene, diethyl ether and common alcohols while being insoluble in highly apolar solvents such as hexane.

The products were characterized by a variety of spectroscopic techniques including FTIR and NMR spectroscopy. The obtained characterization data closely matched that reported by Martinovic et al.[21] Table 1 summarizes the most important spectroscopic data collected for compounds **L1, L2, D1** and **D2**.

Table 1: Selected characterization data of ligands L1-L2 and D1-D2

Compound	IR Spectra (cm^{-1}) (ATR)		ESI MS $(M+H)^+$	^1H NMR (N**H**=C) ppm
	$\nu_{C=N}$	ν_{C-O}		
L1[a]	1632	1275	164	8.22
L2[a]	1633	1276	275	8.37
D1[b]	1632	1277	733	8.32
D2[b]	1629	1271	1182	8.34

[a] Recorded as a neat oil using ATR. [b] Recorded in the solid-state using ATR

With the salicylaldimine model compounds (**L1** and **L2**) and the dendrimers **D1** and **D2** successfully synthesized and characterized we attempted to apply them as ligands in the synthesis of cobalt complexes.

The model cobalt complexes **C1** and **C2** could be obtained by reaction of the appropriate ligands (**L1** and **L2**) with $Co(OAc)_2 \cdot 4H_2O$ in the presence of an appropriate base (Scheme 4).

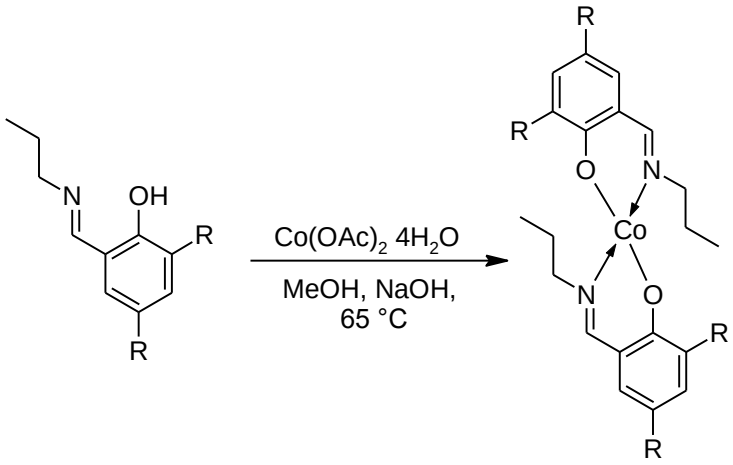

C1: R= H

C2: R= *tert*-Butyl

Scheme 4: Synthesis of model cobalt complexes C1 and C2

The same synthetic protocol could also be applied to yield the analogous metallodendrimers **MD1** and **MD2** using dendritic ligands **D1** and **D2** respectively (Scheme 5). Compounds **MD1** and **MD2** were previously reported by van Wyk et al.[22]

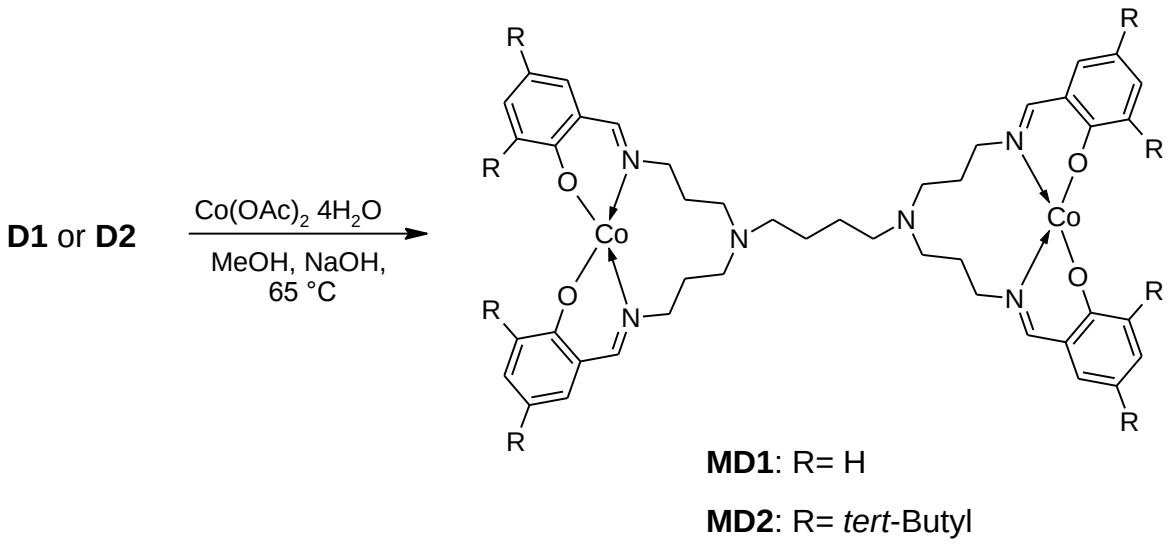

Scheme 5: Synthesis of cobalt salicylaldimine metallodendrimers[22]

These salicylaldimine cobalt complexes were isolated as air stable brown powders soluble in organic solvents such as DCM, THF and acetonitrile while being insoluble in EtOH and MeOH as well as non-polar solvents such as hexane. **C1**, **C2**, **MD1** and **MD2** were characterized by a range of analytical techniques. The most important characterization data is discussed below and summarized in Table 1.

The FTIR spectra of these complexes typically show a shift in the imine absorption band towards lower wavenumbers upon coordination to the Co^{2+} metal centre. Furthermore, the broad band associated with the ν_{O-H} stretch present in the spectrum of the ligand is no longer observed in the spectra of the complexes. In addition to the disappearance of the ν_{O-H} stretch from the spectra of the complexes, a shift in the ν_{C-O} absorption upon coordination of the ligand is observed (Table 2).

Table 2: Selected characterization data of salicylaldimine cobalt complexes

Compound	IR Spectra (cm^{-1})[a]		ESI MS $(M+H)^+$
	$\nu_{C=N}$	ν_{C-O}	
C1	1614	1321	384
C2	1597	1320	608
MD1	1628	1307	847
MD2	1627	1317	1296

[a] Recorded in the solid-state using ATR

C1, C2, MD1 and MD2 were further characterized by UV-Vis spectroscopy. As a representative example only the UV-Vis spectrum of **MD1** is discussed here given the fact spectra of the other complexes show similar properties. The UV-Vis spectrum obtained (in DCM) for **MD1** exhibited absorption maxima at 240 (ligand π-π*) and 360 nm (metal to ligand charge transfer band) with a small shoulder at 410 nm which can likely be assigned to the weak d-d transitions.

The CHN microanalysis of compounds **C1**-**MD2** matched their respective predicted values quite well (results available in experimental section). In some cases, solvent encapsulation into the dendritic architecture was observed.

2.3.2 Synthesis and characterization of iron salicylaldimine metallodendrimers

Soluble methane monooxygenanse (MMO), as discussed in Chapter 1, consists of a diiron core coordinated by oxygen (carboxylate groups) as well as nitrogen donor groups. We envisaged that ligands **D1** and **D2** could also be used to form iron(III) complexes that might have some resemblance to the active site of MMO.

Reaction of **D1** with $FeCl_3$ yielded the first-generation dendritic complex **MD3** (Scheme 6) as a dark brown highly hygroscopic powder.

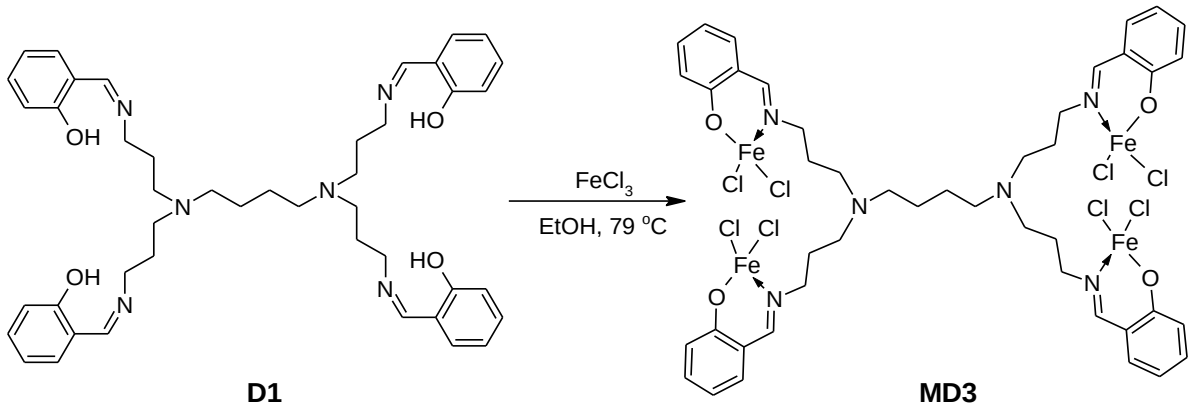

D1 **MD3**

Scheme 6: Synthesis of iron(III) salicylaldimine metallodendrimers

MD3 was characterized by a range of analytical techniques including FTIR spectroscopy, ESI mass spectrometry and elemental analysis. The presence of Fe-Cl bonds could be detected by IR spectroscopy (370 cm^{-1}). The spectroscopic data

collected for **MD3** was fairly similar to that obtained for **MD1** and **MD2** and are summarized in Table 3 and are also available in the experimental section at the end of this chapter.

The obtained microanalysis results differed from those expected for a Fe_2(**D1**)Cl_4 species, instead the results matched those of a system where the **D1** ligand coordinates to four iron centres to yield **MD3** as shown in Scheme 6. Similar products were isolated by Smith et al.[23] However, in their preparation, $FeCl_2$ was employed as the metal precursor. Under their reaction conditions, the Fe(II) centres underwent oxidation during the course of the reaction to yield Fe(III)-alkoxy containing compounds, which were highly insoluble and difficult to characterize (no mass spectrometry data). By employing $FeCl_3$ we hoped to avoid some of these difficulties. However, **MD3** is also highly insoluble in most organic solvents and water.

Table 3: Selected characterization data of D1 and MD3

Compound	IR Spectra (cm^{-1})[a]		ESI-MS $(M+H)^+$
	$\nu_{C=N}$	ν_{C-O}	
MD3 (complex)	1617	1298	912
D1 (ligand)	1632	1277	733

[a] Recorded as solid powders using ATR

With the synthesis of a range of salicylaldimine complexes successfully completed, we turned our attention to imino-pyridine type ligands and complexes.

2.3.3 Synthesis and characterization of N_4 imino-pyridyl ligands and their iron complexes

An important observation made when reviewing oxidation catalyst systems reported in the literature (Chapter 1), is that many of these catalyst precursors incorporate imine, pyridine and amine moieties in the ligand design. This is hardly surprising as these functionalities closely mimic the ligand structure found in heme as previously mentioned in Chapter 1.[1]

With this in mind, we endeavoured to prepare model as well as dendritic ligands that contain pyridine moieties such as model compound **L3** (Scheme 7). **L3** was isolated

as an orange oil that exhibited good solubility in a range of polar solvents and poor solubility in non-polar solvents such as hexane and pentane.

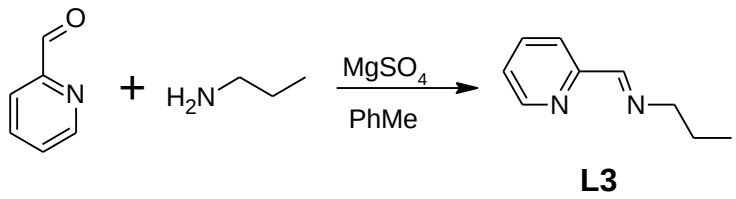

L3

Scheme 7: Synthesis of pyridyl-imine model ligand L3

L3 was characterized by a range of analytical techniques and the obtained characterization data were in good agreement with the data reported in the literature.[24,25]

Building on the successful synthesis of **L3,** we turned our attention to the synthesis of pyridine-imine modified dendrimer **D3** (Scheme 8). The peripheries of the DAB PPI dendrimer were reacted with 2-pyridinecarboxaldehyde (Scheme 8) according to the method reported by Smith et al. to introduce the pyridine-imine functionalities on the periphery.[26] **D3** was isolated as a dark orange viscous oil.

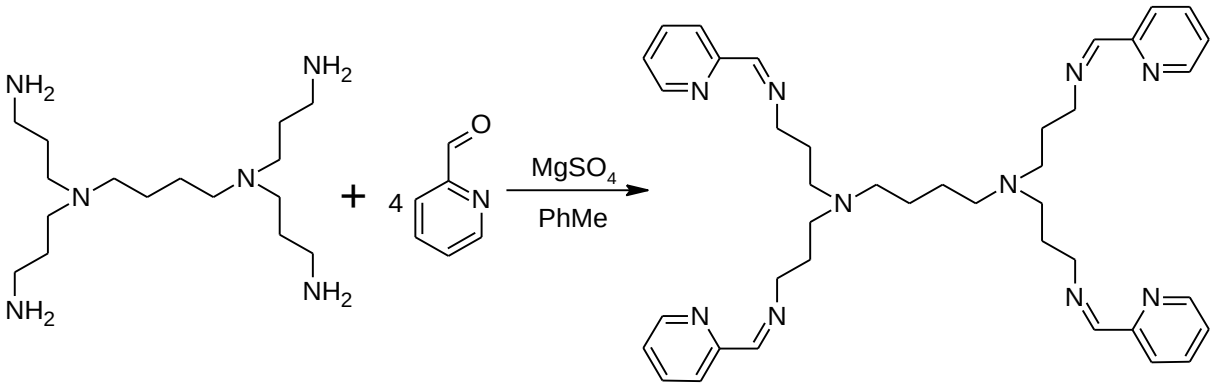

D3

Scheme 8: Synthesis of pyridyl-imine dendrimer

D3 was fully characterized by a range of analytical techniques including FTIR, ^{1}H and ^{13}C NMR spectroscopy as well as ESI mass spectrometry. Comparison with the characterization data reported in the literature confirmed that **D3** was successfully

prepared.[26] Selected characterization data collected for **L3** and **D3** are summarized in Table 4 below.

Table 4: Selected characterization data obtained for L3 and D3

Compound	IR Spectra (cm^{-1})[a]		ESI MS (m/z)	^{1}H NMR (N=C**H**-)[b]
	$\nu_{C=N}$	$\nu_{pyridyl}$		
L3[a]	1648	1607	149 $(M+H)^+$	8.23
D3[a]	1640	1599	673 $(M+H)^+$	8.37

[a] Recorded in the solid-state using ATR. [b] Recorded in $CDCl_3$

With the ligands **L3** and **D3** in hand, we investigated their coordination chemistry using two different iron precursors namely iron(II) chloride and iron(II) triflate.

The reaction of **L3** with $FeCl_2$ was undertaken by employing a modified literature procedure as shown in Scheme 9.[27] The product **C3** was isolated as a hygroscopic purple powder that exhibited solubility in many organic solvents including DCM, THF, MeCN and methanol.

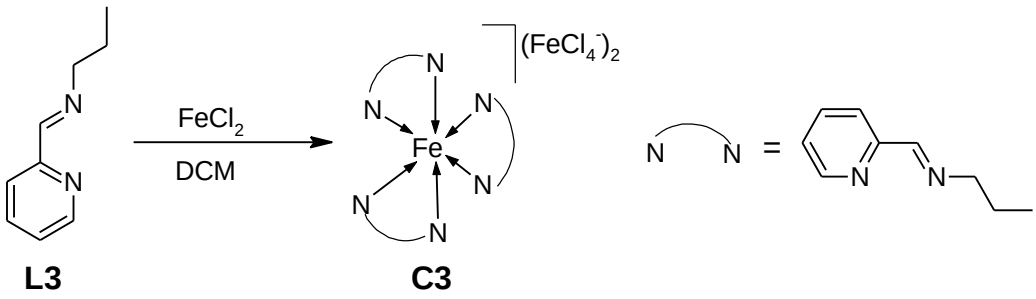

L3 **C3**

Scheme 9: Reaction of model ligand L3 with $FeCl_2$ to yield novel complex C3

The synthesis of the metallodendrimer analogue, **MD4** was performed using the same synthetic protocol established for **C3** as shown below in Scheme 10. However, MD4 was found to be highly insoluble in most organic solvents. Partial solubility in MeCN was observed.

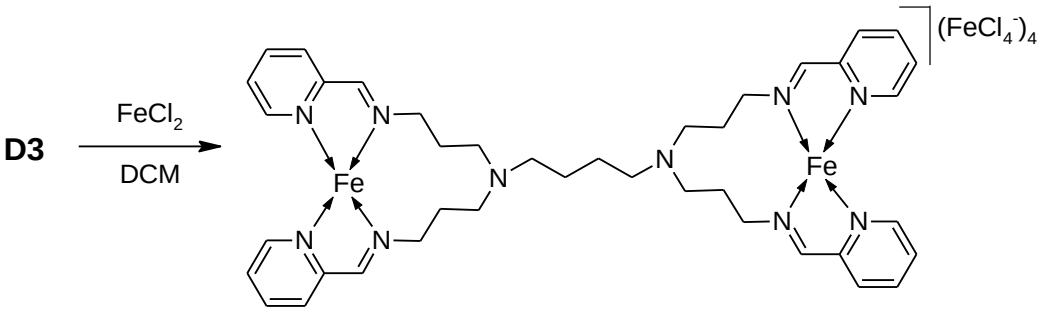

MD4

Scheme 10: Reaction of dendrimer D3 with $FeCl_2$

C3 and **MD4** were characterized by FTIR spectroscopy. From the FTIR spectra of **C3** and **MD4**, we observed a shift in the $\nu_{C=N}$ absorption of both the pyridine and imine moieties (compared to those of the free ligands **L3** and **D3**). The $\nu_{C=N}$ peaks of the imine (1649 cm^{-1} in **L3**) as well as that of the pyridine (1586 cm^{-1} in **L3**) moieties coalesce at around 1610 cm^{-1} in the spectra of the metal complexes, strongly indicating successful complex formation.

The UV-Vis spectrum of **C3** (Figure 2) showed absorption bands at 220 and 286 nm. These peaks are present in **L3** as well and are assigned as π-π* transitions. A shoulder is observed at 350 nm, which is likely the metal-to-ligand charge transfer band. Two further peaks are observed, a peak at 572 nm and a shoulder at 532 nm, these are assigned as the d-d transitions of the metal centre.

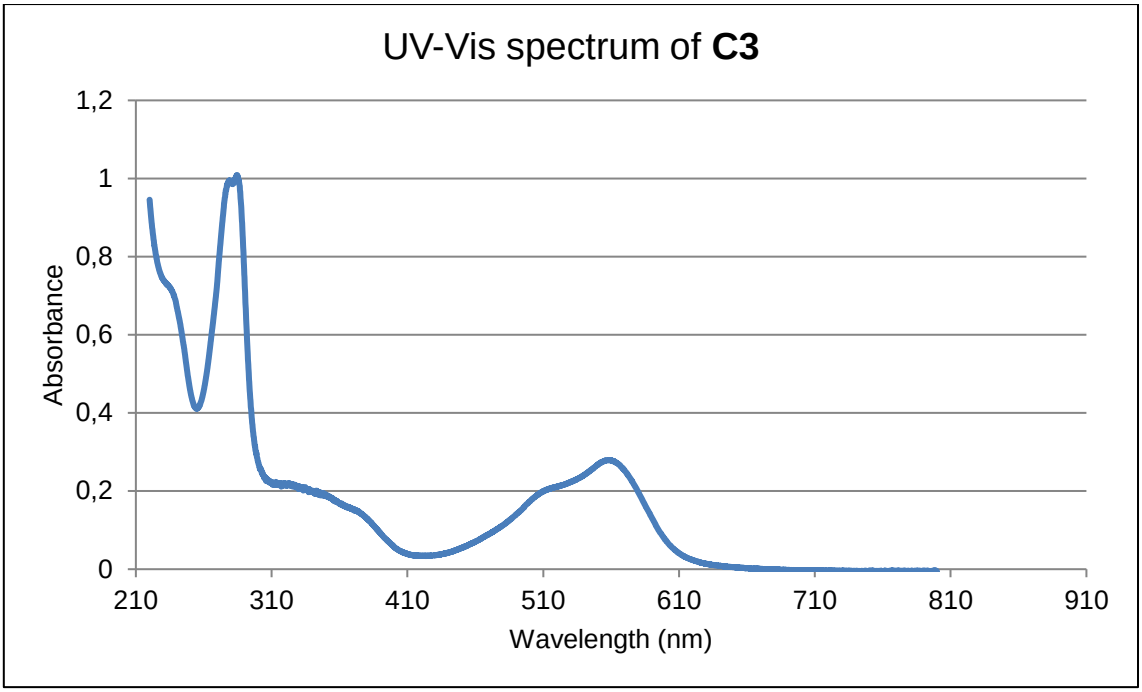

Figure 2: UV- Vis spectrum of novel complex C3 in acetonitrile ($1x10^{-4}$M)

The UV-Vis spectrum of **MD4** shows several absorption bands (Figure 3). π-π* transitions associated with the ligand are observed at 242 and 299 nm. Further bands are observed at 330 nm (shoulder) and 370 nm which are likely ligand to metal charge transfer bands. Broad absorption peaks at 588 and 530 nm (shoulder) are also observed and assigned as d-d transitions.

Further characterization of **C3** by ESI mass spectrometry indicates that it is likely an octahedral iron complex bearing three **L3** ligands. The mass spectrum of **C3** showed the molecular ion at m/z 501 and its' doubly charged analogue at m/z 250 that could be assigned as Fe(**L3**)$_3$. The mass spectrum of **MD4** on the other hand exhibits extensive fragmentation. The doubly charged ion of Fe_2(**D3**) is observed at m/z 392. **MD4** shows the formation of fragment ions due to the loss of pyridine-imine moieties ($C_6H_5N_2$, mass loss of 105) by cleavage of the imine bonds.

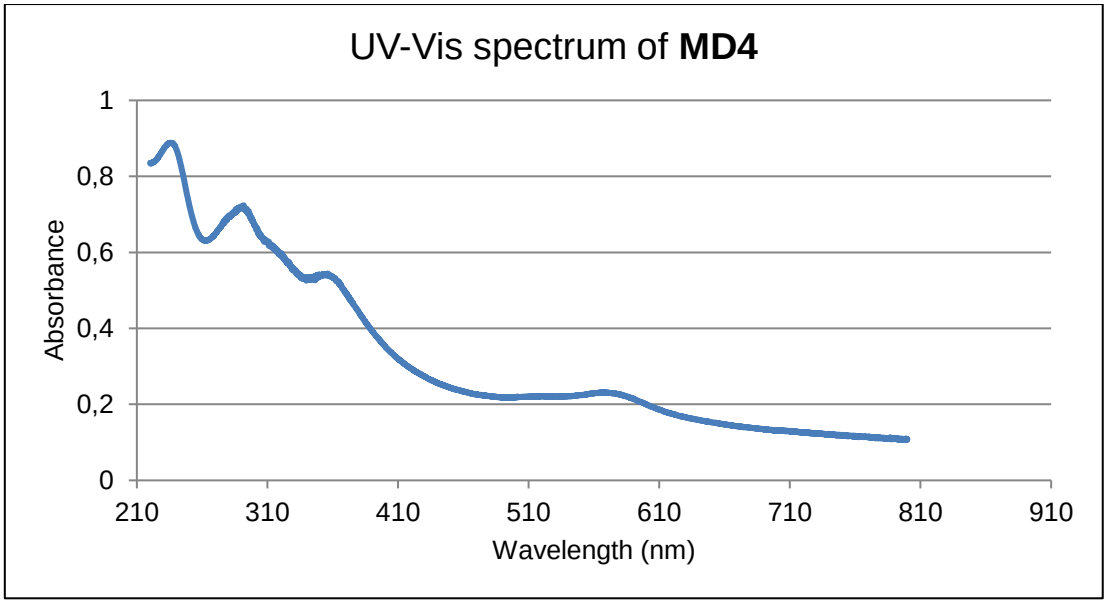

Figure 3: UV-Vis spectrum of MD4 in acetonitrile ($1x10^{-4}$ M)

C3 and **MD4** were submitted for elemental analysis, however, the predicted and obtained experimental values did not match (for the expected Fe(**L3**)$_3$Cl$_2$ and Fe$_2$(**D5**)Cl$_4$ systems). Indeed, even after careful recrystallization and prolonged drying unexpectedly low mass percentages of both carbon and nitrogen were obtained. Attempts at repeating the synthesis also did not help.

In order to shed light on these inconsistent results we also analysed **C3** and **MD4** by negative ion mass spectrometry to probe the nature of the counterions. The mass spectrum of **MD4** in the negative mode exhibited a signal at m/z 197 (Figure 4). This was tentatively assigned as the $FeCl_4^-$ anion. The isotopic pattern of $FeCl_4^-$ was predicted (Figure 4, top spectrum labelled as “Prediction”) and this closely matched the pattern observed in the experimental spectrum of **MD4** (Figure 4 bottom spectrum). Another ion at m/z 162 is also observed and could be assigned to a fragment in which chloride is lost from $FeCl_4^-$ to yield $FeCl_3$.

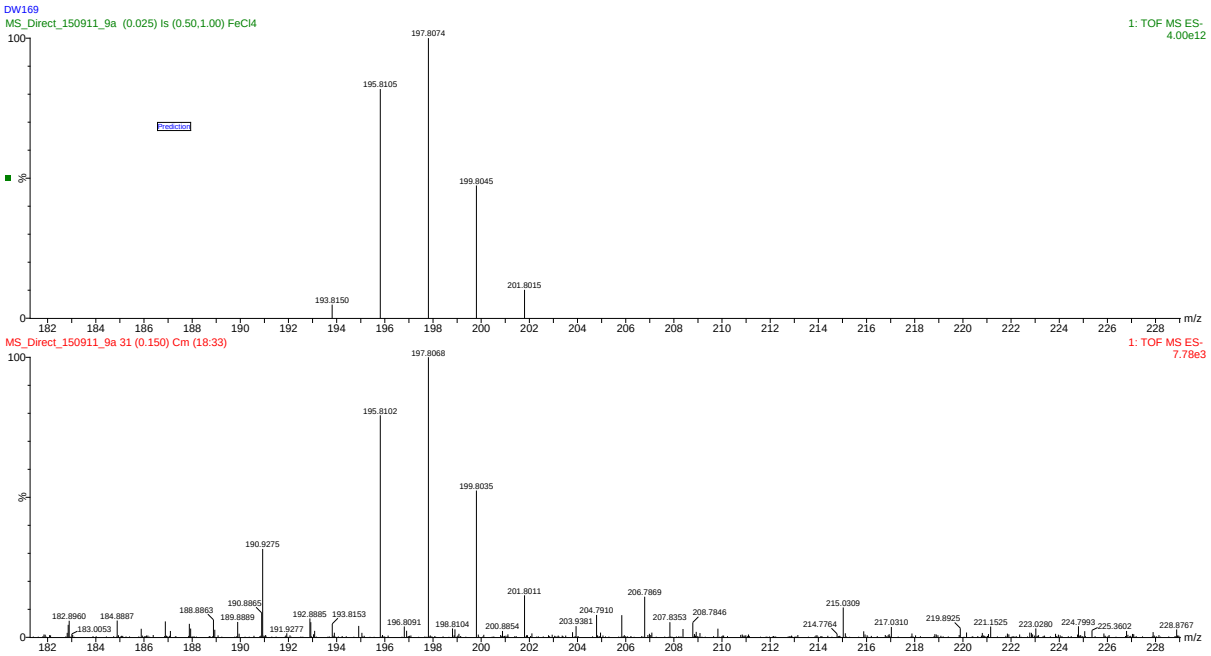

Figure 4: Negative ion mode mass spectrum of MD4

With the detection of $FeCl_4^-$ as counterion, it was speculated that it could potentially be exchanged for another (non-transition metal based) anion. This prompted us to attempt to study an anion exchange reaction of the $FeCl_4^-$ counterion with BPh_4^- and to probe this using mass spectrometry.

The reaction solvent was changed to methanol as both **MD4** as well as $NaBPh_4$ are soluble in methanol. After stirring the mixture of $FeCl_2$ and the ligand **D3** for 24 hours, a small aliquot was withdrawn for analysis by mass spectrometry. $NaBPh_4$ (excess) was then added to the remaining reaction mixture which lead to an immediate precipitation of a dark purple powder that was isolated by filtration and found to be highly insoluble in most organic solvents. However, partial solubility was observed in acetonitrile. The fractions isolated before and after the addition of $NaBPh_4$ were analysed by negative ionization mode mass spectrometry. As can be seen from Figure 5, after anion exchange the BPh_4^- anion is observed while $FeCl_4^-$ was no longer detected by the mass spectrometer.

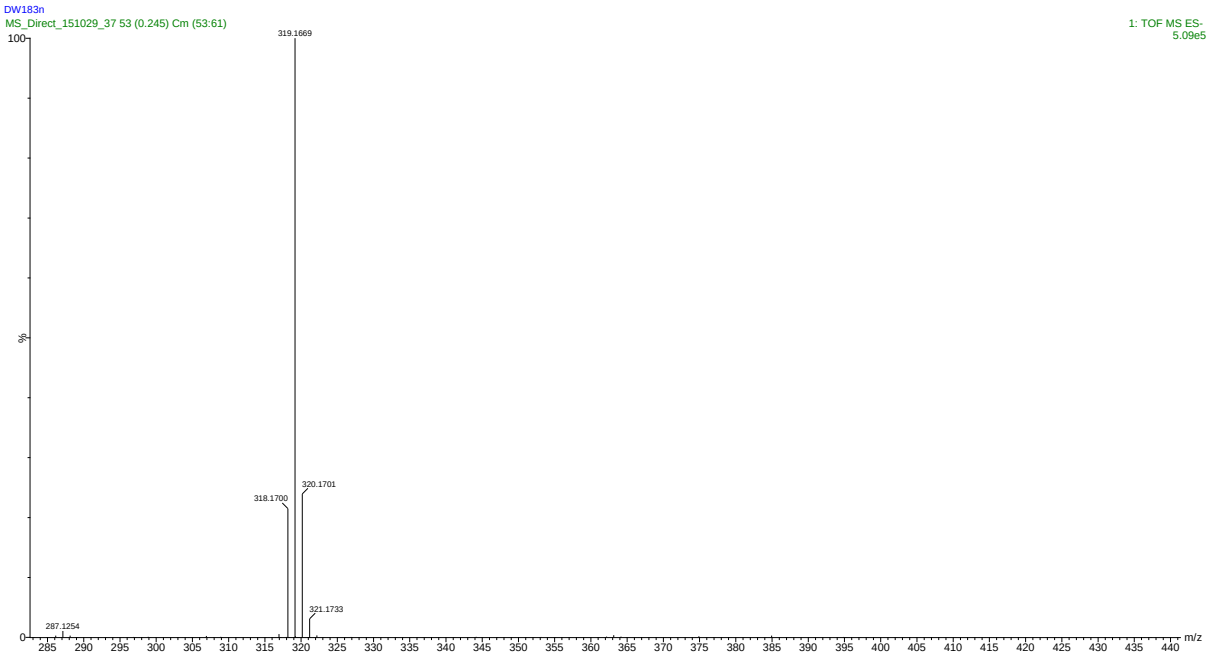

Figure 5:Mass spectrum obtained after exchange of $FeCl_4^-$ for BPh_4^-

The mass spectrometry experiments, conducted on **MD4**, suggest that oxidation of the iron centre is taking place during the reaction of **D3** with $FeCl_2$ and a mixture of anions including $FeCl_4^-$ as well as the expected Cl^- anion are present in the products.

Even when using an excess of $FeCl_2$ along with **MD4**, the oxidation of $FeCl_2$ to $FeCl_4^-$ is incomplete and some chloride anion is also present within the reaction mixture thus yielding a complex mixture of anions. This problem is further exacerbated by the low solubility of these compounds in organic solvents (only partially soluble in MeCN). Presumably, the different products of the **MD4** reaction mixture have very similar solubilities as attempts to use recrystallization to separate and purify the products were unsuccessful.

This problem is exacerbated upon scale up of the reaction. We encountered difficulty in consistently producing the same material particularly upon scaling up. Several attempts employing protocols to prepare **MD4** yielded significantly different results when analysed by elemental analysis. This is likely due to fluctuations in the number of $FeCl_4^-$ moieties in the outer coordination sphere. This prompted us to further investigate the formation of $FeCl_4^-$ during the course of the reaction as well as to attempt to determine which reaction conditions favour or inhibit $FeCl_4^-$ formation.

The formation of $FeCl_4^-$ in reactions where $FeCl_2$ is used as metal precursor for the formation of iron complexes has also been observed by other authors. Nakayama et al. reported on the formation of $FeCl_4^-$ in the reaction of terpyridine with $FeCl_2$ as shown in Scheme 11.[28] The authors did not discuss in depth the formation of the $[Fe(terpyridine)_2][FeCl_4]_2$ derivative however they did note that the complex was a highly active catalyst precursor in their catalytic reactions.

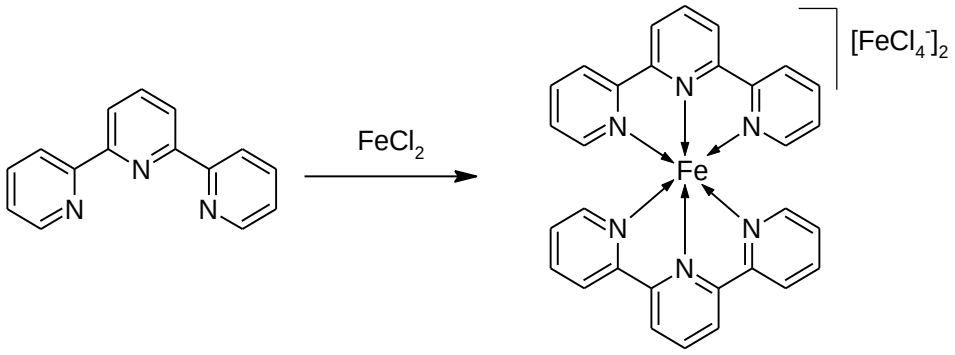

Scheme 11: Formation of $FeCl_4^-$ as a counterion when using $FeCl_2$ as metal precursor reported by Nakayama et al.[28]

This phenomenon was also observed by Glasson et al.[29] In their study of the reaction of $FeCl_2$ with the ligand 5,5'''-dimethyl-2,2':5',5'':2'',2''',quaterpyridine, which yielded a supramolecular architecture that encapsulates the $FeCl_4^-$ anion.

Pelascini et al. also reported the formation of $FeCl_4^-$ counterions in iron complexes of terpyridine derivatives.[30] In this case the presence of the $FeCl_4^-$ counterions in the product mixture was initially detected by far-IR spectroscopy ($\nu_{Fe\text{-}Cl}$ 378 cm^{-1}). In their reaction various species including the expected product $Fe[L]Cl_2$ were detected (where L is a terpyridine ligand). The authors attempted to isolate single crystals of the various products and succeeded in obtaining a crystal structure of the $FeCl_4^-$ containing species. The authors speculated that O_2 might be the oxidizing species; however, it should be noted experiments were conducted under an inert atmosphere. It could thus be a case of unintentional exposure to O_2.

A study by Peck et al. reported and reviewed a large number of complexes that contain the $FeCl_4^-$ anion.[31] In summary these authors suggested that photooxidation of iron halides could be a possible mechanism. The authors tested their hypothesis by stirring

$FeBr_2$ metal salt under complexation reaction conditions but with the exclusion of light. However, oxidation to the $FeBr_4^-$ species was still observed.

Another possible mechanism for the formation of the $FeCl_4^-$ species was suggested by Nguyen et al.[32] In their system the $FeCl_4^-$ species was generated by the photooxidation of chloroform (acting as chloride donor) as shown in Scheme 12. Homolysis of chloroform generates a chloride radical as well as a DCM radical. Further reaction of the chloride radical with another chloroform molecule generates a trichloromethyl radical that oxidizes the Fe(II) centre and facilitates the formation of $FeCl_4^-$.

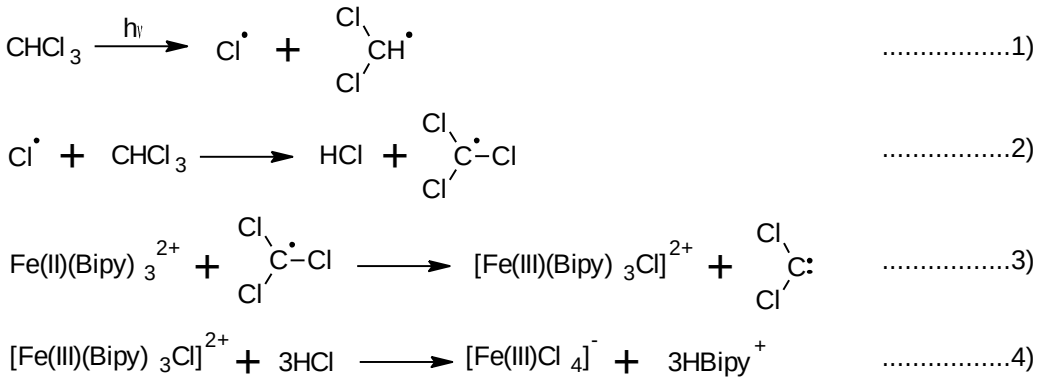

Scheme 12: Mechanism for the formation of $FeCl_4^-$ proposed by Nguyen et al.[32]

This mechanism proposed by Nguyen et al. is certainly feasible, however, in their case the photooxidation is driven by artificial UV radiation.[32] This is not the case during our synthetic reactions. Ambient light is, however, present in our reactions.

We tested the photooxidation hypothesis in our reactions by performing the preparation of **MD4** in the dark however; we still obtained the $FeCl_4^-$ ion in the product stream (confirmed by mass spectrometry). Furthermore, we tested the feasibility of the solvent photooxidation pathway by replacing DCM as the reaction solvent with THF or methanol (in the preparation of **MD4**) in which case the generation of the chloride radical should not be possible (via the above mechanism in Scheme 12). In both cases the formation of the $FeCl_4^-$ species (detected via mass spectrometry) was still observed. In addition to our own investigation it should be noted that in the synthetic experiments conducted by both Nakayama et al. as well as Pelascini et al. the synthesis was performed using THF as reaction solvent, thus the generation of a

chloride radical (as per Scheme 12) should not be possible in these systems. Therefore, the exact mechanism of this reaction still eludes us. We unfortunately could also not avoid the formation of $FeCl_4^-$ in any of our test reactions.

In light of this result we modified the synthesis of **C3** and **MD4** by increasing the reaction time from 6 hours to 48 hours and employing an excess of $FeCl_2$ with the hope of driving the reaction towards a product in which the counterion is exclusively $FeCl_4^-$. This synthetic strategy was successful for **C3** however the preparation of the dendritic complex **MD4** remained problematic on scale-up.

The elemental analysis results (given in Table 5) obtained previously closely matched those predicted for the $FeCl_4^-$ system providing additional proof for the formation of this anion.

Table 5: Elemental analysis results obtained for C3 and MD4

Compound	Formula	Anal. Calcd.(Found) (%)		
		C	H	N
C3	$C_{27}H_{36}Cl_8Fe_3N_6$	44.21(44.21)	4.98(4.87)	11.46(12.66)
MD4	$C_{40}H_{52}Cl_{16}Fe_6N_{10}$	30.50(31.5)	3.58(3.00)	8.59(8.89)

Due to the difficulties encountered when employing $FeCl_2$ as metal precursor in these reactions we also investigated the use of iron(II) triflate as transition metal precursor. The reaction of $Fe(OTf)_2$ with **L3** was performed in an analogous manner to that employed for **C3**. This yielded novel complex **C4** as a pinkish purple powder as shown in Scheme 13.

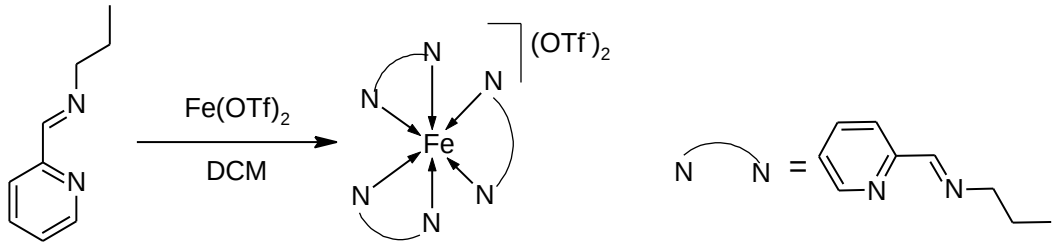

L3 **C4**

Scheme 13: Synthesis of iron triflate Model Complex C4

Similarly reaction of **D3** with 2 equivalents of $Fe(OTf)_2$ (OTf^-= triflate) yielded the generation 1 dendritic complex **MD5** as a dark purple powder (Scheme 14). **C4** as well

as **MD5** are not soluble in most organic solvents. However, partial solubility is observed in chlorinated solvents as well as in acetonitrile.

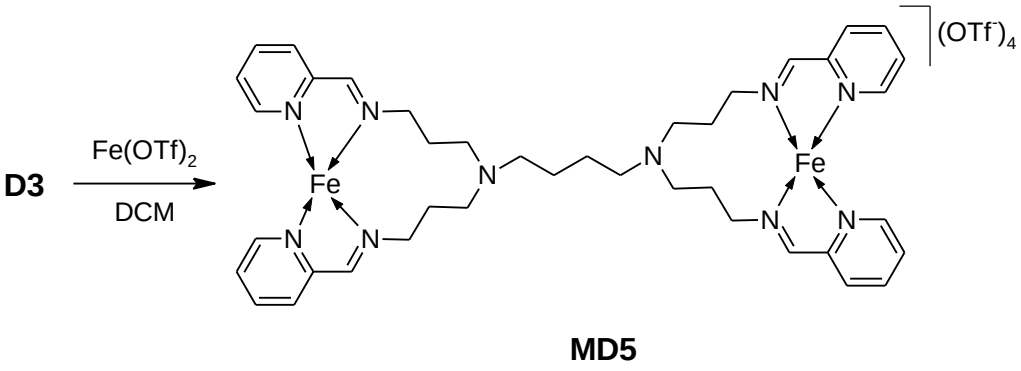

MD5

Scheme 14: Synthesis of pyridine-imine iron metallodendrimer MD5

C4 and **MD5** were characterized by a range of analytical techniques. Characterization by FTIR (ATR) yielded data analogous to that obtained for **C3** and **MD4**, however absorptions due to the triflate counter ions are also observed around 1027 cm^{-1} (ν_{S-O}), 1141 cm^{-1} (symmetric $\nu_{S=O}$) and 1225 cm^{-1}(asymmetric $\nu_{S=O}$).

The mass spectra obtained for **C4** and **MD5** in the positive mode were very similar to those recorded for **C3** and **MD5**. Analysis of the negative ionization mass spectra of **MD5** and **C4** showed only the expected triflate counter ion peak at m/z 148.

The magnetic susceptibilities of **C4** and **MD5** (determined using a Gouy balance) drastically differed from those recorded for **C3** and **MD4**. Both **C4** and **MD5** are low spin, diamagnetic, iron(II) complexes while **C3** and **MD4** are paramagnetic, possibly due to the paramagnetic contribution of the $FeCl_4^-$ anion. This was confirmed by exchanging the $FeCl_4^-$ anions for BPh_4^- anions as described above. Anion exchange lead to a drastic reduction in the observed magnetic susceptibility of the sample, however the material was still paramagnetic likely due to incomplete anion exchange (χ_{mass}= 0.5). As a result of its diamagnetic nature a ^{1}H NMR spectrum of **C4** could be recorded over the normal spectral window (Figure 6).

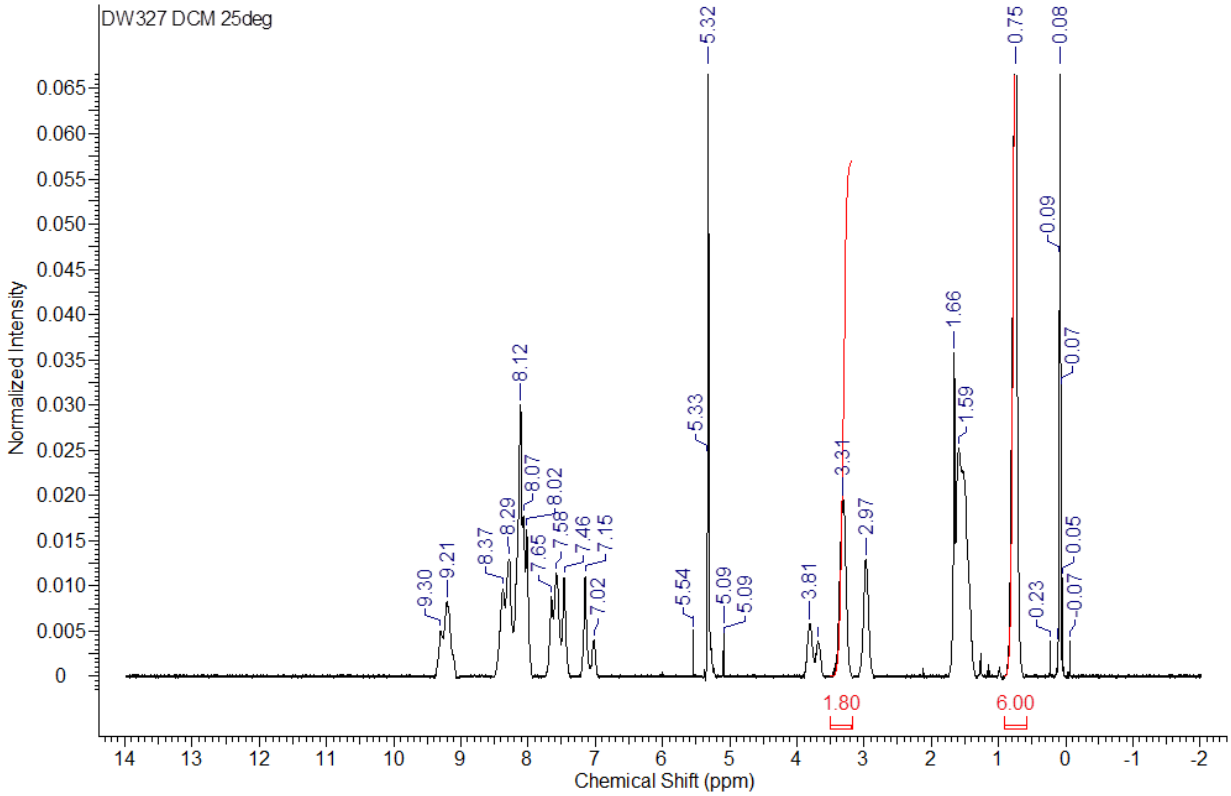

Figure 6: ^{1}H NMR spectrum of C4 in CD_2Cl_2

The obtained spectrum is of low quality possibly due to the fairly low solubility of **C4**. Additionally, multiple resonances for each proton are observed. This is likely due to isomerism in the octahedral complex. Similar racemic mixtures of related octahedral iron complexes have been reported by Howson et al.[33] Stereoisomer formation was observed for less bulky ligands however, for sterically hindered imine pyridine ligands such as phenylethaniminopyridine, isomer formation is not observed.[33] Similar observations were also made by Dragna et al. for a related diamagnetic iron pyridine-imine octahedral complex.[34]

Broad resonances are observed, with very little fine structure evident (possibly due to isomerism). However, imine N=C**H**-resonances are observed around 8.12 ppm (overlapping with aromatic C-**H** resonances) while the resonances of the pyridine moieties (**H**-C=N-) is observed at 9.30 and 9.21 ppm providing further proof of successful complex formation. The peaks due to the aliphatic chain are observed as broad resonances around 0.75, 1.59, 3.31, 2.97, 3.68 and 3.81 ppm. Upon cooling of the sample to -80°C some of the resonances previously observed start to coalesce into broad resonances possibly of a single isomer. However, the solubility of the

material at this temperature is fairly low which could be another reason for the observed broad resonances. No spin crossover event (diamagnetic to paramagnetic) was observed in this temperature range.

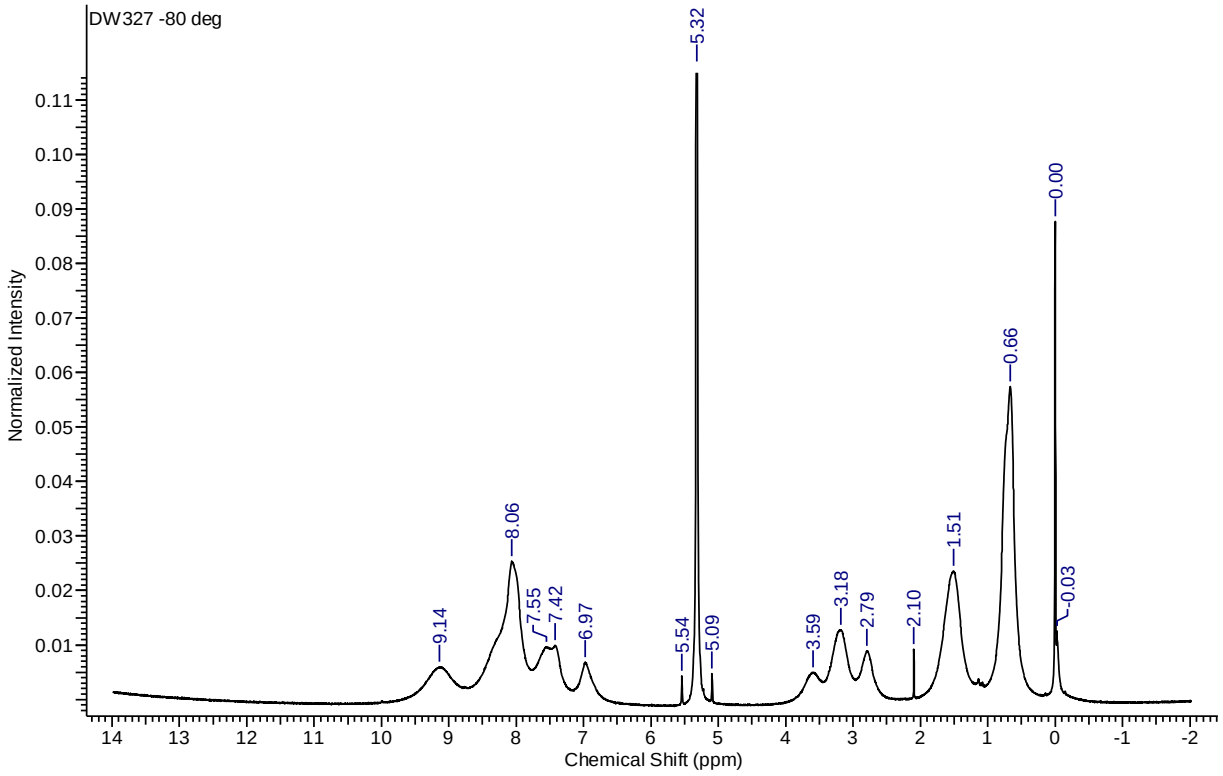

Figure 7: ^{1}H NMR Spectrum of C4 in CD_2Cl_2 at -80°C

Unfortunately attempts to record a ^{1}H NMR spectrum of **MD5**, were unsuccessful due to the low solubility of the material.

Both **C4** as well as **MD5** were characterized by elemental analysis and the obtained results closely matched those predicted for the two complexes as shown in Table 6.

Table 6: Elemental analysis results obtained for C4 and MD5

Code	Formula	Anal. Calcd (Found) (%)		
		C	H	N
C4	$C_{29}H_{36}F_6FeN_6O_6S_2 \cdot 2H_2O$	41.73(41.48)	4.83(4.51)	10.07(10.14)
MD5	$C_{44}H_{52}F_{12}Fe_2N_{10}O_{12}S_4 \cdot H_2O$	37.78 (37.60)	3.89(4.25)	10.01(9.78)

2.3.4 Synthesis and characterization of thioether-amine ligands and their copper and cobalt complexes

It was previously noted that the structure of the active site of the enzyme cytochrome P450, a highly active alkane hydroxylation enzyme, has 4 nitrogen donor sites as well as a sulphur donor site from a cysteine residue.[1, 35] This inspired us to incorporate sulphur donor sites in our ligand design. We targeted compounds containing both thioether and aldehyde moieties with the hope that simple Schiff base condensation could be used to generate thioether-amine ligands as sulphur analogous to the well-known salen ligands. Furthermore, the aldehyde moiety would also allow us to prepare dendrimer analogues.

The first step of this synthetic protocol is the synthesis of appropriate thiol functionalized aldehydes. Andrés et. al. reported the formation of compound **A1** employing a simple aromatic nucleophilic substitution with thiophenol and 2-fluorobenzaldehyde as shown in Scheme 15.[36] This method was successfully employed to yield 2-(phenylsulfanyl)benzaldehyde (**A1**) in near quantitative yield.

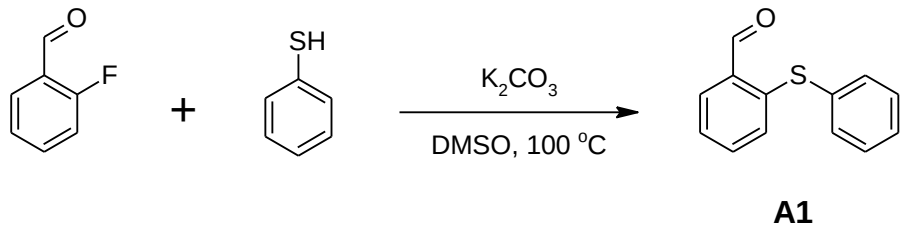

A1

Scheme 15: Synthesis of thiosulphide containing aldehyde A1[36]

FTIR spectroscopic analysis of **A1**, revealed a strong absorption at 1689 cm^{-1} which was assigned as the $\nu_{C=O}$ stretch of the aldehyde. The ν_{C-H} stretch of the aldehyde was observed at 2733 cm^{-1}. Furthermore, the thiol (ν_{S-H} at 2500 cm^{-1}) stretch present in the thiophenol starting material is no longer observed in the product.

The ^{1}H NMR spectrum exhibited a singlet resonance at 10.40 ppm assigned as the proton of the aldehyde functional group. A doublet is observed at 7.88 ppm (integrates for 1 proton) due to the (aromatic) -**H**C-CHO proton. Overlapping resonances are observed in the region 7.44-7.30 ppm which integrate for a total of 7 protons while a

further doublet is observed at 7.11 ppm (1 proton) to give a total of 9 aromatic protons as expected.

The ESI mass spectrum of **A1** exhibited the molecular ion $[M+H]^+$ at m/z 215. No further fragmentation of the molecule was observed.

The above synthetic method was adapted and used in the synthesis of 2-(ethylsulfanyl)benzaldehyde (**A2**) as shown in Scheme 16.[36]

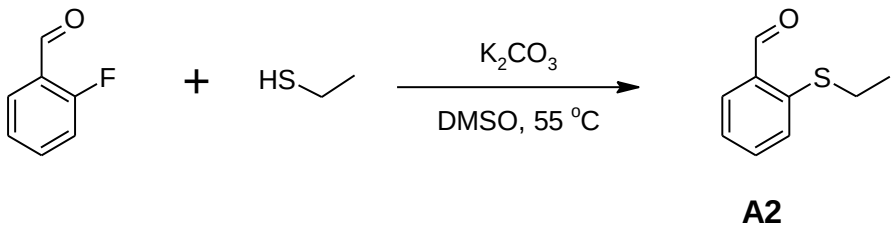

A2

Scheme 16: Synthesis of thiosulphide containing aldehyde A2[36]

In this case a lower reaction temperature (55°C) was employed due to the lower boiling point of ethanethiol. After 5 hours of stirring at 55°C, the reaction mixture was cooled to room temperature and stirred for a further 12 hours. **A2** was isolated as a yellow liquid in very high yield (92%).

FTIR spectroscopic analysis of **A2** revealed a strong absorption at 1689 cm^{-1} which is assigned as the $\nu_{C=O}$ stretch of the aldehyde. Akin to the ^1H NMR spectrum obtained for **A1**, the spectrum of **A2** showed a singlet at 10.38 ppm due to the proton of the aldehyde moiety. Additionally, a triplet (1.34 ppm) and a quartet (2.98 ppm) are observed for the protons of the methyl and methylene groups. Analysis by mass spectrometry (ESI positive) showed the molecular ion at m/z 167 with no further fragmentation observed.

With the modified aldehydes (**A1** and **A2**) in hand, the syntheses of the corresponding Schiff bases were undertaken. By refluxing 1 equivalent of ethylene diamine along with 2 equivalents of either **A1** or **A2** we obtained thioether modified Schiff bases **L4** and **L5** as shown in Scheme 17.

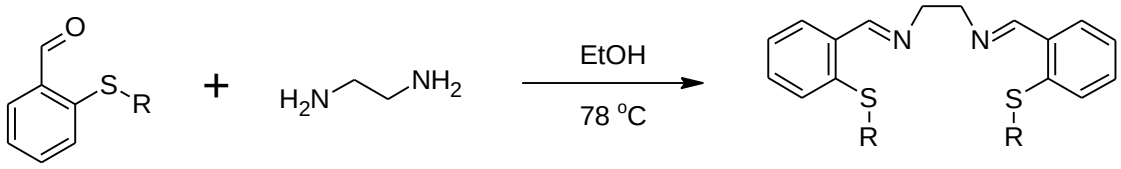

L4: R= Ph
L5: R= CH_2CH_3

Scheme 17: Synthesis of novel thioether-imine Schiff bases

After purification both **L4** and **L5** were fully characterized by ^{1}H and ^{13}C NMR, FTIR spectroscopy as well as ESI mass spectrometry. The characterization data for **L4** is briefly discussed below. The data obtained for compound **L5** is analogous to that obtained for **L4** and is given in full in the Experimental section.

The formation of the imine moiety could once again be followed by both FTIR (C=N absorption at 1632 cm^{-1}) as well as ^{1}H NMR spectroscopy (singlet, 8.81 ppm -**H**C=N- moiety). Furthermore, a sharp singlet at 3.89 ppm in the ^{1}H NMR spectrum of **L4** is assigned as the methylene protons of the =N-C**H₂**-C**H₂**-N= moiety, providing further proof of successful reaction. The mass spectrum of **L4** exhibited the $(M+H)^+$ molecular ion at m/z 453 while at m/z 475 the $(M+Na)^+$ adduct is observed. No other fragmentation species of **L4** are observed under ESI conditions.

The most important characterization data collected for compounds **L4** and **L5** are summarized in Table 7.

Table 7: Selected characterization data of S_2N_2 ligands L4 and L5

Compound	FTIR[a] ($\nu_{C=N}$) (cm^{-1})	ESI-MS (m/z)	^{1}H NMR[b] (N=C**H**) ppm
L4	1634	453 $(M+H)^+$	8.81
L5	1629	357 $(M+H)^+$	8.87

[a] Recorded as neat oils using NaCl windows. [b] Spectra recorded in $CDCl_3$

Compounds **L4** and **L5** in hand, they were tested as potential ligands for the transition metals copper and cobalt. Unfortunately, all attempts to complex these ligands to the mentioned transition metals lead to their hydrolysis resulting in the aldehyde starting materials **A1** and **A2**. In Table 8, below, various reaction conditions that were attempted are listed. In all cases analysis by FTIR revealed the absence of imine

absorptions and the formation of a carbonyl moiety (starting aldehyde). Even when the reaction was attempted for relatively short reaction times (Table 8 Entry 5 and 6), the hydrolysis of the imine moiety was observed. Attempts were undertaken to determine whether the hydrolysis is metal mediated or due to the inherent instability of the ligands.

Table 8: Summary of complexation reaction conditions

Entry	TM Salt	Solvent	Temp (°C)	Time (h)
1	$Cu(OTf)_2$	MeOH	65	6
2	$Cu(OTf)_2$	MeOH	25	6
3	$Cu(OTf)_2$	DCM	25	6
4	$Cu(OTf)_2$	DCM	25	1
5	$Cu(OTf)_2$	DCM	25	0.5
6	Co(OAc)2	MeOH	25	0.5

The hydrolysis of ligand **L5** was further investigated by the use of ^{1}H NMR spectroscopy. **L5** (0.020 g) was dissolved in $CDCl_3$ and the NMR spectrum recorded (Figure 8, time zero). The resonance of the **H**C=N moiety was observed at 8.87 ppm. Distilled water (0.200 ml) was then added and the mixture stirred. NMR spectra were recorded over the subsequent 22-hour time period. The sample was kept at constant temperature (25°C) over this time-period. Under these conditions virtually no hydrolysis of the ligand was observed, over the 22-hour period, when using either $CDCl_3$ or D_2O as NMR solvent (Figure 9).

This led us to believe that metal-mediated hydrolysis of the imine moieties might be occurring as no hydrolysis is apparent in the absence of transition metal and in the presence of water. This has also been observed by other authors for related systems.[37, 38] A possible explanation is that upon coordination, electron density is donated towards the metal centre thereby weakening the C=N bond which can then easily undergo hydrolysis.[39]

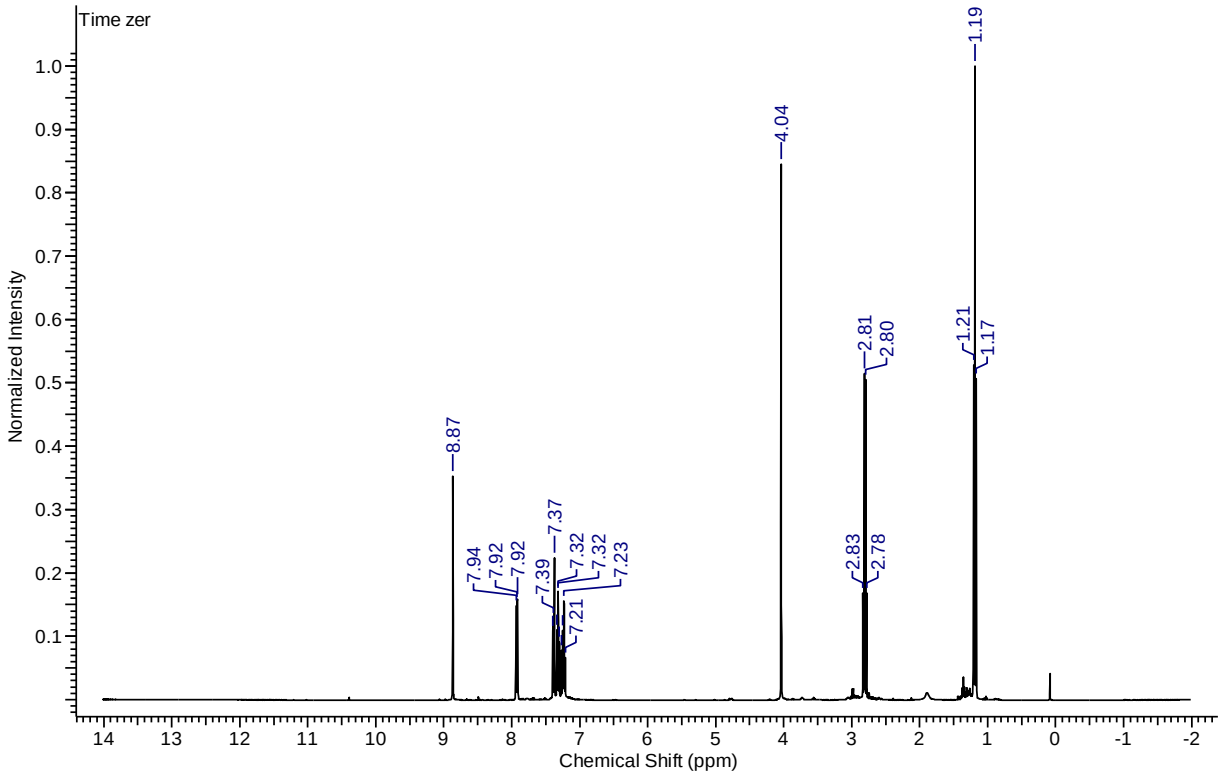

Figure 8: ^{1}H NMR spectrum before the addition of H_2O

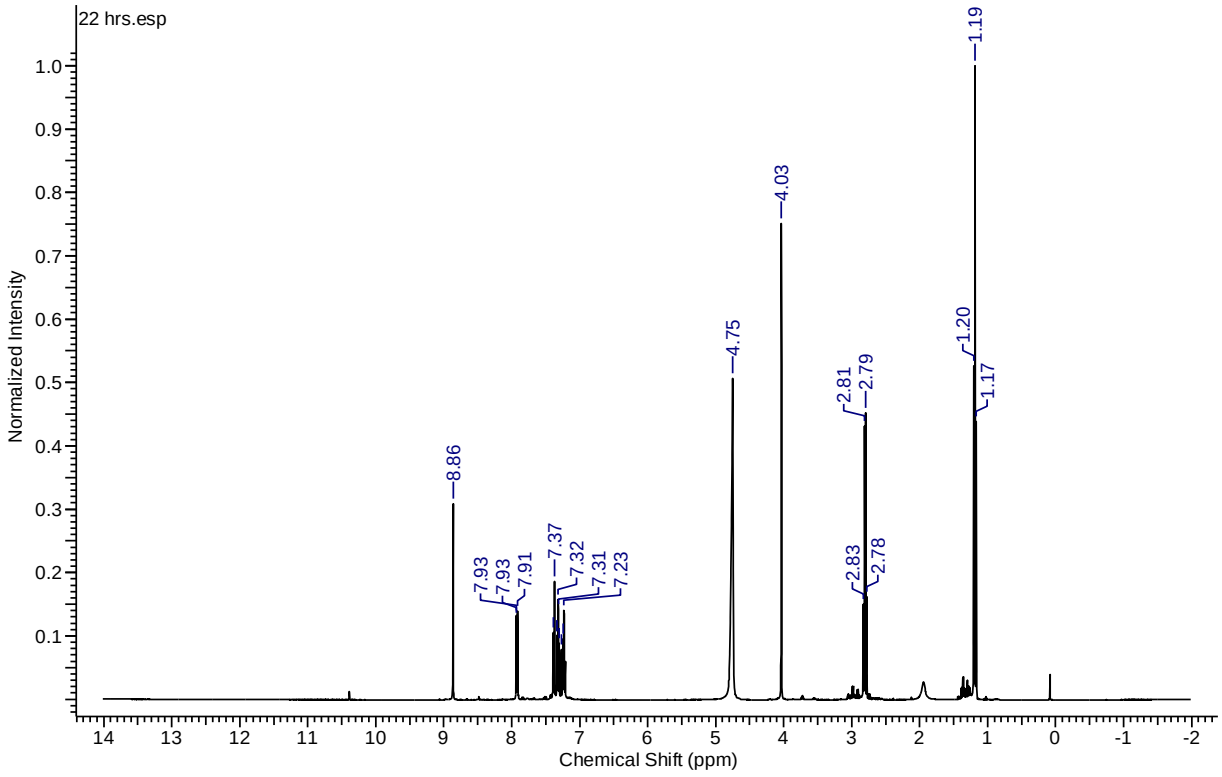

Figure 9: ^{1}H NMR spectrum of L5 in D_2O after 22 hours in the presence of H_2O

In an attempt to avoid the imine hydrolysis, it was decided to reduce the imine moiety to an amine.

The reduction of **L4** and **L5** were performed by adapting the method of Park et al.[40] Treatment of the imine species with $NaBH_4$ yielded the amine derivatives **L6** and **L7** in near quantitative yields.

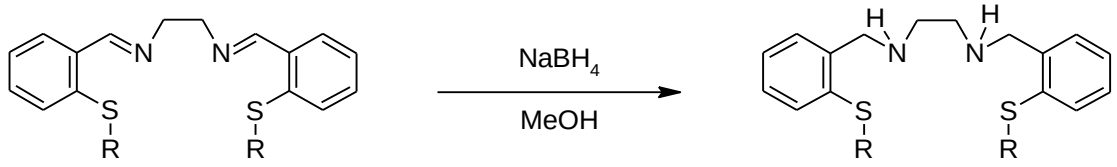

L4 or **L5**

L6: R= Ph
L7: R= CH_2-CH_3

Scheme 18: Synthesis of thioether-amine ligands

Compounds **L6** and **L7** were isolated as light-yellow viscous oils that are soluble in most organic solvents and being insoluble only in highly non-polar solvents such as hexane. The progress of the reaction was followed by FTIR by monitoring the disappearance of the imine C=N stretch and the appearance of the N-H stretch around 3300cm^{-1}. Characterization by ^1H NMR similarly revealed the appearance of a new upfield resonance at around 3.89 ppm (4 protons, singlet resonance) due to the NH-C**H**$_2$- moieties of the reduced product. Furthermore, the imine (proton) resonance is no longer observed in the product spectrum. **L6** and **L7** were fully characterized by a range of analytical techniques.

The same synthetic methodology, developed for the synthesis of **L4** and **L5** as described above, was then employed to synthesize the peripherally imine-modified Schiff base dendrimer analogues **D4** and **D5** as shown in Scheme 19. Modified dendrimers **D4** and **D5** could then also be reduced to the amine derivatives **D6** and **D7** by employing the same reductive method used for **L6** and **L7**.

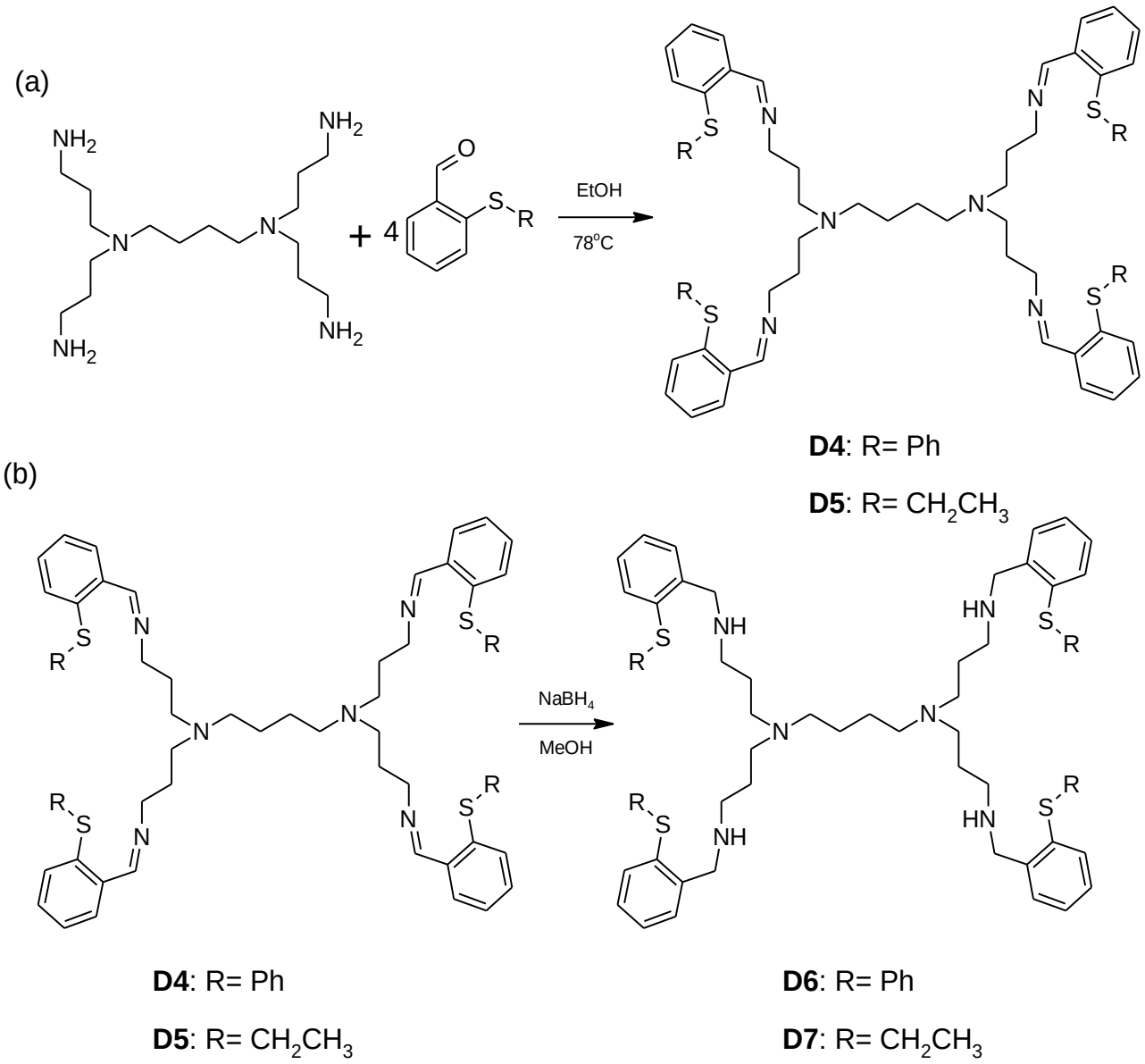

Scheme 19: Synthesis of thioether-amine dendrimers

The spectroscopic characterization data obtained for the dendrimers **D4**-**D7** are very similar to the data obtained for **L4**-**L7** previously discussed and are available in the experimental section. As a representative example the most important characterization data obtained for **D7** are discussed below.

The ^{1}H NMR spectrum obtained for **D7** is shown in Figure 10. The signal due to the imine protons is no longer observed around 8.83 ppm (as in **D5**). Instead a sharp singlet is observed at 3.82 ppm due to the protons of the Ar-C**H$_2$**-NH- moiety serving as proof of successful reduction.

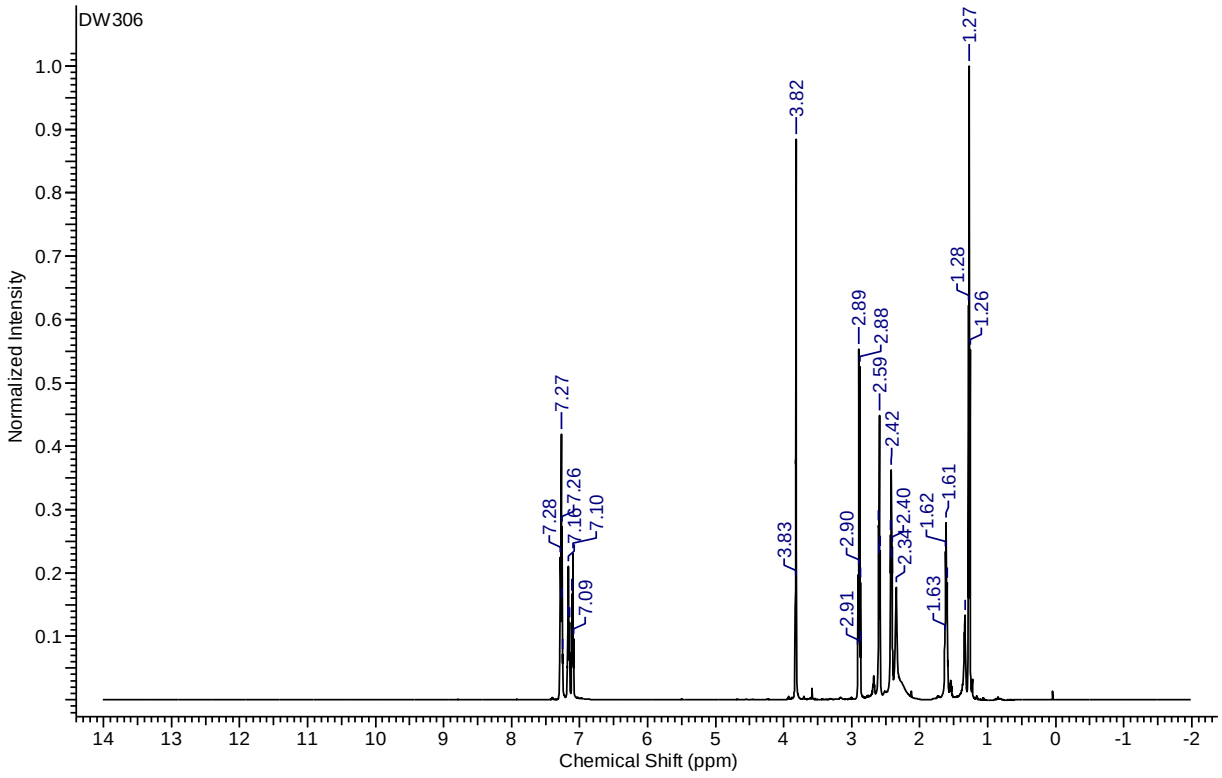

Figure 10: ^{1}H NMR spectrum of D7 in $CDCl_3$

Fragmentation of the molecule is observed under ESI conditions, however the mass spectrum of **D7** (Figure 11) exhibited the molecular ion $(M+H)^+$ at m/z 917 and the doubly charged ion at 459 as the base peak. Another significant fragment is observed at m/z 384 (doubly charged) where cleavage between one of the benzylic carbons and an aromatic ring has taken place ($C_{43}H_{70}N_6S_3$).

The most important characterization data of compounds **D4-D7** are tabulated below in Table 9.

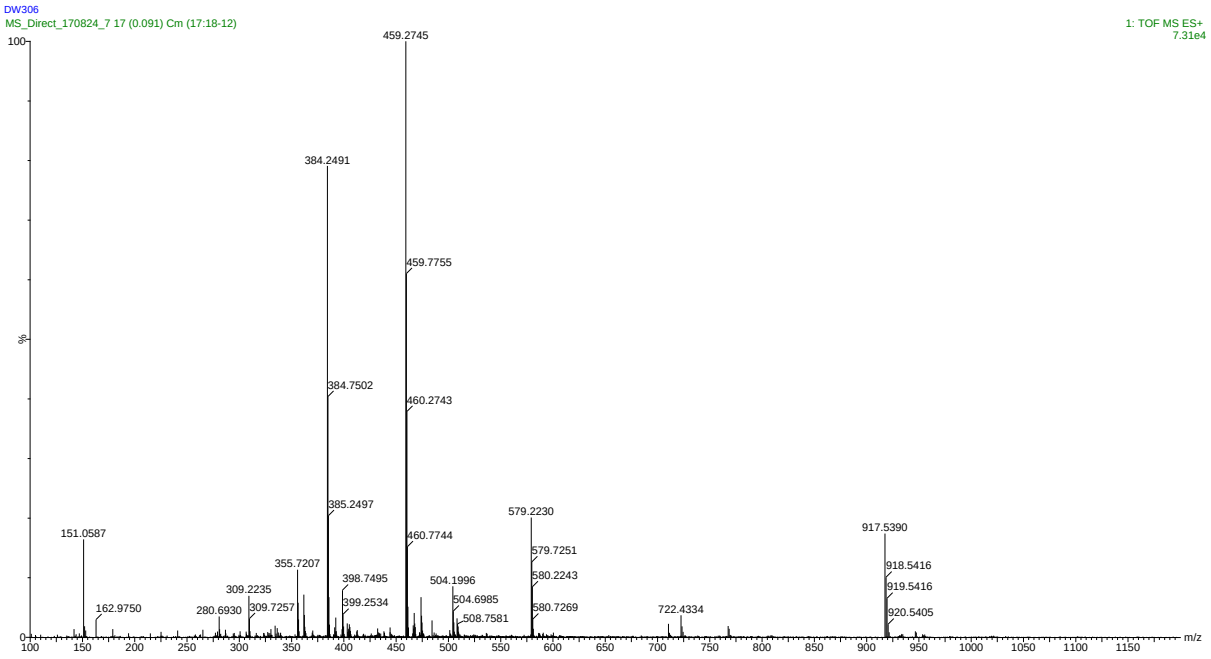

Figure 11: ESI mass spectrum of D7

Table 9: Characterization data of selected thioether-amine compounds

Compound	FTIR (cm^{-1})	ESI-MS (m/z)	^{1}H NMR ppm
D4	1633 ($\nu_{C=N}$)	1101, 551	8.73 (**H**C=N)
D5	1633 ($\nu_{C=N}$)	909	8.83 (**H**C=N)
D6	3285 (ν_{N-H})	1109, 556	3.90 (**H$_2$**C-N)
D7	3306 (ν_{N-H})	917	3.82 (**H$_2$**C-N)

Ligands, **L6**, **L7**, **D6** and **D7** with amine moieties should not undergo hydrolysis. Thus, we set out to employ these compounds as ligands for the transition metals copper and cobalt.

The reaction of ligand **L7** with copper(II)triflate was performed, as shown below in Scheme 20, by employing a modified literature procedure.[41]

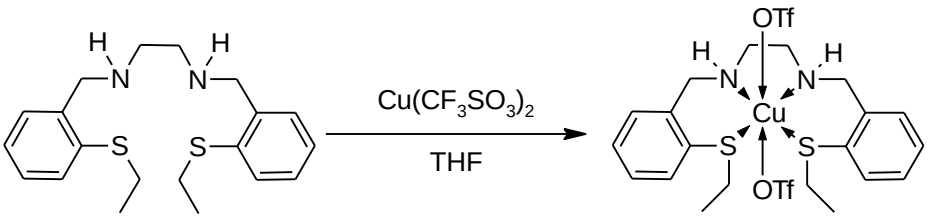

L7 **C5**

Scheme 20: Synthesis of novel Cu(S_2N_2) complex C5

This reaction proceeded at room temperature to yield, after workup, a blue-purple powder. Complex **C5** appears to be fairly air stable and could easily be handled without special precautions. **C5** exhibited good solubility in chlorinated solvents such as DCM and $CHCl_3$, as well as other polar solvents such as THF, MeOH and MeCN while being insoluble in diethyl ether and non-polar solvents such as hexane and pentane.

The FTIR spectrum of **C5** exhibited the expected triflate stretches at 1027 (ν_{S-O}), 1141 (symmetric $\nu_{S=O}$), 1225 (asymmetric $\nu_{S=O}$) and 1253 cm^{-1} (ν_{C-F} stretch) are observed in the FTIR spectrum of complex.

Upon coordination of the ligand to the metal ion via the thioether donor site we would expect to see a shift in the frequency of the C-S stretch, as electron density around the S atom changes. The C-S bond has a fairly low dipole moment with the result that C-S stretches are not usually easily observed with FTIR spectroscopy (small change in dipole moment). For this reason, we attempted the use of Raman spectroscopy as this technique relies on the change in polarizability of a bond.

The Raman spectrum (Figure 12) recorded using a 532 nm laser, showed several peaks that could be assigned to the triflate counterion including $\nu_{S=O}$ and ν_{C-S} stretches occurring in the same spectral regions as the ν_{C-S} bonds of the ligand of **C5**. A peak around 760 cm^{-1} which is absent (or very weak) in the IR spectrum of **C5**, is observed in the Raman spectrum. The position of this stretch shows a shift upon coordination of the ligand (740 cm^{-1}) to the metal centre providing some proof for successful coordination through the sulphur donor site.

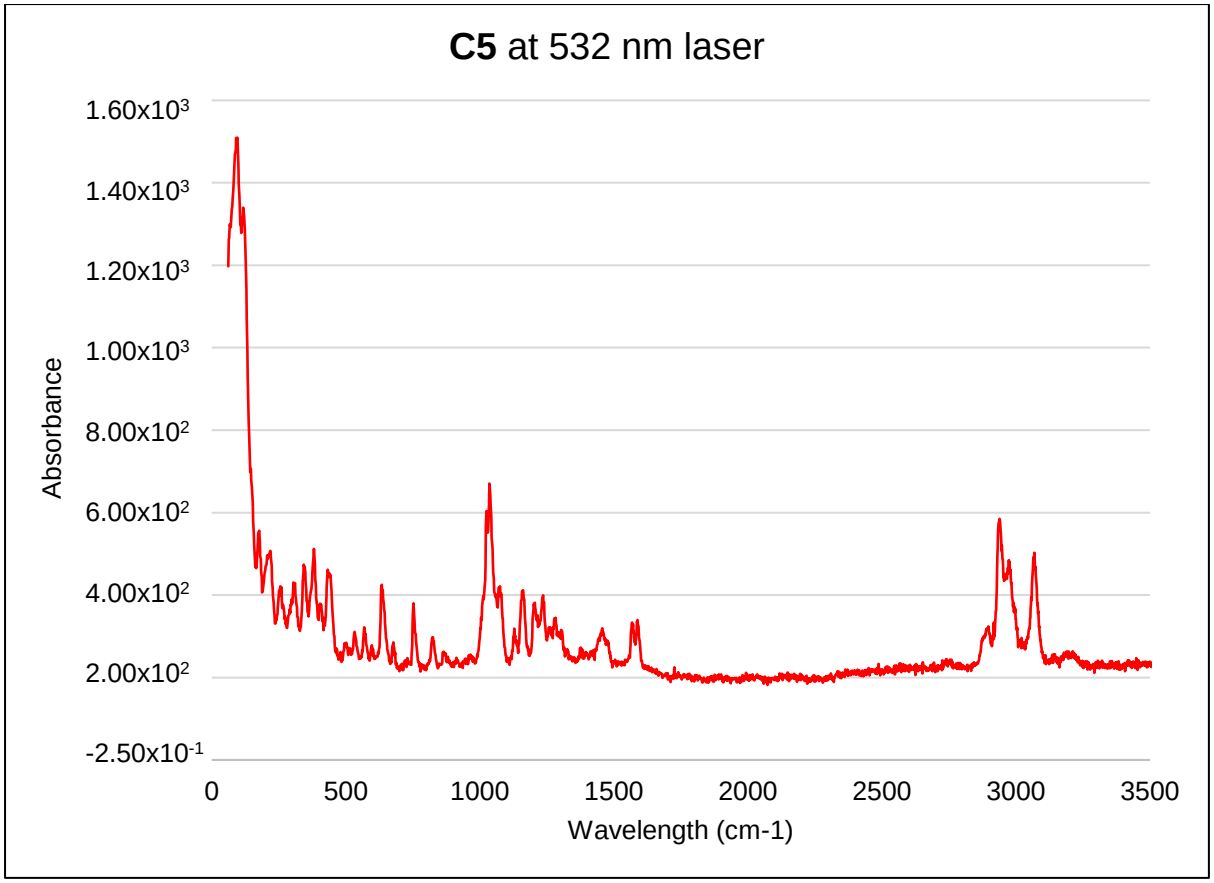

Figure 12: Raman spectrum recorded for complex C5

C5 was further characterized by UV-Vis spectroscopy. Absorption bands are observed at, 274 and 280 nm and can be assigned to transitions associated with the ligand, while a peak at 354 nm is most likely due to a metal to ligand charge transfer band. Furthermore, weak d-d transitions (due to the copper centre) are observed at 595 nm.

The ESI mass spectrum of **C5** exhibited the base peak at m/z 361, which is assigned to the $(M+H)^+$ of the ligand **L7**. A signal at m/z 423 is assigned as the molecular ion $(M+H)^+$ of the cation of **C5**. The complex **C5** with coordinated triflate ligands is not observed under ESI-MS conditions.

Crystals suitable for X-ray diffraction were obtained by slow evaporation of a DCM solution of **C5** to yield large purple needles. From the crystal structure obtained for **C5** (Figure 13) it is observed that **C5** is in a distorted octahedral geometry. The copper centre is coordinated by the 2 secondary amine moieties (blue, Figure 13) as well as the thioether moieties (yellow), furthermore, two triflate ligands are also coordinated

to the copper centre. One of the triflate ligands is disordered and split over 2 positions. The Cu-O bond lengths are quite long (typically Cu-O bonds are around 2.2 to 2.3 Å)[42] for coordinated triflate ligands. This likely indicates that coordination of the triflates to the copper centre is relatively weak. Thus, formation of a vacant site on the metal centre, necessary for oxidation catalysis, should be relatively facile. Crystallographic data and structural parameters are available in the experimental section at the end of the chapter.

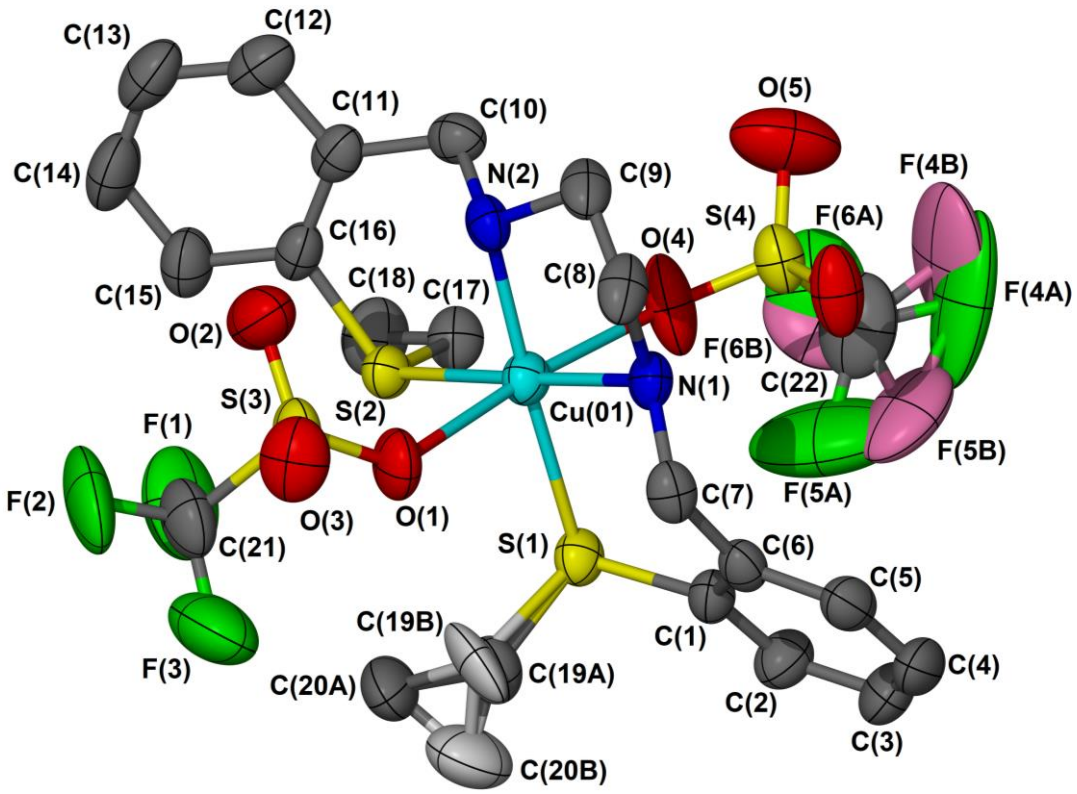

Figure 13: ORTEP plot showing the single crystal X-ray structure of complex C5. Thermal ellipsoids drawn at 50% probability. Hydrogen atoms omitted for clarity. Selected bond lengths (Å) and angles (°): Cu(01)-N(1) 2.016(3), Cu(01)-N(2) 2.017(3), Cu(01)-S(1) 2.3754(11), Cu(01)-S(2) 2.3501(11), Cu(01)-O(1) 2.414 (3), Cu(01)-O(4) 2.548(4), S(1)-Cu(01)-S(2) 87.36(4), S(1)-Cu(01)-N(1) 92.69(8), S(2)-Cu(01)-O(4) 89.57(9), O(1)-Cu(01)-O(4) 175.08(12).

With the successful synthesis of **C5** the analogous reaction of **D7** with $Cu(OTf)_2$ was attempted as shown in Scheme 21 to yield **MD6** as a highly hygroscopic dark green powder soluble in THF and chlorinated solvents.

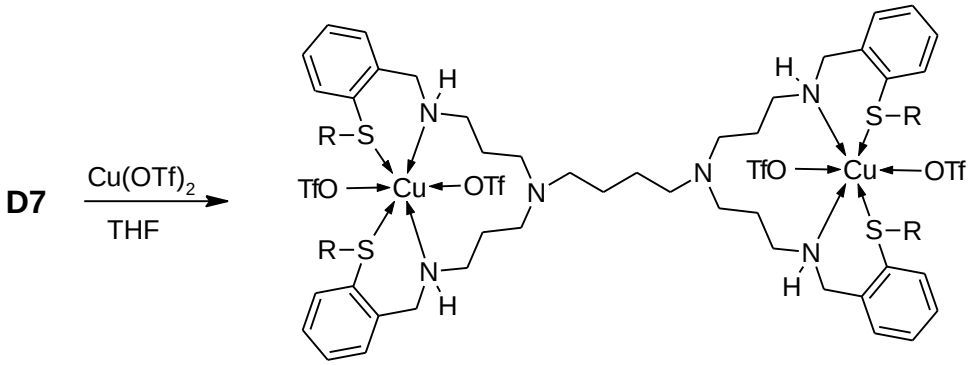

MD6: R= CH_2CH_3

Scheme 21: Synthesis of novel metallodendrimer MD6

The spectroscopic characterization data obtained for dendrimer **MD6** is similar to that obtained for **C5** (previously discussed) and is available in the experimental section. Unfortunately, due to intense fluorescence, Raman spectra of **MD6** could not be recorded. However, the mass spectrum (ESI) showed the molecular ion of the cationic species at m/z 1043.

With the copper complexes in hand we investigated the reaction of **L7** with $CoCl_2$ to form the analogous cobalt complex **C6** as shown in Scheme 22.

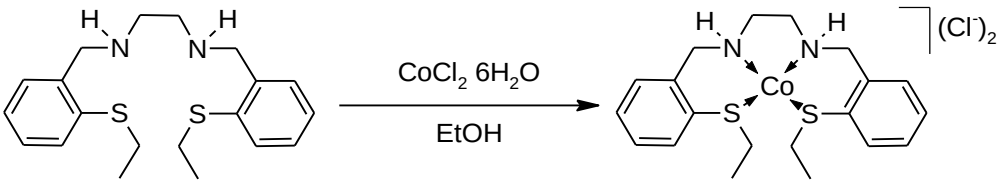

L7 **C6**

Scheme 22: Formation of novel complex C6

C6 was obtained as a light purple-pinkish solid powder that precipitated from solution during the reaction. Complex **C6** is soluble only in acetone, DMF (partial) and DMSO (partial) and is insoluble in almost all other solvents surveyed.

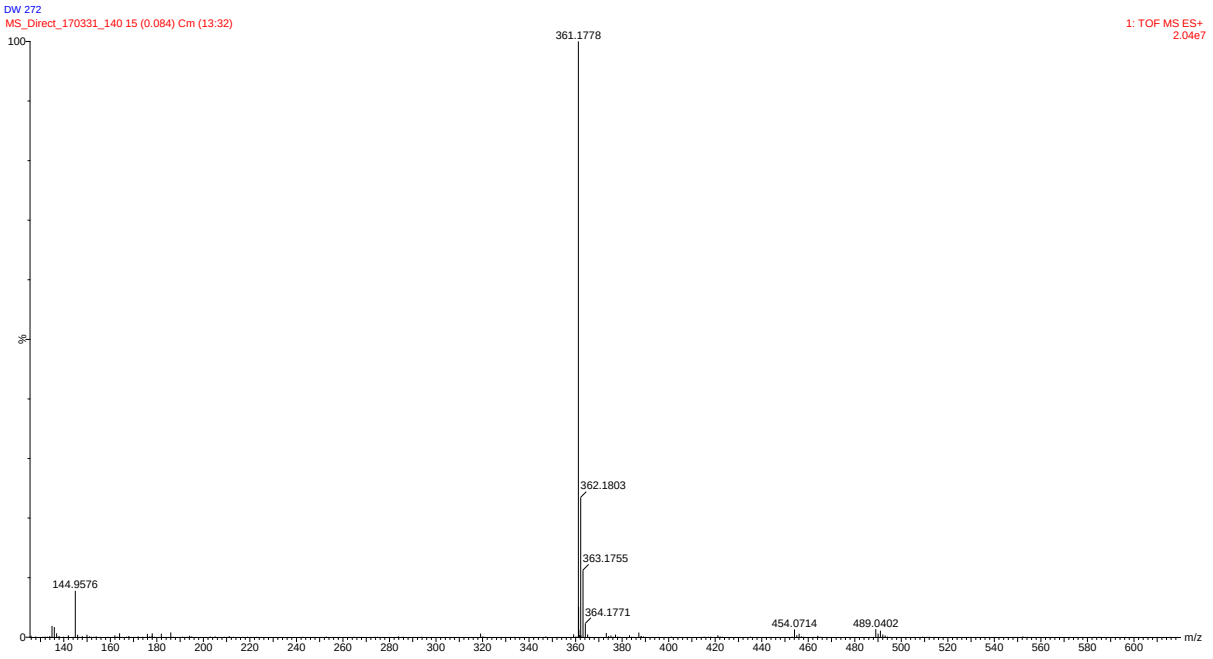

Figure 14: ESI mass spectrum obtained for C6

Complex **C6** undergoes fragmentation under ESI mass spectrometry conditions (Figure 14). The mass spectrum exhibited the base peak at m/z 361, which is assigned to the free ligand. Two other significant fragments are observed. At m/z 489 we observe the fragment corresponding to the octahedral complex in which two chlorides are coordinated to the Co centre. The fragment at m/z 454 is as a result of loss of a chloride from the parent ion at m/z 489. The cationic four-coordinate S_2N_2 cobalt species was not observed.

The mass spectrometry results raised the question of whether the compound is in fact octahedral with two chloride ligands or rather a four-coordinate complex with chloride counter ions. Unfortunately, due to this complex being extremely insoluble (solubility in acetone, partially soluble in THF, DMF and DMSO) we have been unable to grow crystals suitable for x-ray diffraction. In an attempt to get more insight into the nature of complex **C6**, we performed conductivity measurements to determine whether the chlorides were inside or outside the coordination sphere. The molar conductivity determined for **C6** at 23°C was found to be 136.52 (Ω/cm)/M. Unfortunately, due to the low solubility of **C6** in other solvents, the conductivity measurements could only be recorded in acetone. Conductivity results reported in acetone, for fairly similar systems, vary widely between different literature reports as observed in a review by Geary.[43] A

fairly wide range of conductivity values for both 1:1 and 2:1 electrolytes has been reported in acetone.[43] However, the experimental conductivity measurement obtained for **C6** corresponds well with those reported for other 2:1 electrolytes.[44] In the absence of a chloride abstractor such as $AgNO_3$, it seems unlikely that the four-coordinate complex would be generated during the conductivity measurement. Taking the results of both conductivity as well as mass spectrometry experiments into consideration, it would seem that the octahedral species is most likely formed under mass spectrometry conditions.

Raman spectroscopy was again employed in an attempt to monitor changes in frequency of the C-S bond for complex **C6** versus that of the ligand **L7**. However, as can be seen from the spectrum below severe fluorescence is observed when the 532 nm laser is employed, with the entire baseline shifted to higher relative absorbance values. However, it does appear that the peak assigned to the C-S bond is shifted to around 800 cm^{-1} in the complex.

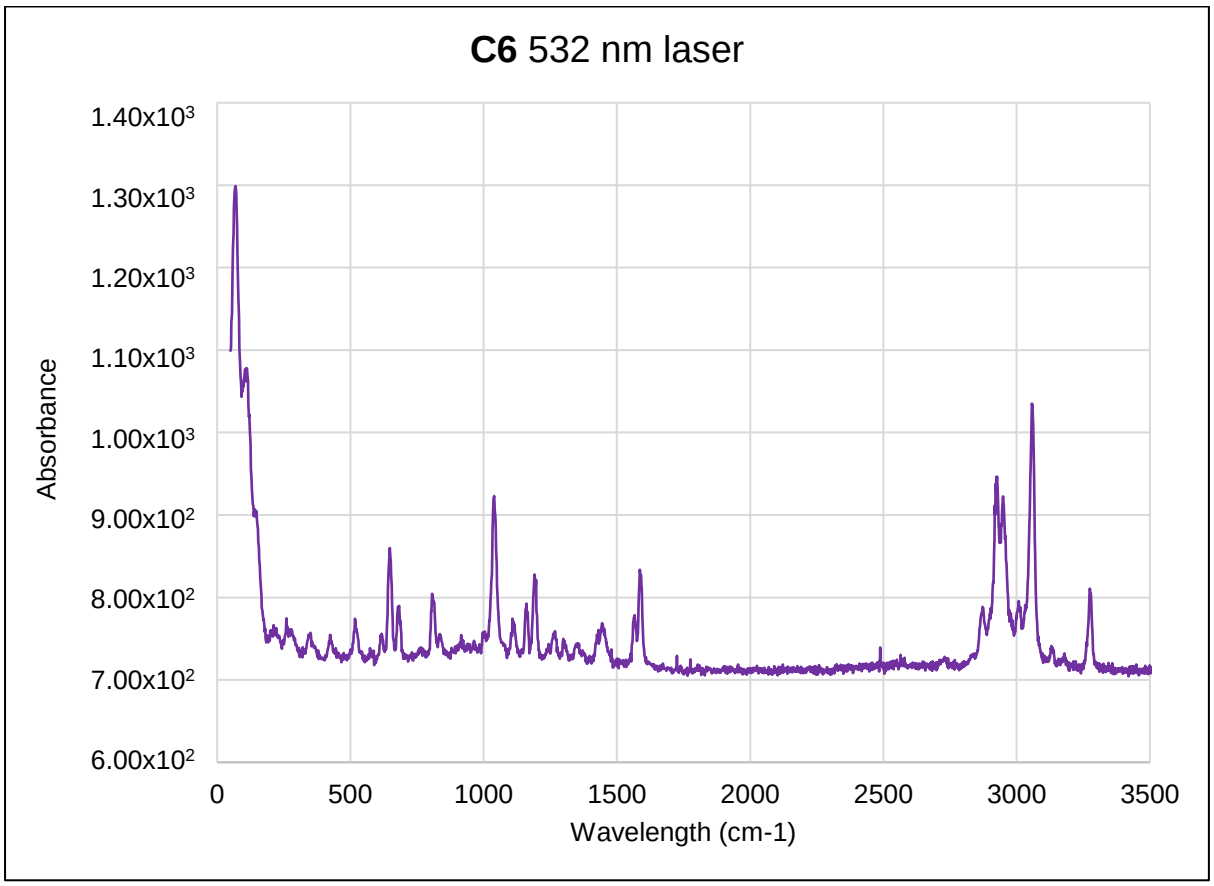

Figure 15: Raman spectrum obtained for C6 using a 532 nm laser

C6 was further characterized by elemental analysis and a good agreement between the experimental results and the values predicted for **C6** were obtained confirming that the complex had been synthesized successfully.

The analogous complexation reactions using **L6** with the same copper and cobalt precursors were attempted but the expected products were not obtained as shown in Scheme 23.

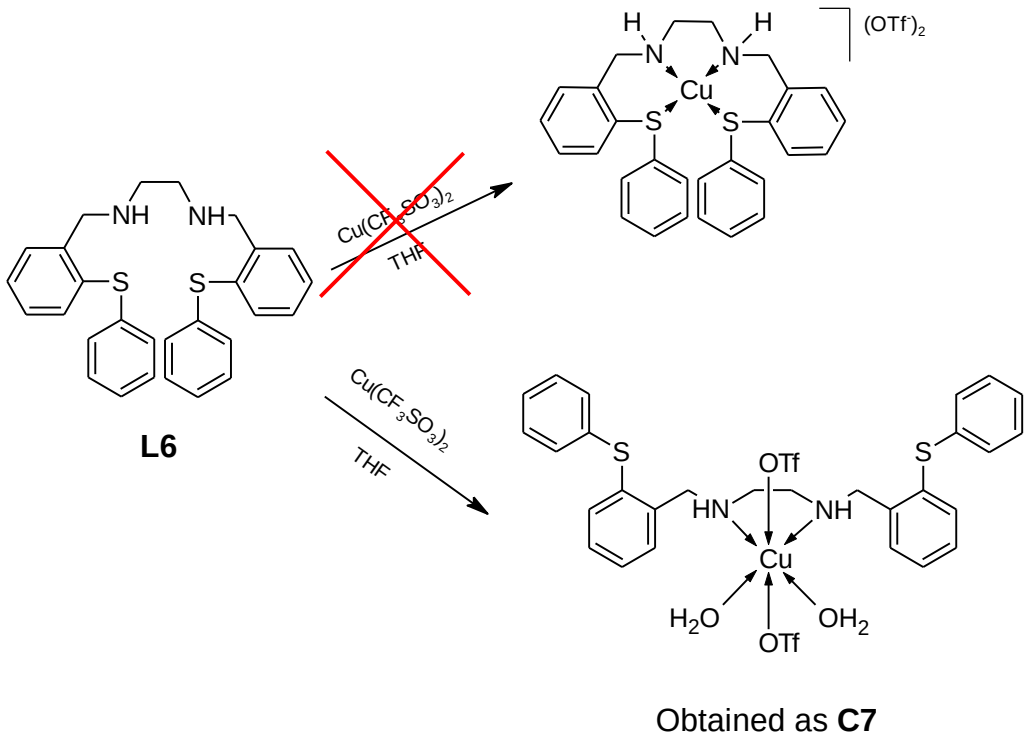

Scheme 23: Attempted synthesis of C7

Instead the reaction of **L6** with $Cu(CF_3SO_3)_2$ yielded a dark green/brown powder the identity of which was confirmed to be that of **C7**. This material was analysed using ESI mass spectrometry as shown below in Figure 16. The molecular ion of the cation of **C7** ($C_{28}H_{28}CuN_2S_2$) is observed at m/z 519. The base peak at m/z 457 can be assigned to the ligand while the doubly charged ion of the complex is observed at m/z 259.

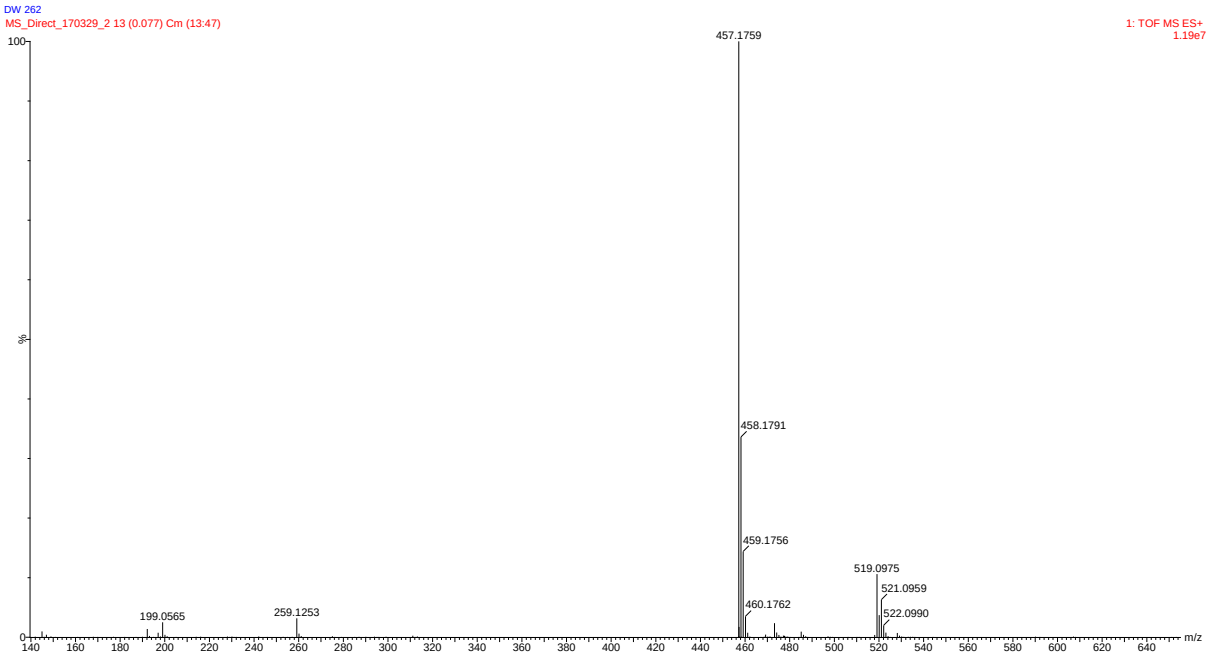

Figure 16: ESI mass spectrum of C7

Complex **C7** was crystalized from a solution of THF and diethyl ether allowing for structure determination by single crystal x-ray diffraction (Figure 17). It was observed that the thioether moieties are not coordinated to the copper metal centre and are relatively far away from the metal ion (in the solid state). Instead, two water molecules as well as the two triflate ligands are coordinated to the metal centre to yield **C7** as a distorted octahedral complex.

The fact that the sulphur donor sites are not coordinated to the metal was also confirmed using Raman spectroscopy. No shift in the C-S stretch is observed for **C7**. The thioether moiety of **L6** is possibly too soft for coordination to the Cu(II) centre (compared to **L7**) due to the electron withdrawing (negative inductive) effect of the aromatic ring adjacent to the thioether moiety. Crystallographic data and structural parameters are available in the experimental section at the end of the chapter.

Similarly, the reaction of **L6** with $CoCl_2$ yielded a highly hygroscopic blue powder. When this material was analysed by FTIR and Raman spectroscopy no shift in the $\nu_{C\text{-}S}$ is observed relative to the $\nu_{C\text{-}S}$ of the ligand. However, large $\nu_{O\text{-}H}$ bands are present around 3300-3400 cm^{-1}.

Similarly, when the dendrimer analogue **D6** was employed as ligand in reactions with $Cu(OTf)_2$ and $CoCl_2$ we obtained oily materials upon isolation of the reaction products. Attempted recrystallization of these materials produced what appeared to be solid materials that became oily upon removal of the solvent. Based on the FTIR as well as Raman spectra of these compounds, we propose that these materials likely incorporate THF (in the case of reaction with $Cu(OTf)_2$) or ethanol (in the case of $CoCl_2$) solvent and/or water inside the coordination sphere.

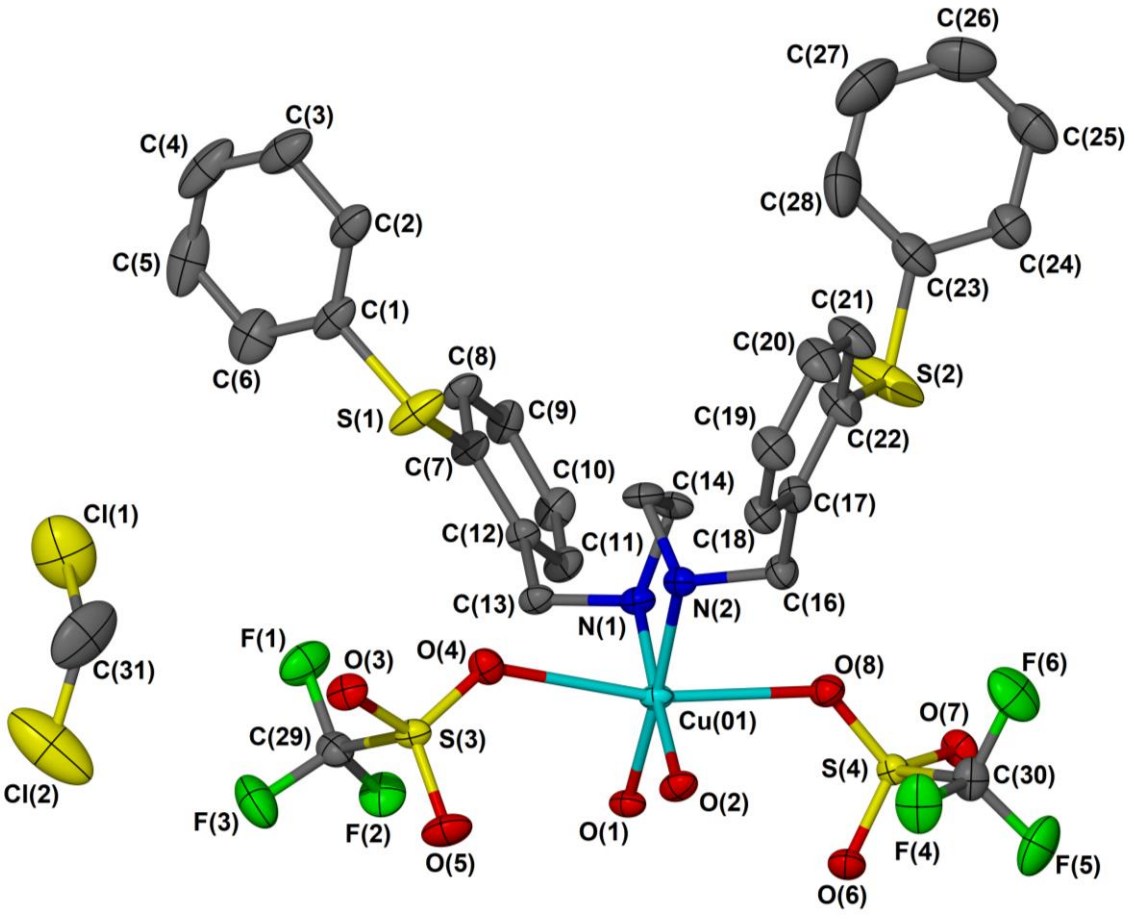

Figure 17: ORTEP plot of C7 showing the copper centre in distorted octahedral geometry with two aqua ligands. Thermal ellipsoids drawn within 50% probability. Hydrogen atoms have been omitted for clarity. Selected bond lengths (Å) and angles (°): Cu(01) -N(1) 2.012(2), Cu(01) -N(2) 2.015(2), Cu(01) -O(1) 1.968(2), Cu(01) -O(2) 1.9664(17), Cu(01)-O(4) 2.5246(17), Cu(01)-O(8) 2.5055(18), O(4)-Cu(01)-O(8) 168.51(6), O(1)-Cu(01)-N(1) 89.35(9).

2.4 Conclusions

In this chapter we described the attempted synthesis of ligands that incorporate the moieties found in both the enzymatic systems as well as other highly successful catalysts such as those reviewed in Chapter 1. The synthesis and characterization of several ligands and transition metal complexes of three classes of compounds that incorporate respectively the N_2O_2, N_4 and N_2S_2 donor sets were successful to some degree. Several of these complexes are novel, notably the metallodendrimers. Included amongst these are a number of salicylaldimine complexes of cobalt and iron. Both mononuclear and metallodendrimers were prepared.

Our attempts to form mononuclear as well as dendritic pyridine-imine complexes using $FeCl_2$ as precursor lead to the isolation of ionic complexes containing $FeCl_4^-$ as counterion which is generated in-situ from $FeCl_2$. This caused some difficulty with respect to the characterization of these materials. The exact mechanism for the formation of $FeCl_4^-$ is not fully known. However, we determined that the photooxidation of $FeCl_2$ in the presence or absence of a chlorinated solvent is not responsible for the formation of $FeCl_4^-$ in our reactions. When the transition metal precursor was changed to $Fe(OTf)_2$ instead of $FeCl_2$, we obtained the expected $Fe(\mathbf{L3})_3(OTf)_2$ and $Fe_2(\mathbf{D3})(OTf)_4$ products for the model and metallodendrimer systems respectively.

The synthesis of thioether-imine ligand systems was also successfully carried out. However, these ligands suffered from metal-mediated hydrolysis of the imine moiety during attempted complexation reactions. The hydrolysis problem was circumvented by reduction of the imines to the corresponding amines.

Finally, a number of copper and cobalt complexes of the S_2N_2 ligands were also prepared. Mononuclear copper complex **C5** bearing the S_2N_2 donor set was characterized by various analytical techniques and its structure confirmed by single crystal X-ray diffraction. Unfortunately, the use **L6** and **D6** as ligands was less successful, possibly due to the soft nature of the thioether moiety.

2.5 Experimental section

2.5.1 General methods and materials

All reagents were obtained from either Merck or Sigma Aldrich and used without any further purification. Solvents were obtained from Merck, Kimix or Protea Chemicals. The solvents THF, toluene, hexane, DCM and diethyl ether were dried using an Innovative Technologies PS-Micro solvent purifier (drying agent: Alusorb aluminium oxide sieves). Acetonitrile was dried by distillation over phosphorous pentoxide. Ethanol and methanol were dried by distillation over a mixture of magnesium filings and iodine.

All reactions were performed using standard Schlenk techniques under an inert atmosphere of nitrogen gas (dried over $CaSO_4$) unless otherwise stated.

FT-IR spectra were recorded on a Thermo Nicolet Avatar 330 FT-IR spectrometer with a Smart Performer (Zn/Se) ATR attachment. NMR spectra were recorded using a Varian Unity Inova NMR spectrometer (400 or 300 MHz). Mass spectra were recorded on a Waters Synapt G2 spectrometer by direct injection into a stream of acetonitrile and formic acid. UV-vis spectra were recorded using a GBC 920 double beam spectrometer using quartz cuvettes. Magnetic susceptibilities were calculated through the use of a Sherwood Scientific MK-1 Gouy balance. Magnetic susceptibilities were in some cases also determined using the Evan's method.[45]

Synthesis 2-[(*E*)-(propylimino)methyl]phenol (L1)

Compound **L1** was prepared as previously described in the literature from propyl amine (0.218 g, 3.69 mmol) and salicylaldehyde (0.300 g, 2.45 mmol) and isolated as a yellow oil (0.331 g, 83% yield).[22] IR (ATR) ν =1632 ($\nu_{C=N}$), 1275 (ν_{C-O}) cm^{-1}; ^1H NMR (400 MHz, $CDCl_3$) δ_H 0.96 (t, 3H, C**H**$_3$, $^3J_{H-H}$ 7.46 Hz), 1.66 (sextet, 2H, -C**H**$_2$-CH_3, $^3J_{H-H}$ 72 Hz), 3.47 (t, 2H, N-C**H**$_2$-CH_2, $^3J_{H-H}$ 7.4 Hz), 6.83 (d 1H, Ar-**H**, $^3J_{H-H}$ 7.4 Hz), 6.96 (d, 1H, Ar-**H**, $^3J_{H-H}$ 7.4 Hz), 7.19 (1H, Ar-**H**), 7.29 (1H, Ar-**H**), 8.23 (s, 1H,N=C-**H**) 13.78 (s,1H, O-**H**) ppm; ^{13}C NMR (101 MHz, $CDCl_3$) δ_C 11.5 (-CH_3), 24.0 (-CH_2-), 59.9 (-CH_2-),119 (Ar), 125.2 (Ar), 126.5 (Ar), 131.2 (Ar), 132.2 (Ar), 157.2 (Ar), 156.1 (C=N) ppm.

Synthesis 2,4-di-*tert*-butyl-6-[(*E*)-(propylimino)methyl]phenol (L2)

Compound **L2** was prepared using the same methodology as described for **L1** from propylamine (0.114 g, 1.92 mmol) and and 3,5-di-*tert*-butyl-2-hydroxybenzaldehyde (0.300 g, 1.28 mmol) isolated as a yellow oil. (0.299 g, 85% yield).[22], IR (ATR) ν =1633 ($\nu_{C=N}$), 1276 (ν_{C-O}) cm^{-1}; ^{1}H NMR (400 MHz, $CDCl_3$) δ_H 1.01 (t, 3H, C**H₃**-CH_2, $^{3}J_{H-H}$ 7.4 Hz), 1.34 (s, 9H, C-(C**H₃**)₃), 1.49 (s, 9H, C-C(C**H₃**)₃), 1.76 (sextet, 2H, CH_3-C**H₂** $^{3}J_{H-H}$ 7.1 Hz), 3.57 (t, 2H, -N-C**H₂**-CH_2-, $^{3}J_{H-H}$ 7.4 Hz), 7.11 (d, 1H, Ar-**H**, $^{3}J_{H-H}$ 4.1 Hz), 7.40 (d, 1H, Ar-**H**, $^{3}J_{H-H}$ 4.1 Hz), 8.37(s, 1H, N=C**H**-), 14.00 (s, 1H, O-**H**) ppm; ^{13}C NMR (101 MHz, $CDCl_3$) δ_C 11.7 (CH_2-**C**H_3), 24.1 (-CH_2-), 59.9 (-CH_2-N), 29.8 (-CH_3), 30.3 (-CH_3), 34.1 (-(CH_3)₃), 34.2 (-(CH_3)₃), 123.1 (Ar), 123.3 (Ar), 128 (Ar), 135.1 (Ar), 135.4 (Ar) 153 (Ar), 158 (**C**=N) ppm.

Salicylaldimine Dendrimer D1

D1 was synthesized as previously reported using salicylaldehyde (0.309 g, 2.53 mmol) and diamino butane (DAB) cored polypropylenimine (PPI) tetramine dendrimer (0.200 g, 0.632 mmol) with the following adaptation.[21] Upon completion of the reaction the oily residue was redissolved in ethanol (20 ml). The sample was then concentrated on a rotary evaporator until precipitation started. The reaction vessel was cooled overnight at 0°C. The precipitate was then filtered and washed with small amounts of cold ethanol (2 x 5 ml) and hexane (10 ml). This yielded **D1** as a yellow powder (0.398 g, 86% yield). M.p. 68°C; IR (ATR) ν = 1632 ($\nu_{C=N}$), 1277 (ν_{C-O}); ^{1}H NMR (400 MHz, $CDCl_3$) δ_H 1.42 (br, 4H, NC**H₂**C**H₂**N), 1.87 (m, 8H, –NC**H₂**CH_2), 2.42 (t, 4H, –NC**H₂**, $^{3}J_{H-H}$ 7.2 Hz), 2.57 (br t, 8H, –NC**H₂**), 3.67 (t, 8H, C=NC**H₂**, $^{3}J_{H-H}$ 6.9 Hz), 6.88 (m, 4H, Ar-H); 7.19–7.35 (m, 12H, Ar-H); 8.32 (s, 4H, N=C**H**-); ^{13}C NMR (101 MHz, $CDCl_3$) δ_C 25.1 (-CH_2-**C**H_2-**C**H_2-CH_2-), 28.6 (-N-CH_2-**C**H_2-), 51.5 (=N-**C**H_2-), 54.1(-N-**C**H_2-), 57.4 (-N-**C**H_2-CH_2-CH_2-**C**H_2-N-), 117.0 (Ar), 118.4 (Ar), 118.8 (Ar), 131.1(Ar), 132.2 (Ar), 161.0 (-H**C**=N-), 164.7 (-H**C**=N-) ppm.

Salicylaldimine Dendrimer D2

D2 was synthesized by following the same method employed in the synthesis of **D1** using 3,5-di-*tert*-butyl-2-hydroxybenzaldehyde (0.592 g, 2.53 mmol) as the aldehyde along with DAB-AM-4 PPI tetramine dendrimer, generation 1 (0.200 g, 0.632 mmol). This yielded **D2** as a yellow powder (0.589 g, 79% yield). M.p. 79°C. IR (ATR) ν = 1630 (ν C=N), 1271 (ν C-O); ^{1}H NMR (400 MHz, $CDCl_3$) δ_H 1.34 (br s, 36H,C(C**H₃**)$_3$), 1.44 (br s, 36H, C(C**H₃**)$_3$), 1.45 (br s, 4H, NC**H₂**C**H₂**N) 1.83 (m, 8H), 2.40 (br, 4H, -N-C**H₂**-C**H₂**-N-), 2.50 (t, 8H, N-C**H₂**-, $^{3}J_{H-H}$ 7.1 Hz), 3.61 (t, 8H, -HCN=C**H₂**-), 7.08 (d, 4H, Ar-**H**, $^{3}J_{H-H}$ 4.1 Hz), 7.30 (d, 4H, Ar-**H**, $^{3}J_{H-H}$ 4.1 Hz), 8.34 (s, 4H, -**H**C=N-) ppm; ^{13}C NMR (75 MHz, $CDCl_3$) δ_C 25.2 (-CH_2-**C**H_2-**C**H_2-CH_2-), 28.6 (-N-CH_2-**C**H_2-), 29.5 (-**C**H_3), 34.1 (-**C**-$(CH_3)_3$), 51.6 (=N-**C**H_2-), 54.1(-N-**C**H_2-), 57.5 (-N-**C**H_2-CH_2-CH_2-**C**H_2-N-), 117.89 (Ar), 125.7 (Ar), 126.6 (Ar), 137.0 (Ar), 139.8 (Ar), 161.2 (Ar) 164.1 (-H**C**=N-) ppm.

General synthetic procedure for cobalt complexes C1, C2, MD1 and MD2

Complexes **C1, C2, MD1** and **MD2** were prepared as previously described in yields ranging from 60-75%.[22] As representative example the synthesis of **MD1** is described below. A round-bottomed flask was charged with a solution of the dendrimer ligand (**D1**) (0.150 g, 0.205 mmol) in methanol (10 ml). To this was added NaOH (0.818 mmol, 0.032 g) as a solid. $Co(OAc)_2 \cdot 4H_2O$ (0.410 mmol, 0.102 g) was then added as a solution in methanol (5 ml). The resultant reaction mixture was then heated to reflux and stirred under nitrogen for 4 hours. During this time the solution darkens in colour (yellow to orange yellow) and a brown precipitate formed. After 4 hours the stirring was stopped, and the reaction mixture was cooled in an ice bath for 30 minutes. The reaction mixture was filtered. The crude product was washed with cold methanol (2 x 5 ml) and dried to yield a fine brown powder.

The crude product was dissolved in DCM (10 ml) and filtered through a syringe filter to remove any inorganic impurities and unreacted starting material. The filtrate was subsequently dried under reduced pressure to yield the pure product as a brown powder (0.116 g, 67%). IR(ATR) ν = 1628 ($\nu_{C=N}$), 1307 (ν_{C-O}) cm^{-1}, UV-Vis (DCM) λ_{max}: 240, 360 nm; MS (ESI): m/z 847 $(M+H)^+$; Anal.calcd for

$C_{44}H_{52}Co_2N_6O_4 \cdot 0.5CH_2Cl_2$: C (60.10), H (6.01), N (9.45) Found: C, (59.89); H, (6.10), N (9.75).

Synthesis of C1

Prepared as described for **MD1**. Isolated as brown powder in 75% yield. IR (ATR) ν: 1614 ($\nu_{C=N}$), 1321 (ν_{C-O}) cm^{-1}. UV-Vis (DCM) λ_{max}: 240; MS(ESI): m/z 384 $(M+H)^+$; Anal.calcd for $C_{36}H_{56}CoN_2O_2$: C, (62.66), H (6.31), N (7.31); Found: C (71.31); H (9.29), N (4.71).

Synthesis of C2

Prepared as described for **MD1**. Isolated as brown powder in 69% yield IR (ATR): ν= 1597($\nu_{C=N}$), 1320 (ν_{C-O}) cm^{-1}; UV-Vis (DCM) λ_{max}: 240, 360 nm; MS(ESI): m/z 608 $(M+H)^+$; Anal.calcd for $C_{36}H_{56}CoN_2O_2$: C (71.14), H (9.29), N (4.61); Found: C (71.31), H (9.29), N (4.71).

Synthesis of MD2

Prepared as described for **MD1**. Isolated as brown powder in 66% yield IR(ATR) ν=1630 ($\nu_{C=N}$), 1317 (ν_{C-O}) cm^{-1}; UV-Vis (DCM) λ_{max}: 240, 359 nm; MS(ESI): m/z 1296 $(M+H)^+$; Anal.calcd for $C_{77}H_{116}Co_2N_6O_4 \cdot H_2O$: C (69.49), H (9.05), N (6.40); Found: C (69.58), H (8.97) N (6.65).

Synthesis of MD3

A round bottomed flask is charged with a solution of the dendrimer ligand, **D1** (0.150 g, 0.205 mmol) in ethanol (20 ml). A solution of $FeCl_3$ (0.133 g, 0.820 mmol) in ethanol (10 ml) was slowly added to the ligand solution via syringe. The resultant reaction mixture was refluxed under nitrogen for 3 hours. During this time a dark brown precipitate formed. After 3 hours the precipitate was isolated by filtration. The filter was washed with ethanol (2 x 10 ml) and dried under vacuum to yield **MD3** as a dark brown

powder (0.154 g, 61% yield,). IR (ATR): ν= 1617 ($\nu_{C=N}$), 1298 (ν_{C-O}) cm^{-1}; MS (ESI): m/z 912 $(M+H)^+$; Anal.calcd for $C_{44}H_{52}Fe_4Cl_8N_6O_4 \cdot 2H_2O$: C (41.55), H (4.44), N (6.61); Found: C (41.10), H (4.85), N (6.35).

Synthesis *of N*-[pyridin-2-ylmethylidene]propan-1-amine (L3)

Compound **L3** was prepared as has been described in the literature and isolated as an orange brown oil (74% yield).[24] IR (ATR) ν= 1648 ($\nu_{C=N}$), 1586 ($\nu_{pyr\ C=N}$), cm^{-1}. ^{1}H NMR (400 MHz, $CDCl_3$) δ_H 0.97 (t, 3H, -N-CH_2-CH_2-C**H$_3$**, $^3J_{H-H}$ 7.42 Hz), 1.75 (sextet, 2H, -N-CH_2-C**H$_2$**-CH_3, $^3J_{H-H}$ 7.04), 3.64 (td, 2H, -N-C**H$_2$**-CH_2-CH_3, $^3J_{H-H}$ 7.02 Hz, $^4J_{H-H}$ 1.56 Hz), 7.25- 7.40 (overlapping multiplets, 2H, Ar-**H**) 7.73 (td, 1H, Ar-**H**, $^3J_{H-H}$ 7.81 Hz, $^4J_{H-H}$ 1.56 Hz), 7.99 (d, 1H, Ar-**H**, $^3J_{H-H}$ 8.02), 8.37 (s, 1H, -N=C**H**-), 8.63 (d, 1H, Ar-**H**, $^3J_{H-H}$ 8.01 Hz) ppm; ^{13}C NMR (75 MHz, $CDCl_3$) δ_C 12.0 (**C**H_3-), 24.7 (CH_3-**C**H_2-), 64.0 (-HC=N-**C**H_2-), 128.8 (Ar), 129.1 (Ar), 131.0 (Ar), 135.5 (Ar), 160.0 (-H**C**=N-) ppm.

Pyridyl-imino dendrimer (D3)

A round-bottomed flask was charged with generation 1 diaminobutane polypropylenimine (DAB-PPI) dendrimer (0.155 g, 0.488 mmol) and toluene (30ml). Anhydrous $MgSO_4$ was then added to the flask. A solution of 2-pyridinecarboxaldehyde (0.210 g, 1.96 mmol) in toluene (5 ml) was then added to the reaction mixture via syringe and the mixture stirred at room temperature e and under nitrogen for 48 hours. After 48 hours the reaction mixture was filtered and the filtrate dried by rotary evaporation. The crude oil obtained from was dissolved in CH_2Cl_2 (20 ml) and washed with water (7 x 50 ml). The organic layer was collected, dried over anhydrous $MgSO_4$ and filtered. Removal of the solvent by rotary evaporation yielded the title product as an orange oil (0.218 g, 74% yield). IR (ATR) ν= 1648 ($\nu_{C=N}$),1586 ($\nu_{C=N}$) cm^{-1}. ^{1}H NMR (600 MHz, $CDCl_3$) 1.42 (br multiplet, 4H, -N-CH_2-C**H$_2$**-C**H$_2$**-CH_2-N-), 1.86 (quintet, 8H, -N-CH_2-C**H$_2$**-CH_2-N=, $^3J_{H-H}$ 7.03 Hz), 2.42 (br multiplet, 4H, -N-C**H$_2$**-CH_2-CH_2-C**H$_2$**-N-), 2.53 (t, 8H, -N-C**H$_2$**-CH_2-CH_2-N=, $^3J_{H-H}$ 7.42 Hz), 3.68 (td, 8H, -N-CH_2-CH_2-C**H$_2$**-N=, $^3J_{H-H}$ 7.03 Hz, $^4J_{H-H}$ 1.17 Hz), 7.28 (overlaps with solvent, 4H, Ar-**H**), 7.71 (td, 4H, Ar-**H**, $^3J_{H-H}$ 7.03 Hz, $^4J_{H-H}$ 1.17 Hz), 7.95(d, 4H, Ar-**H**, $^3J_{H-H}$ 7.81 Hz), 8.37 (s, 4H -**H**C=N-), 8.63 (d, 4H, Ar-H, $^3J_{H-H}$) ppm; ^{13}C NMR (75 MHz, $CDCl_3$)

δ_C 24.6, 27.8, 51.2, 53.5, 59.1 (-**C**H_2-, aliphatic); 120.7 (Ar), 124.0 (Ar), 136.0 (Ar), 148.9 (Ar), 161.4 (Ar), 154.1 (-**C**=N) ppm.

Attempted synthesis of iron(II) complex MD4

A Schlenk tube was charged with a suspension of $FeCl_2$ (1.275 g, 1.01 mol) in DCM (20 ml). To this was added a solution of the ligand **L1** (0.113 g, 0.168 mmol) in DCM (10 ml). An immediate colour change was observed from orange to purple with concomitant formation of a fine purple precipitate. The reaction mixture was stirred for 48 hours at room temperature under nitrogen. After 48 hours the formed precipitate was collected by filtration under nitrogen and washed with cold DCM (10 ml). Drying under reduced pressure yielded **C3** as a purple powder. M.p: 225-233°C (dec); IR (ATR) ν= 1615 ($\nu_{C=N}$); UV-Vis (DCM) λ_{max}: 242, 292, 330, 370, 530, 585 nm.

Attempted synthesis of iron(II) complex C3

The synthesis was performed as described for **MD4**. The product was isolated as a purple powder. IR (ATR) ν= 1615 ($\nu_{C=N}$); UV-Vis (DCM) λ_{max}: 220, 284, 350, 570 nm; MS (ESI positive): m/z 501 $(M+H)^+$; MS (ESI negative): m/z 197 ($FeCl_4^-$).

Synthesis of model iron(II) triflate complex C4

Iron triflate (0.238 g, 0.675 mmol) was added to a nitrogen-filled Schlenk tube. DCM solvent (10 ml) was added to create a suspension of metal salt in DCM. A solution of the ligand N-[(pyridin-2-ylmethylidene]propan-1-amine (**L3**) (0.200g, 1.35 mmol) in DCM (5 ml) was then added via syringe. The reaction mixture is then stirred under nitrogen for 12 hours. The reaction mixture becomes dark purple over the course of the reaction. After 12 hours stirring was stopped and the reaction mixture filtered to remove any unreacted metal salt. The filtrate was then dried under vacuum to yield a purple oil as crude product. Recrystallization from DCM: Et_2O yielded the product as a purple powder which was isolated by filtration under nitrogen (yield 72%, 0.387 g). M.p: 150- 154°C; IR (ATR): ν= 1613 ($\nu_{C=N}$, $\nu_{pyridyl}$), 1253($\nu_{S=O}$), 1141($\nu_{S=O}$), 1027 (ν_{s-}

$_O$) cm^{-1}; ^1H NMR (400 MHz, CD_2Cl_2) 0.75, 1.59, 2.97, 3.31, 3.81, 7.02, 7.15, 7.46-7.65 (overlapping multiplets, Ar-**H**), 8.12-8.37 (overlapping multiplets, Ar-**H**), 9.21(**H**C=N) ppm; UV-Vis (DCM) λ_{max}: 220, 284, 350, 570 nm; MS (ESI) m/z 501 $(M+H)^+$; Anal. (Calc) for $C_{29}H_{36}F_6FeN_6O_6S_2 \cdot 2H_2O$: C(41.73), H(4.83); N(10.07) Found: C(41.48), H(4.51), N(10.14).

Synthesis of piridyl-imine iron metallodendrimer (MD5)

MD5 was synthesized by following the same protocol employed for **C4** using iron(II)trifltate (0.130 g, 0.367 mmol) and **D3** (0.124 g 0.184 mmol) to yield **MD5** as a purple powder (0.142 g, 71% yield). M.p: 230-233°C (dec); IR (ATR) ν= 1620 ($\nu_{C=N}$) 1613($\nu_{pyridyl}$) 1251($\nu_{S=O}$), 1221, 1154 ($\nu_{S=O}$), 1027(ν_{S-O}) cm^{-1}; UV-Vis (DCM) λ_{max}: 242, 286, 340, 575 nm MS (ESI) m/z 392 $(m/2)^{2+}$; Anal.calcd for $C_{44}H_{52}F_{12}Fe_2N_{10}O_{12}S_4 \cdot H_2O$ C(37.78), H(3.89), N(10.01) Found C(37.60), H(4.25), N(9.78).

Synthesis of 2-(phenylsulfanyl)benzaldehyde (A1)

A Schlenk tube was charged with a solution of 2-fluorobenzaldehyde (0.315 g, 0.253 mmol) in DMSO (5ml). To this solution was added K_2CO_3 (3.75 mmol, 0.518 g) as a solid powder. Thiophenol (0.280 g, 0.260 ml, 0.254 mmol) was added via syringe. The resulting reaction mixture was heated to 100°C and stirred under argon for 4 hours. During this time a colour change is observed from colourless to bright yellow. After 4 hours the reaction vessel was cooled and poured into a round bottomed flask containing 30 ml of H_2O. The mixture was extracted with ethyl acetate (3 x15ml) and the combined organic extracts washed with brine (1 x15 ml). The organic layer was dried over sodium sulphate filtered and the filtrate evaporated to dryness under reduced pressure to yield a yellow oil. The crude product was further purified by silica gel chromatography eluting with hexane (100%) as eluent followed by hexane: ethyl acetate (9:1) to yield a light-yellow oil (0.510 g, 94% yield). R_f= 0 (Hexane 100%), 0.6 (hexane: ethyl acetate 9:1); IR (ATR) ν= 2839, 2733, 1689, 1675 cm^{-1}. ^1H NMR (300 MHz, $CDCl_3$) δ_H 7.19 (d, 1H, S-C-CH-C**H**-CH-,$^3J_{H-H}$ 8.20Hz) 7.32 – 7.44 (overlapping, 7H, Ar-**H**), 7.88 (dd, 1H, CHO-C-C**H**-CH-, $^3J_{H-H}$ 1.76, 7.62 Hz) 10.40 (s, 1H, C-C**H**O); ^{13}C NMR (75 MHz, $CDCl_3$) δ_C 126.0 (Ar), 127.1 (Ar), 127.4 (Ar), 129.1 (Ar), 129.6 (Ar),

131.0 (Ar), 131.6 (Ar), 132.2 (Ar-CHO), 135.1 (Ar), 135.4 (Ar), 135.6 (Ar-S), 136.1 (Ar-S), 190.1 (-**C**HO) ppm; MS (ESI): m/z 215 $[M+H]^+$.

Synthesis of 2-(ethylsulfanyl)benzaldehyde (A2)

A Schlenk tube was charged with a solution of 2-fluorobenzaldehyde (0.300 g, 2.42 mmol) in DMSO (4ml). To this solution was added K_2CO_3 (0.502 g, 3.63 mmol) as a solid. Ethanethiol was then added to the reaction mixture via micropipette (0.200 ml 0.168 g, 2.70 mmol). The reaction vessel was sealed and stirred under argon at 55°C for 5 hours and a further 5 hours at room temperature. A colour change is observed from colourless to yellow. The reaction mixture was then poured into a round bottomed flask containing 50ml of water and extracted using 2 x 30ml ethyl acetate. The combined organics were washed with brine 2 x15ml and dried over Na_2SO_4. The reaction mixture was filtered to remove the Na_2SO_4 and the filtrate dried under reduced pressure. The crude product was further purified by silica gel chromatography using the eluent hexane: ethyl acetate (9:1) to yield a yellow oil (0.367 g, 92% yield). IR (ATR) ν= 1636, 1592, 1556 cm^{-1}; ^{1}H NMR (300 MHz, $CDCl_3$) δ_H 1.34 (t, 3H, $^3J_{H-H}$ 7.63Hz, -CH_2-C**H$_3$**), 2.98 (q, 2H, $^3J_{H-H}$ 7.04Hz, C**H$_2$**-CH_3), 7.30 (t, 1H, $^3J_{H-H}$ 7.63 Hz Ar-H), 7.43(d, 1H, $^3J_{H-H}$ 8.22 Hz, Ar-**H**) 7.49 (t, 1H, Ar-**H**) 7.82 (dd, 1H, , $^3J_{H-H}$ 7.63 Hz 8.22, $^4J_{H-H}$ 1.76Hz, 5.87Hz, Ar-**H**), 10.38 (s, 1H, -C**H**O) ppm. ^{13}C NMR (75 MHz, $CDCl_3$) δ_C 14.2 (**C**H_3-CH_2-), 28.8 (CH_3-**C**H_2-),126.1 (Ar), 127.2 (Ar), 128.0 (Ar), 134.2 (Ar), 135.0 (Ar), 140 (Ar-S-) 190.0 (-**C**HO) ppm.

Synthesis of
(1E,1'E)-N,N'-(ethane-1,2-diyl)bis(1-(2-(ethylthio)phenyl)methanimine) (L4)

A round bottomed flask was charged with a solution of **A1** (0.300 g, 1.40 mmol) in ethanol (10 ml). Ethylene diamine (0.042 g, 0.700 mmol) was then added via syringe. The reaction mixture was refluxed for 12 hours under nitrogen. The reaction mixture became faintly yellow over this time period. After 12 hours the reaction was stopped and the solvent removed. Purification by vacuum distillation yielded a light-yellow oil (0.602 g, 90% yield). IR (ATR) ν= 1632 ($\nu_{C=N}$), 1580, 737, 687 cm^{-1}; ^{1}H NMR (300 MHz, $CDCl_3$) δ_H 3.89 (s, 4H, -N-CH_2-CH_2-N-), 7.19-7.32 (m, 14H, Ar-H), 7.97-8.00(m,

2H, Ar-H), 8.81(s, 2H, **H**C=N-) ppm; ^{13}C NMR (100 MHz, $CDCl_3$) δ_C 62.0(-CH_2-), 126.9(Ar), 127.1 (Ar), 127.3 (Ar), 129.3 (Ar), 129.7 (Ar), 131.2 (Ar), 131.6 (Ar), 135.7 (-C-S-, Ar), 136.1(-C-S-, Ar), 139.5 (Ar), 160.5 (-C=N-) ppm; MS (ESI): m/z 452 $(M+H)^+$.

Synthesis of
(1E,1'E)-N,N'-(ethane-1,2-diyl)bis(1-(2-(phenylthio)phenyl)methanimine) (L5)

A solution of **A2** (0.350 g, 2.11 mmol) in EtOH (5 ml) was placed in a round bottomed flask. Ethylenediamine (0.063 g, 1.05 mmol) was added to the reaction mixture via syringe. The mixture was refluxed for 8 hours under nitrogen during which time it changed colour from colourless to faintly yellow. The solvent was then removed under reduced pressure to yield the crude product as a light-yellow oil. The crude material was further purified by vacuum distillation to remove unreacted ethylene diamine. This yielded **L5** as a yellow oil in 92% yield (0.345 g). IR (ATR) ν= 1632, 1585, 747 cm^{-1}. ^{1}H NMR (600 MHz, $CDCl_3$) δ= 1.18 (t, 6H, $^3J_{H-H}$ 7.62 Hz, -C**H$_3$**), 2.79 (q, 4H, $^3J_{H-H}$ 7.03 Hz, -C**H$_2$**), 4.03 (s, 4H, C**H$_2$**-C**H$_2$**-), 7.22 (t, 2H, $^3J_{H-H}$ 7.62 Hz, Ar-H), 7.30(t, 2H, $^3J_{H-H}$ 7.62 Hz, Ar-H), 7.36 (d, 2H, $^3J_{H-H}$ 7.03 Hz, Ar-H), 7.92 (dd, 2H, $^3J_{H-H}$ 8.02 Hz, $^4J_{H-H}$ 1.17 Hz, Ar-H), 8.86(s, 2H, -C**H**=N-) ppm. ^{13}C NMR (100 MHz, $CDCl_3$) δ_C 14.5 (-**C**H_3), 29.1 (-**C**H_2-CH_3), 61.8 (-N-**C**H_2-), 125.1 (Ar), 126.2 (Ar), 129.4 (Ar), 131.1 (Ar), 135.4 (Ar), 141.0 (-**C**-S-, Ar) 161.0 (-**C**=N-) ppm; MS(ESI): m/z 357 $(M+H)^+$.

Synthesis of N^1,N^2-bis(2-(phenylthio)benzyl)ethane-1,2-diamine (L6)

A two necked 50 ml round-bottomed flask was charged with a solution of the imine compound **L4** (0.230 g, 0.508 mmol) in methanol (10 ml). To this was added $NaBH_4$ (0.080 g, 2.032 mmol) as a solid in small portions over 4 hours. The reaction mixture was stirred at room temperature under nitrogen for 12 hours. After 12 hours effervescence had stopped. The reaction mixture was analysed by TLC and a small amount of starting material was still observed. An additional equivalent of $NaBH_4$ (18mg) was then slowly added over an hour and the sample stirred at room temperature for a further hour and then refluxed for 2 hours. The methanol solvent was carefully removed on a rotary evaporator to yield a large amount of a white solid. Water (20 ml) was added and the mixture extracted with chloroform (3 x 20 ml). The organic extracts were combined and washed with brine (1 x 20 ml). The combined

organic fractions were dried over $MgSO_4$, filtered to remove the $MgSO_4$ and the filtrate dried under vacuum extensively. Drying of the sample yielded a faintly yellow oil which solidified upon extended drying. The compound was further purified by silica gel chromatography using first 100% DCM as the eluent, followed by (DCM: MeOH, 6:1) to yield the product as a highly viscous yellow oil (0.223 g, 96% yield). IR (ATR) ν= 3280 (ν_{N-H}), 1108 (ν_{C-N}) cm^{-1}; ^1H NMR (600 MHz, $CDCl_3$) δ_H 2.07 (s, 2H, -N-**H**), 2.73 (s, 4H, N-C**H**$_2$-C**H**$_2$-N), 3.93 (s, 4H, Ar-C**H**$_2$-NH-), 7.19-7.35 (br m, 10H, Ar-**H**), 7.34 (d, 2H, Ar-**H**, $^3J_{H-H}$ 7.62 Hz) 7.46 (d, 2H, Ar-**H**, $^3J_{H-H}$ 7.00 Hz). ^{13}C NMR (151 MHz, $CDCl_3$) δ_C 14.2 (**C**H_3-CH_2-), 29.2 (CH_3-**C**H_2-), 62.1 (-**C**H_2-**C**H_2-), 125.0 (Ar), 126.1 (Ar), 128.8 (Ar), 130.2 (Ar) 136.0 (Ar-S-) 141.2 (-**C**=N-) ppm.

Synthesis of N^1,N^2-bis(2-(ethylthio)benzyl)ethane-1,2-diamine (L7)

A round-bottomed flask was charged with the imine **L5** (0.257 g, $7.20x10^{-4}$ mol). To this was added degassed methanol (50 ml) to yield a pale-yellow solution. $NaBH_4$ (0.109 g, 0.0028 mmol) was then added as a solid in 4 equal portions over 1 hour whilst stirring at room temperature. Upon the addition of the reducing agent mild effervescence was observed which continued throughout the reaction. TLC analysis was employed to follow the reaction and indicated that the reaction was complete after 48 hours. After 48 hours the solvent was removed by rotary evaporation to yield a white solid crude material. To the crude reaction mixture was added 1M NaOH solution (20 ml). The organics phase was extracted from the aqueous solution with DCM (2 x 20ml). The organic fractions were combined and dried over $MgSO_4$. Filtration to remove the drying agent followed by removal of the solvent via rotary evaporation, yielded **L7** as a colourless oil, which solidified to a white solid upon standing. **L7** was purified by silica gel chromatography using (EtOAc: hexane 5:95) to yield a white solid (0.250, 96% yield).M.p. 38-40°C; IR (ATR) ν= 3300 (ν_{N-H}) cm^{-1}; ^1H NMR (300 MHz, $CDCl_3$) δ_H 1.31 (t, 3H, C**H**$_3$-CH_2-S-), 2.79 (s, 4H, -C**H**$_2$-NH-) 2.94 (q, 3H, -C**H**$_2$-S-,$^3J_{H-H}$ 7.42 Hz), 3.89 (s, 4H, Ar-C**H**$_2$-NH-), 7.14 (t, 2H, Ar-**H**, $^3J_{H-H}$ 7.42 Hz), 7.22 (t, 2H, Ar-**H**, $^3J_{H-H}$ 7.42 Hz) 7.30-7.35 (m, 4H Ar-H) ppm; ^{13}C NMR (75 MHz, $CDCl_3$) δ_C 14.1, 27.4, 48.61, 51.68, 125.55, 127.55, 129.07, 135.64, 139.54 ppm. UV-Vis (DCM) 258, 280 (shoulder) nm. MS (ESI): m/z: 361 $(M+H)^+$.

Synthesis of copper S_2N_2 complex (C5)

A Schlenk tube was charged with the ligand **L7** (0.065 g, 1.80x10^{-4} mol) and dissolved in THF (5 ml) to yield a colourless solution. To this was added copper(II)triflate (0.065 g, 1.80x10^{-4} mol) in a solution of THF (3 ml). The reaction mixture was stirred at room temperature under nitrogen for 8 hours. A colour change from blue to purple was observed within the first hour. After 8 hours the reaction was stopped and the THF solvent removed under reduced pressure. The crude product was dissolved in DCM and filtered through a syringe filter to remove unreacted metal precursor. The filtrate was then concentrated to about 5 ml. Diethyl ether (20 ml) was added and a purple blue solid formed. The solid was isolated by filtration and washed with Et_2O. Subsequent drying under vacuum yielded **C5** as a purple solid (0.093 g, 72% yield). IR (ATR) ν= 3275(ν_{N-H}), 1253 (ν_{C-F}), 1225 (asymmetric $\nu_{S=O}$), 1141 (symmetric $\nu_{S=O}$), 1027(ν_{S-O}), cm^{-1}; Raman (532 nm) ν= 760(ν_{C-S}) UV-Vis (DCM) λ_{max} 242, 274, 280 354, 577 nm; MS (ESI): m/z 423 $(M+H)^+$; Anal.calcd for $C_{22}H_{28}CuF_6N_2O_6S_4 \cdot H_2O$: C (35.69), H (4.08), N (3.78), Found: C (35.67), H (3.93), N (3.86).

Synthesis of cobalt S_2N_2 complex (C6)

A round bottomed flask was charged with a solution of **L7** (0.146 g 0.405 mmol) in ethanol (10 ml). To this was added a solution of $CoCl_2$ (0.053 g 0.408 mmol) in ethanol Upon addition of the $CoCl_2$ solution a colour change was observed to purple pink. The reaction mixture was refluxed for 2 hours. A purple-pink precipitate formed almost immediately. After 2 hours the reaction mixture was cooled and filtered to remove the pink-purple precipitate. The filter was washed with ethanol (2 x 10 ml) and dried under vacuum to yield a pink-purple solid (0.148 g, 75% yield). IR (ATR) ν:3271 (ν_{N-H}), 1142 (ν_{C-N}) cm^{-1}; Raman (532 nm): 790 (ν_{C-S}) cm^{-1}; UV-Vis (DCM) λ_{max} 260, 582, 663 nm; MS (ESI) m/z 490 $(M+H)^+$; Anal.calcd for $C_{20}H_{28}Cl_2CoN_2S_2$: C (48.98), H (5.75), N (5.71) Found: C (48.49), H (5.94), N (5.96).

Synthesis of C7

Prepared as described for **C5**. Isolated in 76% yield as a light green solid. IR (ATR) ν:3271(ν_{N-H}), 1142 (ν_{C-N}) cm^{-1}; Raman (532 nm): 910 (ν_{C-S}) cm^{-1}; UV-Vis (DCM) λ_{max}

300, 430 nm. MS (ESI): m/z 519 $(M+H)^+$; Anal.calcd for $C_{30}H_{32}CuF_6N_2O_8S_4$: C (42.17), H (3.78), N (3.28) Found: C (41.91), H (3.82), N (3.33).

Synthesis of D4

Prepared as described for **L4** from **A1** and DAB-PPI dendrimer generation 1. Isolated as a yellow oil in 84% yield. IR (ATR) ν:1633 ($\nu_{C=N}$); ^{1}H NMR (600 MHz, $CDCl_3$) δ_H 1.36 (br, 4H, -N-CH_2-C**H$_2$**-C**H$_2$**-CH_2-N-), 1.73 (p, 8H, -N-CH_2-C**H$_2$**-CH_2-, 7.03 Hz), 2.34(t, 4H, -N-C**H$_2$**-CH_2-CH_2-C**H$_2$**-N-) 2.43 (t, 8H, N-C**H$_2$**-), 3.54 (t, 8H, -C=N-C**H$_2$**-, $^3J_{H-H}$ 7.03 Hz) (br, 4H, N-**H**), 7.15-7.28 (24H, overlapping Ar-**H**) 7.92-7.98 (m, 4H, Ar-**H**), 8.73 (s, 4H, -**H**C=N-) ppm; ^{13}C NMR (75 MHz, $CDCl_3$) δ_C 26.0 (-CH_2-**C**H_2-**C**H_2-CH_2-), 29.8 (-N-CH_2-**C**H_2-CH_2-N-), 53.1 (-C=N-**C**H_2-), 54.5 (-N-**C**H_2-), 55.5(-N-**C**H_2-CH_2-CH_2-**C**H_2-N-), 126.9 (Ar), 127.1 (Ar), 129.1(Ar), 129.9 (Ar), 131.1(Ar), 131.5 (Ar), 136.1 (Ar), 139.1 (Ar), 159.1 (-H**C**=N-) ppm; MS(ESI): m/z 1100 $(M+H)^+$.

Synthesis of D5

Prepared as described for **L5** from **A2** and DAB-PPI dendrimer generation 1. Obtained as a yellow oil in 82 % yield. ^{1}H NMR (600 MHz, $CDCl_3$) δ_H 1.27 (t, 12H, -CH_3, $^3J_{H-H}$ 7.03 Hz), 1.44 (4H, N-CH_2-C**H$_2$**-C**H$_2$**-CH_2-N), 1.85 (p, N-CH_2-C**H$_2$**-CH_2-N, 8H, $^3J_{H-H}$ 7.02 Hz), 2.54 (t, 8H, -HN-C**H$_2$**-, $^3J_{H-H}$ 7.03 Hz), 2.87 (q, 8H, CH_3-C**H$_2$**-, $^3J_{H-H}$ 7.02 Hz) 3.67 (t, 8H,-C=N-C**H$_2$**-), 7.20-7.24 (m, 8H, Ar), 7.30-7.39 (m, 4H, Ar) 7.89 (d, 4H, Ar, $^3J_{H-H}$ 8.20 Hz) ppm; ^{13}C NMR (75 MHz, $CDCl_3$) δ_C 14.2 (CH_3), 25.1 (N-CH_2-**C**H_2-**C**H_2-CH_2-N), 28.4(CH_3-**C**H_2-), 28.7(N-CH_2-**C**H_2- CH_2-N), 51.7 (-HC=N-**C**H_2-), 54.1 (-N-**C**H_2-) 59.9 (-N-**C**H_2-CH_2-CH_2-**C**H_2-N-), 129.5 (Ar), 127.9 (Ar), 130.2 (Ar) 130.5 (Ar), 136.1 (Ar), 136.9 (Ar), 159.3 (-H**C**=N) ppm; MS(ESI): m/z 909 $(M+H)^+$.

Synthesis of D6

Prepared as described for **L6** as a yellow oil in 90% yield. ^{1}H NMR (300 MHz, $CDCl_3$) δ_H 1.30 (br, 4H, -N-CH_2-C**H$_2$**-C**H$_2$**-CH_2-N-), 1.69 (p, 8H, -N-CH_2-C**H$_2$**-CH_2-, $^3J_{H-H}$ 7.03 Hz), 2.30 (t, 4H, -N-C**H$_2$**-CH_2-CH_2-C**H$_2$**-N-), 2.55 (t, 8H, N-C**H$_2$**-), 3.92 (s, 8H, Ar-**H$_2$**C-N-CH_2-), 7.05-7.15 (24H, overlapping Ar-**H**), 7.65-7.70 (m, 4H, Ar-**H**) ppm; ^{13}C NMR (75 MHz, $CDCl_3$) δ_C 26.0 (-CH_2-**C**H_2-**C**H_2-CH_2-), 29.9 (-N-CH_2-**C**H_2-CH_2-N-) 36.5 (-Ar-**C**H_2-N-CH_2-), 51.1 (Ar-**C**H_2-NH-), 52.2 (-N-CH_2-), 56.0 (-N-**C**H_2-CH_2-CH_2-**C**H_2-N-), 123.3 (Ar), 123.4 (Ar), 126.2 (Ar), 127.2 (Ar), 130.0 (Ar), 131.2 (Ar), 131.6 (Ar), 133.2 (Ar), 133.6 (Ar), 134.5 (Ar) ppm; MS(ESI): m/z 1109 $(M+H)^+$.

Synthesis of D7

Prepared as described for **L7**. Obtained as a light-yellow oil in 92% yield ^{1}H NMR (600 MHz, $CDCl_3$) δ_H 1.27(t, 12H, -CH_3, 7.03 Hz) 1.33 (4H, N-CH_2-C**H$_2$**-C**H$_2$**-CH_2-N), 1.61 (p, 8H N-CH_2-C**H$_2$**-CH_2-N, $^{3}J_{H-H}$ 7.03 Hz). 2.34 (br, 4H, N-**H**), 2.42 (t, 8H,HN-CH_2-CH_2-C**H$_2$**-N-,$^{3}J_{H-H}$ 6.44 Hz), 2.59 (t, 8H, HN-C**H$_2$**-, $^{3}J_{H-H}$ 7.03 Hz), 2.87-2.91 (8H, S-C**H$_2$**-), 3.82 (s, 8H HN-C**H$_2$**-Ar) 7.09-7.18 (m, 4H, overlapping Ar-**H**), 7.15-7.18 (m, 4H, Ar-**H**) 7.25-7.28 ppm (m, 8H, overlapping Ar-**H**); ^{13}C NMR (151 MHz, $CDCl_3$) δ_C 14.1 (-S-CH_2-**C**H_3), 24.8 (-N-CH_2-**C**H_2-**C**H_2-N-), 27.3 (-S-**C**H_2-CH_3), 47.8 (-**C**H_2-NH-CH_2-Ar), 51.9(-N-CH_2-**C**H_2-**C**H_2-N-), 52.1 (-N-**C**H_2-), 53.9 (Ar-**C**H_2-NH-), 125.5 (Ar), 127.3 (Ar), 128.3 (Ar) , 129.0 (Ar), 135.5(Ar-C-S-), 139.4 (Ar-S) ppm; MS(ESI): m/z 917 $(M+H)^{+}$.

Synthesis of MD6

Prepared as described for **C5** from **D7** (0.200 g, 0.218 mmol) and Cu(OTf) (0.157 g, 0.109 mmol). Isolated in 67% yield (0.196 g) as a hygroscopic dark green solid. IR (ATR) ν = IR (ATR) ν = 3270(ν_{N-H}), 1253 (ν_{C-F}), 1225 (asymmetric $\nu_{S=O}$), 1145 (symmetric $\nu_{S=O}$), 1027(ν_{S-O}), cm^{-1}; UV-Vis (DCM) λ_{max} 240, 272, 280 355, 530 nm; MS (ESI): m/z 1043 $(M+H)^{+}$; Anal.calcd for $C_{56}H_{80}Cu_2F_{12}N_6O_{12}S_8 \cdot 4H_2O$ C (39.27), H (5.18), N(4.91), Found: C (38.7), H (5.40), N (4.80).

Table 10: Crystallographic data and structure refinement parameters for complexes C5 and C7

Parameter	**C5**	**C7**
Empirical formula	$C_{22}H_{28}CuF_6N_2O_6S_4$	$C_{30.39}H_{32.77}Cl_{0.77}CuF_6N_2O_8S_4$
Mr (g/mol)	722.24	887.05
Crystal system	Triclinic	Triclinic
Space group	*P-1*	*P-1*
a (Å)	9.7461(7)	7.8587(13)
b (Å)	12.4780(9)	13.537(2)
c (Å)	13.1803(9)	18.336(3)
α (deg)	91.533(4)	110.791(3)
β (deg)	111.454(4)	96.349(3)
γ (deg)	90.761(5)	93.086(3)
Volume (Å^3)	1490.83(19)	1803.3(5)
Z	2	2
D_{calc} (g/cm^3)	1.609	1.634
F(000)	738	906
λ (MoK_a) (Å)	0.71073	0.71073
Temperature (K)	100(2)	100(2)
2*θ* min (deg)	1.633	2.338
2*θ* max (deg)	27.102	27.103
absorption corrections applied (mm^{-1})	1.090	0.977
Goodness-of-fit on F^2	1.056	1.029
Final R_1 indices [$I>2\sigma(I)$]	0.0538	0.0380
wR_2 (all reflections)	0.1277	0.0888

2.7 References

1 M. Sono, M. P. Roach, E. D. Coulter and J. H. Dawson, *Chem. Rev.*, 1996, **96**, 2841–2888.

2 G. E. Oosterom, J. N. H. Reek, P. C. J. Kamer and P. W. N. M. van Leeuwen, *Angew. Chem. Int. Ed. Engl.*, 2001, **40**, 1828–1849.

3 S. M. Grayson and J. M. J. Frechet, *Chem. Rev.*, 2001, **101**, 3819–3868.

4 E. Buhleier, W. Wehner and F. Vögtle, *Synthesis*, 1978, 155–158.

5 D. A. Tomalia, H. Baker, J. Dewald, M. Hall, G. Kallos, S. Martin, J. Roeck, J. Ryder and P. Smith, *Polym. J.*, 1985, 17, 117–132.

6 C. J. Hawker and J. M. J. Frechet, *J. Am. Chem. Soc.*, 1990, **112**, 7638–7647.

7 S. Svenson and D. A. Tomalia, *Adv. Drug Deliv. Rev.*, 2012, **64**, 102–115.

8 M. S. Diallo, S. Christie, P. Swaminathan, J. H. Johnson and W. A. Goddard, *Environ. Sci. Technol.*, 2005, **39**, 1366–77.

9 K. Wichmann, B. Antonioli, T. Söhnel, M. Wenzel, K. Gloe, K. Gloe, J. R. Price, L. F. Lindoy, A. J. Blake and M. Schröder, *Coord. Chem. Rev.*, 2006, **250**, 2987–3003.

10 J. Villa and A. Warshel, *J. Phys. Chem. B*, 2005, **109**, 692–704.

11 C. Francavilla, F. V. Bright and M. R. Detty, *Org. Lett.*, 1999, **1**, 1043–1046.

12 T. Mizugaki, M. Ooe, K. Ebitani and K. Kaneda, *J. Mol. Catal. A Chem.*, 1999, **145**, 329–333.

13 A. W. Kleij, R. A. Gossage, J. T. B. H. Jastrzebski, J. Boersma and G. Van Koten, *Angew. Chem. Int. Ed. Engl.*, 2000, **3**, 176–178.

14 P. G. Cozzi, *Chem. Soc. Rev.*, 2004, **33**, 410–21.

15 A. R. Silva, T. Mourão and J. Rocha, *Catal. Today*, 2013, **203**, 81–86.

16 J. Tang, P. Gamez and J. Reedijk, *Dalton Trans.*, 2007, 4644–4646.

17 S. Guieu, F. Cardona, J. Rocha and A. M. S. Silva, *New J. Chem.*, 2014, **38**, 5411–5414.

18 S. Liu, H. Sun, Y. Ma, S. Ye, X. Liu, X. Zhou, X. Mou, L. Wang, Q. Zhao and W. Huang, *J. Mater. Chem.*, 2012, **22**, 22167–22173.

19 H. Oie, A. Sudo and T. Endo, *J. Polym. Sci. Part A Polym. Chem.*, 2011, **49**, 3174–3183.

20 A. Yada, W. Liao, Y. Sato and M. Murakami, *Angew. Chemie - Int. Ed.*, 2017, **56**, 1073–1076.

21 J. Martinovic, A. M. Chiorcea-Paquim, V. C. Diculescu, J. Van Wyk, E. Iwuoha, P. Baker, S. Mapolie and A. M. Oliveira-Brett, *Electrochim. Acta*, 2008, **53**, 4907–4919.

22 S. F. Mapolie and J. L. van Wyk, *Inorganica Chim. Acta*, 2013, **394**, 649–655.

23 G. S. Smith, *An investigation into the synthesis, characterization and some applications of novel metal-containing polymers and dendrimers of transition metals. PhD Thesis. University of the Western Cape, 2003. https://etd.uwc.ac.za/handle/11394/1681*.

24 A. C. Gomes, S. M. Bruno, S. Gago, R. P. Lopes, D. A. MacHado, A. P. Carminatti, A. A. Valente, M. Pillinger and I. S. Gonalves, *J. Organomet. Chem.*, 2011, **696**, 3543–3550.

25 S. Karlsson, J. Lindberg and H. Sörensen, *Org. Process Res. Dev.*, 2013, **17**, 1552–1560.

26 G. Smith, R. Chen and S. Mapolie, *J. Organomet. Chem.*, 2003, **673**, 111–115.

27 G. J. P. Britovsek, J. England, S. K. Spitzmesser, A. J. P. White and D. J. Williams, *Dalt. Trans.*, 2005, 945–955.

28 Y. Nakayama, Y. Baba, H. Yasuda, K. Kawakita and N. Ueyama, *Macromolecules*, 2003, **36**, 7953–7958.

29 C. R. K. Glasson, J. K. Clegg, J. C. McMurtrie, G. V. Meehan, L. F. Lindoy, C. A. Motti, B. Moubaraki, K. S. Murray and J. D. Cashion, *Chem. Sci.*, 2011, **2**,

540–543.

30 F. Pelascini, M. Wesolek, F. Peruch, A. De Cian, N. Kyritsakas, P. J. Lutz and J. Kress, *Polyhedron*, 2004, **23**, 3193–3199.

31 M. A. Peck, G. R. Hearne, C. Obuah and J. Darkwa, *Phys. Chem. Chem. Phys.*, 2018, **20**, 11682–11691.

32 T. H. Nguyen, P. J. Shannon and P. E. Hoggard, *Inorganica Chim. Acta*, 1999, **291**, 136–141.

33 S. E. Howson, L. E. N. Allan, N. P. Chmel, G. J. Clarkson, R. J. Deeth, A. D. Faulkner, D. H. Simpson and P. Scott, *Dalt. Trans.*, 2011, **40**, 10416–10433.

34 J. M. Dragna, G. Pescitelli, L. Tran, V. M. Lynch, E. V. Anslyn and L. Di Bari, *J. Am. Chem. Soc.*, 2012, **134**, 4398–4407.

35 S. Shaik, M. Filatov, D. Schröder and H. Schwarz, *Chem. - A Eur. J.*, 1998, **4**, 193–199.

36 M. Andrés, M. Bravo, M. A. Buil, M. Calbet, M. Castillo, J. Castro, P. Eichhorn, M. Ferrer, M. D. Lehner, I. Moreno, R. S. Roberts and S. Sevilla, *Eur. J. Med. Chem.*, 2014, **71**, 168–184.

37 D. E. Fenton, G. P. Westwood, A. Bashall, M. McPartlin and I. J. Scowen, *J. Chem. Soc. Dalt. Trans.*, 1994, 2213.

38 P. Bhattacharyya, J. Parr and A. M. Z. Slawin, *J. Chem. Soc. Dalt. Trans.*, 1998, 3263–3268.

39 L. F. Lindoy, *Q. Rev. Chem. Soc.*, 1971, **25**, 379–391.

40 W. Park, M. H. Shin, J. H. Chung, J. Park, M. S. Lah and D. Lim, *Tetrahedron Lett.*, 2006, **47**, 8841–8845.

41 R. R. Fernandes, J. Lasri, A. M. Kirillov, M. F. C. Guedes da Silva, J. A. L. da Silva, J. J. R. Fraústo da Silva and A. J. L. Pombeiro, *Eur. J. Inorg. Chem.*, 2011, 3781–3790.

42 J. Valdés-Martínez, R. A. Toscano and J. Ramirez-Ortíz, *Polyhedron*, 1995, **14**, 579–583.

43 W. J. Geary, *Coord. Chem. Rev.*, 1971, **7**, 81–122.

44 C. S. Kraihanzel and S. C. Grenda, *Inorg. Chem.*, 1965, **4**, 1037–1042.

45 D. F. Evans, *J. Chem. Soc.*, 1959, 2003–2005.

Chapter 3: The Effect of Cobalt Salicylaldimine and Iron Pyridine-Imine Complexes on Oxidant Decomposition, Mechanistic and Kinetic Aspects

3.1 Introduction to the oxidation reactions of transition metals with peroxide oxidants

The use of peroxide based oxidants such as hydrogen peroxide (H_2O_2) and *tert*-butyl hydroperoxide (TBHP, or *t*BuOOH) are ubiquitous in the study of catalytic hydrocarbon oxidation reactions.[1–4] However, as was discussed in Chapter 1, the mechanistic aspects of the reactions of metal complexes with commonly employed oxidants can be quite complex and difficult to study. This has resulted in extensive discourse (as discussed in Chapter 1) in the chemical literature, concerning the mechanism of various catalytic systems employed in oxidation reactions.[5] In Chapter 1, the two common mechanisms of the reaction of an oxidant (such as hydrogen peroxide) with a transition metal catalyst were mentioned briefly. The first of these involve a situation where the transition metal induces homolytic cleavage in the peroxide (oxidant). (Scheme 1, Reaction 1) while the second mechanism entails heterolytic cleavage of O-O bonds (Scheme 1, Reaction 2).

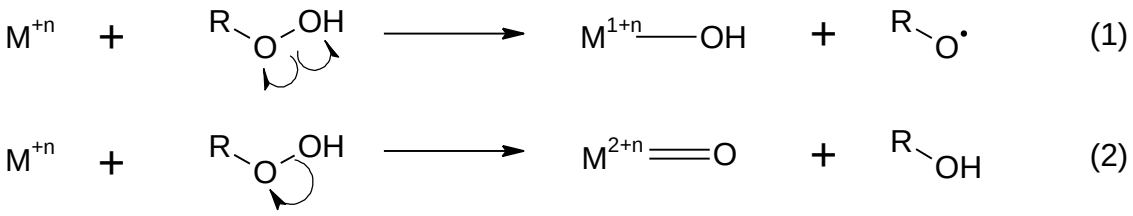

Scheme 1: Reaction of a metal complex (M^{n+}) with a peroxide-based oxidant

Many factors influence the mechanism by which the reactions in Scheme 1 occur and it is virtually impossible to predict (for new systems) whether homolytic or heterolytic cleavage of an oxidant will occur for a particular system. The high reactivity and poor stability of the formed M^{n+1} or the M^{n+2} species are among these factors.[6, 7] Careful choice of the ligand present in a complex of M^{n+} will play an important role in stabilizing the high oxidation states of a potential M^{n+2} species.[8] Furthermore, some catalyst systems have been reported in the literature that seemingly operate simultaneously via both mechanistic pathways identified above.[9]

Many of the catalyst precursors discussed in Chapter 1 are likely to operate via the pathway depicted in Reaction 1 (Scheme 1). Consequently, the generation of a free radical species and the subsequent reaction of this radical species with the hydrocarbon substrate is responsible for oxidative transformation of the organic substrate.

However there exists another possible reaction *viz*. the decomposition of the oxidant by the metal complex to H_2O and O_2 (Scheme 2) in a catalase-like process.[10]

$$2H_2O_2 \xrightarrow{[TM\ Catalyst]} 2H_2O + O_2$$

Scheme 2: Metal mediated decomposition reaction of hydrogen peroxide to oxygen and water[10]

This phenomenon and its impact on catalytic oxidation reactions is, however, much less studied.

In this chapter the catalytic decomposition of oxidants such as hydrogen peroxide in the presence of several synthesized metal complexes (reported in Chapter 2) are investigated. Various analytical techniques are employed in an attempt to identify intermediates formed during these reactions. The nature of such intermediates could potentially aid in determining the mechanism by which (hydroxyl radical formation, decomposition to oxygen or metal-oxo formation) potential oxidation reactions could occur.

3.2 Metal-oxo compounds as catalysts in oxidation reactions

Metal-oxo complexes have been identified as active oxidants and catalytically active species in many oxidation processes.[11] Similarly, metal-oxo moieties have been invoked as the active centres in many enzymatic systems such as heme-containing metalloenzymes such as cytochrome P450.[12] These systems operate via the so-called rebound mechanism during which a high valent oxo-iron complex is generated capable of abstracting protons from unsaturated hydrocarbons. Similarly the formation of a high valent Co(IV)-oxo species has been suggested for the synthetic metalloprotein coboglobin and its various analogues.[7, 13]

Isolation of such high valent metal-oxo species is quite rare, possibly due to the instability of the highly charged metal centre. A number of such structures have, however, been isolated and reported. Analytical techniques such as mass spectrometry and Mössbauer spectroscopy as well as UV-Vis spectroscopy have been used in attempts to characterize the metal-oxo intermediates.[14–16]

Many oxidation catalyst systems however operate under a radical mechanism, as was discussed in Chapter 1. The direct detection of the formed radical species is however quite difficult due to their highly reactive and short-lived nature.

Typically, metal-oxo catalysts have proven to be highly selective in hydrocarbon oxidation processes compared to the non-selective radical based oxidations. This observation has spurred research towards discovering non-heme systems capable of forming such desirable metal-oxo intermediates.

In this chapter the reaction of some of the metal complexes reported in Chapter 2 with peroxide oxidants is discussed. Additionally, attempts at characterizing intermediates of these reactions are discussed. Secondly the results of our mechanistic study which could inform our subsequent choice of reaction conditions are also discussed. This is with the aim of employing these complexes as hydrocarbon oxidation catalysts (Chapter 4).

3.3 Electrospray ionization mass spectrometry and UV-Vis spectroscopy aided identification of reaction intermediates

3.3.1 Reaction of cobalt complexes, C1 and MD1 with peroxide oxidants

Mass spectrometry as well as UV-Vis spectroscopy have previously been used by Mitra et al.[14] and Das et al.[17] to shed light on the nature of the oxidizing species in their catalytic oxidation reactions.

With this in mind, we set out to study the reaction of the cobalt salicylaldimine complexes, **C1** and **MD1**, with hydrogen peroxide. Thus, for example a solution of the generation 1 (G1) dendritic complex **MD1** in acetonitrile was treated with an excess of hydrogen peroxide (1:20 metal to peroxide). The ESI mass spectrum of **MD1** before peroxide addition is shown in Figure 1 while Figures 2 and 3 show the spectra after hydrogen peroxide addition.

The mass spectrum of unreacted **MD1** (Figure 1) exhibits the $(M+H)^+$ signal at m/z 847 (indicated by the red arrow) as well as the doubly charged species at m/z 423 while the disodium adduct is observed at m/z 891.

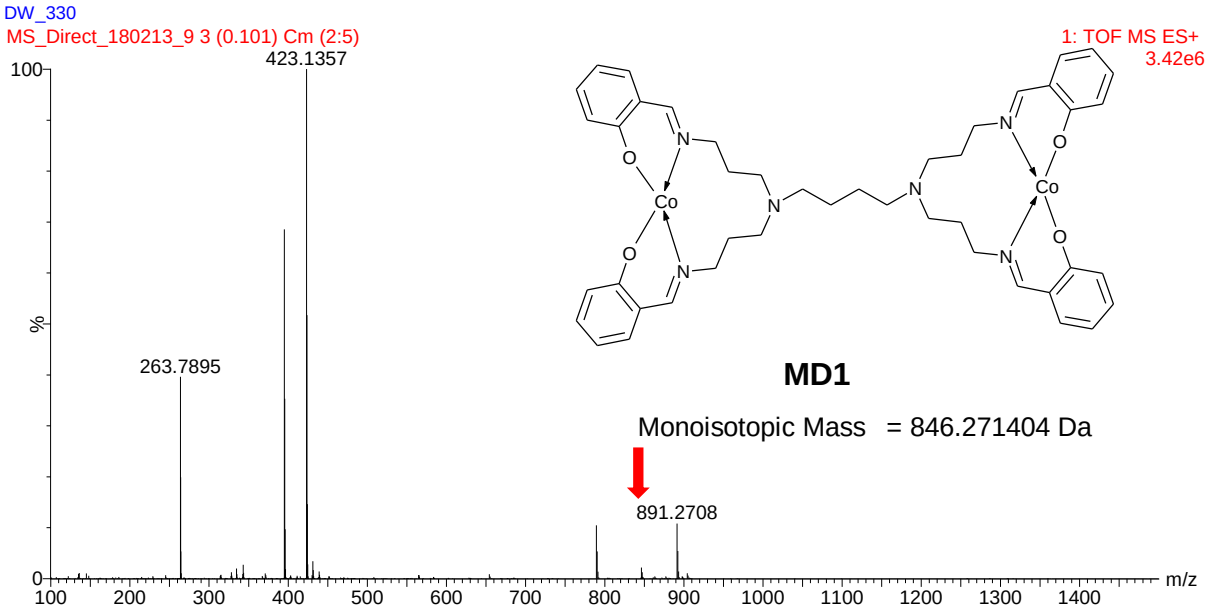

Figure 1:Mass spectrum of Cobalt complex MD1 before the addition of H_2O_2

Upon addition of the hydrogen peroxide solution a gradual colour change from brown to yellow-brown is observed over time. The colour change can be correlated with substantial changes in the mass spectrum of **MD1** (Figure 2). A new signal is observed at m/z 431 while a small cluster of peaks are observed between m/z 850 and 950.

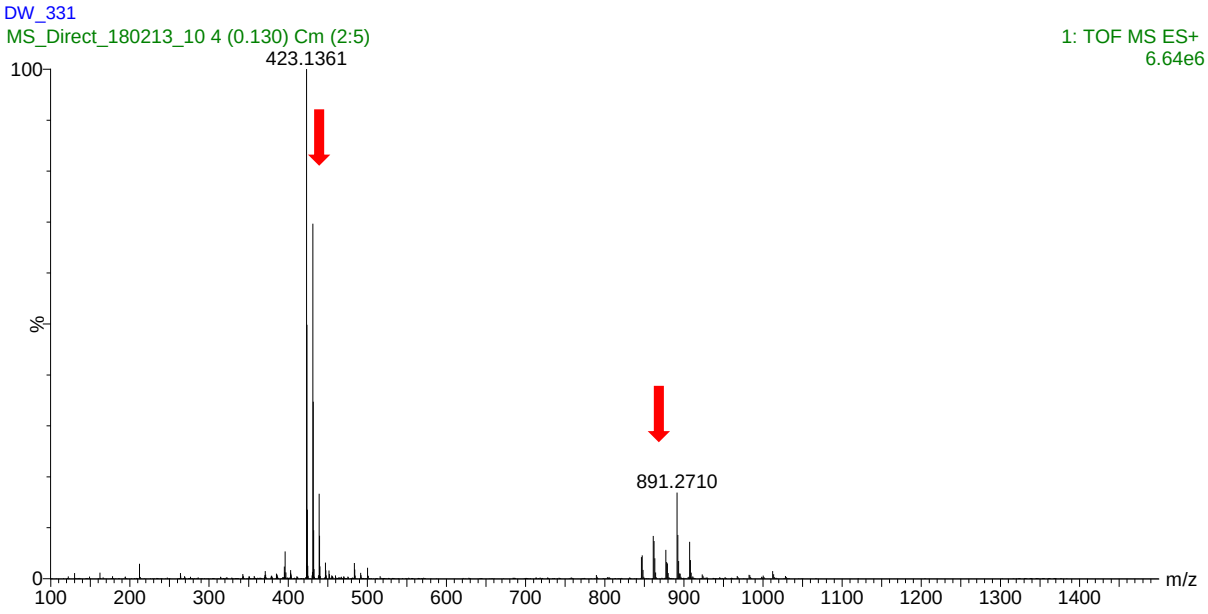

Figure 2: Mass spectrum of MD1 after the addition of H_2O_2

The peak observed at 431 is 8 mass units higher than the doubly charged ion of **MD1** observed at m/z 423. This suggests that incorporation of an oxygen atom into **MD1** is taking place, with the possible formation of a terminal Co-oxo species. Furthermore, new peaks are observed at m/z 923, 907 and 891 coinciding with a mass loss of 16 mass units between each of these ions (Figure 3).

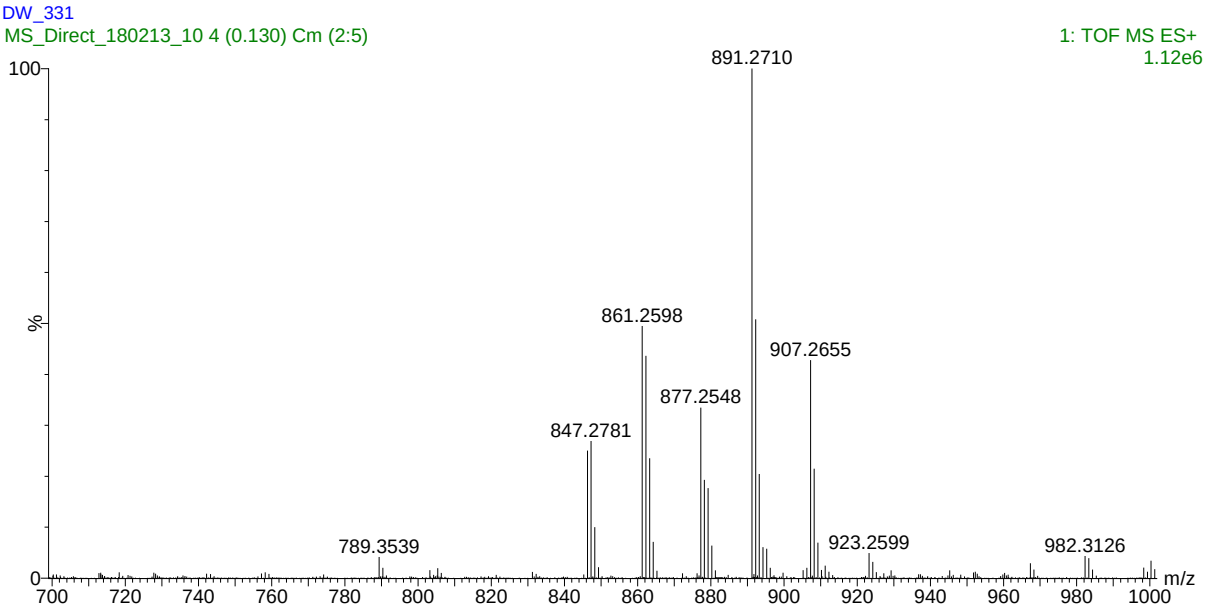

Figure 3: Mass spectrum of MD1 after H_2O_2 addition between m/z 700 and 1000

This result seems to suggest that Co-oxo moieties are being formed under these conditions. The species observed at m/z 907 and 923 could possibly be the disodium adducts of the species shown in Figure 4. Alternatively a performic acid adduct could also form in-situ during the mass spectrometry process (1% formic acid solution used during ionization) as has been observed in the case where a mixture of hydrogen peroxide and acetic acid was used (formation of peracetic acid).[17]

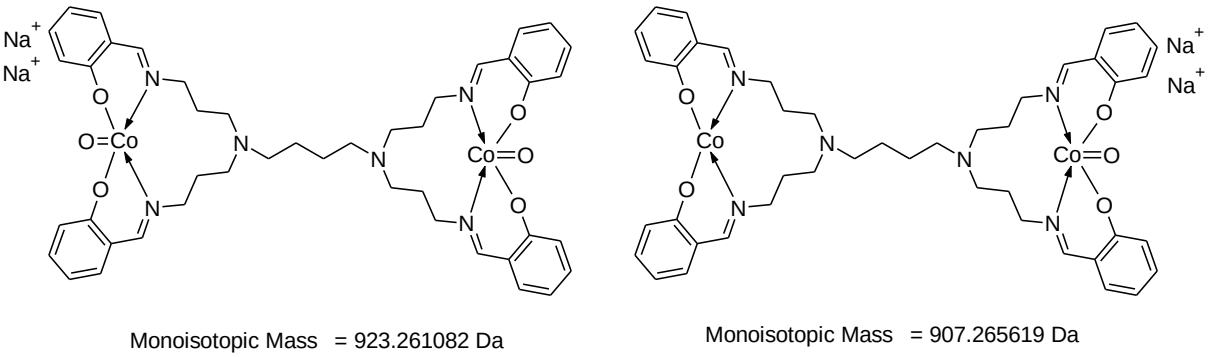

Figure 4: Possible oxygen-containing derivatives of MD1

Encouraged by this result the same experiment was performed using the model cobalt complex **C1** (Scheme 4) along with the oxidants H_2O_2 and TBHP.

The mass spectrum of **C1** before the addition of oxidant exhibits the molecular ion at m/z 383.

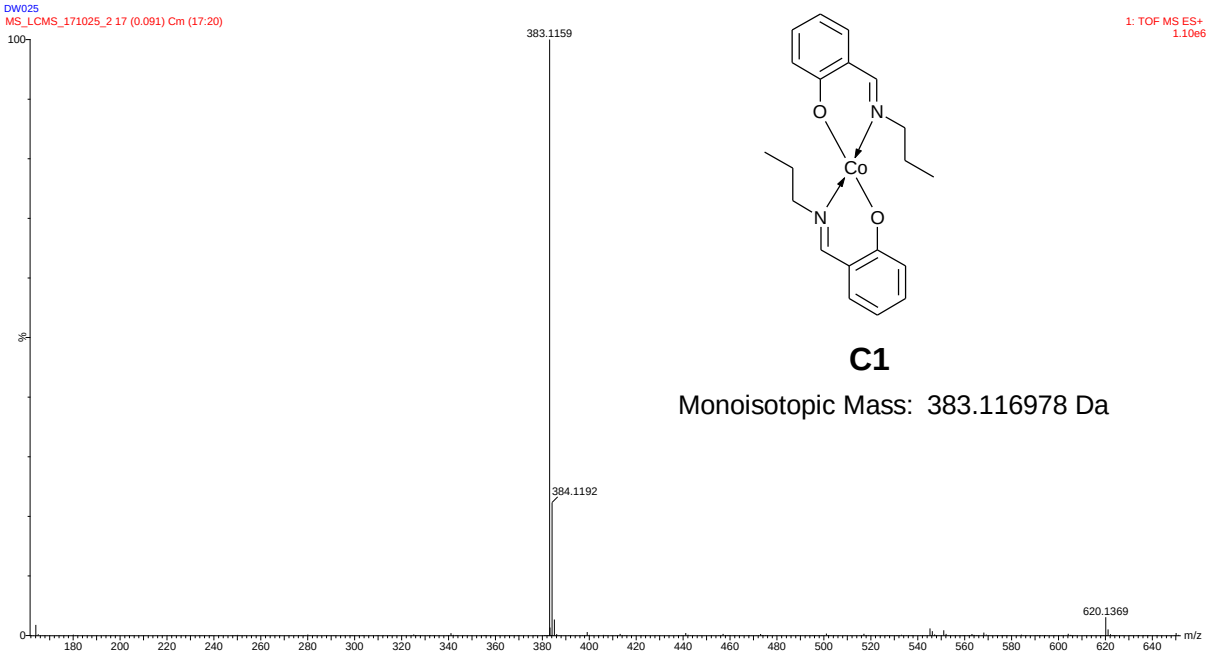

Figure 5: Mass spectrum obtained for C1 before the addition of oxidant

When H_2O_2 (1:20 **C1** to oxidant ratio) is added to **C1**, rapid effervescence of the reaction mixture is observed. The mass spectrum of the obtained reaction mixture was recorded. A number of relatively high mass ions (close to double the mass of **C1**) was observed in the obtained mass spectrum. Abundant signals are also observed between m/z 500 and 710 as shown in Figure 6.

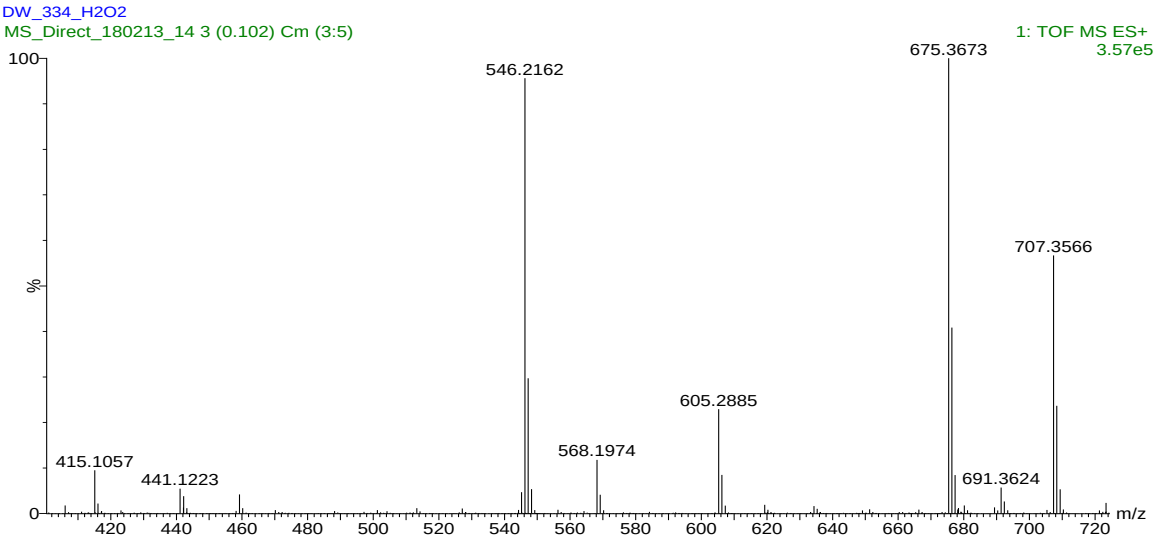

Figure 6: Mass spectrum obtained after the addition of H_2O_2 to C1

The ion observed at m/z 546 is likely an octahedral cobalt species similar to the one shown in Figure 7 (stereochemistry of such a species is unknown). The ion observed at m/z 568 could possibly be the sodium adduct of the species shown in Figure 7.

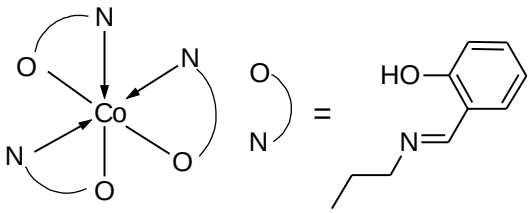

Molecular Formula: $C_{30}H_{37}CoN_3O_3$

Monoisotopic Mass: 546.217241 Da

Figure 7: Potential structure of species formed upon the addition of H_2O_2 to C1

The other signals observed between 605 and 707 have not been unambiguously assigned however it could be that a dimerization process followed by fragmentation (under ESI-MS conditions) takes place which could account for these high m/z ions. However, some information may be gleaned from these high m/z signals. The mass loss between m/z 707, 691 and 675 are 16 mass units, suggesting that possible sequential loss of oxygen atoms is taking place.

When TBHP is used as oxidant instead of H_2O_2 (shown in Figure 8), significant differences are observed compared to the spectrum obtained when H_2O_2 is employed (Figure 6). Again, signals at relatively high m/z values are observed. However, these differ from the signals observed in the previous spectrum, where H_2O_2 was employed (Figure 6). Various signals not present in the mass spectrum of **C1** are observed at m/z 680, 783 and 928 respectively. Identification of the formed species is, again, quite challenging due to possible fragmentation under ESI-MS conditions.

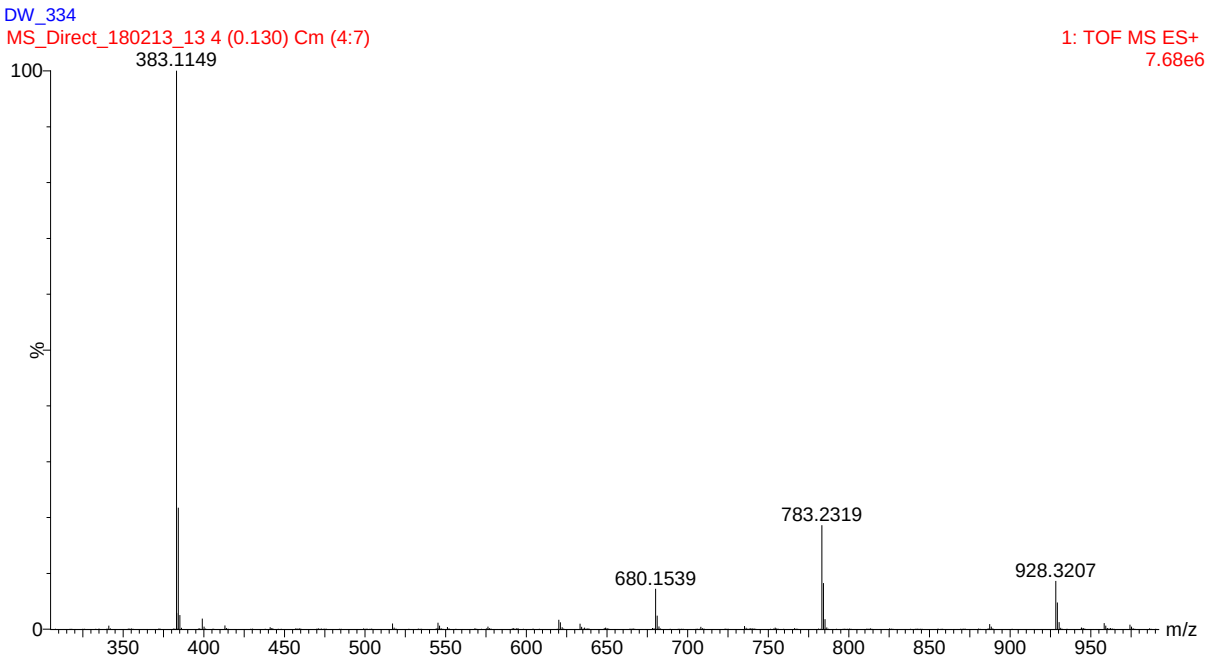

Figure 8: Mass spectrum obtained after addition of TBHP to C1

Tentative assignment of these structures was accomplished by comparison with similar experiments reported in the literature. Mimoun et al. studied the reaction of $Pd(OAc)_2$ with TBHP.[18] Upon addition of TBHP to the metal-containing solution orange crystals started to form. The nature of this species was investigated using single crystal X-ray diffraction and determined to be a multiply peroxy-bridged species, $(CCl_3CO_2PdOO\text{-}t\text{-}Bu)_4$.[18] Turra et al. proposed the formation of μ-hydroxo bridged cobalt dimers in the reaction of cobalt(II) acetylacetonate with TBHP.[19] A number of similar peroxy- and alkoxy-bridged structures are present in the Cambridge Structural Database. Anson et al.[20] reported a number of crystal structures of the general formula $[M_2Co_2(\mu_3\text{-}OtBu)_2(\mu_2\text{-}OtBu)_4]$ where M represents either Na, K or Rb. However, these complexes were obtained by the reaction of cobalt halides with various metal alkoxides

of the formula MO*t*Bu (M= Na, K or Rb) and not under oxidative conditions with TBHP. A similar method was employed by Meyer et al. in the synthesis of $[Co(Al(O\textit{t}Bu)_4)_2]$.[21]

However, a number of terminal cobalt-peroxy structures have been reported under oxidative conditions using TBHP or H_2O_2.[22, 23]

Based on the structures reported in the literature, it is feasible that the species formed during the reaction of **C1** with TBHP could be assigned as either cobalt complexes bearing terminal alkoxy or peroxy moieties or as peroxy/ alkoxy bridged species. The ion observed at m/z 928 can be tentatively assigned as a bridged dimeric complex, the structure of which is presented in Figure 9.

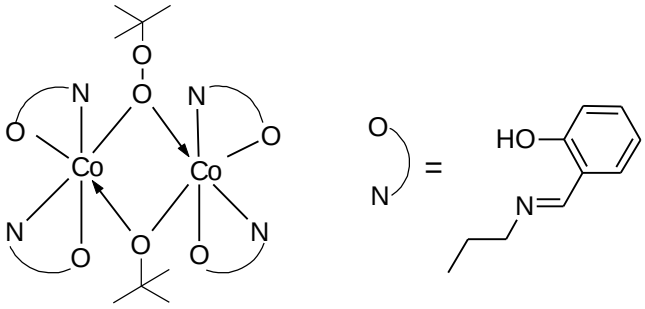

Molecular Formula: $C_{48}H_{66}Co_2N_4O_7$

Monoisotopic Mass: 928.361745 Da

Figure 9: Potential structure of the species observed at m/z 928

The ion at m/z 783 could possibly be assigned as a peroxo-bridged dinuclear cobalt species (Figure 10). In this suggested structure one cobalt centre is coordinated by two N,O salicylaldimine ligands while the other cobalt centre is coordinated by only one N,O salicylaldimine ligand; a N, O ligand is presumably lost under ESI-MS conditions. The two cobalt centres are bridged by two *tert*-butylperoxo ligands.

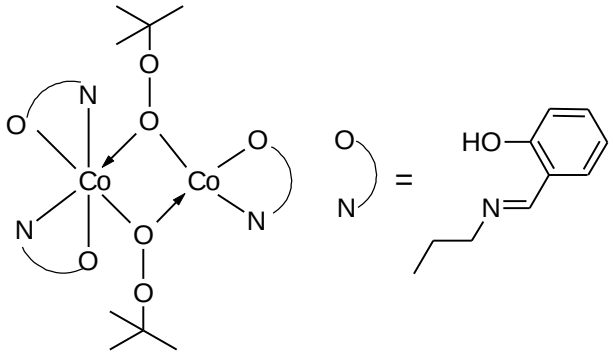

Monoisotopic Mass: 782.264222 Da

Molecular Formula: $C_{38}H_{54}Co_2N_3O_7$

Figure 10: Potential structure of the species observed at m/z 782

Very similar peroxo-bridged structures have been suggested as intermediates in the oxidation of hydrocarbons with TBHP catalysed by analogous copper Schiff base complexes.[24]

Unfortunately, similar experiments could not be performed using **C2** or **MD2**, since upon addition of the oxidant a fine, highly insoluble, precipitate formed which could not be injected into the mass spectrometer. Similar precipitates form during the initial stages of catalytic experiments described in Chapter 4. However, upon completion of the reaction the precipitates are fully dissolved.

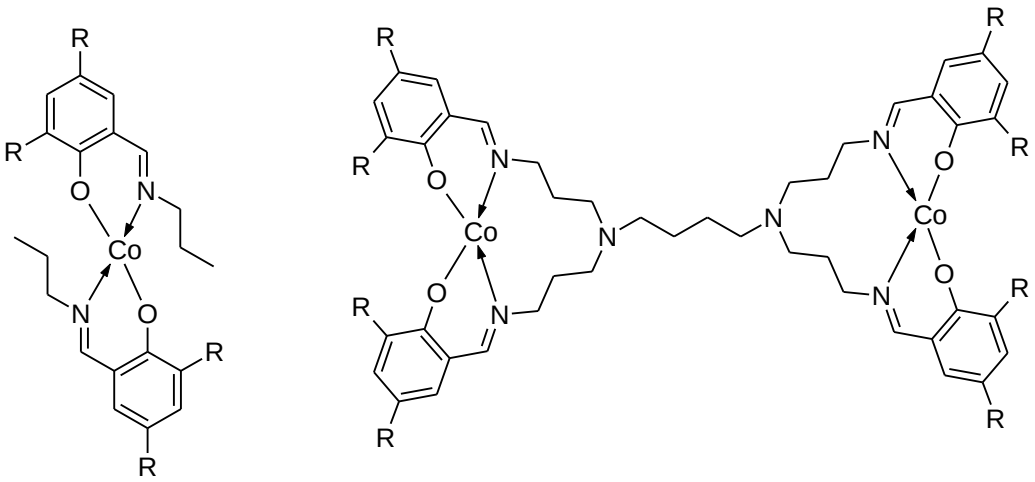

C2 **MD2**

R= *t*-Butyl

Figure 11: Structures of C2 and MD2 that formed precipitates upon addition of oxidant

Previous studies on cobalt-catalysed hydrocarbon oxidation have also utilized UV-Vis spectroscopy in an attempt to characterize the active catalysts/intermediates formed. [7, 13] Thus, we decided to employ UV-Vis spectroscopy to study the interaction of our complexes with the oxidant.

A stock solution of **MD1** in MeCN (1 X 10^{-3} M) was prepared and the UV-Vis spectrum of recorded (Figure 12). Two peaks are observed for **MD1** the first at 240 nm (charge transfer band, omitted for clarity) and the second at 356 nm. The solution was then treated with oxidant, either H_2O_2 or TBHP (in identical molar ratios, 1:20, complex to oxidant). Two minutes after addition of the oxidant another spectrum was recorded. Both the charge transfer band as well as the peak at 356 nm appear to shift towards higher wavenumbers. Over time, the intensity of the peak at 356 nm decreases and a shoulder is formed around 410 nm (compare for instance Figure 12, 1 hour vs Figure 12, 2 mins).

The results of the UV-Vis experiment seem to indicate that a non-reversible change in the coordination environment of the cobalt centre is occurring. The spectral changes observed in Figure 12 are not consistent with the spectral changes reported for the

formation of a Co(IV) species in the literature.[7, 13] It might be that a Co(III) species is formed instead (based on the mechanism shown in Scheme 1).

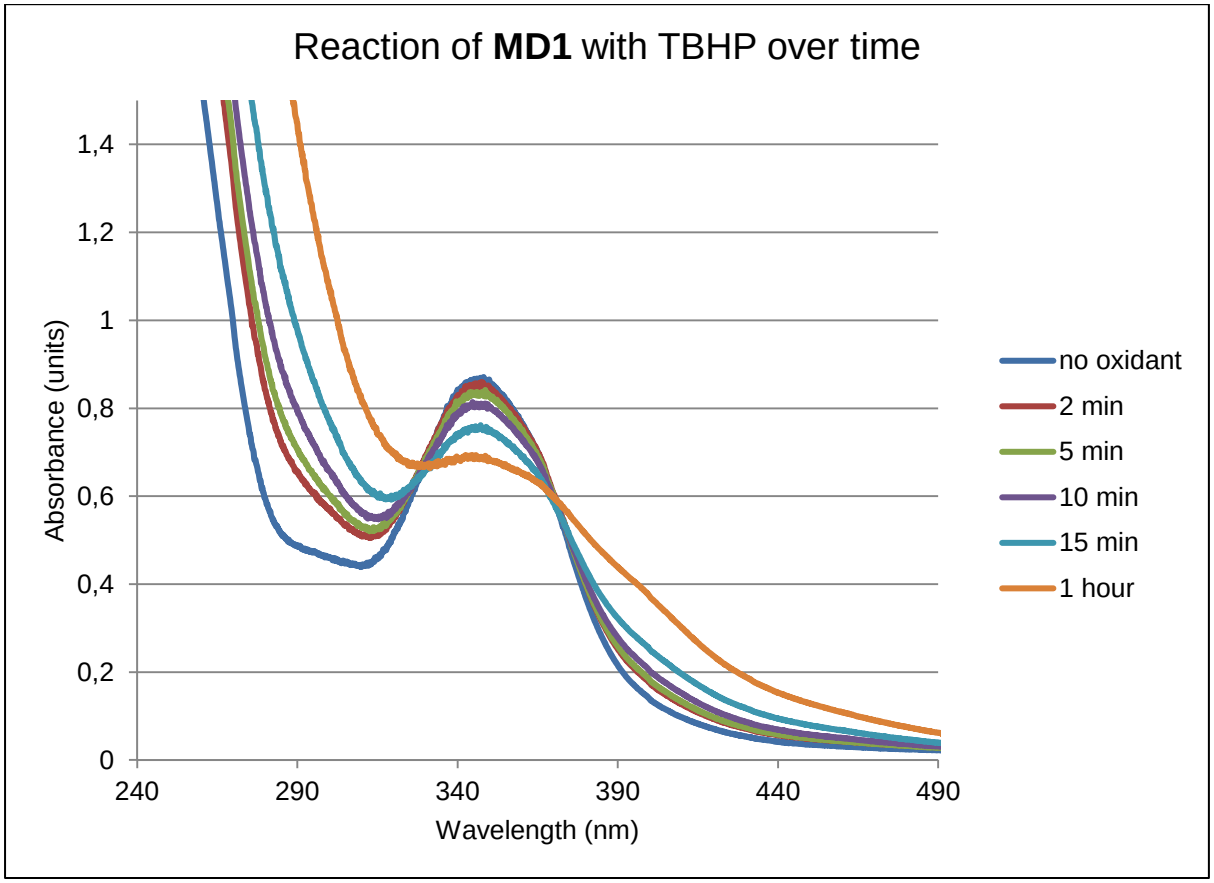

Figure 12: Change in the UV-Vis spectrum of C1 in the presence of TBHP over time (in acetonitrile).

Similar observations were made when UV-Vis spectra were recorded in the presence of H_2O_2. In this case a decrease in intensity of the peak at 350 nm is accompanied with a simultaneous increase of the absorption around 400 nm. Interestingly, this transformation is almost instantaneous in the presence of H_2O_2 (Figure 13) compared to the analogous TBHP reaction, under the same conditions.

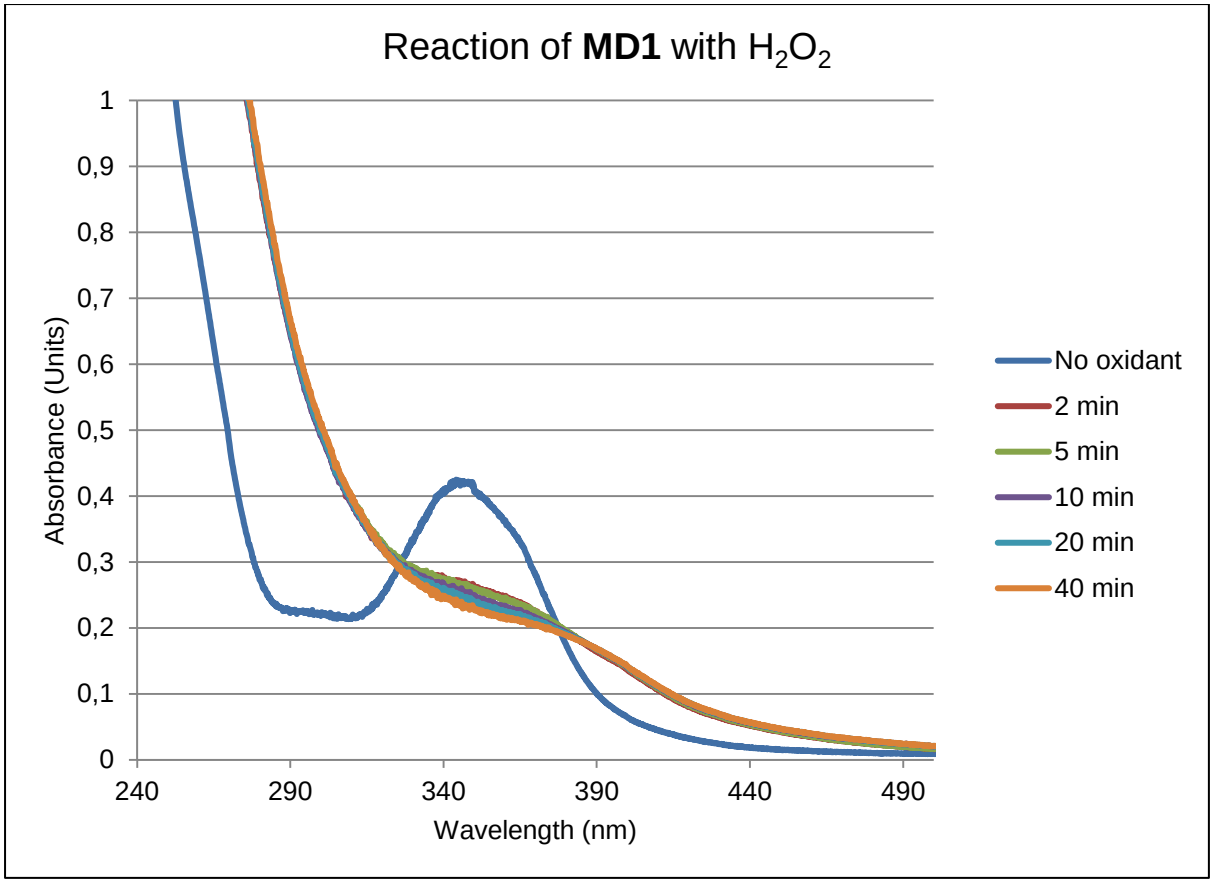

Figure 13: UV-Vis spectrum of the reaction of MD1 with H_2O_2 in MeCN over time

The observed spectral changes (when using either H_2O_2 or TBHP) do not match those reported for the formation of a Co(IV) species,[7, 13] The obtained UV-Vis spectra also do not match those of known isolated bridged cobalt complexes[20], however such species could be unstable and possibly not detected on the UV-Vis spectroscopy timescale. However, the spectra shown in Figures 12 and 13 are similar to the spectra obtained for octahedral Co(III) oxide species (absorption between 400 – 415 nm).[25–27]

Thus, the use of either oxidant leads to the (eventual) formation of a possibly identical species. This transformation appears to occur more quickly when H_2O_2 is employed as oxidant. The formed species is likely a Co(III)-oxide or a Co(III)-hydroxo species, which is consistent with the reaction products shown in Scheme 1, Reaction 1.

3.3.2 Reaction of iron complex C4 with peroxide oxidants

Encouraged by the positive results obtained for the cobalt complexes, **MD1** and **C1**, the reaction of the mononuclear iron complex **C4** with TBHP and H_2O_2 was also investigated using ESI mass spectrometry.

The mass spectrum of **C4**, before the addition of oxidant, is shown in Figure 14.

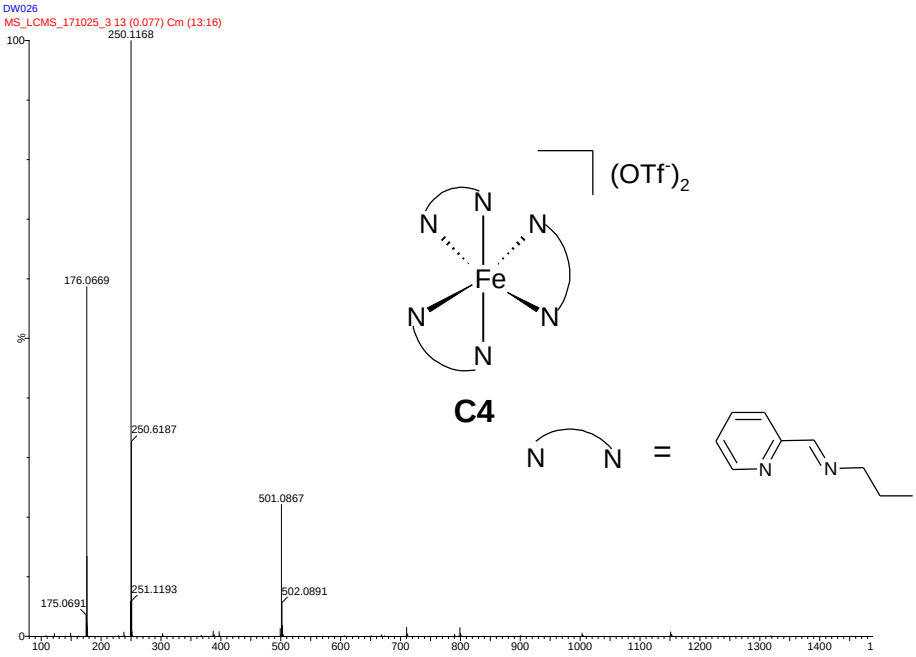

Figure 14: ESI mass spectrum of C4 before the addition of TBHP

The molecular ion of **C4** is observed at m/z 501 while the doubly charged molecular ion of **C4** is observed at m/z 250. TBHP was then added to a solution of **C4** in acetonitrile and the ESI mass spectrum of the oxidation reaction mixture recorded immediately (Figure 15). New signals are observed at m/z 198, 238 and 530 as indicated in Figure 15. The absolute identification of these ions is not possible using only ESI-MS in isolation. However, some useful information may still be gleaned from these spectra.

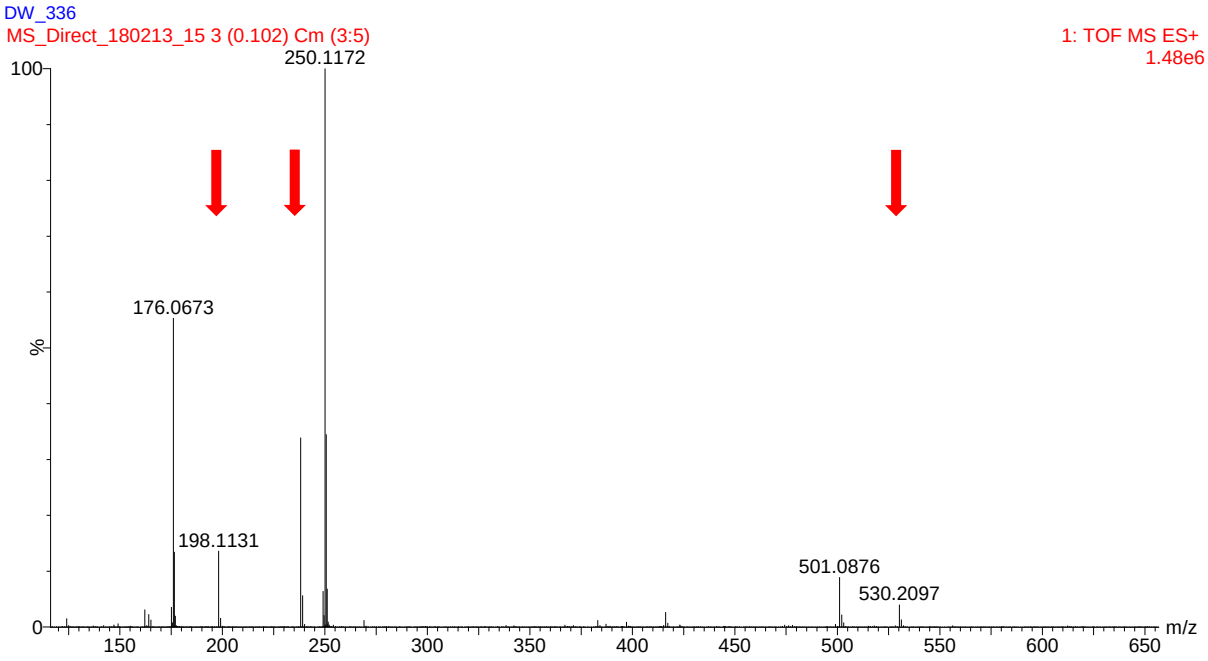

Figure 15: Mass spectrum recorded for the reaction of C4 with TBHP

The signal observed at m/z 198 (Figure 15) has not been identified and could possibly be formed via fragmentation of a more complex ion.

The ion observed at m/z 238 is not doubly charged (isotope signals are more than 0.5 m/z apart), thus it is likely also formed by fragmentation of an oxidized species. This ion could possibly be assigned to the structure proposed in Figure 16 consisting of the iron centre coordinated by a single pyridine-imine ligand and two hydroxyl ligands, the latter generated by homolytic cleavage of the oxidant (Scheme 1). Such a species (containing two hydroxyl groups) has been invoked by Rizkalla et al. in their kinetic model for the decomposition of hydrogen peroxide by EDTA iron complexes.[28]

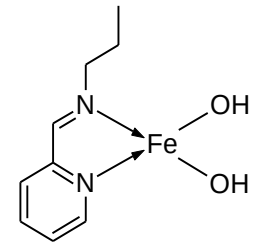

Molecular Formula = $C_9H_{14}FeN_2O_2$
Monoisotopic Mass = 238.04047 Da

Figure 16: Possible structure of species observed at m/z 238

Figure 17 shows the isotopic pattern obtained around m/z 238 as well as the predicted pattern for the species suggested in Figure 16. A fairly close match between the predicted and obtained patterns as well as the literature precedence for such species lends credence to the structure suggested in Figure 16.

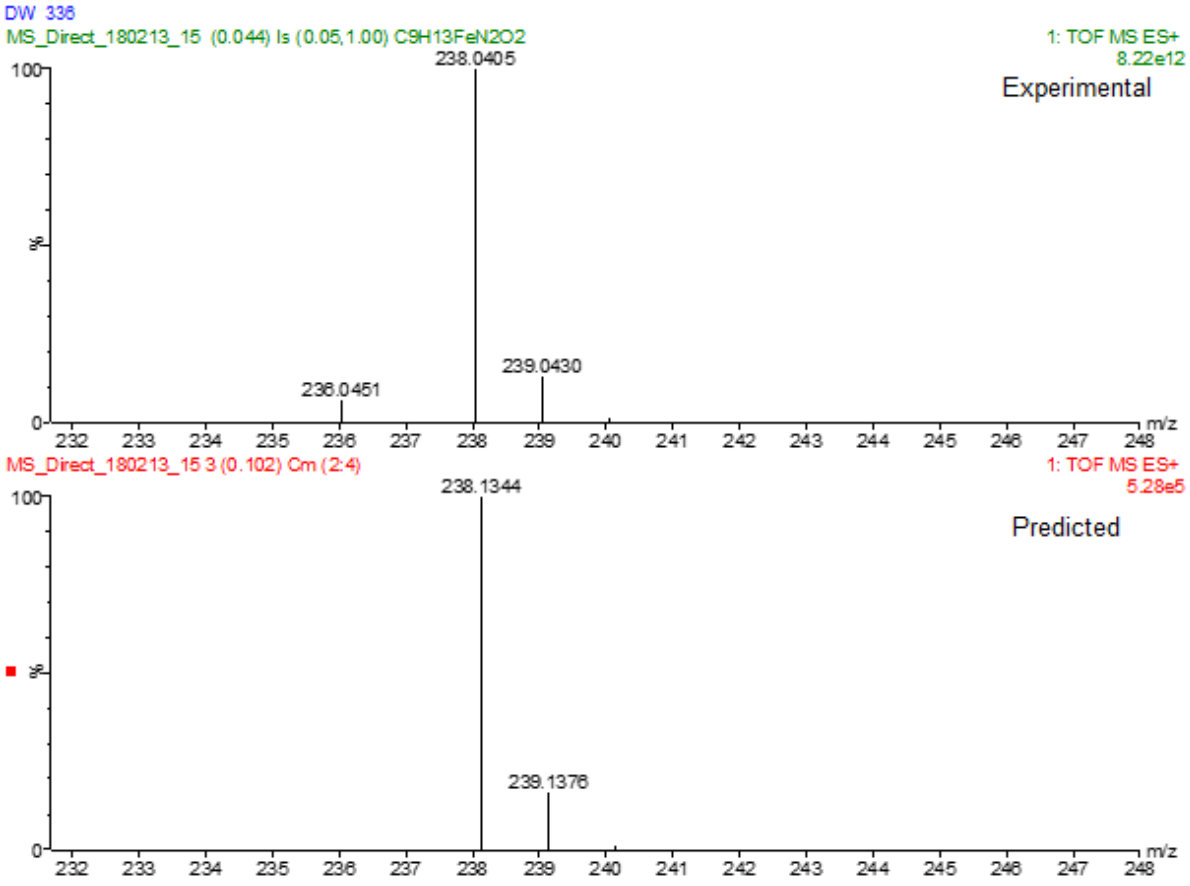

Figure 17: Predicted and obtained isotopic patterns

Figure 15 shows that a new signal is observed at m/z 530 after treatment of the complex with TBHP. The mass loss between the ions observed at m/z 530 and 501 (29 mass units) does not correspond directly to any expected mass loss, such as loss of oxygen (16 mass units or alternatively 32; loss of 2 oxygen atoms). As such, the ion at m/z 530 is probably not generated directly from the parent ion at m/z 501. However, metal-peroxo structures have previously been reported to form under similar oxidative conditions by Nguyen et al. when studying iron complexes.[29] On this basis, the ion observed at m/z 530 could possibly be an iron-peroxo species as proposed in Figure 18.

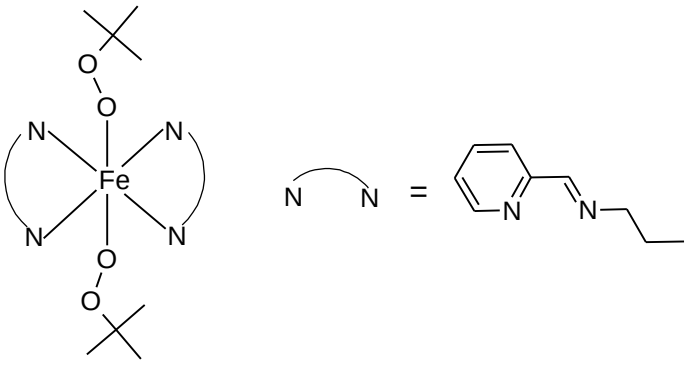

Molecular Formula = $C_{26}H_{42}FeN_4O_4$

Monoisotopic Mass = 530.255548 Da

Figure 18: Proposed structure of the ion observed at m/z 530

If the species observed at m/z 530 contains *tert*-butyl peroxo moieties; as suggested in Figure 18, then the ion observed at m/z 530 (Figure 15) should be absent if the same experiment was performed using H_2O_2 instead of TBHP as oxidant.

Figure 19 shows the ESI mass spectrum obtained when **C4** is reacted with H_2O_2. The signal at m/z 530, observed in Figure 15 (when TBHP oxidant is used), is not observed when H_2O_2 is used. Furthermore, when TBHP is replaced by H_2O_2, under the same experimental conditions, severe fragmentation is observed in the ESI mass spectrum (Figure 19).

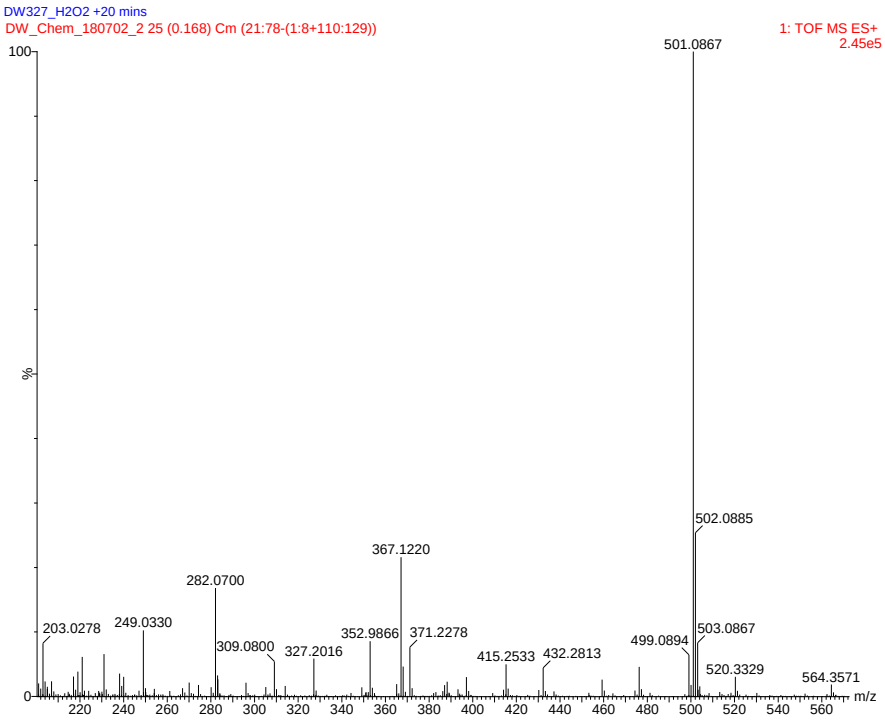

Figure 19: ESI mass spectrum of the reaction of C4 with H_2O_2

When employing H_2O_2 as oxidant, the molecular ion is still observed at m/z 501. Most of the other ions are quite difficult to assign due to extensive fragmentation coupled with adduct formation. The ion at m/z 564 is likely a $(M + MeCN + Na)^+$ adduct. A potential hydroxy analogue with the structure suggested in Figure 20 is observed around m/z 386, albeit in very low abundance (Figure 20).

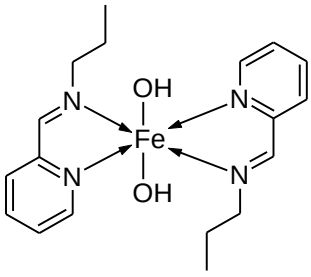

Monoisotopic Mass: 386.140518 Da

Figure 20: Suggested structure of the ion observed at m/z 386

The species suggested in Figures 16, 18 and 20 are similar to intermediates reported in several oxidation reactions that occur in processes involving free radicals.[28, 30]

3.4 Decomposition of peroxide oxidants mediated by cobalt and iron complexes

During the ESI-MS experiments described above it was observed that the addition of hydrogen peroxide to solutions of cobalt model complexes **C1** and **C2** resulted in vigorous gas evolution. This seems to indicate some sort of catalase-like activity of the model cobalt complexes. This entails decomposition of the hydrogen peroxide to form water and oxygen (Scheme 2). Kinetic data obtained for the reaction of the metal complexes with hydrogen peroxide could provide insight into the mechanism operative in these reactions.

A study was conducted with the aim of determining the rate of hydrogen peroxide decomposition in the presence of the metal complexes. This was done by monitoring hydrogen peroxide concentrations at various reaction times by $KMnO_4$ titrations, using an adapted literature procedure.[31]

In contrast to the model complexes, the dendritic cobalt complex **MD1** reacts relatively slowly with the hydrogen peroxide, with only about 5% of the active hydrogen peroxide decomposed after the first 15 minutes, while more than half the initial concentration of hydrogen peroxide remains after an hour (Figure 21). In contrast the model cobalt complex **C1**, decomposes about 80% of the initial hydrogen peroxide after only 15 minutes.

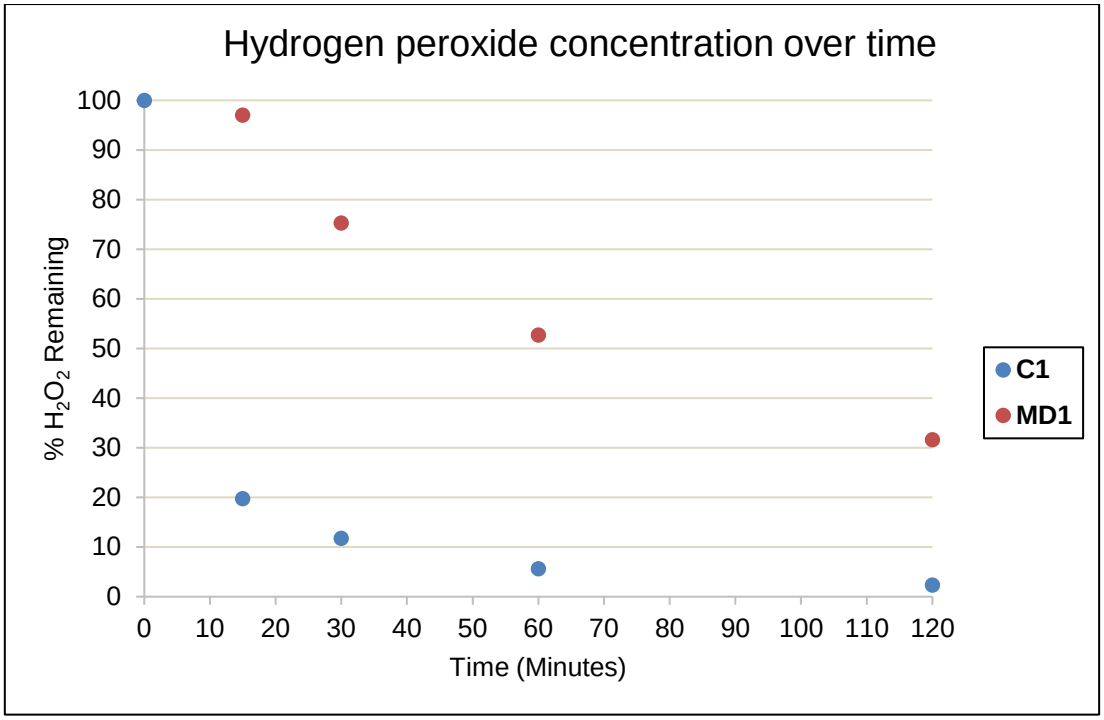

Figure 21: Decomposition of H_2O_2 by model complex C1 and generation 1 metallodendrimer MD1. 7.27 x 10^{-3} M cobalt concentration in MeCN, 6 mmol H_2O_2, total reaction volume 2.75 ml, 25°C

Similar observations were made for the *tert*-butyl derivatives **MD2** (metallodendrimer) and **C2** (model complex), with **C2** decomposing virtually all of the hydrogen peroxide within the first 5 minutes of the reaction. **MD2** on the other hand gradually decomposes the oxidant over three hours.

By employing lower concentrations of the model complexes, the decomposition reactions could be retarded sufficiently to allow decomposition curves to be obtained (Figure 22). The cobalt concentration was reduced to 3.64 x 10^{-3} M leading to a much slower decomposition of the peroxide (using **C1** as catalyst). About 25% of active hydrogen peroxide was still present after 45 minutes (Figure 22). This was, however, not the case for **C2**, which decomposed about 70% of the hydrogen peroxide within the first 5 minutes.

The above results were then used to determine the kinetics of the decomposition reaction catalysed by the aforementioned metallodendrimers and model complexes.

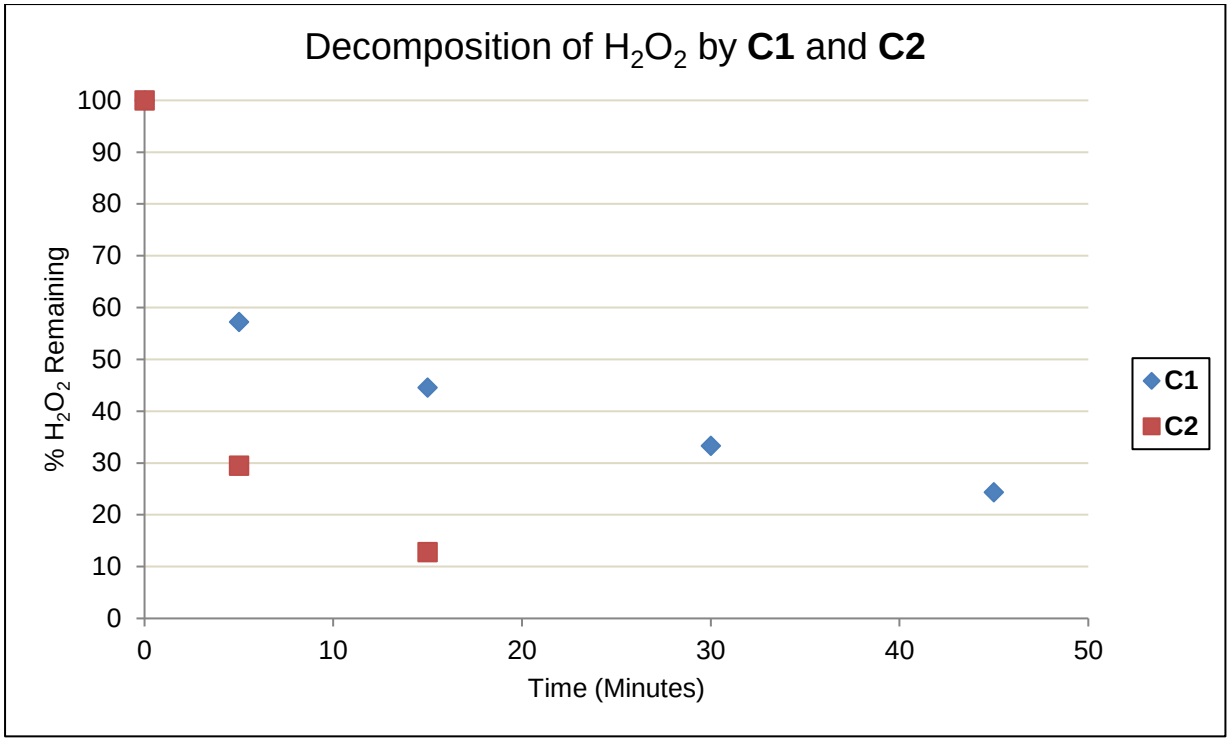

Figure 22: Decomposition of H_2O_2 by C1 and C2. 3.64 x 10^{-3} M cobalt concentration in MeCN, 6 mmol H_2O_2, total reaction volume 2.75 ml, 25°C

Due to its high reactivity, the concentration of **C2** had to be decreased even further to obtain acceptable decomposition curves. It was found that at a concentration of 1.81 x 10^{-3} M of **C2**, about 20% active hydrogen peroxide was still present after 45 minutes (Figure 23). However, the rate of decomposition is still relatively fast, even at this lower catalyst concentration. About 40% of the hydrogen peroxide decomposed within the first 5 minutes of the reaction catalysed by **C2**.

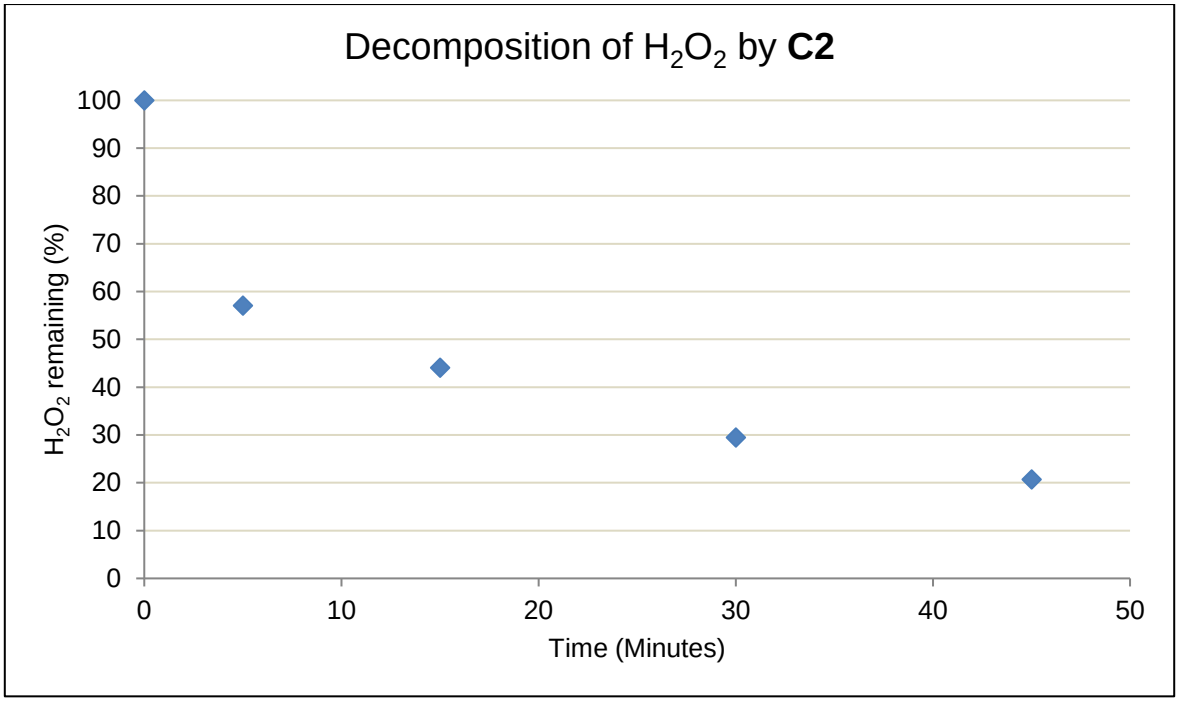

Figure 23: Decomposition of H_2O_2 by 1.81 x 10^{-3} M of C2. 1.81 x 10^{-3} M cobalt concentration in MeCN, 6 mmol H_2O_2, total reaction volume 2.75 ml, 25°C

A mechanism for the decomposition of hydrogen peroxide to oxygen using cobalt catalysts has previously been described by Sigel and Pasternack.[32] Based on the kinetics of the process, the catalase activity exhibited by cobalt(III)-hematoporphyrin (CoHP) could be described by the mechanism shown in Scheme 3. The first step of the mechanism is coordination of the hydrogen peroxide to the metal centre. Subsequently neither homo- nor hetero-lytic cleavage of the O-O bond takes place, instead the hydrogen peroxide is deprotonated. How this deprotonation takes place is not described in detail (Scheme 3, Step 2). This process does not occur via oxidative addition of the H_2O_2, instead, water could possibly act as base to facilitate Step 2. Reaction with a further equivalent of hydrogen peroxide leads to the formation of hydroxide anions and O_2.

$$Co^{3+}HP + H_2O_2 \rightleftharpoons Co^{3+}HP(H_2O_2) \quad (1)$$

$$Co^{3+}HP(H_2O_2) \rightleftharpoons Co^{3+}HP(HOO^-) + H^+ \quad (2)$$

$$Co^{3+}HP(HOO^-) + H_2O_2 \rightleftharpoons Co^{3+}HP(HOO^-)(H_2O_2) \quad (3)$$

$$Co^{3+}HP(HOO^-)(H_2O_2) \rightleftharpoons Co^{3+}HP + H_2O + HO^- + O_2 \quad (4)$$

Scheme 3: Mechanism for the decomposition of H_2O_2 by cobalt hematoporphyrin described by Sigel et al.[32]

If the decomposition of hydrogen peroxide catalysed by the model cobalt complexes occurs predominantly via the above mechanism, then radical species would not be expected to form.

This mechanism could also possibly explain why **C2** decomposes hydrogen peroxide more rapidly than **C1**. Due to the electron donating effects of the *tert*-butyl groups, the cobalt centre of **C2** is more electron rich and thus better able to stabilize the intermediate formed in Step 2.

Another hydrogen peroxide decomposition pathway has been suggested by Turrá et al. on the basis of kinetic arguments and a computational study. These authors proposed that inhibition of catalytic activity in cobalt-catalysed reactions could be explained through the formation of hydroxo-bridged cobalt dimers (Scheme 4, reaction 1).[19] The formation of such dimers could typically occur at relatively high cobalt concentrations and lead to the inhibition of catalytic activity. Reaction with peroxyl radicals leads to the formation of a peroxo-bridged dimer as well as the formation of peroxide species (Scheme 4, reactions 2 and 3). According to Turrá et al. the peroxo-bridged dimer should spontaneously dissociate to form two cobalt(II) species and O_2 (based on their computational study).[19] The intermediates proposed by Turrá et al. are similar to the species proposed on the basis of the ESI-MS results in Section 3.3.1. Thus, the decomposition pathway described by Turrá et al. could possibly be responsible for the catalase-like activity observed for **C1** and **C2**.

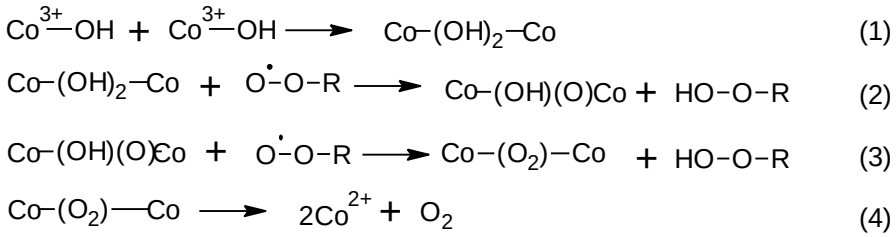

Scheme 4: Formation of bridged cobalt dimers suggested by Turrá et al.[19]

Similar hydrogen peroxide decomposition experiments were attempted for the pyridine-imine iron complexes **C4** and **MD5**. Both of these complexes are intensely coloured, even in highly dilute solutions. Due to the highly intense colour, the hydrogen peroxide concentration could not be determined by titration with $KMnO_4$ nor using iodometric titration. Instead the endpoint of the titration was determined by continuously measuring the oxidation potential of the reaction mixture while titrating with standard $KMnO_4$. Presumably once the endpoint of the titration is reached, the oxidation potential measured in the solution should increase dramatically due to the presence of excess $KMnO_4$. Thus, small aliquots of $KMnO_4$ were added using a burette, while simultaneously recording the oxidation potential with an ORP (oxidation reduction potential) probe. A plot of the oxidation potential versus the volume $KMnO_4$ added was then constructed. The endpoint of the titration was then determined using the derivative method (see experimental section for further details).

The H_2O_2 decomposition reaction catalysed by **C4** displays an induction period of about 20 minutes during which very little change in the active hydrogen peroxide concentration occurs (Figure 24). This could possibly be due to **C4** gradually being transformed to the active species over the first 20 minutes of reaction. The observation of an induction period could also possibly be due to the fact that **C4** is an octahedral complex with three pyridine-imine ligands. Thus, prior to reaction with hydrogen peroxide, the generation of a vacant site on the metal centre is required. After the first 20 minutes a steady decrease in hydrogen peroxide concentration is observed over the next hour. After 90 minutes about 70% of the original hydrogen peroxide had decomposed.

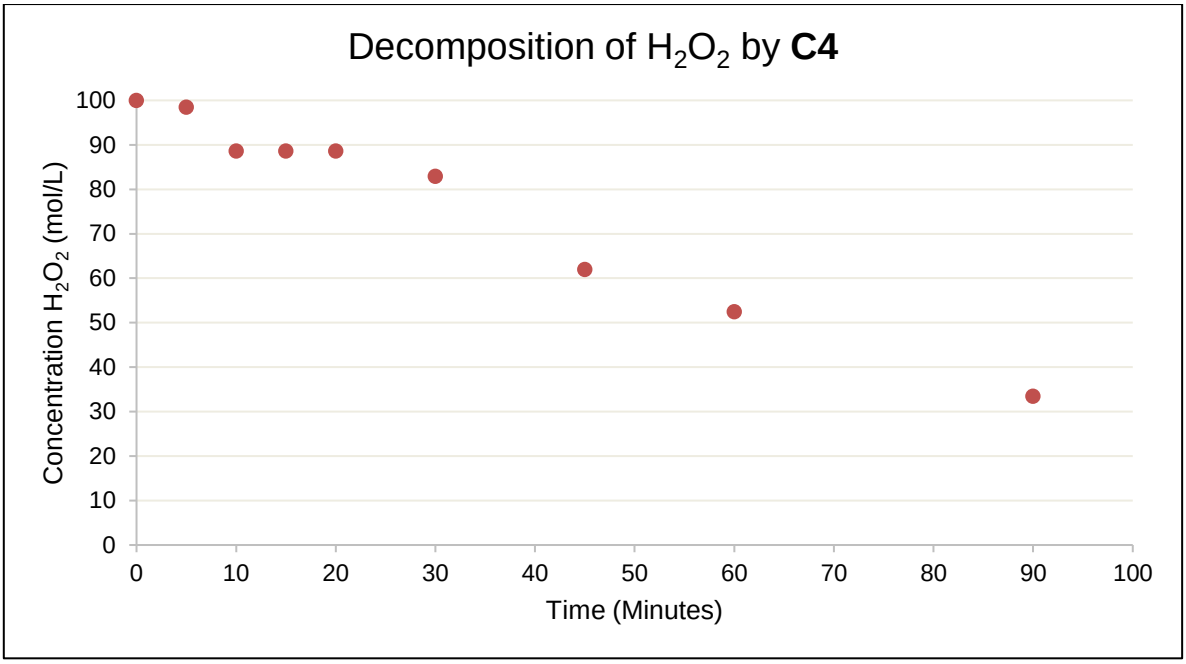

Figure 24: Decomposition of H_2O_2 by the iron complex C4. 3.64 x 10^{-3} M iron concentration in MeCN, 6 mmol H_2O_2, total reaction volume 2.75 ml, 25°C

The H_2O_2 decomposition catalysed by the metallodendrimer **MD5** does not show an induction period as was observed for **C4** and the rate of decomposition is initially relatively fast. Neither of **C4** nor **MD5** exhibited the rapid decomposition observed for **C1** and **C2**.

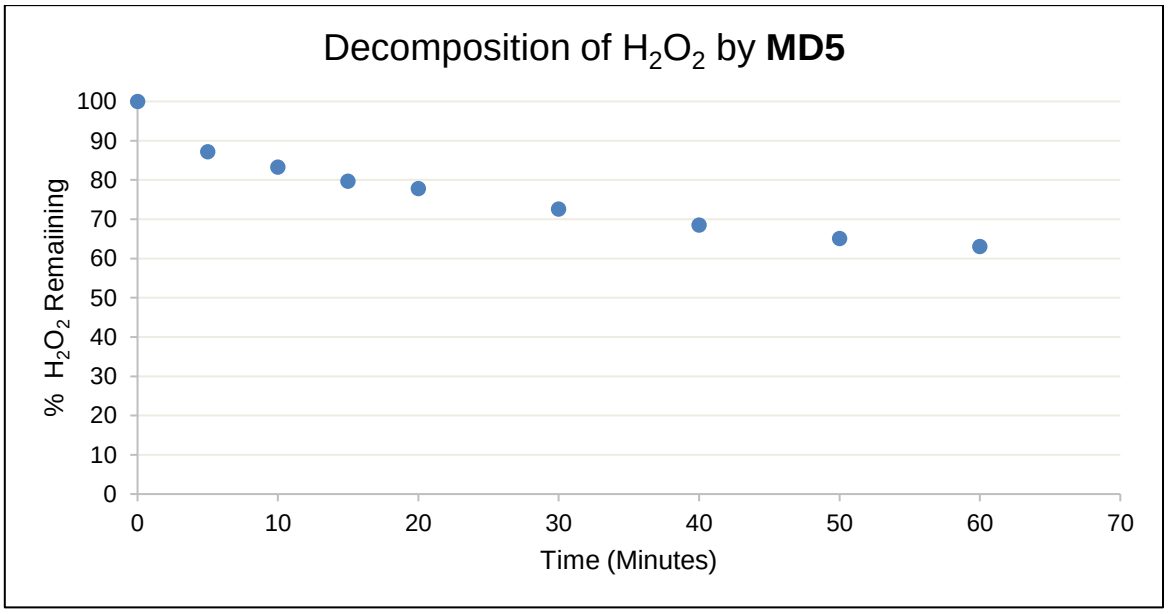

Figure 25: Decomposition of H_2O_2 by the iron complex MD5. 3.64 x 10^{-3} M iron concentration in MeCN, 6 mmol H_2O_2, total reaction volume 2.75 ml, 25°C

The kinetics of the decomposition of hydrogen peroxide by some cobalt and iron complexes and its dependence on reaction temperature and initial oxidant concentration will be discussed further in Chapter 5.

Another factor that can influence the metal complex's ability to participate in redox processes is the catalyst's oxidation and reduction potentials.[33] This was further investigated for a number of the cobalt and iron complexes by the use of cyclic voltammetry.

3.5 Oxidative potentials of cobalt and iron complexes

Cyclic voltammetry (CV) experiments were conducted on complexes **C1**, **C2**, **C4**, **MD1** and **MD2**. As oxidation of the metal centre occurs during oxidation catalysis, the oxidation potential of these complexes could provide insight into the catalytic results presented in Chapter 4. Measurements were done on the solutions of metal complex in acetonitrile using tetrabutylammonium hexafluorophosphate as electrolyte.

The cyclic voltammogram obtained for **C4** is shown in Figure 26. No reversible redox pairs are observed at anodic potentials, while irreversible redox processes are observed for the ligands in this range (-2 to 0 V). However, a reversible redox process at $E_{1/2}$= 0.559 V [Fe(II)/Fe(III)] is observed (relative to ferrocene Fc/Fc^{+}). The oxidation potential of **C4** is comparable to those obtained for analogous iron pyridine systems.[34]

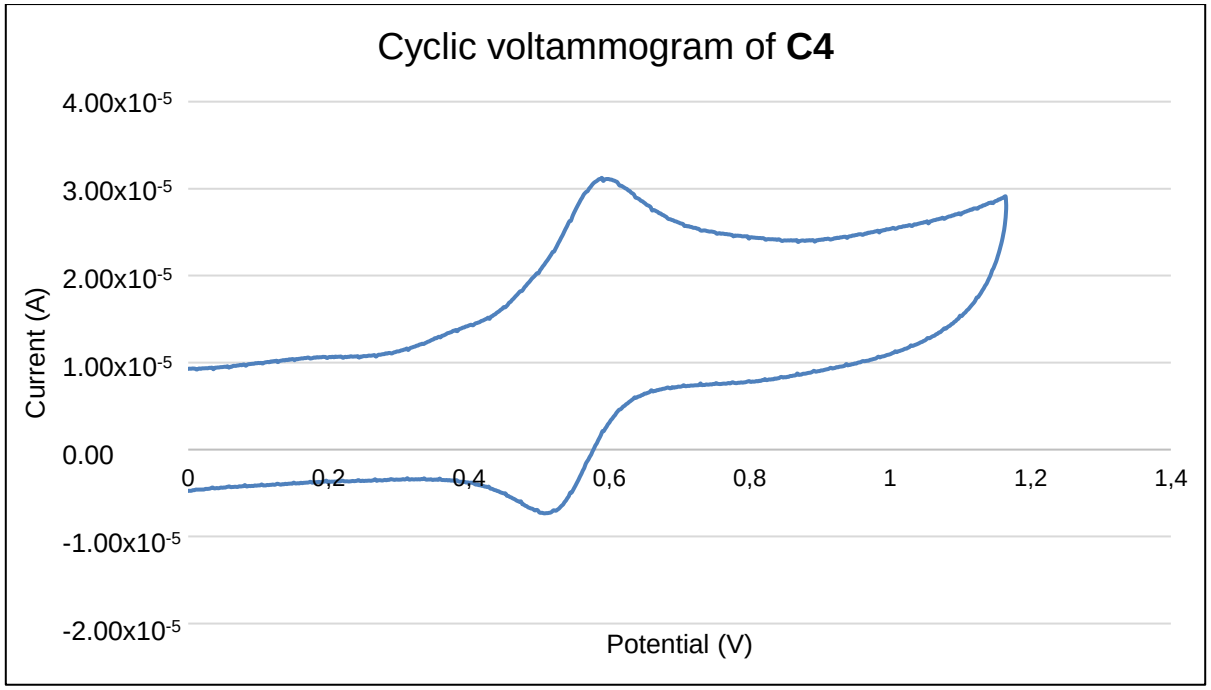

Figure 26: Cyclic voltammogram obtained for C4 (3.00 x 10^{-3} M in MeCN)

In the case of the cobalt complexes **C1** and **MD1** (Figure 27 as representative example), a large reversible redox process is observed at around -1 V. This is likely due to the Co(II)/Co(I) redox pair also typically observed for analogous cobalt salen complexes. The Co(II)/Co(III) redox pair is normally observed at around +0.8 V.[35]

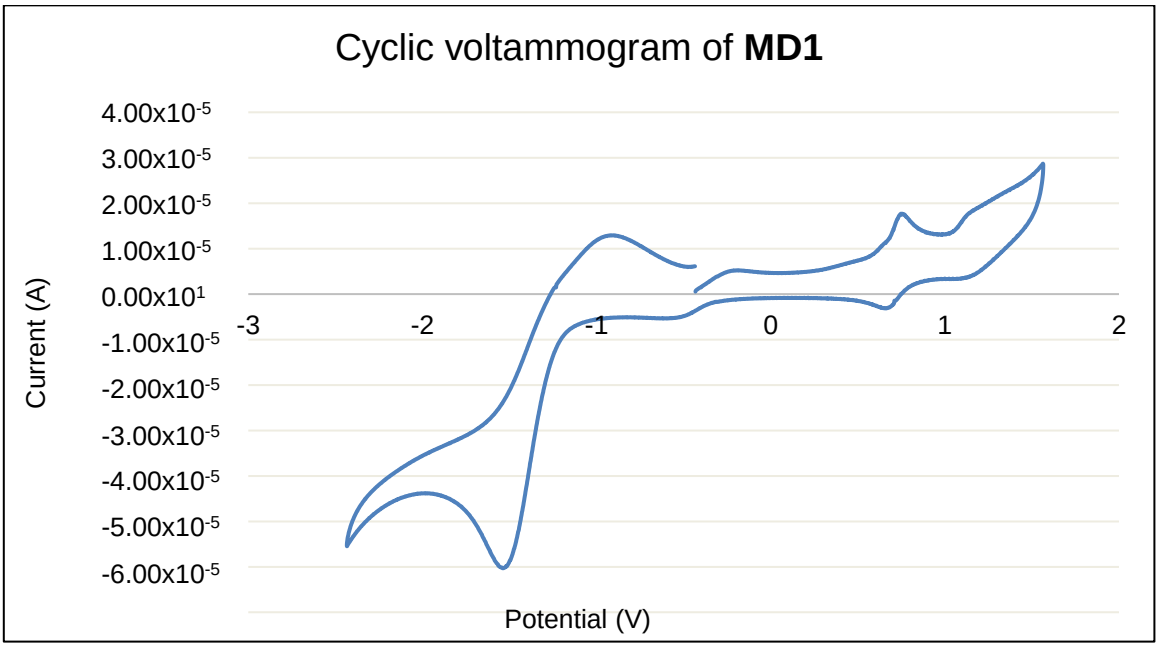

Figure 27: Cyclic voltammogram of MD1 (3.00 x 10^{-3} M in MeCN)

By evaluating the standard oxidation potentials in Table 1 (relative to ferrocene) of these complexes we observed that the model cobalt complexes are more easily oxidized than their dendritic analogues. Typically, iron complexes have lower oxidation potentials than their analogous cobalt complexes. It is expected that **C4** should have a relatively low oxidation potential. However, the oxidation potential obtained for **C4** (neutral ligands) is comparable to those obtained for **C1** and **C2**, bearing anionic ligands.

MD1 and **MD2** have relatively high oxidation potentials for the Co(II)/Co(III) redox process. This could possibly be explained by the relative difference in charge densities of the metallodendrimers and the model complex. If the metallodendrimer undergoes oxidation, the resulting Co(III) systems would have a high charge density compared to the model complex. Other authors have speculated that sterically hindered cobalt(II) complexes are oxidized to relatively less stable Co(III) species due to the tendency of Co(III) to form octahedral complexes.[36]

The *tert*-butyl substituted complexes **C2** and **MD2** tended to have lower oxidation potentials than **C1** and **MD1**, possibly due to the electron donating effects of the *tert*-butyl groups increasing electron density on the metal centre. An increase in the positive inductive effect of the ligands lead to a shift of the oxidation potential to more negative values, while negative inductive effects lead to an increase in the oxidation potential to more positive potentials. Interestingly both the model as well as dendritic cobalt complexes have significantly higher Co(II)/Co(III) oxidation potentials when compared to the well-known cobalt salen complexes ($E_{1/2}$ 0.25 V, tetrafluoroborate used as electrolyte).[35] The multinuclear dendritic species has a higher oxidation potential than the mononuclear complexes. Astruc et al. reported that when dendrimer branches are sufficiently long, redox processes occurring at the peripheries are independent from one another. However, when the peripheries are not sufficiently separated from one another the redox processes at the peripheries are not independent.[37] This would explain why the dendritic systems **MD1** and **MD2** have higher oxidation potentials than the model complexes **C1** and **C2**. If the cobalt centres are not electronically isolated, oxidation of one cobalt centre is influenced by the other cobalt centre. Oxidation of either **MD1** or **MD2** possibly leads to the formation of an unfavourable di-cation species. These relatively high oxidation potentials might

indicate that a strong oxidant will be required for these complexes to be effective catalysts in oxidation chemistry.

Table 1: Standard potentials determined for C1, C2, C4, D1 and MD2

Complex	$E_{1/2}$ M(II)/M(III)	E_{pc}	E_{pa}
C1	0.604	0.610	0.598
C2	0.621	0.627	0.615
C4	0.559	0.601	0.516
MD1	0.728	0.770	0.686
MD2	0.704	0.730	0.677

CV recorded on 0.003M complex solutions with a sweepwidth -2.5 to 2.5 V at a scanning rate of 100 mV/s. $E_{1/2}$ is the calculated halfwave potential, E_{pc} the cathodic current and E_{pa} the anodic current.

3.6 Conclusions

The reactions of several cobalt salicylaldimine and iron pyridine-imine complexes with peroxide-based oxidants were investigated. Mass spectrometry was used to characterize intermediates of the reaction of the cobalt complexes **MD1** and **C1** with the oxidants H_2O_2 and TBHP. A potential cobalt-oxo species was identified in the reaction of **MD1** with H_2O_2. However, mass spectrometry (alone) could not be used to determine the presence of such a species during a catalytic test reaction. Therefore, it is possible that such a species is formed in an extremely low concentration or could be formed on-line during the ionization process in the mass spectrometer and not necessarily during the catalytic test reactions. UV-Vis spectroscopy seems to indicate that a cobalt-oxide or hydroxide species is formed during reaction, however intermediate species are not detected by UV-Vis. Spectral changes do not match those reported for Co(IV) species, which would indicate a possible metal-oxo, rebound mechanism (Scheme 1, Reaction 2).

The model cobalt complex **C1,** in the presence of H_2O_2, appears to undergo a process whereby oxo or peroxo bridged complexes are formed with high m/z signals observed in the mass spectrum of the oxidation reactions. When hydrogen peroxide is added to the model complexes, **C1** and **C2**, effervescence is observed, an indicator that the oxidant is decomposed to oxygen instead of generating radical species. The catalase-like activity is only observed for **C1** and **C2**. In contrast the dendritic analogues, **MD1**

and **MD2** react very slowly with hydrogen peroxide. In this case the relatively high oxidation potentials of **MD1** and **MD2** could possibly be the reason for the retarded decomposition. However, complexes **MD1** and **MD2** are only the catalyst precursors, the oxidation potential of the active species likely differs significantly. In such a case the difficulty might lie in forming the active species from **MD1** and **MD2**.

Similar experiments were performed on the mononuclear iron complex **C4**. In this case intermediates containing alkoxy and peroxy ligands were detected by mass spectrometry. Such intermediates have previously been invoked for complexes that generate free radicals from peroxides. The decomposition of H_2O_2 by **C4** and the metallodendrimer **MD5** was also investigated. Both **C4** and **MD5** decompose the oxidant gradually (compared to **C1** and **C2**). An induction period is observed for **C4.** The active catalyst is possibly being formed during this induction period.

The observations made for these iron and cobalt complexes, as discussed in this chapter, inform the choice of reaction conditions and reaction optimization in Chapter 4. Possible identification of reaction intermediates described in this chapter forms the basis of further mechanistic investigations reported and collated in Chapter 5.

3.7 Experimental

3.7.1 General Methods and instrumentation

All chemicals were purchased from Sigma Aldrich and used without any further purification. Solvents used were distilled and dried using the appropriate drying agents and methods prior to use. Hydrogen peroxide decomposition reactions were performed in a Radleys 12-stage carrousel parallel reactor with a gas distribution system. Cyclic voltammograms were recorded on a Nuvant Systems, EZstat pro potentiostat/ galvanostat/ battery cycler. UV-Vis spectra were recorded on a GBC UV-Vis 920 spectrometer. Mass spectrometry was performed on a Waters Synapt G2 mass spectrometer. ORP measurements were obtained through the use of a Eutech Instruments Meter with ATC probe.

3.7.2 ESI-MS experiments

Stock solutions of the various metal complexes were prepared by dissolving 2 mg of the relevant complex in 2.65 ml MeCN. 1 ml aliquots were then taken from these stock solutions to prepare 1 ml samples that were analysed by direct injection ESI-MS (positive). This yielded the mass spectrum of the material before the addition of oxidant. 0.100 ml oxidant (TBHP or H_2O_2) was then added to the remaining stock solution. A 1 ml aliquot was withdrawn and analysed by ESI-MS (positive ion mode) immediately.

3.7.3 Oxidant decomposition titration experiments

3.7.3.1 Decomposition of H_2O_2 by cobalt complexes

Stock solutions (3.64 x 10^{-3} M cobalt) of the cobalt complexes (**C1**, **C2**, **MD1** and **MD2**) in acetonitrile were prepared. This solution was placed in a parallel reactor tube. H_2O_2 (4 mmol, 0.612 ml) was then added to the reaction mixture to yield a final reaction volume of 2.75 ml. The tube was sealed and stirred at room temperature. Aliquots (0.600 ml) were sampled at various reaction times. The samples were diluted by the addition of 10 ml H_2SO_4 (3M) and heated in a water bath (60°C) for about 30 seconds. The resulting reaction mixture was titrated against a standardized $KMnO_4$ (0.02 M) solution to determine the concentration of H_2O_2 remaining. This was then used to calculate the extent of H_2O_2 decomposition.

3.7.3.2 Decomposition of H_2O_2 by Iron complexes C4 and MD5

The decomposition of H_2O_2 by the iron complexes was measured by titrating H_2O_2 decomposition mixtures against standardized $KMnO_4$ (0.02 M) solution, as described above, while continuously measuring the oxidation potential of the $KMnO_4$ and H_2O_2 titration mixture using an oxidation/reduction probe. Titration curves of oxidation potential vs $KMnO_4$ volumes, were then constructed. The endpoint of the titration was then determined by determining the 1st and 2nd derivatives of the titration curve.

3.7.4 Cyclic voltammetry experiments.

Cyclic voltammograms were recorded by first preparing a stock solution of 0.100 M tetrabutylammonium hexafluorophosphate (supporting electrolyte) in acetonitrile. The complexes were dissolved in 10 ml of the supporting electrolyte solution to yield solutions with a complex concentration of 0.001 M. The ferrocene reference was also prepared by the method described above. The complex solutions were then placed in an electrochemical cell equipped with a glassy carbon working electrode, a platinum wire auxiliary electrode and an AgCl reference electrode. Three cycles scanning between 2.5 V and -2.5 V were then recorded at a scanning rate of 100 mV/s. Standard potentials were determined relative to a ferrocene reference.

3.8 References

1 R. A. Sheldon, *J. Mol. Catal.*, 1980, **7**, 107–126.

2 D. H. R. Barton and V. N. Le Gloahec, *Tetrahedron*, 1998, **54**, 15457–15468.

3 A. N. Vedernikov, *Acc. Chem. Res.*, 2012, **45**, 803–813.

4 N. Mizuno and K. Kamata, *Coord. Chem. Rev.*, 2011, **255**, 2358–2370.

5 I. W. C. E. Arends, K. U. Ingold and D. D. M. Wayner, *J. Am. Chem. Soc.*, 1995, **117**, 4710–4711.

6 I. Prat, J. S. Mathieson, M. Güell, X. Ribas, J. M. Luis, L. Cronin and M. Costas, *Nat. Chem.*, 2011, **3**, 788–793.

7 B. Wang, Y.-M. Lee, W.-Y. Tcho, S. Tussupbayev, S.-T. Kim, Y. Kim, M. S. Seo, K.-B. Cho, Y. Dede, B. C. Keegan, T. Ogura, S. H. Kim, T. Ohta, M.-H. Baik, K. Ray, J. Shearer and W. Nam, *Nat. Commun.*, 2017, **8**, 1–10.

8 M. Chen, Y. Pan, H.-K. Kwong, R. J. Zeng, K.-C. Lau and T.-C. Lau, *Chem. Commun.*, 2015, **51**, 13686–13689.

9 R. A. Leising, J. Kim, M. A. Pérez and L. Que Jr., *J. Am. Chem. Soc.*, 1993, **115**, 9524–9530.

10 C. Glorieux and P. B. Calderon, *Biol. Chem.*, 2017, **398**, 1095–1108.

11 W. P. Griffith, *Coord. Chem. Rev.*, 1970, **5**, 459–517.

12 B. Meunier, S. P. de Visser and S. Shaik, *Chem. Rev.*, 2004, **104**, 3947–3980.

13 S. Hong, F. F. Pfaff, E. Kwon, Y. Wang, M.-S. Seo, E. Bill, K. Ray and W. Nam, *Angew. Chemie Int. Ed.*, 2014, **53**, 10403–10407.

14 M. Mitra, H. Nimir, D. A. Hrovat, A. A. Shteinman, M. G. Richmond, M. Costas and E. Nordlander, *J. Mol. Catal. A Chem.*, 2017, **426**, 350–356.

15 A. Company, I. Prat, J. R. Frisch, D. R. Mas-Ballesté, M. Güell, G. Juhász, X. Ribas, D. E. Münck, J. M. Luis, L. Que and M. Costas, *Chem. - A Eur. J.*, 2011, **17**, 1622–1634.

16 A. R. McDonald and L. Que, *Coord. Chem. Rev.*, 2013, **257**, 414–428.

17 B. Das, A. Al-Hunaiti, M. Haukka, S. Demeshko, S. Meyer, A. A. Shteinman, F. Meyer, T. Repo and E. Nordlander, *Eur. J. Inorg. Chem.*, 2015, **2015**, 3590–3601.

18 H. Mimoun, R. Charpentier, A. Mitschler, J. Fischer and R. Weiss, *J. Am. Chem. Soc.*, 1980, **102**, 1047–1054.

19 N. Turrà, U. Neuenschwander, A. Baiker, J. Peeters and I. Hermans, *Chem. Eur. J.*, 2010, **16**, 13226–13235.

20 C. E. Anson, W. Klopper, J.-S. Li, L. Ponikiewski and A. Rothenberger, *Chemistry*, 2006, **12**, 2032–2038.

21 F. Meyer, R. Hempelmann and M. Veith, *Materials.*, 1999, **4**, 1755–1763.

22 L. Saussine, E. Brazi, A. Robine, H. Mimoun, J. Fischer and R. Weiss, *J. Am. Chem. Soc.*, 1985, **107**, 3534–3540.

23 F. A. Chavez, C. V. Nguyen, M. M. Olmstead and P. K. Mascharak, *Inorg. Chem.*, 1996, **35**, 6282–6291.

24 S. Rayati, S. Zakavi, M. Koliaei, A. Wojtczak and A. Kozakiewicz, *Inorg. Chem. Commun.*, 2010, **13**, 203–207.

25 J.-W. Kim, S. H. Choi, P. T. Lillehei, S.-H. Chu, G. C. King and G. D. Watt, *Chem. Commun.*, 2005, 4101–4103.

26 A. P. Katsoulidis, D. E. Petrakis, G. S. Armatas, P. N. Trikalitis and P. J. Pomonis, *Microporous Mesoporous Mater.*, 2006, **92**, 71–80.

27 J. Taghavimoghaddam, G. P. Knowles and A. L. Chaffee, *J. Mol. Catal. A Chem.*, 2012, **358**, 79–88.

28 E. N. Rizkalla, L. H. J. Lajunen and G. R. Choppin, *Inorganica Chim. Acta*, 1986, **119**, 93–98.

29 C. Nguyen, R. J. Guajardo and P. K. Mascharak, *Inorg. Chem.*, 1996, **35**, 6273–6281.

30 E. Neyens and J. Baeyens, *J. Hazard. Mater.*, 2003, **98**, 33–50.

31 S. Skounas, C. Methenitis, G. Pneumatikakis and M. Morcellet, *Bioinorg. Chem. Appl.*, 2010, **2010**, 1–9.

32 H. Sigel and R. F. Pasternackt, *J. Inorg. Nucl. Chem.*, 1975, **37**, 1093–1095.

33 C. P. Andrieux, C. Blocman, J. M. Dumas-Bouchiat, F. M'Halla and J. M. Savéant, *J. Electroanal. Chem. Interfacial Electrochem.*, 1980, **113**, 19–40.

34 S. Taktak, W. Ye, A. M. Herrera and E. V. Rybak-Akimova, *Inorg. Chem.*, 2007, **46**, 2929–2942.

35 F. Bedioui, E. Labbe, S. Gutierrez-Granados and J. Devynck, *J. Electroanal. Chem. Interfacial Electrochem.*, 1991, **301**, 267–274.

36 M. Hirotsu, M. Kojima, K. Nakajima, S. Kashino and Y. Yoshikawa, *Bull. Chem. Soc. Jpn.*, 1996, **69**, 2549–2557.

37 D. Astruc, C. Ornelas and J. Ruiz, *Acc. Chem. Res.*, 2008, **41**, 841–856.

Chapter 4: Catalytic Oxidation of Hydrocarbons by Iron, Cobalt and Copper Complexes

4.1 Introduction to the oxidation of alkenes and alkanes

Hydrocarbons are extremely important chemical feedstocks. Large scale production of alkenes occurs industrially via the cracking process.[1] Alternatively, alkenes such as cyclohexene, are obtained via the partial reduction of unsaturated hydrocarbons such as benzene.[2, 3] Alkanes and alkenes are also generated on a large scale during the Fischer-Tropsch process, particularly as operated by SASOL[4] in South Africa.[5] These hydrocarbons find application in many different fields and are used industrially as solvents, fuels or as platform chemicals in fine chemical synthesis.[6, 7]

The partial oxidation of hydrocarbons to oxygen-containing products is of particular interest as was highlighted in Chapter 1. Various oxidative processes have been developed for the oxidation of alkenes, including some that have been applied industrially. Some of these processes include the Wacker oxidation process (oxidation of alkene to aldehyde or ketone)[8], ozonolysis- a process in which the alkene double bond is often cleaved[9]- and also various reactions of alkenes with stoichiometric or catalytic oxidants such as such OsO_4.[10]. The oxidation of ethene (to epoxide products) is carried out industrially by silver catalysts along with oxygen as the oxidant, however long chain alkenes typically require stronger oxidants such as hydrogen peroxide.[11, 12] Such oxidative transformations are also performed biologically by enzymatic systems such as the previously discussed cytochrome P450 enzymes.[13, 14] These oxidation reactions yield the more valuable oxygenates from the relatively inexpensive alkene substrates. These oxygen-containing products are sold in bulk or act as platform chemicals and find application in the synthesis of fine chemicals and pharmaceuticals.[6] However, the need for catalytic processes capable of efficiently performing these transformations still remains.

The above is also true for alkanes. However, the saturated hydrocarbons are even less reactive (in oxidation processes) than their alkene counterparts.[15] The generation of oxygen-containing products from saturated hydrocarbons under mild conditions is the subject of ongoing research efforts world-wide but remains both an academic as well as an industrial challenge.[16–19]

In this chapter the oxidation of cyclohexene catalysed by iron, copper and cobalt complexes (preparation reported in Chapter 2) in the presence of suitable oxidants such as hydrogen peroxide and *tert*-butyl hydroperoxide are discussed. Subsequently, the most promising catalysts precursors are also evaluated in the catalytic oxidation of octane.

The importance of a process capable of using cheap and green oxidants such as hydrogen peroxide and providing access to industrially relevant products (economically) cannot be overstated.

4.2 Cyclohexene oxidation mediated by metal complexes.

4.2.1 Introduction to cyclohexene as a model substrate

Cyclohexene is a popular model substrate in the literature due to its relatively low cost, industrial relevance and due to its symmetric nature, which results in a fairly simple product stream.[20] Three major products are usually reported for the oxidation of cyclohexene namely cyclohexene oxide and the two allylic oxidation products, 2-cyclohexen-1-ol and 2-cyclohexen-1-one.

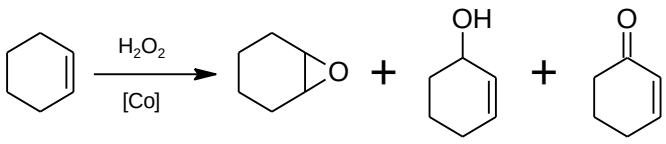

Scheme 1: Oxidation of cyclohexene to various oxygenates

Generally speaking, the economically important cyclohexene oxide is formed as the major product under a metal-oxo centred mechanism, the so-called rebound mechanism (Chapter 3, Scheme 1, Reaction 2). On the other hand, free radical

mediated processes tend to favour the formation of the allylic products namely 2-cyclohexen-1-ol and 2-cyclohexen-1-one.[20] The α, β- unsaturated ketones and alcohols formed, are also important industrial intermediates and find application in the fragrance and synthetic organic chemistry sectors.[6] With this in mind some of the metal complexes reported in Chapter 2 were tested as catalyst precursors in the catalytic oxidation of cyclohexene.

4.2.2 Iron complexes as catalyst precursors for the oxidation of cyclohexene

A large number of iron complexes, especially iron pyridine complexes, have been reported as active catalyst precursors for the oxidation of various alkenes.[21–25] Complexes **C4**, **MD3**, **MD4** and **MD5**, reported in Chapter 2, were tested as catalyst precursors in the oxidation of cyclohexene. Initial test conditions were adapted from those reported by White et al.[21] Acetonitrile is commonly employed in hydrocarbon oxidation reactions and was used as solvent during the evaluation of the iron complexes (complexes soluble in MeCN) as catalyst precursors. Acetonitrile has high chemical stability and resistance to oxidation, which makes it attractive for use in hydrocarbon oxidation reactions.[26] The influence of various other parameters on the catalytic oxidation reaction were also evaluated in order to optimize the catalytic system. These include catalyst concentration, reaction temperature and time. Additionally, two different oxidants, namely hydrogen peroxide and *tert*-butyl hydroperoxide (TBHP), were tested.

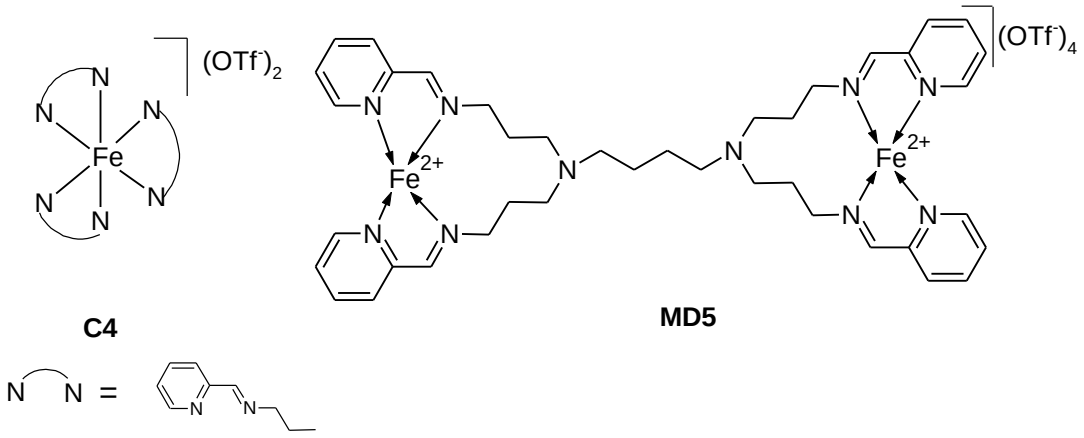

Figure 1: Iron complexes used to optimize cyclohexene oxidation

4.2.2.1 Blank control oxidation reactions

Before the evaluation of the complexes as catalyst precursors for the oxidation of cyclohexene a number of control experiments were conducted. In these experiments, the substrate (cyclohexene) was added to the reaction mixture, but either the oxidant or the catalyst precursor was excluded from the experiment. When the catalyst precursor **C4** is added to the experiment in the absence of oxidant, virtually no conversion of the substrate is observed (GC-FID). However, when either H_2O_2 or TBHP is present in the absence of catalyst small amounts of oxidation products are detected (Figure 2, no TBHP and no H_2O_2, < 2% conversion).

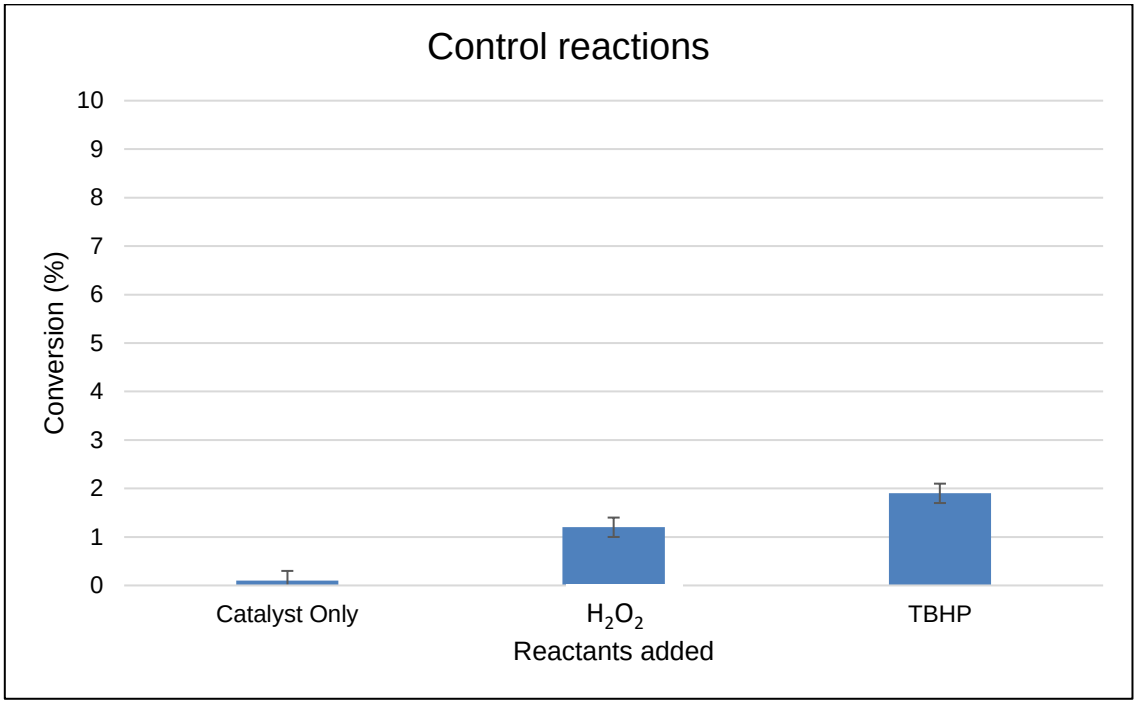

Figure 2: The effects of the different components on the catalytic oxidation reaction. Reaction conditions: 2.00 mmol, cyclohexene, 6.00 mmol Oxidant or 0.5 mol% catalyst, 3 hours, 25 °C, MeCN.

4.2.2.2 Effect of catalyst concentration

Catalyst **C4** was chosen as model complex to optimize the conditions for the iron complexes. Test reactions were performed at three different catalyst loadings namely 0.1, 0.5 and 1 mol% iron relative to the cyclohexene substrate (Figure 3). The reactions were stirred at room temperature for 3 hours. Based on the oxidant decomposition studies reported on in Chapter 3, most of the hydrogen peroxide is

expected to have decomposed after 3 hours and therefore this was chosen as the standard reaction time.

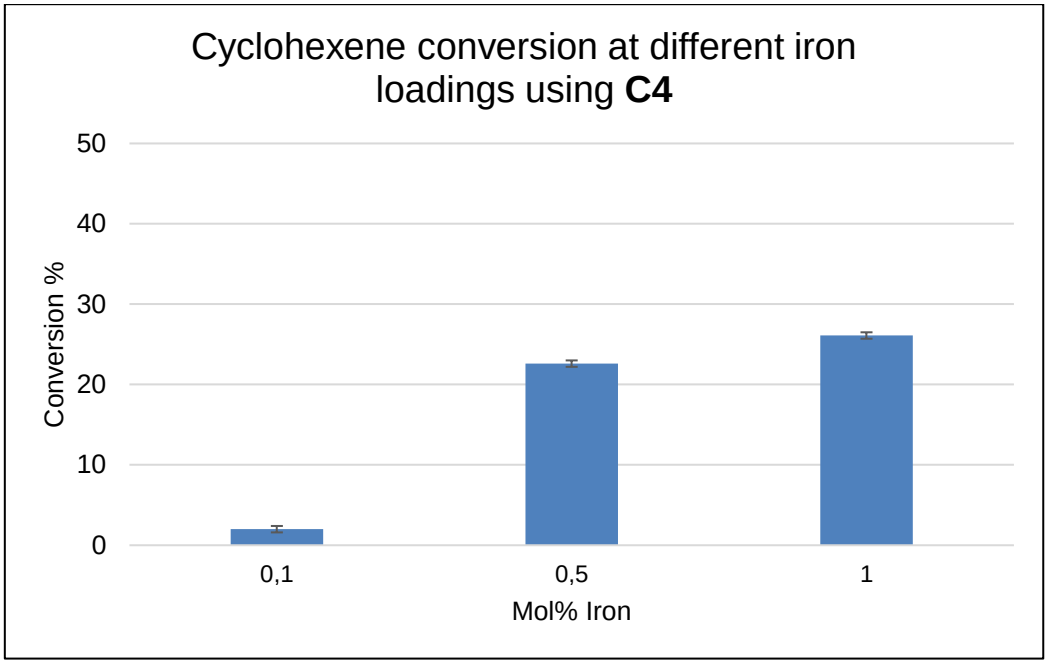

Figure 3: Effect of iron loading on catalytic conversion of cyclohexene using C4 as catalyst precursor. Reaction conditions: 2.00 mmol, cyclohexene, 6.00 mmol H_2O_2, ,3 hours, 25 °C, MeCN.

At 0.1 mol% iron concentration (relative to substrate) **C4** did not display any appreciable catalytic activity, with only traces of the oxidation products detected via GC-FID. The highest substrate conversion was obtained at 1 mol% iron. In the presence of H_2O_2 as oxidant around 26% conversion was obtained while at 0.5 mol% iron, 22% conversion was achieved. A test reaction at 1.5 mol% iron was also attempted, however increasing the catalyst loading beyond 1 mol% iron relative to substrate did not increase the obtained conversion. In all cases very high selectivity towards 2-cyclohexen-1-one is observed as the major product. 2-Cylohexen-1-ol and cyclohexene oxide were observed in low concentrations. In addition, low concentrations of a number of unknown products were also detected. It was hypothesized that these trace level products could be overoxidized products. GC-MS analysis revealed that these other oxidation products are likely 1,2-cyclohexanediol, 2-hydroxycyclohexanone and 2,3-epoxycyclohexanone (Scheme 2). GC standards for some of these trace level compounds are not readily available and their

combined concentrations are therefore labelled as “Other products” in further discussions. Their concentrations were determined algebraically (mol others = mol substrate converted - mol products).

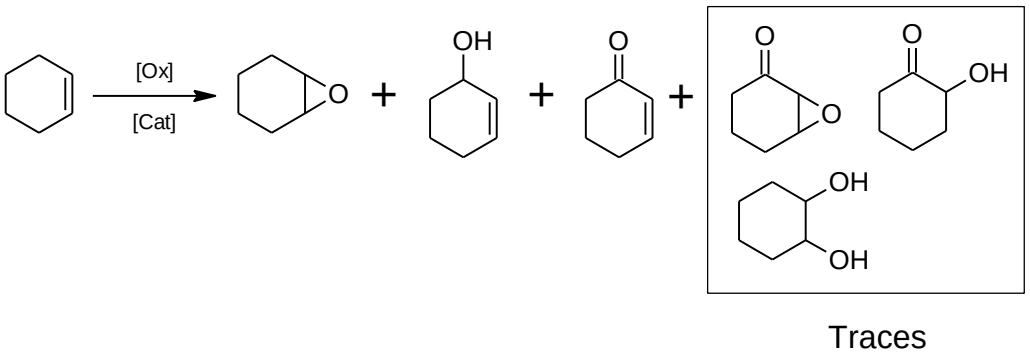

Traces

Scheme 2: Product distribution of iron catalysed oxidation of cyclohexene.

The reaction was repeated (with **C4**) but the hydrogen peroxide oxidant was replaced with *tert*-butyl hydroperoxide (TBHP). Similarly, when TBHP was used as oxidant, 32% substrate conversion is observed at 0.5 mol% iron, while 39% conversion is obtained when using 1 mol% iron. Again, only traces of products (< 3% conversion) are obtained when working at 0.1 mol% iron. Similarly, when TBHP was used as oxidant 2-cyclohex-1-one was the major product of the oxidation reaction (Figure 4).

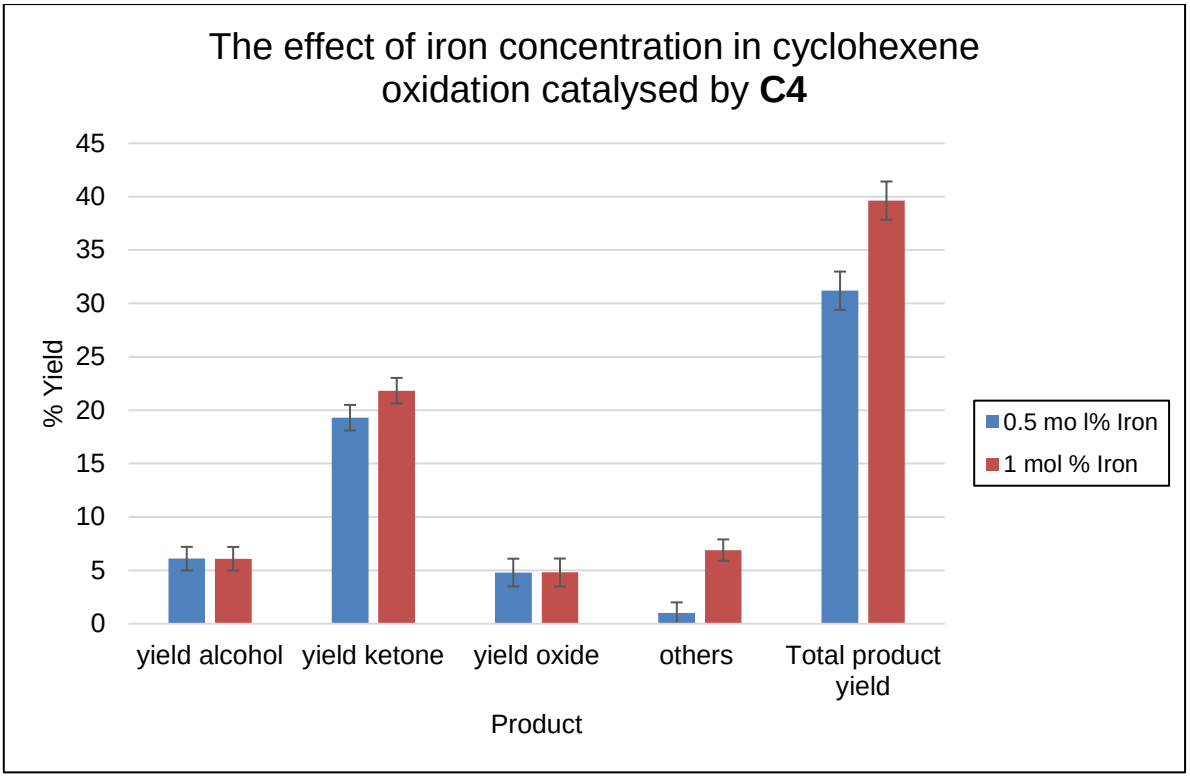

Figure 4: Effect of metal concentration on catalytic conversion when using TBHP as oxidant. Reaction conditions: 2.00 mmol, cyclohexene, 4.00 mmol TBHP, 0.5 mol % iron, 3 hours, 25 °C, MeCN.

The highest substrate conversion was obtained at a catalyst precursor loading of 1 mol% iron (relative to substrate) when using either H_2O_2 or TBHP. However, the conversion obtained at a catalyst loading of 0.5 mol% iron was only slightly lower than that obtained at the higher concentration of 1 mol% iron, and thus the former was used for further experimentation. The highest turnover number is achieved at a catalyst loading of 0.5 mol% iron relative to substrate.

4.2.2.3 Effect of reaction temperature

Often reactions employing hydrogen peroxide as oxidant are performed at room temperature to minimize the degradation of the thermally unstable oxidant.[21, 27] The catalytic activity of the catalyst precursor **C4** was thus evaluated at three different temperatures using H_2O_2 as oxidant. At 0°C very little oxidation of the substrate was observed over the three-hour period (< 5% conversion). At 25°C around 22% conversion was obtained. Increasing the temperature to 40°C did not drastically

improve the conversion obtained in the presence of H_2O_2 (26% conversion). A test reaction was also attempted at 60°C however, vigorous effervescence of the solution was observed, indicative of rapid peroxide disproportionation to oxygen and water. The seemingly high pressure inside of the reactor lead to leaking of the reactor and thus no further reactions at higher temperatures were attempted.

A set of experiments were performed where H_2O_2 was replaced with TBHP and the influence of temperature on these reactions evaluated. In the presence of TBHP, an increase in conversion is observed with increasing temperature. However, the selectivity towards the over-oxidized “other” products increased dramatically at 60°C. Thus, reactions at 40°C were preferred for further experimentation.

4.2.2.4 Rate of oxidant addition and oxidant concentration

In the experiments described thus far, a substrate to H_2O_2 ratio of 1:3 was employed. The use of excess of hydrogen peroxide is to compensate for the decomposition of the oxidant over the course of reaction. The rate of oxidant addition can thus potentially affect the extent of oxidant decomposition.[27, 22] Experiments were performed using **C4** as catalyst precursor where hydrogen peroxide is slowly added over time in portions (1 equivalent H_2O_2 relative to substrate per hour for three hours), however the conversion obtained when this method of addition was employed was almost identical to the result obtained when adding all of the oxidant at the start of the experiment (at 25°C). Thus, it appears that the rate of oxidant addition to **C4** catalysed reactions does not significantly affect the obtained cyclohexene conversion. However, if the ratio of substrate to H_2O_2 was reduced to 1:1 or 1:2 a severe decrease in catalytic activity was observed with low conversions of 9.5 and 15% obtained respectively. An excess of oxidant is therefore needed to counteract the effect of oxidant decomposition.

4.2.2.5 Effect of reaction time

During the oxidant decomposition studies, discussed in Chapter 3, it was observed that the oxidant is consumed at a high rate during the early stages of the reaction.

Thus, the effect of time on the reaction progress was also evaluated. The conversion was determined after 1, 3 and 6 hours for catalysts **C4** (monomeric iron) and **MD5** (iron metallodendrimer). When hydrogen peroxide was used the conversion after 6 hours was virtually identical to that after 3 hours, most likely because all the oxidant had already decomposed within the first 3 hours.

When the reaction was performed using TBHP as oxidant, around 25% conversion was obtained within the first hour of the reaction. Over the next two hours the conversion slowly increased, resulting in 35% total conversion being obtained after 3 hours.

Both **MD5** and **C4** exhibit high TOF values within the first hour of the reaction (Figure 5). However over longer reaction times the TOFs decrease drastically. This is most likely due to the high concentration of oxidant at the start of the reaction. However, catalyst decomposition could also be occurring over time, especially if unselective free radical species are being formed.

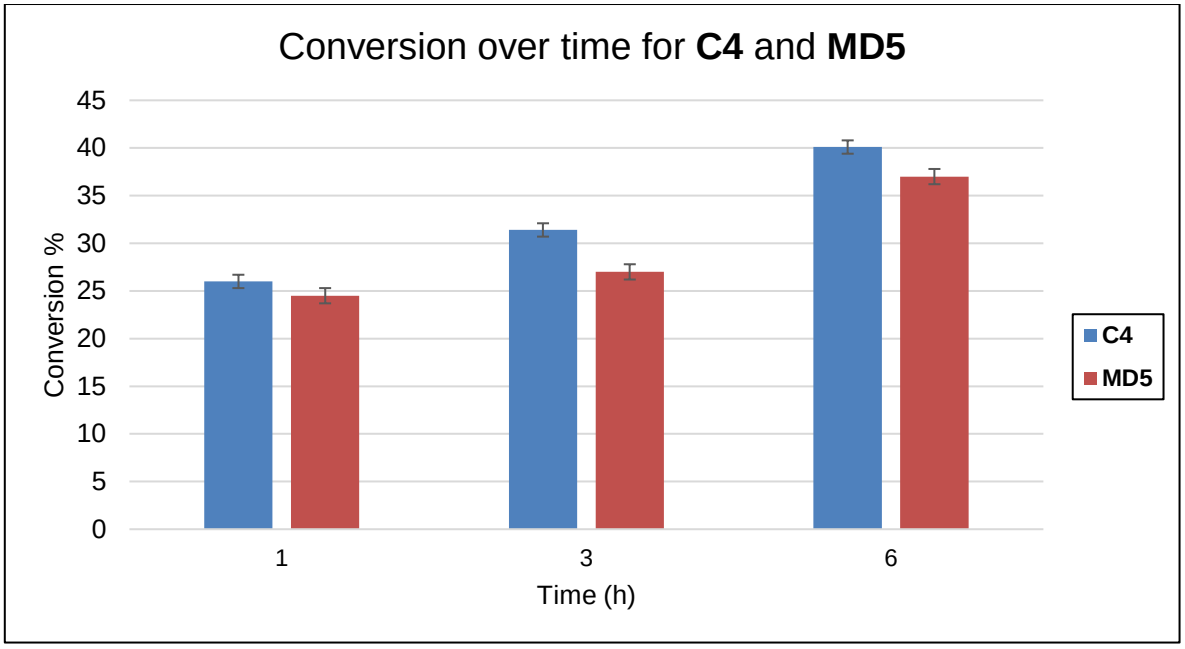

Figure 5: Effect of time on catalytic oxidation of cyclohexene by C4 and MD5. Reaction conditions: 2.00 mmol, cyclohexane, 6.00 mmol TBHP, 0.5 mol % iron,3 hours, 40 °C, MeCN.

Under these optimized conditions catalysts **C4** and **MD5** achieved respectable TON and TOF values (after 1 hour). **C4** obtained slightly higher TON values than **MD5** (Table 1).

Table 1: Activity data for cyclohexene oxidation using various iron catalyst precursors in conjunction with TBHP as oxidant

Reaction time (h)	Complex	TON	TOF (mol product/mol catalyst.h)
3	**C4**	62.9	20.1
3	**MD5**	52.4	17.7
1	**C4**	51.3	51.3
1	**MD5**	49.6	49.6
3	**MD3**	39.3	13.1
3	**MD4**	32.3	10.8

Reaction conditions: 2.00 mmol, cyclohexane, 4.00 mmol TBHP, 0.5 mol% Fe, 40°C, MeCN (0.2138 ml.). TON calculated as mol total product/ mol catalyst. TOF calculated as TON/ Time (h). Reaction time as indicated.

The TOF values obtained for **C4** and **MD5** are fairly similar to one another with both catalyst precursors yielding fairly similar TON and TOF values. This observation is especially valid over the first hour of reaction. **C4** has slightly higher TON and TOF values than **MD5** after 3 hours of reaction, which might indicate that the decomposition of the active catalyst species occurs less readily for **C4** than when using **MD5** as catalyst precursor. The TON and TOF values obtained for **C4** and **MD5** also compare favourably to other iron catalyst systems reported in literature.[25]

Das et al. reported on the use of an oxo-bridged iron pyridine-amine complex for the oxidation of cyclohexene.[25] In their work, a maximum TOF value of 72 h^{-1} was achieved at 30°C, using a mixture of acetic acid and H_2O_2 (in order to form peracetic acid according to the authors) as oxidant.[25]

The Fe(III) complex **MD3** was less active than the Fe(II) complexes. A possible explanation for this can be obtained by considering the well-known Fenton system. During the Fenton cycle, Fe(III) reacts more slowly than Fe(II) with H_2O_2 with the former producing peroxyl species rather than hydroxyl species.[28] During this initial step, Fe(III) is reduced to Fe(II). The newly formed Fe(II) complex reacts with H_2O_2 to form hydroxyl radical species. In our case, Fe(III) complex **MD3** is expected to undergo a similar series of reactions, leading to much slower overall reaction.

Complex **MD3** is also insoluble at the start of the catalytic reaction, thus resulting in a much lower concentration of the active species being in solution during the initial stages of the reaction.

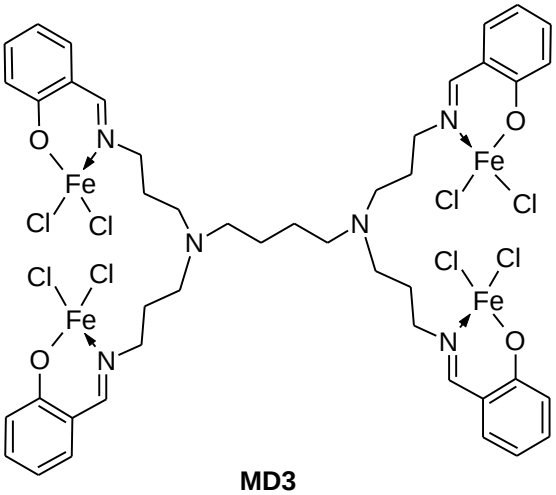

MD3

Figure 6: Iron(III) complex MD3 employed in catalytic cyclohexene oxidation

Complex **MD3** has salicylaldimine ligands coordinated to Fe(III) and is neutral due to the presence of Cl ligands in the inner sphere. On the other hand, **MD5** has pyridine-imine ligands and is cationic Fe(II). If the first step of the reaction mechanism is activation of the oxidant by the metal complex (coordination of oxidant), this should be favoured for the 4-coordinate cationic complex. In contrast coordination of a negatively charged or radical species should be more favourable for a Fe(III) species than for a Fe(II) species.

A similar study was performed by Silva et al. who reported on the oxidation of various hydrocarbon substrates using different homogeneous iron catalyst precursors (Figure 7). Silva et al. studied the oxidation of cyclohexane and n-hexane and observed that the Fe(N_2O_2)Cl complexes generally achieved the highest turnover numbers. Furthermore, it was found that increasing the electron density on the metal via inductive effects lead to an increase in catalytic activity (**R2**<**R1**<**R3**). **R4** was found to be the most selective catalyst precursor. A metal based oxidant, rebound type mechanism was suggested for **R4**, while the Fe(III) complexes were suggested to occur via radicals based on their selectivity results.

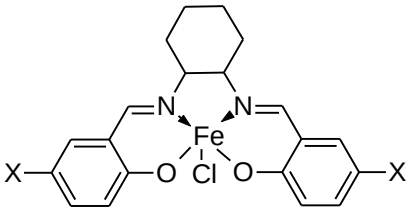

R1: X= H
R2: X= Br
R3: X= Me

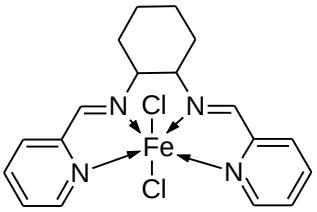

R4

Figure 7: N_2O_2 and N_4 Iron complexes utilized by Silva et al. for the oxidation of various hydrocarbons

The complexes **C4**, **MD3**, **MD4** and **MD5** are similar in structure to the complexes reported by Silva et al.[29] However, in our study it was found that the Fe(N_4) type complexes were more active than the Fe(N_2O_2)Cl (**MD3**) complex. Unfortunately, complexes **MD4** and **MD3** were insoluble in most organic solvents including acetonitrile. This makes direct comparison of these complexes (**C4**, **MD3**, **MD4** and **MD5**) based solely on electronic effects impossible. Furthermore, comparison to the results obtained by Silva et al. is also problematic. Many of the complexes reported by Silva et al. were soluble during catalytic test reactions in contrast to **MD4** and **MD3**.

The selectivity results obtained for the different catalyst precursors are quite similar. In all cases, relatively high selectivity towards 2-cyclohexen-1-one as the major product was obtained. The mononuclear complex **C4** was the most selective catalyst as well as the most active catalyst for the oxidation of cyclohexene. **MD5** is however only marginally less active with similar selectivity towards 2-cyclohexn-1-one. It appears overoxidation to the “other” products occurs readily as the reaction progresses leading to a decrease in the ketone selectivity over time. Interestingly, only small amounts of 2-cyclohexen-1-ol is observed- even when test reactions are performed at short reaction times.

Table 2: Product selectivities obtained for various iron complexes during the oxidation of cyclohexene using TBHP as oxidant

Entry	Time(h)	Catalyst	Selectivity (%)			
			cyclohexen-1-ol	cyclohexen-1-one	cyclohexene oxide	others
1	1	**C4**	19.5	65.7	3.1	11.7
2	1	**MD5**	15.7	65.4	2.9	16.0
3	3	**C4**	18.8	61.4	2.5	17.3
4	3	**MD5**	18.0	59.4	2.2	20.4
5	3	**MD3**	15.4	56.3	4.0	24.3
6	3	**MD4**	16.1	55.4	1.5	27.0

Reaction conditions: 2 mmol, cyclohexene, 4 mmol TBHP, 0.5 mol% Fe, 40°C, MeCN (0.2138 ml.)

The strikingly similar selectivity results obtained for the different catalyst precursors, seems to indicate that the active species (reactive oxygen species) might be the same in these reactions (for example a hydroxyl radical). High selectivity towards ketones has also been reported in the literature.[30] This could either be due to autooxidation of the alcohol product or it might indicate that the ketone and alcohol products are generated via different mechanisms.[22, 30, 31]

Mukherjee et al. also obtained high selectivity towards 2-cyclohexen-1-one in their study of the oxidation of cyclohexene using copper Schiff base complexes in the presence of TBHP.[32] Mukherjee et al. suggested that the use of TBHP results in the formation of 2-cyclohexen-1-one preferentially while the yield of 2-cyclohexene-1-ol is increased when using H_2O_2 as oxidant. The authors rationalized this by suggesting that selectivity is governed by the relative pKa values of the acidic protons in H_2O_2 and TBHP. Reaction of the metal complex and a peroxide oxidant leads to the formation of a metal peroxo complex (Scheme 3). Reaction with cyclohexene results in the formation of the epoxide intermediate and tert-butoxide or hydroxide ions (depending on oxidant). Subsequent deprotonation occurs to reform the allylic double bond. It is suggested by Mukherjee et al. that the next step is dependent on oxidant pKa. In the case of TBHP, the α proton on the substrate is abstracted with subsequent formation of 2-cyclohexen-1-one, *tert*-butanol and a metal-hydroxo species. In the case of hydrogen peroxide, the hydrogen peroxide is deprotonated to form a metal-hydroperoxide species (Cu-OOH eventually) and 2-cylcohexen-1-ol. However, in the mechanism presented by Mukherjee et al. no free radical species

are proposed. Unfortunately, the authors did not test this hypothesis by employing a radical scavenger and they also did not comment on the possibility of a free radical pathway for the reactions under investigation.

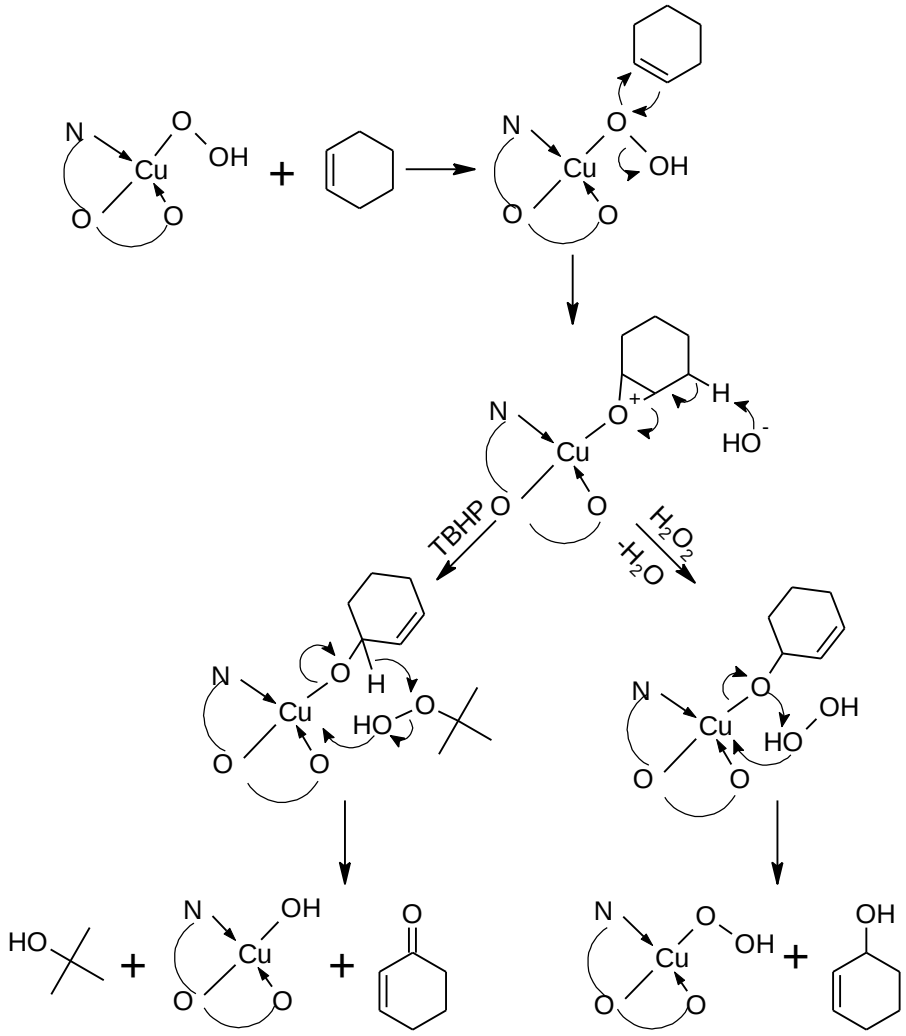

Scheme 3: Selectivity in cyclohexene oxidation reactions based on oxidant as proposed by Mukherjee et al.[32]

Other authors have reported similar product selectivities when using iron catalyst systems in the oxidation of cyclohexene. Sehlotho et al. investigated the oxidation of cyclohexene by iron phthalocyanine complexes.[33] In their study, the use of TBHP as oxidant, resulted in the formation of a 2-cyclohexen-1-one as the major product with selectivities above 70%. These results are comparable to our results presented in Table 2.[33] The authors attempted to rationalize their selectivity by suggesting that when TBHP is used as oxidant, free radical species are formed. However, the

authors did not suggest a mechanism to explain why the radical species would favour the formation of 2-cyclohexen-one. Other authors have made some suggestions to explain this observation as discussed below.

MacFaul et al. attempted to explain the high selectivity towards ketone products in free radical mediated, hydrocarbon oxidation reactions.[34] According to Scheme 4, cyclohexen-1-one could be formed via various routes including a free radical mediated alcohol oxidation (autoxidation, Scheme 4, reactions 4 and 5), which explains the high selectivity towards the ketone product. Similar reactions have been proposed by Weiner et al.[35] as well as Fu et al.[35]

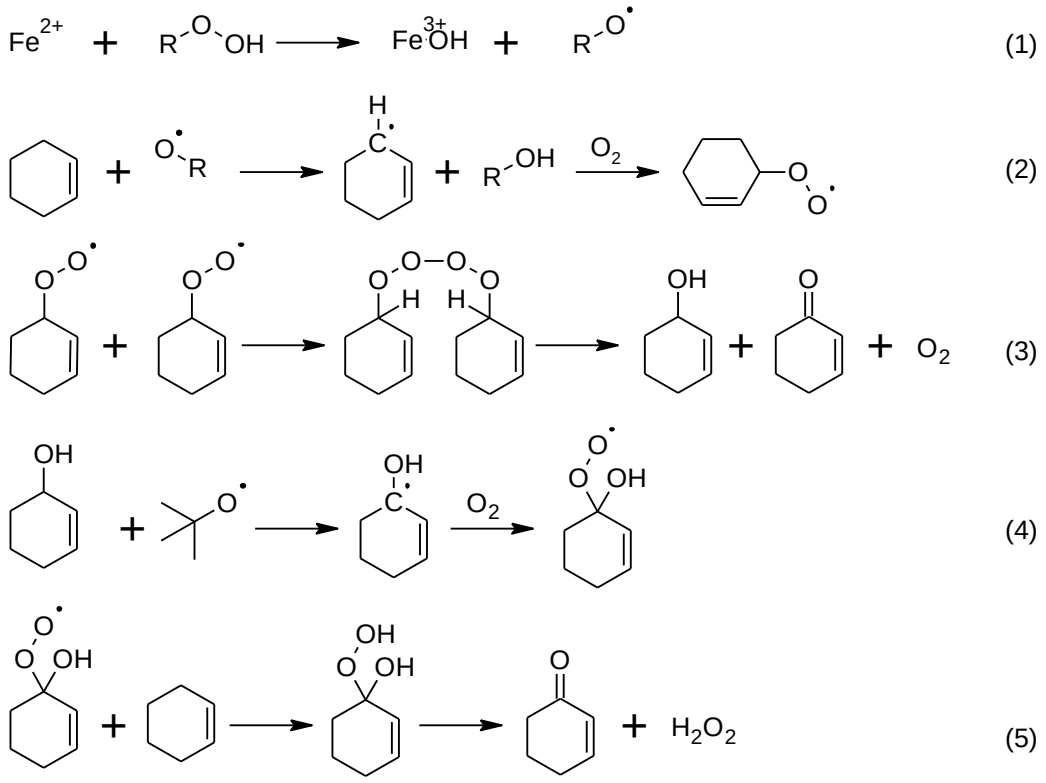

Scheme 4: Oxidation of cyclohexene to 2-cyclohexen-1-ol and 2-cyclohexen-1-one[34–36]

In our reactions, only traces of cyclohexene oxide are detected (< 10%, Table 2). Other authors have proposed that epoxide products are formed from alkenes (in iron mediated catalysis) via a metal-based oxidant (Fe(IV)=O or Fe(V)=O), in the rebound mechanism.[37] In these reactions high valent iron-oxo species are formed and these species facilitate the formation of the epoxide product. Such high oxidation state

species are thought to be highly unstable, with the result that characterization data and concrete evidence for such species are often lacking in the literature.[38] However, several porphyrin and haem derivatives are thought to follow such a mechanism (Scheme 5, (1) rebound mechanism).

McAteer et al. suggested an alternative mechanism that could possibly explain the formation of epoxide products in “Fenton-like” systems (generation of free radicals as reactive oxygen species).[39] In their work an iron-hydroperoxo species (with very poor stability and low lifetime) was thought to be the active catalyst for epoxidation (Scheme 5 (2) Fenton-like).

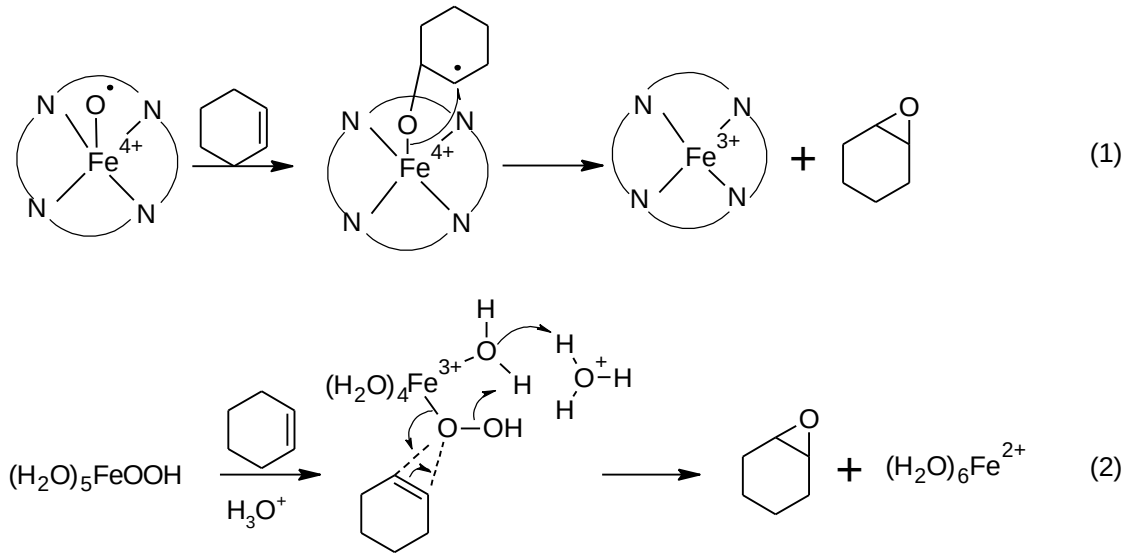

Scheme 5: Formation of epoxide products catalysed by iron catalysts[39]

In cyclohexene oxidation reactions performed using our iron complexes, TOF and TON values obtained when using TBHP as oxidant are higher than those in which hydrogen peroxide was employed as oxidant. Similar observations have been made in the literature for iron phthalocyanine (Pc) systems.[40] In these cases, it was found that the use of hydrogen peroxide as oxidant readily leads to catalyst decomposition, involving oxidation of the aromatic Pc ring. Catalyst decomposition, however does not occur as readily when TBHP is used as oxidant.[41, 40] Similar catalyst decomposition might be occurring when using **C4** or **MD5** as catalyst precursors. During the course of the reaction a colour change from purple to orange is observed (UV-Vis spectra of this colour change was recorded and discussed in Chapter 3).

Also, a drop in TOF is observed for both catalyst precursors with increasing reaction time. Thus, it appears that a similar catalyst decomposition pathway to that reported for iron phthalocyanine systems could possibly occur. In the event of free radicals forming during the oxidation reactions, decomposition of the catalyst is expected to be exacerbated due to the extremely reactive and unselective nature of these radical species.[40–42]

The iron complexes proved to be relatively successful as catalyst precursors for the oxidation of cyclohexene showing moderate TON/TOF values compared to other iron catalyst systems reported in literature. This is especially true in the presence of TBHP where TON and TOF values were obtained comparable to those reported in literature by Das et al. as discussed above (TOF, 72 h^{-1}, mixed oxidant H_2O_2/ CHOOH).[25] Our results are also comparable to those of Sehlotho et al. who obtained high TON values (maximum 494), albeit over much longer reaction times and thus did not report TOF values (up to 4 weeks reaction times).[43] The catalytic activities obtained for **C4** and **MD5** are also comparable to some of the porphyrin systems, such as the iron, manganese and cobalt metalloporphyrins catalyst systems reported by Połtowicz et al. and Serwicka et al.[44, 45] **C4** and **MD5** showed cyclohexene conversions which were slightly higher than those reported for a manganese porphyrin catalyst system, which showed 28.1% cyclohexene conversion using PhIO as oxidant after 16 hours at 25 °C.[44] The iron porphyrin system reported by Serwicka et al. obtained 29% conversion under reaction conditions identical to those employed by Połtowicz et al. (16 hours using PhIO as the oxidant at 25 °C). [44, 45] The metalloporphyrin systems reported by Połtowicz and Serwicka et al. show selectivity towards the epoxide product, while **C6** and **MD5** are much more selective towards the allylic oxidation products. This might indicate a difference in the mechanism of oxidation as many metalloporphyrins are known to operate via the rebound mechanism (Scheme 5, Reaction 1).[46]

However, far more active catalyst systems have also been reported in literature, White et al. reported an iron catalyst precursor, generated *in situ* from a pyridine-amine ligand and $Fe(II)(SbF_6)_2$, capable of oxidizing various alkenes to the corresponding epoxide products (with very high selectivity) using H_2O_2 as the oxidant in as little as five minutes.[21] White et al. however only studied the oxidation of

straight long-chain alkenes such as 1-decene and did not report any results on cyclic alkenes. Other catalyst systems have been reported in which oxygen is employed as the oxidant, which is highly desirable from an economic and green chemistry perspective. Hughes et al. reported on the oxidation of cyclohexene over nanocrystalline gold catalysts using oxygen as the oxidant. In their reactions, cyclohexene conversions around 30% were obtained which are comparable to the results obtained for **MD5** and **C4**. However, in their reactions only a small amount of TBHP (typically 5 mol% relative to substrate) is added as initiator and the system pressurized with oxygen which acts as the oxidant (typical conditions include: 1% Au/C catalyst, 80 °C, 24 hours, 1,2,3,5- tetramethylbenzene as solvent, 2.96 Bar O_2). Both the activity and the selectivity of the catalyst could be fine-tuned through the use of different promotors but in most cases 2-cyclohexen-1-one was a major product, similar to what was observed for **C4** and **MD5**. However, the authors found that in a number of cases over-oxidation to CO_2, formic acid and oxalic acid had occurred. Given the moderate success with our iron-based catalysts, it was decided to explore the use of other earth-abundant metals. Thus, the oxidation of cyclohexene using cobalt and copper catalyst precursors was subsequently investigated.

4.2.3 Cobalt and copper complexes for the oxidation of cyclohexene

Various cobalt and copper Schiff base complexes[47–50] (for example cobalt salen) as well as cobalt MOFS[51, 52] have previously been reported as active catalyst precursors in the oxidation of alkenes and alkanes. With this in mind, complexes **C1**, **C2**, **MD1** and **MD2** (pictured in Figure 8) were evaluated as catalyst precursors in the oxidation of cyclohexene.

However, when **C1**, **C2**, **MD1** and **MD2** were applied as catalyst precursors along with the oxidant, hydrogen peroxide, under conditions similar to those reported in literature (and fairly similar to the optimized conditions employed for the iron complexes discussed above), relatively low conversions were obtained (Figure 9). All four catalyst precursors tested yielded conversions of less than 10% over a three-hour reaction period. The oxidant decomposition studies described in Chapter 3,

indicated that, under the reaction conditions employed, virtually all of the oxidant would be expected to have decomposed after about three hours reaction time.

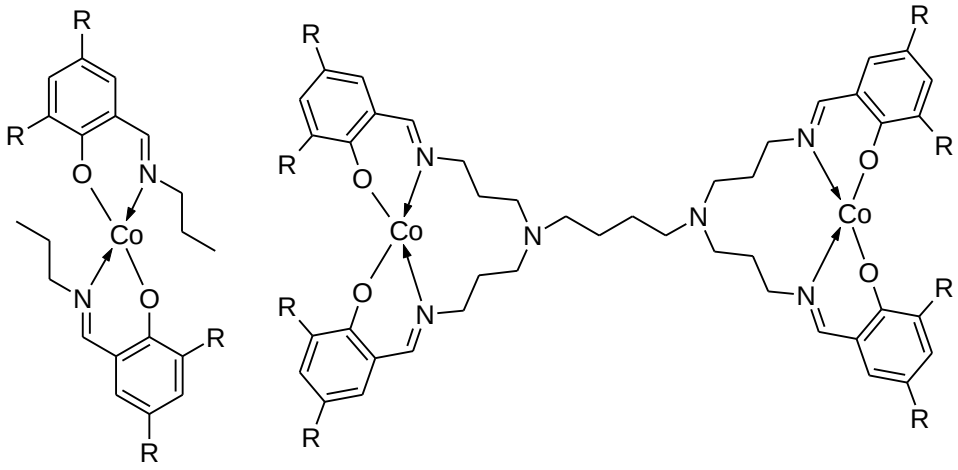

C1: R= H

C2: R= *tert*-Butyl

MD1: R= H

MD2: R= *tert*-Butyl

Figure 8: cobalt salicylaldimine complexes for cyclohexene oxidation

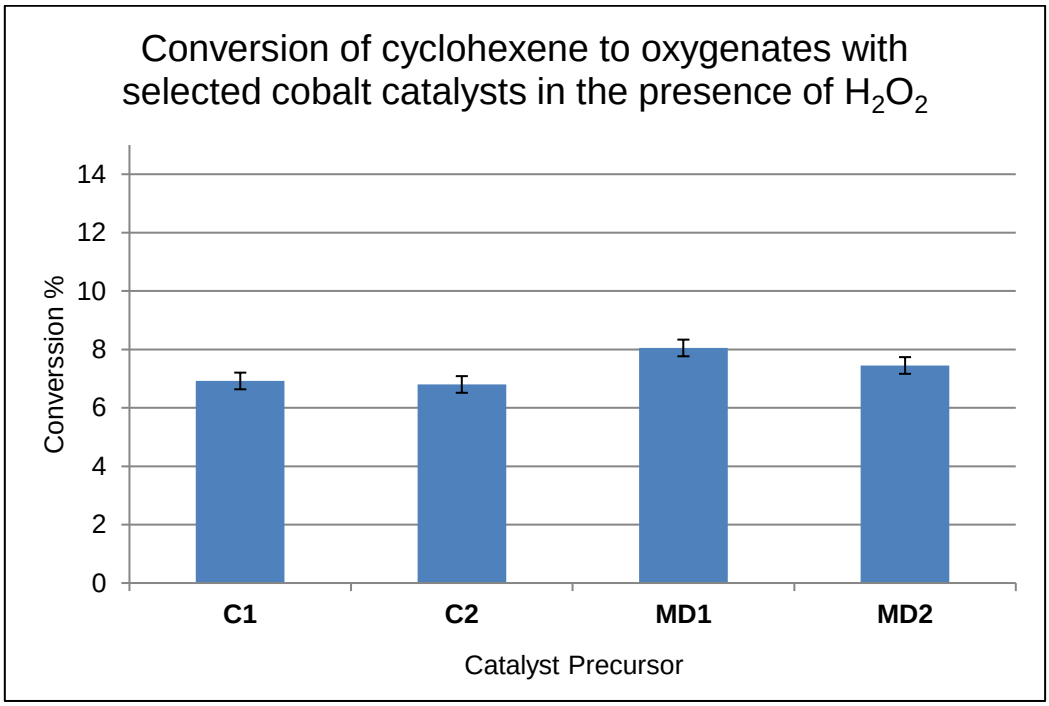

Figure 9: Oxidation of cyclohexene by cobalt complexes in the presence of H_2O_2. Reaction conditions: 2.00 mmol, cyclohexene, 6.00 mmol H_2O_2, 1mol% Co, 3 hours, 25 °C, MeCN (0.214 ml).

A possible reason for the low conversions obtained for the **C1**- and **C2** catalysed reactions, could be the hydrogen peroxide disproportionation activity observed for complexes **C1** and **C2** (discussed in Chapter 3). Reactions employing **C1** or **C2** in the presence of hydrogen peroxide tend to effervesce vigorously leading to build up of pressure inside of the reaction vessel. It was therefore decided to explore a decrease in the concentration of the catalyst precursor, with the hope that it could lead to better catalytic activity for the model complexes. In addition, the influence of various reaction parameters such as catalyst concentration, temperature, oxidant concentration and the nature of the oxidant was investigated for these cobalt catalysed test reactions. Optimization of the cobalt based catalytic reaction was accomplished by employing **C1** (mononuclear complex) and **MD1** (dendritic complex) as catalyst precursors.

4.2.3.1 Effect of catalyst concentration on catalytic activity

In Chapter 3 it was observed that by decreasing the concentration of **C1** and **C2** in the reaction mixture, the decomposition of the oxidant is slowed down significantly. Test reactions were thus performed at both 0.1, 0.5 as well as 1 mol% cobalt concentration (relative to substrate). Neither **C1** nor **MD1** displayed any catalytic activity at 0.1 mol% cobalt (result within experimental error of blank reaction containing only oxidant, ~1% conversion), while some activity is observed at 0.5 mol% cobalt. The highest conversion of the substrate was observed at 1 mol% cobalt. Any further increase in catalyst concentration did not lead to a higher conversion for **C1**, while **MD1** displayed slightly higher conversions at 1.5 mol% cobalt.

Reducing the concentration of the cobalt catalyst below 0.1 mol% did not seem to improve the conversion either. However, it was noted that even at the lower catalyst concentration effervescence of the reaction mixture (though less than at higher concentrations) occurs. Based on these exploratory results a cobalt concentration (relative to substrate) of 1 mol% was selected for further experimentation.

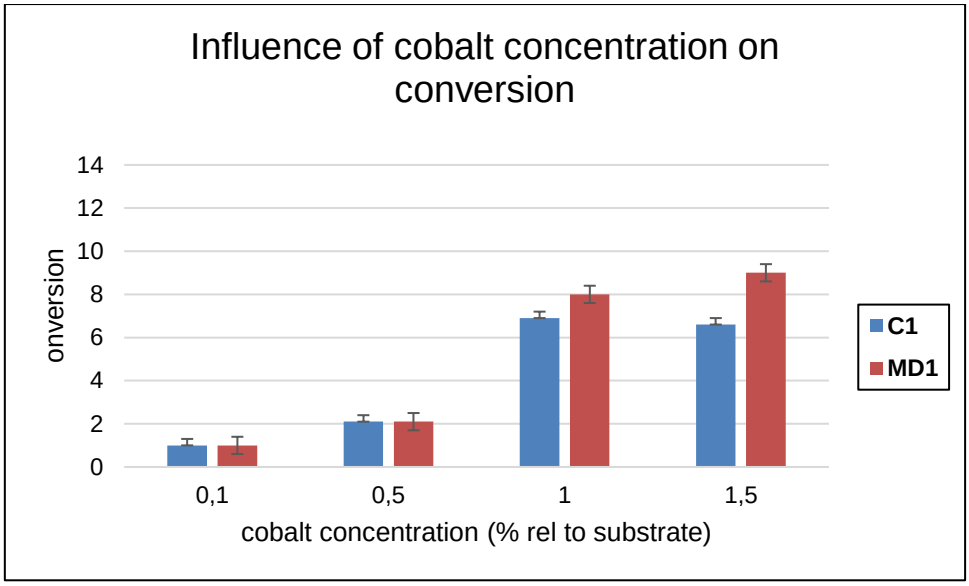

Figure 10: Oxidation of cyclohexene by C1 and MD1 at different cobalt concentrations in the presence of H_2O_2. Reaction conditions: 2.00 mmol, cyclohexene, 6.00 mmol H_2O_2, 3 hours, 25 °C, MeCN (0.214 ml).

Hydrogen peroxide is known to be thermally unstable, thus the temperature dependence of the reaction was evaluated next.

4.2.3.2 Effect of temperature on catalytic reactivity

Cyclohexene oxidation was attempted at three different temperatures namely 0, 25 and 40 °C. It was hoped that at 0°C the decomposition of the oxidant would be suppressed and that some catalytic activity would be observed for the model complex **C1**. At 0°C very little effervescence is observed in the **C1** catalysed reactions. Unfortunately, at this temperature virtually no oxidation products were detected either (GC-FID). Higher substrate conversions were obtained at both 25 and 40 °C. The results obtained for both **C1** and **MD1** at 40 °C were nearly identical to those obtained at 25 °C. Further increases in the reaction temperature was attempted for both **C1** and **MD1**. **MD1** achieved a conversion of less than 3% at 60 °C. When a **C1** catalysed reaction was attempted at 60 °C, the internal pressure of the reaction vessel increased past the threshold of the test reactor. Thus, these high temperature reactions were subsequently attempted in a high-pressure reactor.

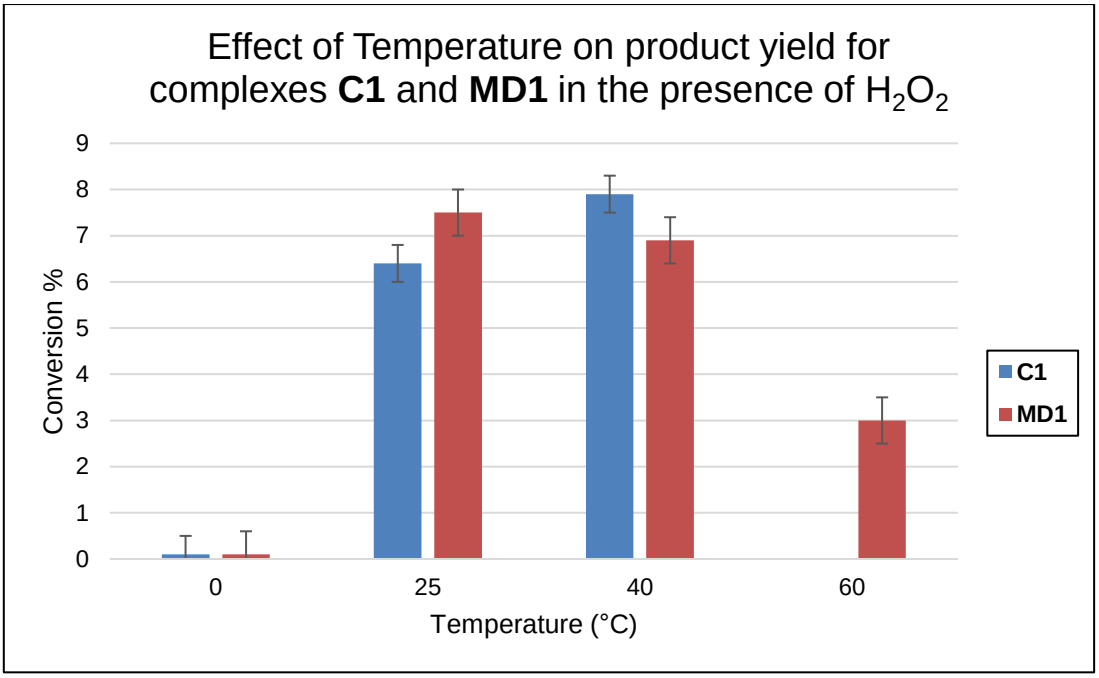

Figure 11: Effect of temperature on conversion for C1 and MD1. Reaction conditions: 2.00 mmol, cyclohexene, 6.00 mmol H_2O_2, 3 hours,1 mol% cobalt, MeCN (0.214 ml).

Catalytic test reactions using both **C1** and **MD1** were therefore attempted in a glass high pressure reactor (Q-tube^{TM} glass reaction tube). Two reactions at 60 °C were attempted. In the first experiment **C1** was employed as catalyst precursor at 60 °C as described above. Low conversions were also obtained in the high-pressure reactor (< 1.5%). **C1** performed even worse in this reaction setup possibly due to physical differences between the reactor setups e.g. reactor volume, different mixing regimes. However, it seems that decomposition of the oxidant to O_2 and H_2O is the main decomposition pathway when using **C1** as catalyst precursor. It appears that very little homolytic cleavage of the oxidant (to form radical species) occurs in the temperature range evaluated.

Some authors have reported on the use of oxygen as co-oxidant. **C1** and **MD1** were thus evaluated as described above (at 60 °C), with the inclusion of oxygen as co-oxidant. The results of these experiments are discussed below.

4.2.3.3 Effect of oxidant

The use of molecular oxygen as oxidant is highly desirable due to its green nature and low cost. Complexes **C1** and **MD1** were tested as oxidation catalysts using a combination of H_2O_2 (2 mole equivalent relative to substrate) and O_2 as oxidants in a high-pressure reactor. However even under O_2 pressures as high as 10 bar, and temperatures up to 60 °C only traces of products were detected (~2% conversion). Thus, it appears that the catalase-like mechanism (Scheme 6) under which **C1** decomposes the oxidant, hydrogen peroxide, is much more favourable than the generation of a radical species under the reaction conditions employed. It appeared that both hydrogen peroxide as well as oxygen were ineffective as oxidants in this oxidative process.

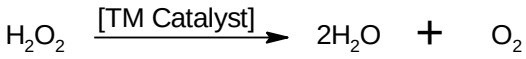

Scheme 6: Hydrogen peroxide disproportionation by transition metal catalyst

Tert-butyl hydroperoxide (TBHP) is commonly employed as oxidant in hydrocarbon oxidation processes.[53] TBHP was chosen to replace H_2O_2 as oxidant due to its higher thermal stability relative to other alkyl hydroperoxides (and hydrogen peroxide).[54] It was hoped that disproportionation of the TBHP oxidant did not occur as readily as was the case for H_2O_2.

The use of TBHP resulted in the highest substrate conversion obtained for both **MD1** and **C1**. Therefore, the refined optimum reaction conditions involved the use of TBHP in these cobalt catalysed reactions. The TOF and TON values obtained under these conditions are reported in Table 3.

When H_2O_2 was replaced by TBHP as oxidant in **C1** or **C2** catalysed reactions, virtually no effervescence was observed. Additionally, enhanced catalytic activity was obtained in these reactions. Reactions catalysed by either **C1** or **C2** achieved around 22% conversion with selectivity towards 2-cyclohex-1-one as the major product while small amounts of 2-cyclohex-1-ol and cyclohexene oxide are also obtained.

Table 3: TON and TOF values obtained for cyclohexene oxidation by cobalt and copper complexes using TBHP as oxidant

Complex	Conversion (%)	TON	TOF
MD1	15.29	15.29	5.10
C1	21.77	21.77	7.26
MD2	19.28	19.28	6.43
C2	20.46	20.46	6.82
C5	24.63	24.63	8.21
C6	15.88	15.88	5.29
C7	13.90	13.90	4.633

Reaction conditions: 2 mmol, cyclohexene, 4 mmol TBHP, 1 mol% metal, 40 °C, MeCN (0.2138 ml.). TON calculated as mol total product / mol catalyst. TOF calculated as TON / Time (h).

Similarly, an increase in catalytic activity is observed in the oxidation reactions catalysed by the metallodendrimers, **MD1** and **MD2** in the presence of TBHP. However, these conversions are lower than the analogous, mononuclear model compounds **C1** and **C2**. This could possibly be due to the relatively higher oxidation potentials of **MD1** and **MD2** (as discussed in Chapter 3). Oxidation of the metal centre and thus subsequent catalytic activity occurs more readily for the model complexes. Furthermore, the model complexes are relatively more soluble than their dendritic counterparts (especially true in the case of **C2** and **MD2**).

The catalytic activities obtained for **C1** and **C2** are comparable to those reported for cobalt catalyst systems in the literature. Salavati-Niasari reported on cobalt(II) Schiff base complexes as catalyst precursors for the oxidation of cyclohexene.[55] In their study a cobalt(II) salicylaldimine complex, similar in structure to **C1**, showed around 30% conversion of the cyclohexene substrate using TBHP as oxidant.[55] The substrate conversion was vastly improved by immobilization of the catalyst on an alumina support (above 70% conversion). In both cases high selectivity towards the allylic oxidation products was obtained. In another report by Salavati-Niasari, conversions of around 45% for their homogeneous cobalt Schiff base complex was achieved after 8 hours.[56] Again, the authors improved upon this result by immobilizing the cobalt Schiff base complex (zeolite support), obtaining 59% cyclohexene conversion with selectivity towards 2-cyclohex-1-one (> 80%) using TBHP as oxidant at 40°C. These authors proposed that decomposition of the catalytically active species takes place when employing the homogeneous catalyst

and decomposition of the catalytically active species is inhibited when the complex is supported. Mirkhani et al. obtained very good catalytic activity in the oxidation of cyclohexene using a cobalt Schiff base complex covalently bonded to a polyoxometalate.[57] Nishinaga et al. reported on the use of four-coordinate cobalt Schiff base complexes (bearing the N_2O_2 donor set) for the oxidation of various alkenes.[58] Good catalytic activity was obtained using O_2 as the oxidant at 60°C, however, only activated alkenes containing aromatic or other electron withdrawing groups were evaluated as substrates. The cobalt metallodendrimers, **MD1** and **MD2** are less active than the literature systems discussed above.

The cationic copper(II) thioether-amine catalyst precursor with triflate counterion, **C5** (Figure 12), achieved the highest conversion of around 25%. Similar conversions, (30-50%) were obtained by Maurya et al. in the oxidation of cyclohexene with TBHP and copper(II) complexes bearing N, O ligands.[59] The analogous cobalt complex with chloride counterion showed the lowest substrate conversion (Figure 12). **C6** is insoluble in most organic solvents and remains mostly insoluble during the course of the reaction. However, after 3 hours the reaction mixture had changed colour to a very pale pink. This suggests that some of the cobalt species dissolves into solution. It is possible that the Co(III)-OH species (an intermediate which could possibly form during free radical mediated oxidation) might be soluble.

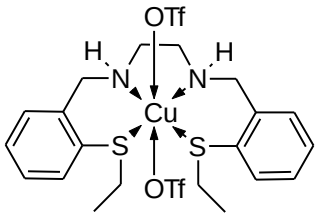

C5

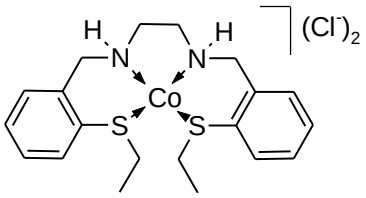

C6

Figure 12: Cobalt and copper complexes for cyclohexane oxidation

While several catalyst systems exhibiting relatively low conversions (< 50%), similar to those reported in Table 3, have been reported in literature, a number of highly active and selective oxidation catalyst systems are also known. Jacobsen's catalyst (and derivatives thereof) is a highly efficient, enantioselective epoxidation catalyst, widely employed in pharmaceutical synthesis.[60, 61] Some reported catalyst systems

use O_2 as the only oxidant, which is highly desirable from both a green chemistry as well as an economic standpoint.[62, 63] The complexes **C1**, **C2**, **C5**, **C6**, **MD1** and **MD2** compare unfavourably to these catalyst systems.

Reactions catalysed by **C2** and **MD2** exhibited slightly higher conversions than their **C1** and **MD1** counterparts. Both **C2** and **MD2** have *tert*-butyl substituents on the aromatic rings of the salicylaldimine ligands. The inductive effects of these tert-butyl groups should cause the cobalt centre to be have relatively more electron density than their **MD1** and **C1** counterparts, which have no substituents on the salicylaldimine ligands. Thus the oxidation of the metal centre from Co(II) to Co(III) is expected to be more facile for **C2** and **MD2**. The oxidation potential as measured by cyclic voltammetry (Chapter 3) for complexes **C2** and **MD2** are lower than their **MD1** and **C1** counterparts and might explain their higher catalytic activity.

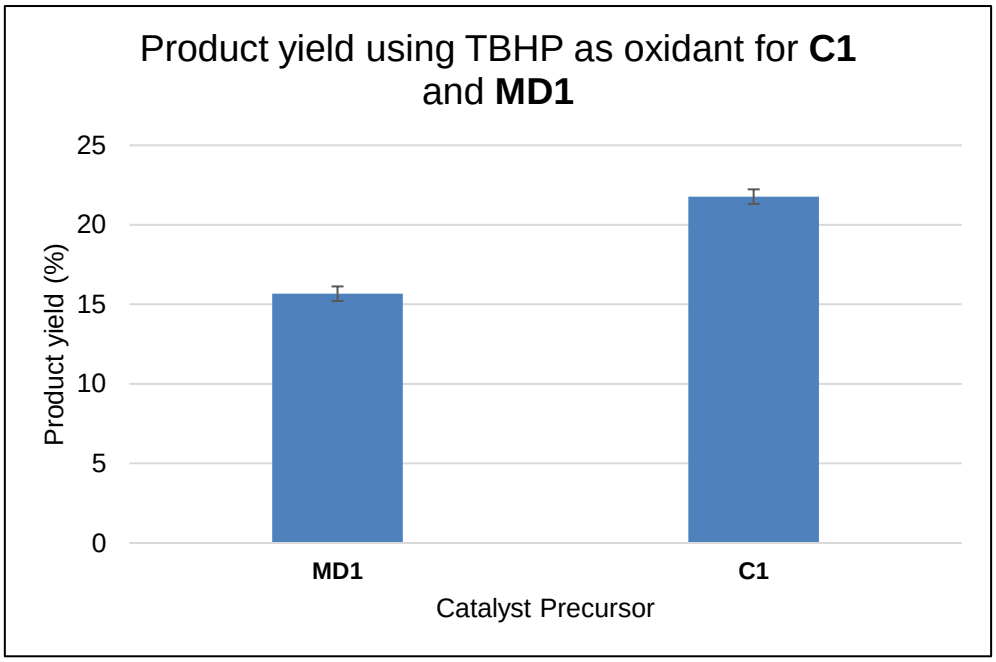

Figure 13: Catalytic oxidation of cyclohexene by MD1 and C1 employing TBHP as the oxidant. Reaction conditions: 2.00 mmol, cyclohexane, 6.00 mmol TBHP, 1 mol % Co,3 hours, 40 °C, MeCN (0.214 ml).

During the GC-FID analysis of these reactions a peak was observed that did not correlate to any products (including those observed in the iron catalysed reactions and labelled as “other”). This peak is absent from the GC-trace when using hydrogen peroxide as oxidant. Further analysis of the product stream by GC-MS, revealed that

the product is likely 1-(*tert*-butylperoxy)-2-cyclohexene. Similar observations were previously made by Salavati-Niasari et al. who also detected peroxide containing products in the oxidation of cyclohexene with TBHP.[55] Salavati-Niasari et al. employed various metal salen complexes in their catalytic test reactions and detected 1-(*tert*-butylperoxy)-2-cyclohexene in the product stream with selectivity to this species as high as 25%.[55] Similar selectivity towards 1-(*tert*-butylperoxy)-2-cyclohexene was obtained in our reactions. 2-cyclohexen-1-one and 1-(*tert*-butylperoxy)-2-cyclohexene were the major products of the reaction as shown in Table 4.

Table 4: Product selectivities obtained for cobalt and copper catalysed oxidation of cyclohexene

Catalyst	Selectivity %			
	2-cyclohexen-1-ol	2-cyclohexen-1-one	peroxide	oxide
MD1	13.5	56.1	24.1	6.3
MD2	5.2	62.8	27.4	4.7
C1	13.0	52.3	28.0	6.7
C2	15.0	49.9	30.5	4.7
C5	6.2	48.7	41.1	3.9
C6	8.6	65.1	20.3	5.9
C7	6.0	50.1	39.1	4.8

Reaction conditions: 2 mmol, cyclohexene, 4 mmol TBHP, 1 mol% metal, 40°C, MeCN (0.2138 ml.).

An attempt was made to reduce the 1-(*tert*-butylperoxy)-2-cyclohexene product with PPh_3 (Shul'pin's method) as described by other authors for the reduction of alkylhydroperoxides.[64] However, reduction of the peroxide product to 2-cyclohexen-1-ol and 2-cyclohexen-1-one did not occur quantitatively (even when employing gentle heating during reduction). This suggested that the peroxide product is relatively stable. The detection of such peroxide products would suggest a free radical centred mechanism being operative.

The 1-(*tert*-butylperoxy)-2-cyclohexene product could probably be formed by reaction of a cyclohexene radical (formed by abstraction of a proton by another radical species) with a *tert*-butylperoxo radical species in a radical chain termination process (Scheme 7).

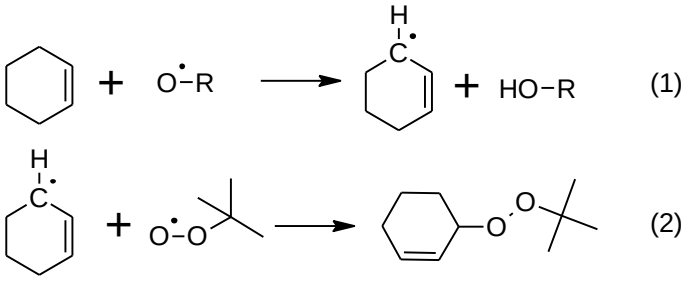

Scheme 7: Radical chain termination to form 1-(*tert*-butylperoxy)-2-cyclohexene

Decomposition pathways leading to the formation of peroxyl radical have been described for metals such as cobalt and copper.[65] Deprotonation and coordination of the hydroperoxide yields a metal peroxo species. The alkylperoxo complexes then decompose to release free radical species (Scheme 8).

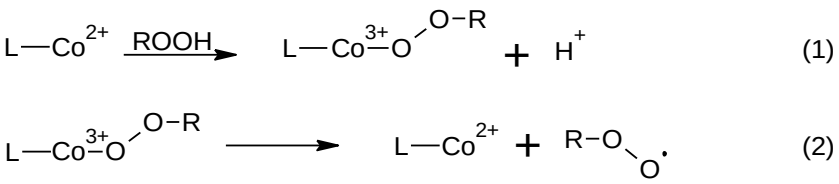

Scheme 8:Formation of metal-peroxo species[65]

A number of stable cobalt(III) alkylperoxo compounds have also been reported and even isolated.[66] These systems are often used as stoichiometric oxidants. In these cases, oxidation of the substrate only occurs once the metal peroxo species decomposes to yield the free alkylperoxo radical species (or hydroperoxo in the case of H_2O_2).

MD1 and **MD2** exhibited enhanced catalytic activity in the presence of TBHP, however the catalytic activity is still relatively low compared to other systems in the literature. Other authors have suggested that reaction of the cobalt complex with the oxidant leads to the formation of cobalt(III) alkylperoxo species. In such cases where these cobalt alkylperoxo species are relatively stable, the catalytic activity will be poor. The cobalt peroxyl species must first be cleaved in order to generate a radical species which then abstracts a proton from the hydrocarbon substrate (Scheme 7).[67]

Such species were postulated as possible intermediates based on ESI-MS data obtained in the reaction of **C1** and **MD1** with TBHP as described in Chapter 3.

4.3 Catalytic oxidation of cyclohexene- mechanistic studies

In all the catalytic reactions discussed above the major product of the oxidation reactions was (in all cases) 2-cyclohex-1-one. Even when reactions were conducted for shorter time periods, greater selectivity towards 2-cyclohex-1-one is still observed, while very little 2-cyclohex-1-ol is detected.

The higher levels of 2-cyclohexen-1-one could possibly be ascribed to the auto-oxidation of 2-cyclohexen-1ol to the ketone product, 2-cyclohex-1-one. Thus, to test this hypothesis a catalytic experiment was performed where the cyclohexene substrate was replaced by 2-cyclohex-1-ol as substrate (Scheme 9). The optimized reaction conditions described in Section 4.2.2.3 were then employed to evaluate the auto-oxidation of the alcohol.

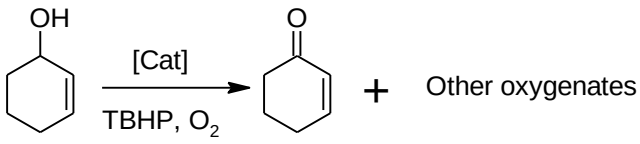

Scheme 9: Oxidation of the substrate 2-cyclohexen-1-ol

Under these reaction conditions full conversion of 2-cyclohex-1-ol substrate is observed within the 3-hour reaction time in the **MD5** catalysed reaction. 2-cyclohex-1-one formed in 83% yield while other oxidation products such as 2-hydroxycyclohexanone and 2,3-epoxycyclohexanone were also present (17%) as confirmed by GC-MS experiments. Thus, the auto-oxidation of 2-cyclohex-1-ol could serve as a possible explanation for the high selectivity observed towards 2-cyclohex-1-one. When **MD1** was employed as catalyst precursor in the above (Scheme 9) experiment, around 65% conversion of the starting material is obtained.

Other authors have made similar observations. Sawyer et al. has discussed results showing selectivity towards cyclohexanone and 2-cyclohex-1-one in the oxidation of

cyclohexane and cyclohexene, catalysed by various iron bipyridine and pyridine complexes.[68] Similarly, the so-called Gif systems (well-known iron complexes used in hydrocarbon oxidation reactions) prepared by Barton et al. show selectivity towards cyclohexanone in the oxidation of cyclohexane. Barton et al. suggested a metal-based oxidant mechanism, centred around high valent iron (Fe(V)=O intermediate) to explain the ketone selectivity of these catalyst systems.[69] In contrast, Sawyer et al. suggested that the unusually high ketone selectivity could be due to what the authors termed “oxygenated Fenton chemistry”. These authors proposed that the hydrocarbon substrate incorporates atmospheric oxygen to produce the ketone product. Other authors have tested for the “oxygenated Fenton chemistry” mechanism by performing reactions under an inert atmosphere such as argon.[22] If atmospheric oxygen is really involved during these oxidation reactions, then the catalytic activity should be inhibited under an inert atmosphere. This is indeed observed, in some cases.

The catalytic activities of **C4** and **MD5** were thus evaluated under an argon atmosphere, at the optimized reaction conditions discussed earlier. In the case of **C4** and **MD5** virtually no inhibition of the catalytic activity is observed. However, the role of oxygen in these reactions cannot be completely excluded on the basis of this experiment. Sawyer et al. suggested that formation of oxygen occurs during the decomposition of the oxidant thereby generating gaseous oxygen in situ.[70] Wei et al. has suggested a similar, radical-centred mechanism for the oxidation of cyclohexene to the products 2-cylohexen-1ol (selectivity: 36.9%) and 2-cylcohexen-1-one (selectivity: 55.7%) in the presence of oxygen.[30]

In our catalytic reactions described above, very little cyclohexene epoxide is formed, (typically less than 5%). Furthermore, various overoxidized products are also detected by GC-MS. These observations are typical of a free radical-centred process. Thus, an experiment was performed where a radical inhibitor was added to the reaction mixtures.

Butylated hydroxytoluene (BHT) is a well-known radical scavenger. BHT was added to cyclohexene oxidation reactions catalysed by **C4**. The effect of various ratios (relative to metal catalyst) of butylated hydroxytoluene (BHT) was then determined (Figure 14). The addition of increasing equivalents of BHT leads to a sharp decrease

in the observed catalytic activity of **C4**. This suggests that free radicals are likely to be involved in these oxidation reactions.

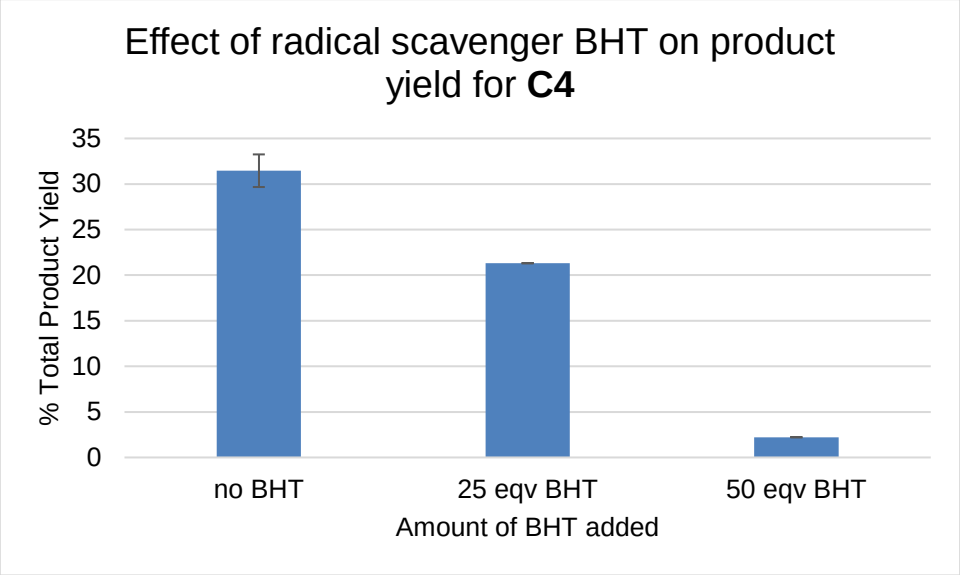

Figure 14: Inhibition of cyclohexene oxidation by BHT. Reaction conditions: 2.00 mmol cyclohexene, 6.00 mmol TBHP, 0.5 mol % Fe, 3 hours, 40 °C, MeCN (0.2138 ml).

Similar experiments conducted on **MD1** yielded similar results. Addition of 50 equivalents of BHT (relative to metal) to **MD1**- catalysed reactions successfully inhibited the oxidation of cyclohexene, thereby confirming the radical pathway.

The cobalt and copper complexes were generally less active in the oxidation of cyclohexene than their iron counterparts. However, all complexes formed 2-cyclohexen-1-one as the major product. Employing the cobalt and copper complexes as catalyst precursors in the oxidation of cyclohexene resulted in the formation of a significant amount of peroxide products as well. Only traces of peroxide products are observed in reactions catalysed by the iron complexes. All the complexes successfully catalysed the oxidation of cyclohexene to some degree. Subsequently the oxidation of the much more challenging substrate, octane, was attempted.

4.4 Octane oxidation catalysed by iron, copper and cobalt complexes.

The catalytic oxidation of octane is relatively more challenging compared to cyclohexene. The allylic C-H bond in cyclohexene is slightly more reactive than the C-H bonds of octane. Furthermore, the potential products in the oxidation of octane are numerous and include octanaldehyde, octanoic acid, various alcohols (including diols) and ketones. GC standards for all possible products are not readily available, thus, catalytic results are reported as % product yield (% yield of observed known products) instead of conversion (initial octane concentration – final octane concentration).

The oxidation of octane (Scheme 10) was carried out by employing the optimum conditions obtained for the oxidation of cyclohexene. Under these conditions, the complexes are largely inactive in the catalytic oxidation of octane. Only the iron complexes **C4**, **MD3** and **MD5** exhibited catalytic activity significantly higher than those obtained for blank control reactions (Table 5, Entry 1, no catalyst, TBHP oxidant). High selectivity towards the various ketones were obtained (2-octanone, 3-octanone and 4-octanone). This result suggests that autooxidation of the alcohol products takes place, as was observed when using cyclohexene as substrate. Furthermore, a decrease in alcohol selectivity is observed over the course of the reaction, while increasing the temperature of the reaction leads to an increase in the overall ketone selectivity with virtually no change in total product yield.

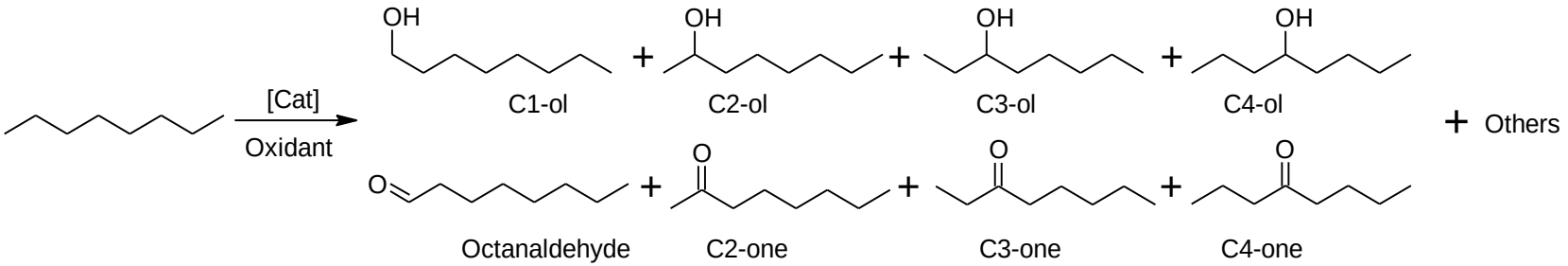

Scheme 10: Oxidation of n-octane to various oxygenates

Table 5: Product yields obtained for various iron complexes in the catalytic oxidation of octane

nr	Cat	Temp (°C)	Time (h)	% Yield of product							Total (%)
				C1-ol	C2-ol	C3-ol	C4-ol	C2-one	C3-one	C4-one	
1	None	60	12	3.00×10^{-4}	5.00×10^{-4}	1.00×10^{-4}	4.00×10^{-4}	0.301	0.302	0.201	0.81
2	**MD5**	40	4	0.260	0.450	0.35	0.300	0.800	1.04	1.76	4.96
3	**MD5**	40	12	0.110	0.100	0.107	0.100	1.75	1.38	1.8	5.23
4	**MD5**	60	4	1.00×10^{-3}	2.00×10^{-3}	2.00×10^{-3}	1.00×10^{-3}	1.46	1.64	2.22	5.33
5	**MD5***	25	4	3.00×10^{-4}	4.60×10^{-4}	1.60×10^{-3}	2.00×10^{-3}	0.33	0.32	0.28	0.94
6	**C4***	25	4	4.00×10^{-4}	6.00×10^{-4}	2.00×10^{-3}	2.00×10^{-4}	0.41	0.4	0.35	1.17
7	**C4**	60	4	2.00×10^{-3}	3.00×10^{-3}	3.00×10^{-3}	2.00×10^{-3}	2.25	2.18	2.18	6.62
8	**MD3**	60	4	1.80×10^{-3}	1.50×10^{-3}	2.10×10^{-3}	2.00×10^{-3}	1.35	1.31	1.31	3.98
9	**C5**	60	4	1.20×10^{-3}	2.50×10^{-3}	1.40×10^{-3}	1.00×10^{-3}	0.45	0.52	0.82	1.80

conditions: 2 mmol octane, 4 mmol TBHP, 3ml MeCN, 0.5 mol% metal

* 2 mmol octane, 6 mmol H_2O_2, 2 ml MeCN, 0.5 mol% metal, 3 hours

Complexes **C4** and **MD5** were the most active for this transformation, obtaining close to 7% total product yield (Table 5, Entry 6). The use of TBHP as oxidant yielded significantly better results than the use of hydrogen peroxide. However, the total product yield of oxygenates remains relatively low. Some unknown products, possibly diols as well as octanal and octanoic acid are also detected at ultra-trace levels (below the limit of quantification) in the GC analysis of the reaction mixtures. Octane and linear, relatively, long chain alkanes are not common test substrates in literature. This is most likely due to the potential complexity of the product streams obtained (aldehydes, carboxylic acids, various alcohols and ketones). The product yields reported in Table 5, are generally quite low and at first glance seem poor. However, the results compare favourably to data reported in the literature for the oxidation of n-octane.[71, 72] Cele et al. reported on the oxidation of n-octane using various iron-porphyrin complexes encapsulated in zeolites.[73] In their study, the zeolite-encapsulated iron complexes achieved conversions between 1 and 3% at optimized reaction conditions (80°C, H_2O_2 or TBHP). The authors also tested the homogeneous catalyst precursor Fe(III)tetraphenylporphyrin chloride and achieved conversions as high as 19% (H_2O_2 as oxidant) and 12% (TBHP as oxidant).[74] In their reactions, selectivity towards the various ketone products were obtained (similar to the results reported in Table 5), with very little alcohol product formation. Cele et al. also reported on the use of Fe-MOF-5 catalysts for n-octane oxidation. In this study conversions ranging between 5-10% were reported (10.5% conversion, 4 hours, 80°C, H_2O_2).[75]

Similar results were also reported by Kadwa et al. These authors employed heterogenous catalysts, viz. iron(III) Schiff base complexes immobilized on montmorillonite clay, in the oxidation of n-octane using either H_2O_2 or TBHP as the oxidant.[76] Conversions of less than 10% were obtained (TON values < 5). In their work, selectivity towards the ketone products was observed, comparable to the results reported by Cele et al.[74, 77] and those in Table 5.

When the copper and cobalt complexes (**C1**, **C2**, **C5**, **C6**, **MD1** and **MD2**) were employed as catalyst precursors virtually no oxygenated products were observed (under these conditions). The conversions obtained (for **C1**, **C2**, **MD1** and **MD2**) in the presence of TBHP are within experimental error of the control reaction containing TBHP but no catalyst. The S_2N_2 cobalt catalysts (**C6**, 1.2% product yield) showed

marginal activity similar to the other cobalt complexes, while the copper S_2N_2 catalyst (**C5**) exhibited some catalytic activity towards octane oxidation, yet significantly lower than the Fe(II) catalyst precursors. In contrast to these results, a number of highly active cobalt catalyst precursors for the oxidation of n-octane have previously been reported. Naicker et al. reported Co(II) aminodiphosphine complexes (coordination to cobalt in bidentate fashion via -$P(Ph)_2$ moieties).[78] In the presence of the oxidant, TBHP, a maximum conversion of 14% was achieved with selectivity towards ketone products.[78] Similarly cobalt(II) SNS complexes (thioether-amine ligands, Figure 15) reported by Soobramoney et al. managed to obtain relatively high conversion of the n-octane substrate.[79] In their study conversions as high as 23% were obtained (TBHP, 80°C, 48 h). However, this result relied on the use of a substrate to oxidant ratio of 1:20. At this extremely high oxidant concentration, the metal salt $CoCl_2$ showed 7% conversion (under the same reaction conditions). Significantly lower conversions were obtained when working at lower oxidant concentrations. This prerequisite, high oxidant concentrations, represents the greatest hurdle to employing this process economically. The complexes reported by Soobramoney et al. are fairly similar in structure (Figure 15) to complexes **C5** and **C6** (reported in this thesis) yet their activity for n-octane oxidation reactions are strikingly different.

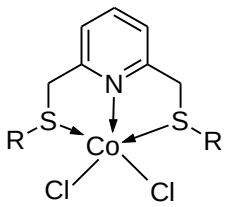

R5

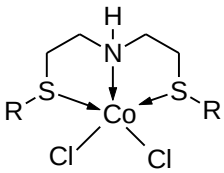

R6

Figure 15: Co(II) SNS complexes for n-octane oxidation reported by Soobramoney et al.[79]

Complexes of the type **R6** (R= ethyl or butyl) were the most active for n-octane oxidation. These complexes are similar to the cobalt complex **C6** reported by us. The authors make no mention of whether complex **R6** (with ethyl substituents) is soluble in the reaction mixture, which makes direct comparison to complex **C6** difficult. Complex **C6** does however differ in the ligand donor set, S_2N_2 as opposed to SNS for **R6**. The authors found that changing the alkyl substituent in complexes of the

type **R6**, from ethyl to butyl lead to a decrease in conversion of the substrate and reasoned that steric hinderance around the metal centre had a pronounced effect on catalytic activity. This is especially true when using the bulky oxidant TBHP. Thus, **C6** with the S_2N_2 chelating donor set might be even more sterically hindered than the analogous **R6** complex. **C6** is thought to be four-coordinate with chloride counterions outside the coordination sphere (based on conductivity results). Characterization of **R6** relied on the use of elemental analysis as well as mass spectrometry. However, no crystal structure or conductivity studies (to determine whether Cl^- species are inside or outside coordination sphere) are available, thus the theory (steric hinderance around metal centre) presented above is speculation based on the data available.

A report by Chavez et al. highlighted the differences in reactivity for a number of stable Co(III)-*tert*-BuOO complexes in cyclohexane oxidation reactions.[80] Different reactivities of the complexes were rationalized by invoking a thermodynamic parameter called the "radical strength" of both the *tert*-BuO· (97 kcal.mol^{-1}) and *tert*-BuOO· (83 kcal.mol^{-1}) radicals. Comparison of the radical strengths with the bond dissociation energy of a C-H bond in cyclohexane (95 kcal.mol^{-1}) indicated that only the tBuO· radical could abstract a proton from cyclohexane.[80]

Chavez et al. suggested that cleavage of the Co(III)-O bond of a *tert*-BuO· species is necessary for such complexes to be active in alkane oxidation reactions (Scheme 11).[67] If *tert*-BuOO· radicals form instead, further homolytic cleavage of the O-O bond must occur for the generation of the *t*-BuO· species. Only the latter species can abstract a proton from the alkane substrate.

If complexes **MD1** and **MD2** produce mainly *t*-BuOO· radicals, then abstraction of a proton from octane will likely not occur.

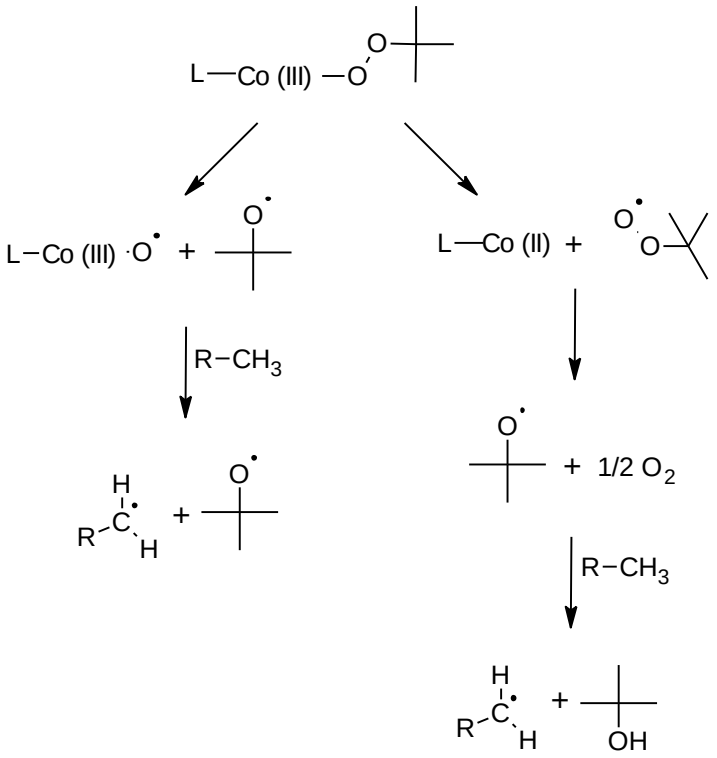

Scheme 11: Decomposition and subsequent oxidative activity of cobalt(III)-alkylperoxide complexes[67]

Evidence for the existence of these *t*-BuOO· radicals was obtained in the oxidation of cyclohexene by **MD1** and **MD2**. During these reactions 1-(*tert*-butylperoxy)-2-cyclohexene was detected (in relatively high concentrations) in the product stream using GC-MS. This product can only form if *t*-BuOO· radicals are present (refer to Scheme 6).

The half-life of a radical species is a convenient measure of the reactivity of the radical species. Table 6 shows typical half-life values reported in the literature for various radical species.[81–83] The half-life of peroxyl radicals are several orders of magnitudes larger than the analogous hydroxyl and peroxyl radicals due to their lower reactivity.[83]

Table 6: Typical lifetimes of various radical species[83]

Reactive oxygen species	Half Life (s)
Hydroxyl radical	$1x10^{-9}$
Alkoxyl radical	$1x10^{-5}$
Peroxyl radical	7

Thus, the nature of the formed radical species in free radical mediated oxidation processes is of tremendous importance. The concentration of the various radical species formed during our oxidation experiments, could explain the stark differences in activity observed for the iron and cobalt complexes.

4.5 Conclusions

The oxidation of hydrocarbons remains a challenging academic as well as industrial problem. Iron complexes **C4**, **MD3**, **MD4** and **MD5** were evaluated as catalyst precursors for the oxidation of cyclohexene. These complexes achieved moderate conversions of the cyclohexene substrate when using H_2O_2 as oxidant. Improved conversions were obtained when using TBHP as oxidant. Complex **C4** gave the highest TOF (50 mol product/mol catalyst. h). In all cases high selectivity towards the 2-cyclohexen-1-one was obtained. However, a number of overoxidized products were also obtained.

These iron complexes were also employed as catalyst precursors in the oxidation of octane. The pyridine-imine iron(II) complexes, **MD5** and **C4**, exhibited the highest catalytic activity obtaining total product yields of around 7%. However, a number of products are formed including various alcohols and ketones. High selectivity towards ketone products was obtained. The high selectivity towards the ketone product was investigated in more detail. It was determined that the oxidation of 2-cylohexen-1-ol to 2-cyclohoxen-1-one is facile under the reaction conditions employed. Thus, accounting for the high ketone selectivity.

A radical scavenger (BHT) was added to the **C4**-catalysed cyclohexene oxidation reactions. The presence of BHT inhibited the oxidation of the substrate, providing further evidence for a free radical-centred mechanism.

The cobalt and copper complexes were less active than the iron complexes in the oxidation of hydrocarbons. The model complexes **C1** and **C2** mediates the facile disproportionation of H_2O_2 into O_2 and H_2O and were thus rather unsuccessful as catalyst precursors when using H_2O_2. **MD1** and **MD2** were also relatively inactive as catalyst precursors, in the presence of H_2O_2, for the oxidation of cyclohexene. Improved conversions were obtained when using TBHP as oxidant. In these

reactions and reactions employing the S_2N_2 cobalt and copper complexes, 1-(*tert*-butylperoxy)-2-cyclohexene was detected in the product stream, which suggests that free radicals are present in the reaction mixture. The cobalt and copper complexes were fairly inactive in the oxidation of octane. Only marginally better product yields, than for the control reactions employing only TBHP, were obtained.

4.6 Experimental details

4.6.1 General Methods and instrumentation

All chemicals were purchased from Sigma Aldrich and used without any further purification. Solvents used were distilled and dried using the appropriate drying agents and methods prior to use. Oxidation catalysis test reactions were performed in a Radleys Carousel 12 batch reactor.

4.6.2 Catalytic oxidation of hydrocarbons.

A typical cyclohexene oxidation experiment using **C4** is described below as a representative example.

A reaction vessel (glass reactor tube) was charged with a solution of catalyst precursor (0.5 mol% iron relative to substrate, 7.98 mg, 10 mg/ml solution in acetonitrile). The reaction tube is then sealed and cyclohexene (2.00 mmol, 0.200 ml) is added via pipette through the removable septum. The sample is diluted with MeCN (total reaction volume including oxidant 2.75 ml). The reaction vessel is heated to the appropriate temperature whilst stirring. The oxidant, H_2O_2 (30% solution, 6.00 mmol, 0.612 ml) or TBHP (70% solution, 4.00 mmol, 0.554 ml) is then added to the reaction vessel to initiate the reaction. The reaction mixtures were stirred for 3 hours. After the allotted time had passed, the reaction mixture is filtered through a syringe filter and a 0.950 ml aliquot is sampled for GC analysis. *p*-xylene (0.050 ml) is added to the GC sample as internal standard. The sample is then analysed by GC (Agilent Cyclosil-B GC-column).

4.7 References

1 N. Rahimi and R. Karimzadeh, *Appl. Catal. A Gen.*, 2011, **398**, 1–17.

2 H. Nagahara, M. Ono, M. Konishi and Y. Fukuoka, *Appl. Surf. Sci.*, 1997, **121**–**122**, 448–451.

3 H. Liu, S. Liang, W. Wang, T. Jiang and B. Han, *J. Mol. Catal. A Chem.*, 2011, **341**, 35–41.

4 R. L. Espinoza, A. P. Steynberg, B. Jager and A. C. Vosloo, 1999, **186**, 13–26.

5 H. Jahangiri, J. Bennett, P. Mahjoubi, K. Wilson and S. Gu, *Catal. Sci. Technol.*, 2014, **4**, 2210–2229.

6 Y. Cao, H. Yu, F. Peng and H. Wang, *ACS Catal.*, 2014, **4**, 1617–1625.

7 P. D. De María, *ChemSusChem*, 2011, **4**, 327–329.

8 J. Smidt, W. Hafner, R. Jira, J. Sedlmeier, R. Sieber, R. Rüttinger and H. Kojer, *Angew. Chemie*, 1959, **71**, 176–182.

9 T. J. Fisher and P. H. Dussault, *Tetrahedron*, 2017, **73**, 4233–4258.

10 M. Schröder, *Chem. Rev.*, 1980, **80**, 187–213.

11 M. D. Hughes, Y.-J. Xu, P. Jenkins, P. McMorn, P. Landon, D. I. Enache, A. F. Carley, G. A. Attard, G. J. Hutchings, F. King, E. H. Stitt, P. Johnston, K. Griffin and C. J. Kiely, *Nature*, 2005, **437**, 1132–1135.

12 Appl. EP 87–-201439, 1988.

13 A. D. N. Vaz, D. F. McGinnity and M. J. Coon, *Proc. Natl. Acad. Sci.*, 1998, **95**, 3555–3560.

14 B. Meunier, S. P. de Visser and S. Shaik, *Chem. Rev.*, 2004, **104**, 3947–3980.

15 S. J. Blanksby and G. B. Ellison, *Acc. Chem. Res.*, 2003, **36**, 255–263.

16 A. E. Shilov and G. B. Shul'pin, *Chem. Rev.*, 1997, **97**, 2879–2932.

17 G. B. Shul'pin, *J. Mol. Catal. A Chem.*, 2002, **189**, 39–66.

18 R. H. Crabtree, *J. Organomet. Chem.*, 2004, **689**, 4083–4091.

19 G. Shul'pin, *Catalysts*, 2016, **6**, 50.

20 I. M. Denekamp, M. Antens, T. K. Slot and G. Rothenberg, *ChemCatChem*, 2018, **10**, 1035–1041.

21 M. C. White, A. G. Doyle and E. N. Jacobsen, *J. Am. Chem. Soc.*, 2001, **123**, 7194–7195.

22 J. Tang, P. Gamez and J. Reedijk, *Dalton Trans.*, 2007, 4644–4646.

23 A. D. Chowdhury, R. Ray and G. K. Lahiri, *Chem. Commun.*, 2012, **48**, 5497.

24 D. Clemente-Tejeda and F. A. Bermejo, *Tetrahedron*, 2014, **70**, 9381–9386.

25 B. Das, A. Al-Hunaiti, M. Haukka, S. Demeshko, S. Meyer, A. A. Shteinman, F. Meyer, T. Repo and E. Nordlander, *Eur. J. Inorg. Chem.*, 2015, **2015**, 3590–3601.

26 J. Brazdil, *J. Catal.*, 1986, **100**, 516–519.

27 T. Okuno, S. Ito, S. Ohba and Y. Nishida, *J. Chem. Soc. Dalt. Trans.*, 1997, 3547–3551.

28 A. D. Bokare and W. Choi, *J. Hazard. Mater.*, 2014, **275**, 121–135.

29 A. R. Silva, T. Mourão and J. Rocha, *Catal. Today*, 2013, **203**, 81–86.

30 Y. N. Wei, H. Li, F. Yue, Q. Xu, J. D. Wang and Y. Zhang, *RSC Adv.*, 2016, **6**, 107104–107108.

31 I. Hermans, P. Jacobs and J. Peeters, *Chem. - A Eur. J.*, 2007, **13**, 754–761.

32 S. Mukherjee, S. Samanta, B. C. Roy and A. Bhaumik, *Appl. Catal. A Gen.*, 2006, **301**, 79–88.

33 N. Sehlotho and T. Nyokong, *J. Mol. Catal. A Chem.*, 2004, **209**, 51–57.

34 P. A. MacFaul, D. D. M. Wayner and K. U. Ingold, *Acc. Chem. Res.*, 1998, **31**, 159–162.

35 H. Weiner, A. Trovarelli and R. G. Finke, *J. Mol. Catal. A Chem.*, 2003, **191**, 217–252.

36 Y. Fu, D. Sun, M. Qin, R. Huang and Z. Li, *RSC Adv.*, 2012, **2**, 3309.

37 Y. Yang, J. Guan, P. Qiu and Q. Kan, *Transit. Met. Chem.*, 2010, **35**, 263–270.

38 B. McAteer, N. Beattie and D. T. Richens, *Inorg. Chem. Commun.*, 2013, **35**, 284–289.

39 B. McAteer, N. Beattie and D. T. Richens, *Inorg. Chem. Commun.*, 2013, **35**, 284–289.

40 N. Grootboom and T. Nyokong, *J. Mol. Catal. A Chem.*, 2002, **179**, 113–123.

41 S. A. Borisenkova, E. P. Denisova, E. A. Batanova, E. G. Girenko, O. L. Kaliya, E. A. Lukyanets and G. N. Vorozhtsov, *J. Porphyr. Phthalocyanines*, 2000, **4**, 684–688.

42 E. T. Saka and Z. Biyiklioğlu, *J. Organomet. Chem.*, 2013, **745**–**746**, 50–56.

43 N. Sehlotho and T. Nyokong, *J. Mol. Catal. A Chem.*, 2004, **209**, 51–57.

44 J. Połtowicz, E. . Serwicka, E. Bastardo-Gonzalez, W. Jones and R. Mokaya, *Appl. Catal. A Gen.*, 2001, **218**, 211–217.

45 E. M. Serwicka, J. Połtowicz, K. Bahranowski, Z. Olejniczak and W. Jones, *Appl. Catal. A Gen.*, 2004, **275**, 9–14.

46 J. T. Groves, *J. Chem. Educ.*, 1985, **62**, 928–931.

47 A. S. Amarasekara, A. R. Oki, I. McNeal and U. Uzoezie, *Catal. Commun.*, 2007, **8**, 1132–1136.

48 V. Mirkhani, M. Moghadam, S. Tangestaninejad, I. Mohammadpoor-Baltork and N. Rasouli, *Catal. Commun.*, 2008, **9**, 219–223.

49 A. Kumar, G. S. Mishra and A. Kumar, *Transit. Met. Chem.*, 2003, **28**, 913–917.

50 K. C. Gupta and A. K. Sutar, *Coord. Chem. Rev.*, 2008, **252**, 1420–1450.

51 H. Y. Ren, R. X. Yao and X. M. Zhang, *Inorg. Chem.*, 2015, **54**, 6312–6318.

52 T. Zhang, Y. Q. Hu, T. Han, Y. Q. Zhai and Y. Z. Zheng, *ACS Appl. Mater. Interfaces*, 2018, **10**, 15786–15792.

53 R. A. Sheldon, *J. Mol. Catal.*, 1980, **7**, 107–126.

54 Y.-W. Wang and C.-M. Shu, *Ind. Eng. Chem. Res.*, 2010, **49**, 8959–8968.

55 M. Salavati-Niasari and A. Amiri, *Appl. Catal. A Gen.*, 2005, **290**, 46–53.

56 M. Salavati-Niasari, *J. Mol. Catal. A Chem.*, 2008, **283**, 120–128.

57 V. Mirkhani, M. Moghadam, S. Tangestaninejad, I. Mohammadpoor-Baltork and N. Rasouli, *Catal. Commun.*, 2008, **9**, 219–223.

58 A. Nishinaga, T. Yamada, H. Fujisawa, K. Ishizaki, H. Ihara and T. Matsuura, *J. Mol. Catal.*, 1988, **48**, 249–264.

59 M. R. Maurya, P. Saini, C. Haldar, A. K. Chandrakar and S. Chand, *J. Coord. Chem.*, 2012, **65**, 2903–2918.

60 E. N. Jacobsen, W. Zhang, A. R. Muci, J. R. Ecker and L. Deng, *J. Am. Chem. Soc.*, 1991, **113**, 7063–7064.

61 L. Deng and E. N. Jacobsen, *J. Org. Chem.*, 1992, **57**, 4320–4323.

62 C. Döbler, G. Mehltretter and M. Beller, *Angew. Chemie Int. Ed.*, 1999, **38**, 3026–3028.

63 I. Y. Skobelev, A. B. Sorokin, K. A. Kovalenko, V. P. Fedin and O. A. Kholdeeva, *J. Catal.*, 2013, **298**, 61–69.

64 K. T. Mahmudov, M. N. Kopylovich, M. F. C. G. da Silva, P. J. Figiel, Y. Y. Karabach and A. J. L. Pombeiro, *J. Mol. Catal. A Chem.*, 2010, **318**, 44–50.

65 S. Goldstein, *Acc. Chem. Res.*

66 F. A. Chavez and P. K. Mascharak, *Acc. Chem. Res.*, 2000, **33**, 539–545.

67 F. A. Chavez, C. V. Nguyen, M. M. Olmstead and P. K. Mascharak, *Inorg. Chem.*, 1996, **35**, 6282–6291.

68 D. T. Sawyer, A. Sobkowiak and T. Matsushita, *Acc. Chem. Res.*, 1996, **29**,

409–416.

69 H. R. B. Derek and D. Doller, *Acc. Chem. Res.*, 1992, **25**, 504–512.

70 D. T. Sawyer, A. Sobkowiak and T. Matsushita, *Acc. Chem. Res.*, 1996, **29**, 409–416.

71 T. C. O. Mac Leod, M. V. Kirillova, A. J. L. Pombeiro, M. A. Schiavon and M. D. Assis, *Appl. Catal. A Gen.*, 2010, **372**, 191–198.

72 E. Kadwa, M. D. Bala and H. B. Friedrich, *Appl. Clay Sci.*, 2014, **95**, 340–347.

73 M. N. Cele, H. B. Friedrich and M. D. Bala, *React. Kinet. Mech. Catal.*, 2014, **111**, 737–750.

74 M. N. Cele, H. B. Friedrich and M. D. Bala, *React. Kinet. Mech. Catal.*, 2014, **111**, 737–750.

75 M. N. Cele, H. B. Friedrich and M. D. Bala, *Catal. Commun.*, 2014, **57**, 99–102.

76 E. Kadwa, M. D. Bala and H. B. Friedrich, *Appl. Clay Sci.*, 2014, **95**, 340–347.

77 M. N. Cele, H. B. Friedrich and M. D. Bala, *Catal. Commun.*, 2014, **57**, 99–102.

78 D. Naicker, H. B. Friedrich and B. Omondi, *RSC Adv.*, 2015, **5**, 63123–63129.

79 L. Soobramoney, M. D. Bala and H. B. Friedrich, *Dalt. Trans.*, 2014, **43**, 15968–15978.

80 F. A. Chavez, J. A. Briones, M. M. Olmstead and P. K. Mascharak, *Inorg. Chem.*, 1999, **38**, 1603–1608.

81 H. Sies, W. Stahl and Sundquist, *Ann. NY Acad. Sci.*, 1992, **20**, 669.

82 W. A. Pryor, *Annu. Rev. Physiol.*, 1986, **48**, 657–667.

83 H. Sies, *Eur. J. Biochem.*, 1993, **215**, 213–219.

Chapter 5: Kinetic and Mechanistic Studies of Dendritic Iron- and Cobalt-Catalysed Decomposition of H_2O_2

5.1 Introduction and summary of mechanistic observations for some iron and cobalt complexes

The catalytic activity of various iron and cobalt complexes in the oxidation of some hydrocarbon substrates was discussed in Chapter 4. In general, the iron complexes exhibited better catalytic activities than the cobalt complexes. In Chapter 3 it was shown that the model cobalt complexes (**C1** and **C2**) causes disproportionation of the oxidant, hydrogen peroxide, in a catalase-like process. In contrast to the model complexes, the cobalt metallodendrimers (**MD1** and **MD2**) appeared not to rapidly decompose the oxidant. Despite this **MD1** and **MD2** were however, found to be relatively inactive as catalyst precursors for oxidative hydrocarbon transformations; especially when hydrogen peroxide is used as oxidant. The iron pyridine-imine complexes **MD5** and **C4**, in contrast, exhibit relatively high activities in these transformations. It was thought that exploring the kinetics of oxidant decomposition in the presence of various catalyst precursors could potentially provide insight into the observations regarding the characteristics of the above-mentioned reactions.

Such a study was performed by Skounas et al.[1] In their study, the kinetics of the decomposition of hydrogen peroxide by two different copper(II) complexes was investigated. A mechanism for this oxidant decomposition was then suggested on the basis of the kinetic model. Skounas et al. only studied the oxidant decomposition reactions and did not attempt to associate the obtained kinetic modelling results with the catalysts precursors' performance in other oxidation processes involving organic substrates.

Rizkalla et al. also investigated the kinetics of the reaction of an ethylenediaminetetraacetato-iron(III) complex (Fe(III)[EDTA]) with H_2O_2.[2] The complex was found to mimic both catalase (H_2O_2 disproportionation) as well as peroxidase (oxidation with H_2O_2) oxidative activity through the generation of free radical species. Based on the results of their kinetic study, Rizkalla et al. were able to suggest a mechanism which was closely related to the Fenton cycle to account for these observations.

In this chapter, the reactions of two of the metallodendrimers (Figure 1), **MD1** (Co) and **MD5** (Fe) with H_2O_2 is discussed. With the aid of kinetic modelling, an attempt is made to provide insight into the different catalytic activities observed for these two complexes during hydrocarbon oxidation reactions. In addition, an attempt was made to elucidate the mechanism of the reaction of the metal complex with oxidant and by extension the oxidation of hydrocarbons catalysed by these complexes as reported in Chapter 4.

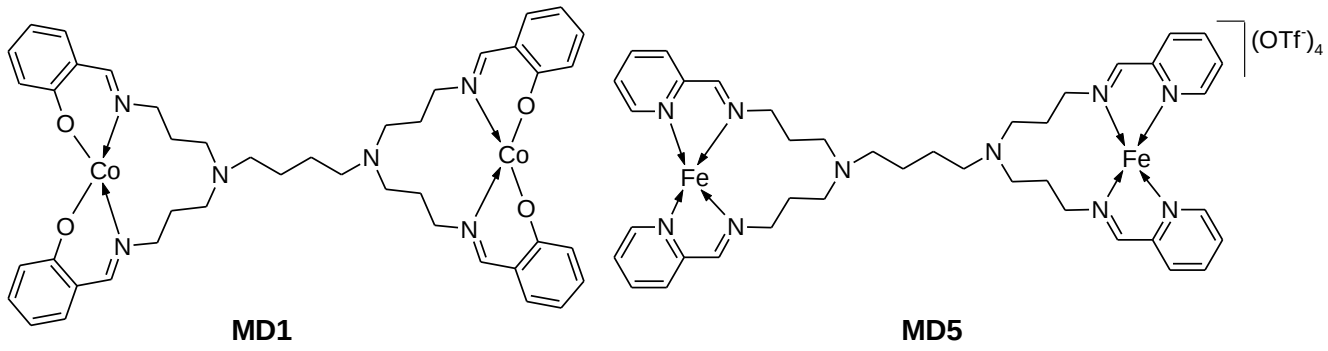

Figure 1: Metallodendrimers MD1 and MD5 utilized in kinetic investigation of the decomposition of H_2O_2

5.2 Kinetic modelling of H_2O_2 decomposition catalysed by MD5 and MD1

The dendritic iron complex, **MD5**, and the dendritic cobalt complex, **MD1** (soluble in water in contrast to **MD2**) were selected for further kinetic analysis as representative examples of an active iron catalyst and a less active cobalt catalyst. The decomposition of hydrogen peroxide in the presence of these two complexes were investigated. The

temperature of the decomposition reaction (Figure 2 and Figure 4) as well as the oxidant concentration (Figure 3 and Figure 5) were varied.

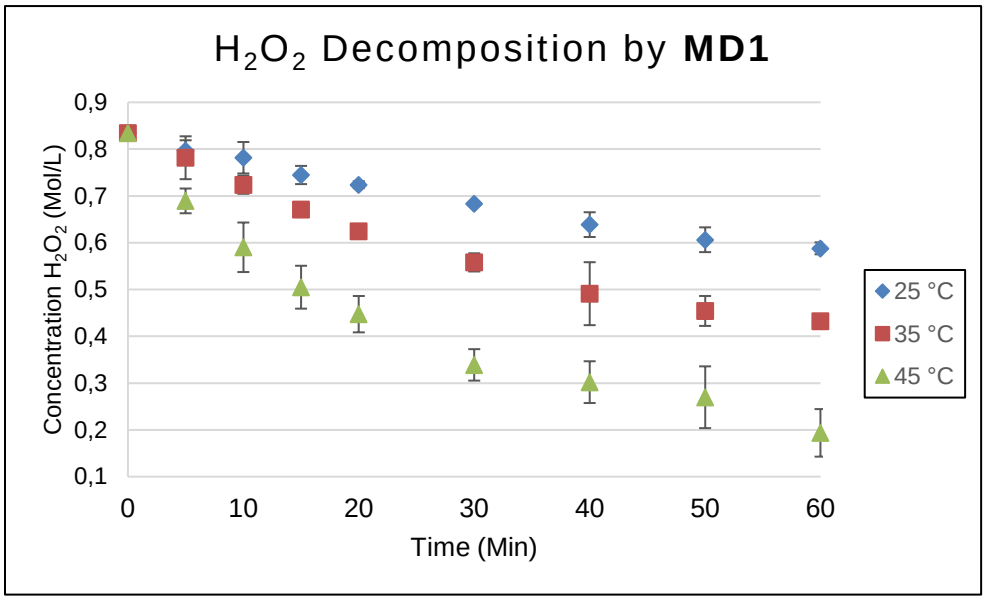

Figure 2: Decomposition of hydrogen peroxide by dendritic Co complex MD1 at various temperatures. Catalyst precursor concentration (4.3 x 10^{-3} M metal). Initial oxidant concentration (0.835 M).

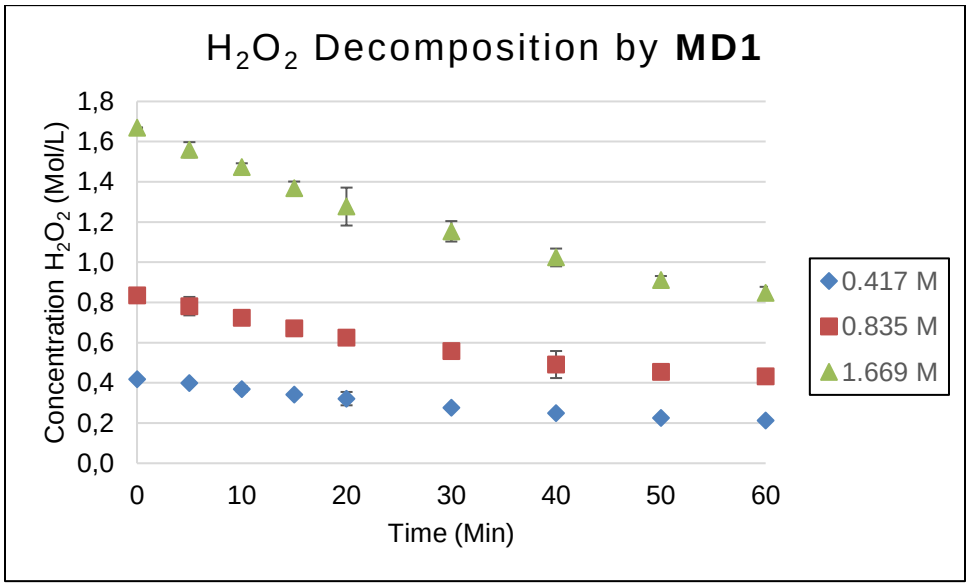

Figure 3: Decomposition of hydrogen peroxide by dendritic Co complex MD1 while varying initial H_2O_2 concentration. Catalyst precursor concentration (4.3 x 10^{-3} M metal). Temperature (35 °C).

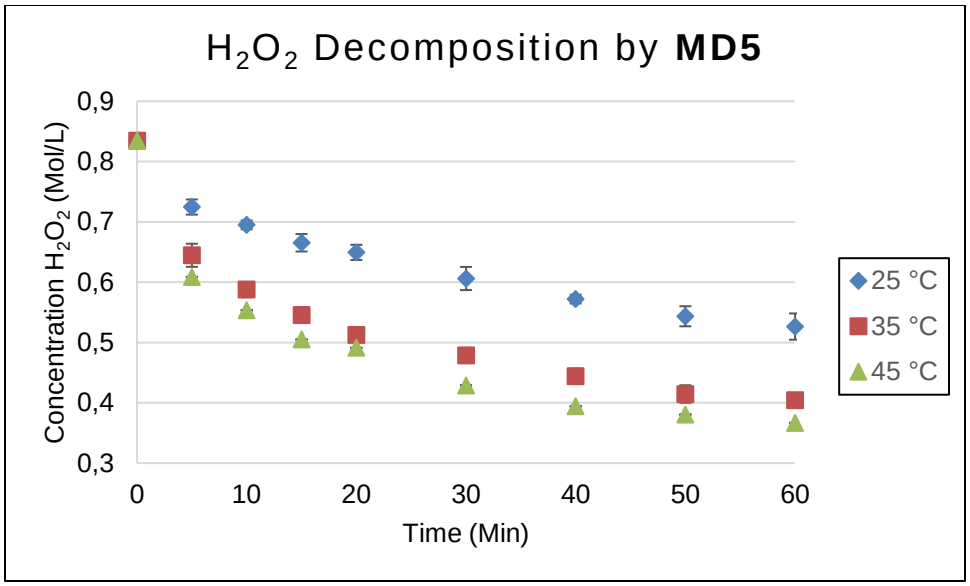

Figure 4: Decomposition of hydrogen peroxide by dendritic Fe complex MD5 with varying temperature. Catalyst precursor concentration (4.3 x 10^{-3} M metal). Initial oxidant concentration (0.835 M).

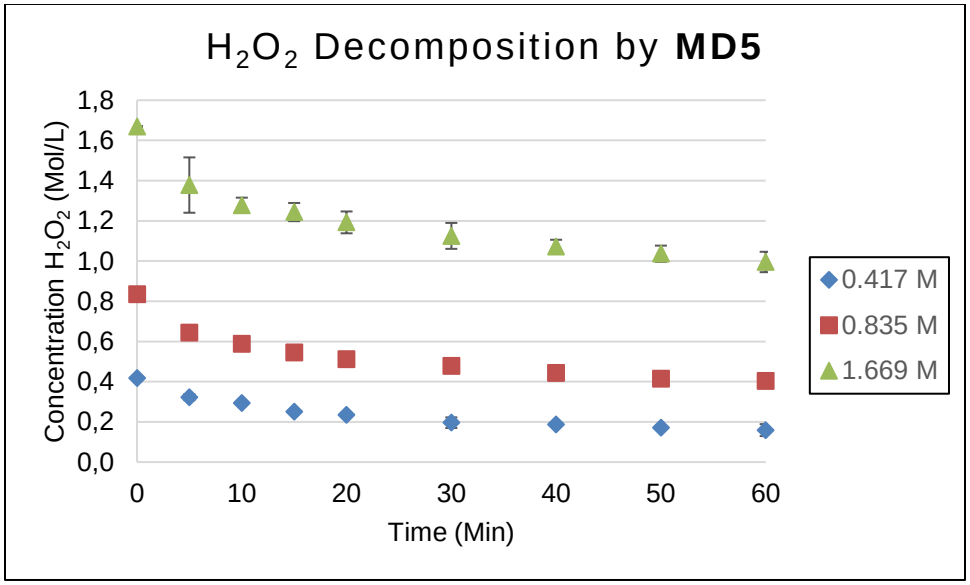

Figure 5: Decomposition of hydrogen peroxide by dendritic Fe complex MD5 while varying initial H_2O_2 concentration. Catalyst precursor concentration (4.3 x 10^{-3} M metal). Temperature (35 °C).

As expected, an increase in the reaction temperature over the temperature range investigated (25 - 45°C) leads to an increase in the rate of oxidant decomposition for both **MD1** and **MD5** (Figures: 2 and 4). The increase in the rate of oxidant decomposition is quite pronounced for **MD1** (Figure 2), with large differences in reaction rates observed over the three different temperatures surveyed. In contrast the rate of oxidant decomposition by the dendritic iron complex, **MD5** (Figure 4), does not drastically change with increasing temperature. This is consistent with observations made in Chapter 4. In cyclohexene oxidation reactions catalysed by **MD5** in the presence of H_2O_2, increasing the reaction temperature was found to have minimal effect on the catalytic activity of the system.

A higher initial oxidant concentration leads to an increase in the decomposition reaction rates for both catalyst precursors. (Figures: 3 and 5). These reactions appear to be pseudo-first order with respect to H_2O_2 concentration. The experimental H_2O_2 decomposition data was used to determine the rate of decomposition under the reaction conditions employed. Arrhenius plots (Figures 6 and 7) were then generated to determine the activation energy ($\Delta G^{\ddagger}$) of the hydrogen peroxide decomposition reaction. Subsequently, Eyring plots were used to evaluate the entropy ($\Delta H^{\ddagger}$) and enthalpy ($\Delta S^{\ddagger}$) of activation for a given catalyst precursor (Figures 8, and 9).

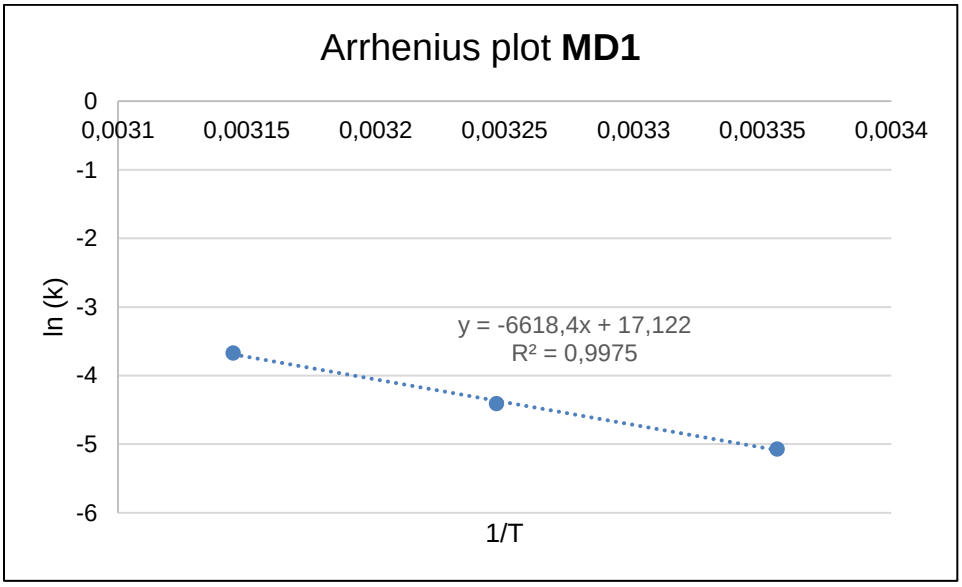

Figure 6: Arrhenius plot obtained for MD1

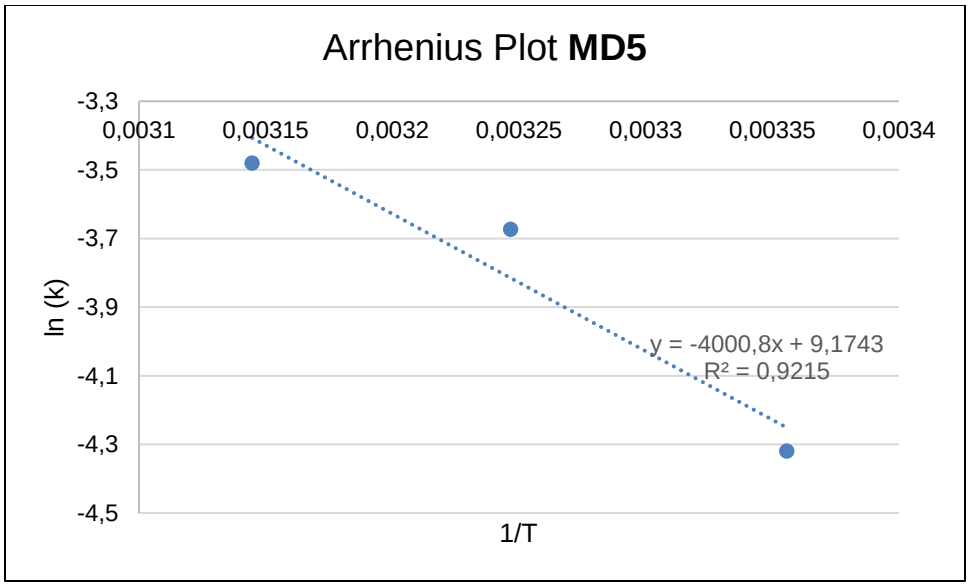

Figure 7: Arrhenius plot obtained for MD5

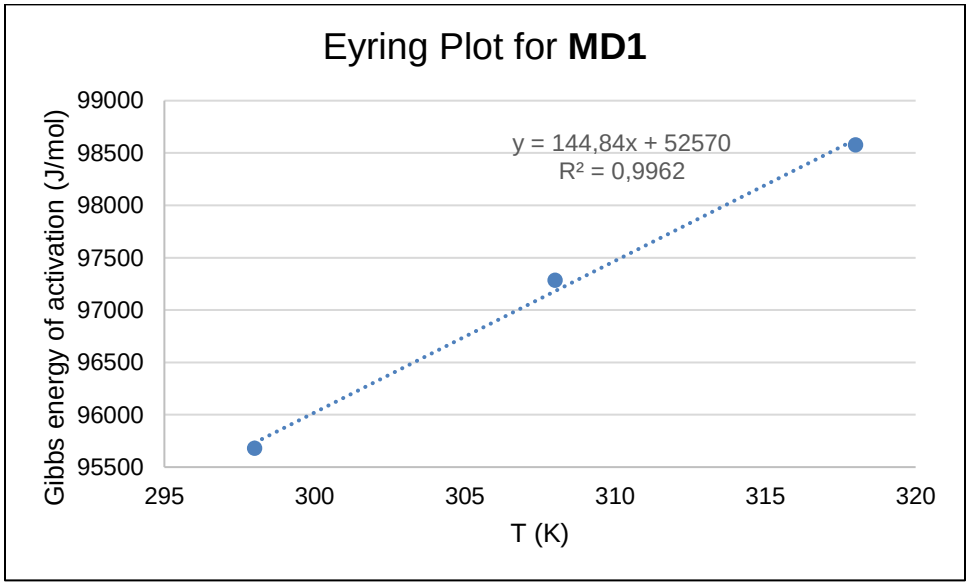

Figure 8: Eyring plot obtained for MD1

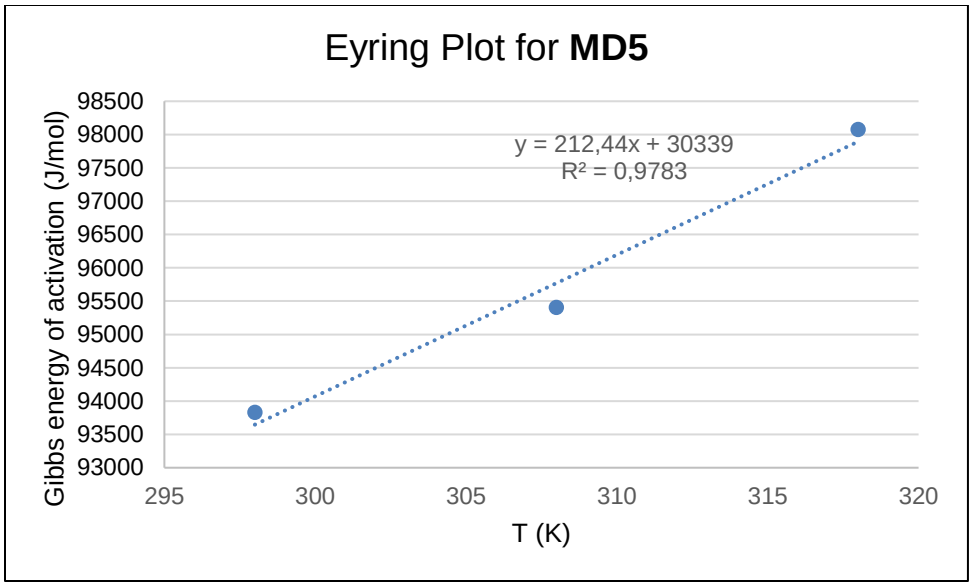

Figure 9: Eyring plot obtained for MD5

Table 1: H_2O_2 decomposition kinetic parameters obtained for MD1 and MD5 as catalyst

Catalyst	$\Delta G^{\ddagger}$ (kJ/Mol)	$\Delta H^{\ddagger}$ (kJ/mol)	$\Delta S^{\ddagger}$ (J/mol.K)
MD1	55.03	52.57	-144.84
MD5	33.26	30.70	-211.26

Parameters measured by varying temperature (25, 35 and 45°C) and initial oxidant concentration (0.417, 0.835 and 1.67 M). Catalyst precursor concentration was kept constant throughout (4.3×10^{-3} M metal)

The activation energy ($\Delta G^{\ddagger}$) of the cobalt complex **MD1** is significantly higher than that for the iron complex, **MD5**. Therefore, the latter is much more active for the decomposition of H_2O_2 at lower temperatures (e.g. Figure 4, 25°C) in comparison to **MD1**, especially during the early stages of the reaction. The entropy of activation ($\Delta S^{\ddagger}$) is negative for both **MD1** and **MD5**, which does not favour the overall activation energy. A possible explanation for this is thought to be the result of prior coordination of H_2O_2 to the metal center in order to form a transition state via an associative pathway.[3, 4] Such an associative mechanism was previously proposed by Rizkalla et al. who also obtained relatively large negative entropy values in their kinetic study of the decomposition of

H_2O_2 by iron complexes. Rizkalla et al. suggested that these entropy values could indicate that a rate-determining substitution (most likely of solvent molecules) reaction[5] is occurring.[2] The exact nature of the species involved in these reactions is unknown but the authors suggested that coordination of either hydrogen peroxide (Scheme 1, Route 1) or a hydroperoxide ligand (Scheme 1, Route 2) (depending on pH of the reaction) leads to the formation of the activated complex as shown in Scheme 1.

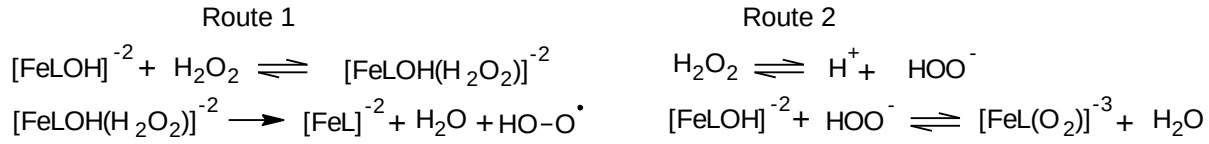

Scheme 1: Formation of the activated complex as described by Rizkalla et al.[2]

In contrast, Prasad et al. obtained positive entropy values in their study of the decomposition of hydrogen peroxide by cobalt(II) complexes of 1-phenyl 1-hydrazonyl 2-oximinopropanedione (HPHOPD).[6] They proposed that a dissociative pathway might be operative. They made this proposition on the basis that coordinating bases such as pyridine and quinoline inhibit the reaction entirely, presumably by competition for the coordination sites. Prasad et al. suggested that the decomposition of H_2O_2 occurs via the formation of an activated complex wherein the hydrogen peroxide is loosely bound (instead of substituting a ligand or solvent molecule) to the metal complex (Scheme 2), as the activation entropy for the overall reaction is moderately positive at 63.3 J/(mol.K). Reaction of a second equivalent of H_2O_2 results in the decomposition of the peroxide.[6]

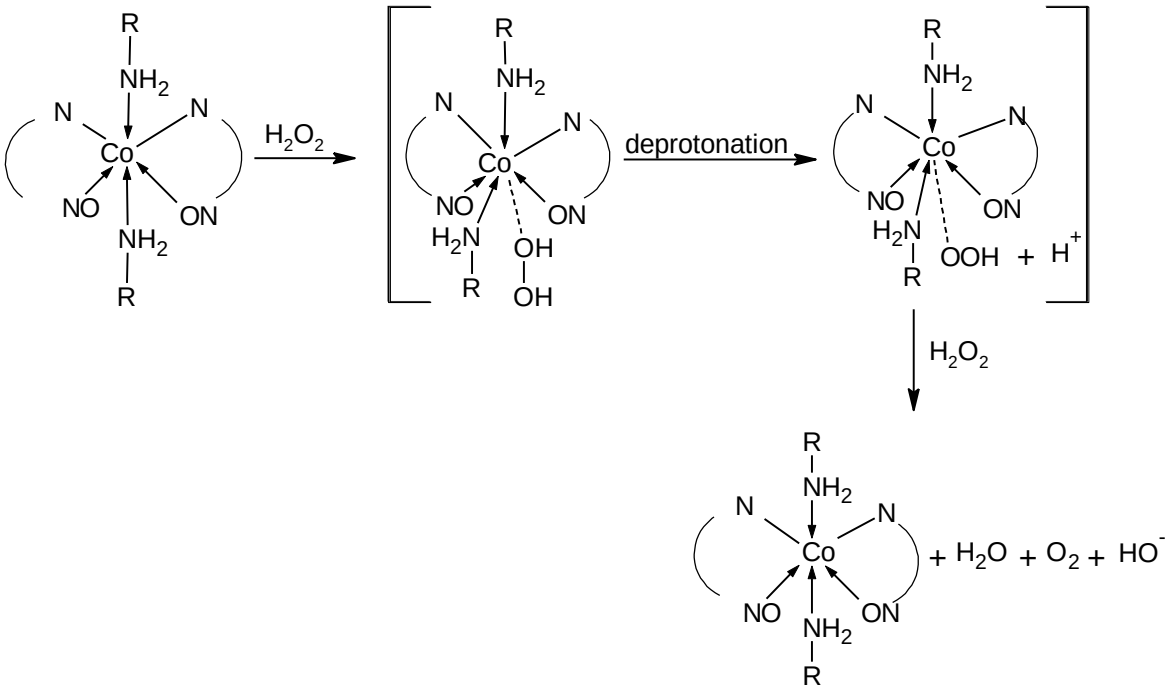

Scheme 2: Formation of an activated complex via a dissociative pathway as described by Prasad et al.[6]

The large difference in $\Delta S^{\ddagger}$ between **MD1** and **MD5** is more difficult to explain without knowledge of the structure of the transition state. **MD1** contains salicylaldimine ligands while **MD5** contains pyridine-imine ligands, thus there are significant differences in the electronic and vibrational states (and the number of possible states) of these complexes which could explain the difference in $\Delta S^{\ddagger}$.

The enthalpy of activation ($\Delta H^{\ddagger}$) is related to the height of the electronic energy barrier that must be overcome in order to reach such a transition state.[3, 4] The transition state is significantly higher for the cobalt complex **MD1** than for the iron complex **MD5.** This could serve as a possible explanation for the poor catalytic activity, in oxidation reactions, observed for **MD1**.

Based on the observations made in Chapter 3 (attempts to characterize the intermediates) and Chapter 4 (mechanistic work) it appears that these complexes, **MD1** and **MD5**, operate via a free radical-centered mechanism. The Haber-Weiss cycle (which forms part of the expanded Fenton cycle) has been used by other authors to

describe the catalytic decomposition of hydrogen peroxide to radical species by transition metals.[7–9] Thus, the experimental decomposition data, obtained in the current investigation was modelled and fitted to the Haber-Weiss model (Table 2) in an attempt to obtain insight into individual mechanistic steps.[10, 11]

Table 2: Reactions of the Haber-Weiss cycle and their rate laws

Description	Reaction	Rate law
RXN 1, forward	$M^{2+} + H_2O_2 \rightarrow M^{3+}OH^- + OH\cdot$	$r_1 = k_1[M^{2+}][H_2O_2]$
RXN 2, forward	$M^{3+}OH^- + H_2O_2 \rightarrow M^{2+} + H_2O + HOO\cdot$	$r_2 = k_2[M^{3+}OH^-][H_2O_2]$

Nonlinear regression of the experimental data, obtained in the experiments with **MD1** and **MD5** was performed to determine the parameters of the Arrhenius equation that best fit the Haber-Weiss model. The decomposition of hydrogen peroxide by cobalt complex **MD1** fit the modelled data quite well (Figure 10) with very little deviation from that of the predicted Haber-Weiss model.

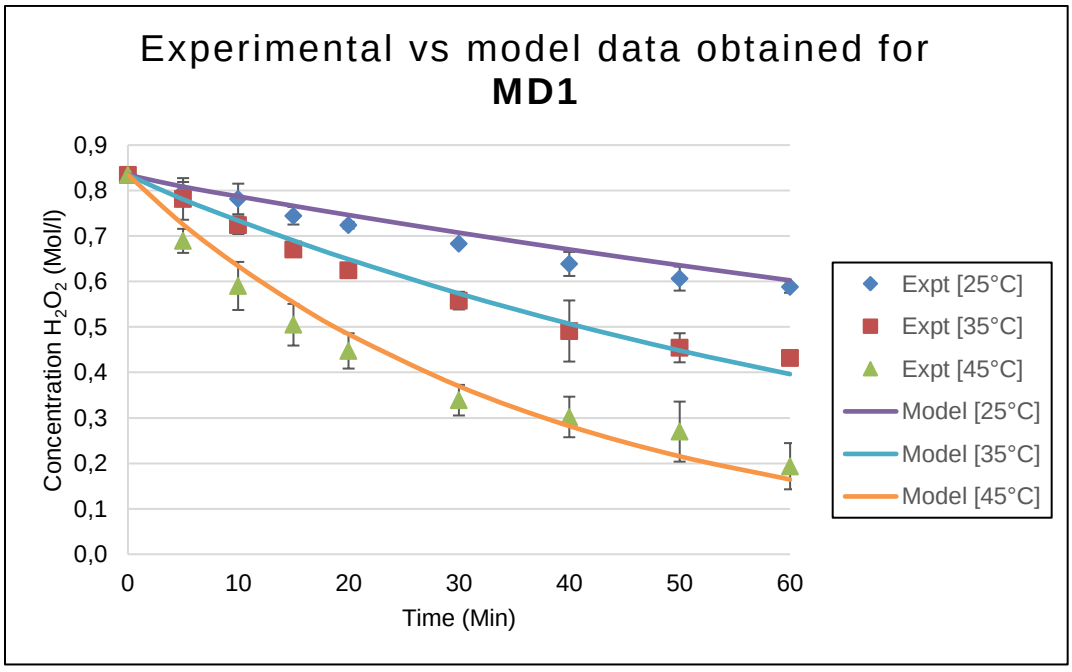

Figure 10: Comparison of the Haber-Weiss model to experimental data obtained for decomposition of H_2O_2 by complex MD1

Table 3 shows the kinetic parameters that best fit the model data obtained for both reaction 1 and reaction 2 (as defined in Table 2) through the regression of the experimental data (obtained for **MD1**).

Table 3: Kinetic parameters of the Haber-Weiss cycle calculated for MD1

Parameter	RXN 1	RXN 2
Activation Energy (k*J/mol)*	57.43	63.90
Frequency Factor (*L/mol/min)*	91.94	0.63
Enthalpy of Activation (*J/mol)*	54.91	61.38
Entropy of Activation (*J/mol/K)*	-57.11	-76.80

The iron species, **MD5** deviates from the model (Figure 11), especially at the start of the reaction. The full Fenton reaction cycle, which the Haber-Weiss cycle forms a part of, may prove to be a better model and possibly fit the experimental data better. The Fenton cycle attempts to explain the formation of other radical species such as superoxide during Fenton reactions. However, use of the more complex model would require more experimental data than simply the measurement of H_2O_2 concentration over time.[12, 13] Barb et al. investigated the effect of other reaction parameters such as reaction pH in conjunction with the measurement of oxygen evolution over time to construct more accurate models.[12]

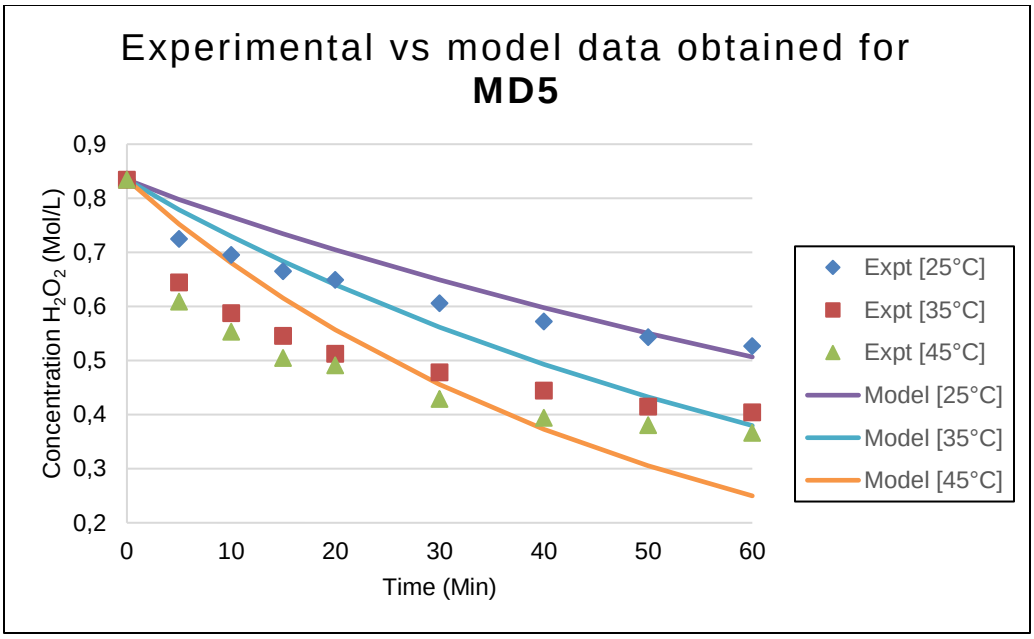

Figure 11: Comparison of the Haber-Weiss model to experimental data obtained for decomposition of H_2O_2 by MD5

Table 4: Kinetic parameters of the Haber-Weiss cycle calculated for MD5

Parameter	RXN 1	RXN 2
Activation energy (KJ/mol/K)	41.8	49.79
Frequency factor (L/mol/min)	53.30	50.51
Enthalpy of activation (KJ/mol)	36.75	47.27
Entropy of activation (J/mol/K)	-122.57	-87.72

Analysis of the results obtained in Tables 3 and 4 indicates that the cobalt species, **MD1** has relatively high activation energies for the two Haber-Weiss reactions (as defined in Table 2); much higher than the corresponding activation energies for the iron complex, **MD5**. The decomposition of hydrogen peroxide by **MD5** to a radical species will therefore occur more readily and at a higher rate than for **MD1**. The reformation of the M^{2+} species from M^{3+}-OH (Table 2, RXN 2) is less favourable for both **MD1** and **MD5** than the initial oxidation of the M^{2+} species to M^{3+} (Table 2, Reaction 1). This regeneration of the M^{2+} species is most likely the rate-determining step (under the reaction conditions employed).

The decomposition of hydrogen peroxide mediated by **MD1** and **MD5** appears to be pseudo first order which is typical for oxidation reactions occurring via a free radical mechanism.[1]

The obtained experimental data fit the Haber-Weiss model reasonably well especially for **MD1**. Further information regarding the nature of the reactive oxygen species in the oxidation reactions presented in Chapter 4, is required to support the validity of the Haber-Weiss model for these catalyst systems.

5.3 Identification of the reactive oxygen species

The cobalt metallodendrimer **MD1** fits the proposed kinetic model relatively well. In this particular model, hydroxyl radicals are generated in the first step of the reaction. Such a reaction is often referred to as “Fenton-like”.[9] Houghton et al. and Goldstein et al. reviewed these so called Fenton-like reactions for transition metals such as cobalt.[14, 15] Numerous possible mechanisms were identified. Goldstein et al. remarked that there is no general reaction mechanism for these cobalt catalysed “Fenton-like” reactions. Instead, for each case, a detailed mechanistic study should be performed to determine whether hydroxyl radicals are being formed for a specific system.[15] Knowledge of the reactive oxygen species (ROS) in **MD1** catalysed reactions could aid in determining whether these “Fenton like” reactions are possible for the cobalt metallodendrimers.

Xu et al. investigated the reactive oxygen species (ROS) in the oxidative degradation of methylene blue by a Co(II)/ HCO_3^- system using H_2O_2 as oxidant.[16] The authors used disodium terephthalate (NaTA) as a probe to determine the type of radical formed during the oxidation reaction. Disodium terephthalate has been shown to react selectively with hydroxyl radicals.[17, 18] No reaction is observed in the presence of other radical or oxidative species such as H_2O_2 or peroxyl radicals (Scheme 3).[17, 18]

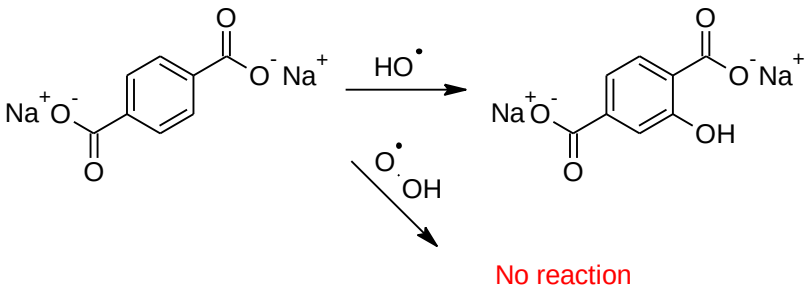

Scheme 3: Selective oxidation of disodium terephthalate by hydroxyl radicals[18]

The formation of 2-Hydroxy terephthalate (HTA) and by implication the presence of hydroxyl radicals, can be monitored using fluorescence spectroscopy. HTA exhibits a strong fluorescence signal around 420 nm while NaTA does not fluoresce strongly.

The experiment proposed in Scheme 3 was tested and optimized by using the catalyst precursor described by Xu et al. for comparison with catalyst precursors **C4**, **MD1** and **MD5**.[16] A solution of cobalt(II) acetate, sodium hydrogen carbonate and NaTA in water was prepared. Upon addition of hydrogen peroxide the fluorescence spectrum of the reaction mixture was recorded. An increase in the intensity of the fluorescence signal around 420 nm was observed after only 30 seconds (Figure 12). The intensity of this fluorescence signal increased over time implying that HTA is being formed due to the oxidation of NaTA by hydroxyl radicals. These observations are also in line with those made by Xu et al.[16]

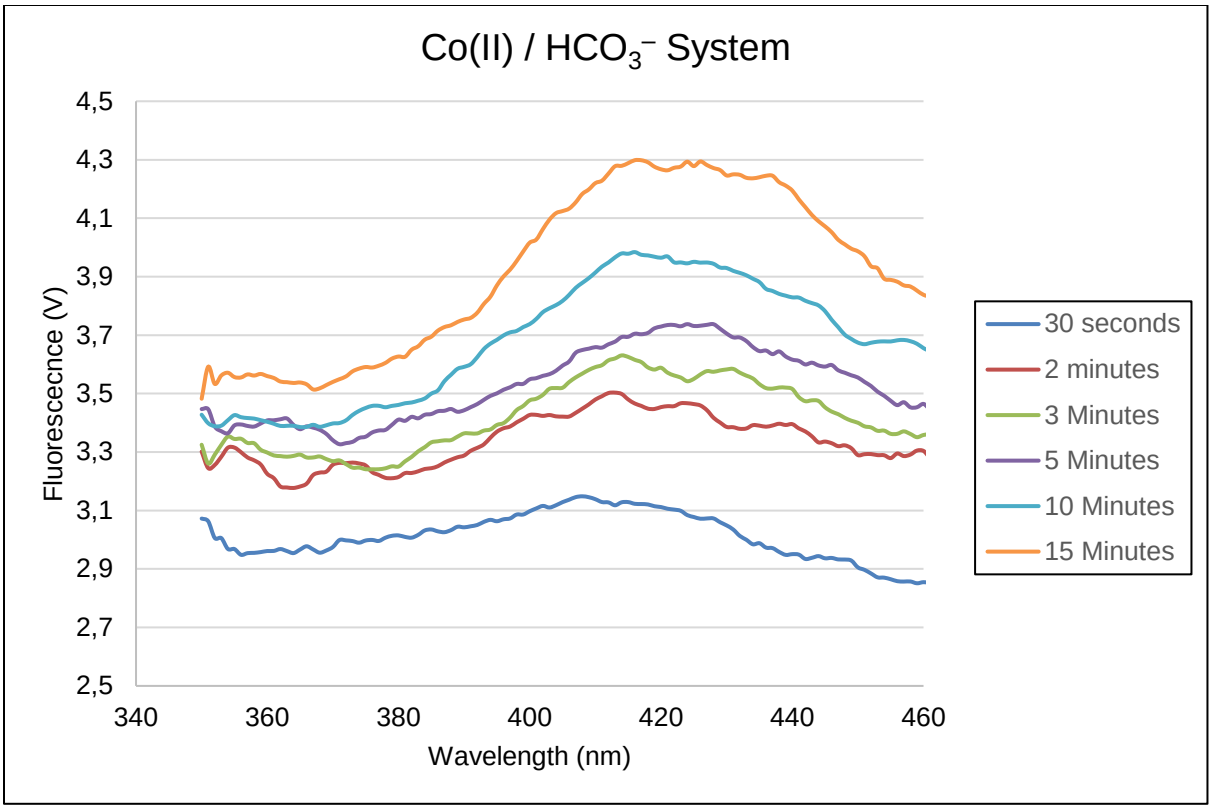

Figure 12: Fluorescence spectra recorded during the oxidation of NaTA to HTA by a Co(II)/HCO_3^- and H_2O_2 catalyst system. 20 µM Co^{2+}, 25 mM HCO_3^-, 0.134 M NaTA, 0.134 M H_2O_2 at 25°C

With the system optimized, the experiment was repeated using the iron pyridine-imine complexes **C4** and **MD5**. The metallodendrimer **MD5** proved to be insoluble in the reaction mixture, thereby complicating the acquisition of fluorescence spectra over time. The fluorescence signal due to the formation of HTA was however still observed. Complex **C4** dissolved readily in the reaction mixture and the formation of HTA could be studied over time. A steady increase in the intensity of the fluorescence signal at 420 nm is observed over the first 20 minutes of reaction (Figure 13). Interestingly after 30 minutes the intensity of the fluorescence signal at 420 nm had decreased slightly. This could possibly be due to formation of a secondary (over-oxidized) oxidation product such as 2,5-dihydroxy terephthalate, or coordination of the product to the iron metal center.

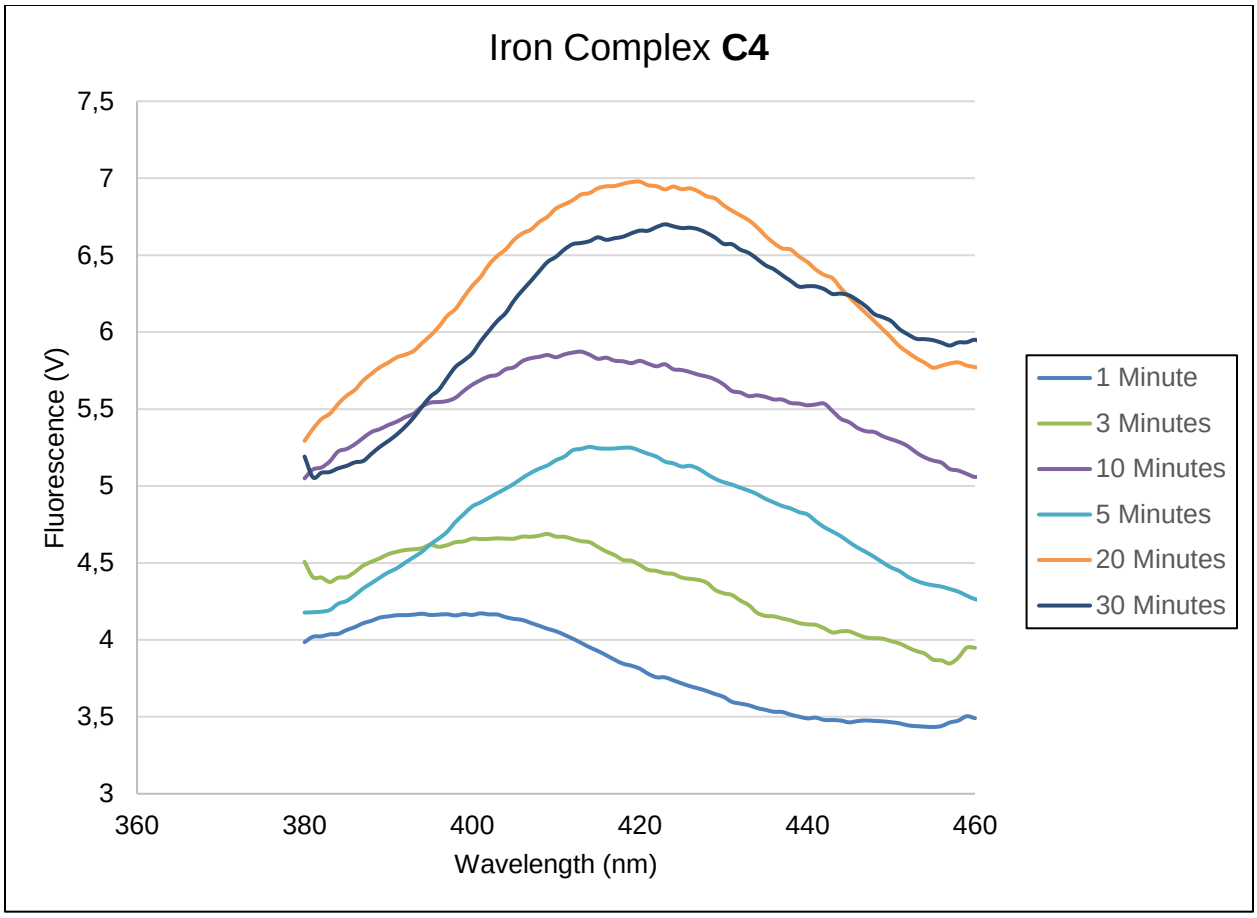

Figure 13: Fluorescence spectra recorded during the oxidation of NaTA to HTA by C4 and H_2O_2. 20 µM Fe^{2+}, 0.134 M NaTA, 0.134 M H_2O_2 at 25°C

MD1 was then evaluated employing the same experimental protocol established for the Co(II)/HCO_3^- and **C4** catalyst precursors. However, after the addition of H_2O_2 to the solution containing **MD1** and NaTA virtually no increase in the fluorescence signal intensity at 420 nm was observed over a 30 minute period (Figure 14). No fluorescence signal is apparent with only noise observed around 420 nm.

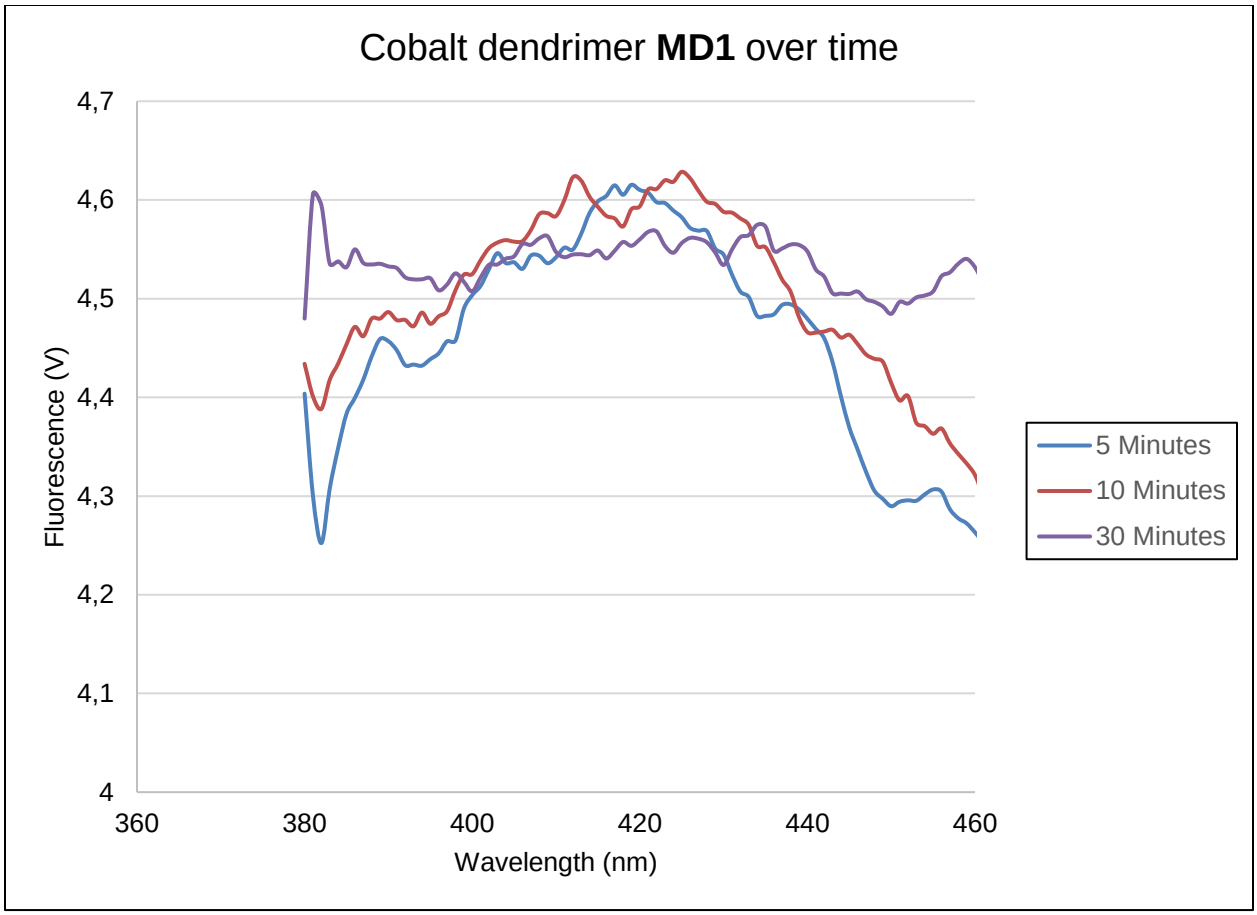

Figure 14: Fluorescence spectra recorded when MD1 and H_2O_2 are employed in an attempt to oxidize NaTA to HTA. 20 µM Co^{2+}, 0.134 M NaTA, 0.134 M H_2O_2 at 25°C

Comparison of **MD1** with the Co(II)/HCO_3^- and **C4** systems suggests that hydroxyl radicals are likely not formed, or formed in very low concentration, in the reaction of **MD1** with hydrogen peroxide (at 25°C). This suggests that **MD1**-catalysed oxidation reactions in all likelihood do not follow the proposed "Fenton-like" mechanistic pathway as depicted and modelled in Section 5.2. Even though the fit of the experimental data to the model is quite good, it seems that another mechanism which does not involve hydroxyl radicals, (not detected in our experiments) is (also) operative and possibly in competition with these "Fenton-like" reactions.

5.4 Conclusions

The calculated activation energy for dendritic cobalt complex **MD1** is significantly higher than that of **MD5** and may represent a barrier to reaction that is not easily overcome under the reaction conditions employed. If this barrier is not overcome; subsequent generation of the reactive oxygen species does not occur readily during the oxidation test reactions as performed in Chapter 4.

As was discussed in Chapter 4, the catalytic oxidation of cyclohexene was inhibited by the addition of a radical scavenger, butylated hydroxytoluene, (BHT) to **MD1**-catalysed reactions. Thus, oxidation reactions catalysed by **MD1** still occur via a radical species. However, the nature of this radical species is unknown. By studying the oxidation of NaTA (disodium terephthalic acid) it was shown that hydroxyl radicals are likely not generated (from the oxidant) in high concentrations during **MD1** catalysed reactions. Thus, the Haber-Weiss model does not accurately describe **MD1** catalysed oxidation reactions, even though the fit of the model to the kinetic data seems good. However, the model is generated by calculating the kinetic parameters from the decomposition data in order to obtain the best fit. In Chapter 4 it was observed that **MD1** catalysed the oxidation of the substrate, cyclohexene (at the allylic position), while being inactive in the oxidation of octane. Based on these results, it is proposed that **MD1** catalysed oxidation reactions occur via free radicals. Such a radical species could possibly be a hydroperoxyl radical. Hydroperoxyl and peroxyl (when using TBHP) radicals have been reported to form by other authors during the reaction of some oxidants (H_2O_2 and TBHP) with cobalt(II).[19–21] Similar observations have been made by Kadiiska et al. who employed a radical spin trap and electron spin resonance (ESR) spectroscopy in order to quantify the relative amounts of different radical species formed during the reaction of a Co(II) complex with H_2O_2.[22] It was found that peroxyl radicals were produced in great excess relative to hydroxyl radicals. Such a species would likely be capable of oxidizing an allylic C-H bond while being unreactive towards the C-H bond in octane.[23, 24] This could also possibly explain why, in our experiments, very little activity is observed in the catalytic oxidation of octane. The peroxyl radical is less reactive than hydroxyl radicals and do not readily react with unsaturated hydrocarbons such as cyclohexane and

octane.[24] Decomposition of hydrogen peroxide likely occurs via another mechanism possibly in competition with the Haber-Weiss mechanism.

The iron-pyridine-imine systems showed some deviation from the modelled Haber-Weiss reactions (Section 5.2). The fit of the experimental data to the model could possibly be improved by consideration of the full Fenton cycle, however further experimentation would be required in this case. Deviation from the model could also signify potential catalyst decomposition. A number of intermediates, consistent with the Haber-Weiss reaction mechanism, were possibly detected for complex **C4** and described in Chapter 3. The catalysis results presented in Chapter 4 are typical of a free radical-centered process. Furthermore, oxidation test reactions of NaTA catalysed by **C4** and **MD5** suggests that hydroxyl radicals are formed and act as the ROS. The Haber-Weiss reactions are likely a good representation of the mechanism of the oxidation reactions catalysed by **MD5** and **C4** in the presence of H_2O_2.

5.5 Experimental details

5.5.1 General Methods and instrumentation

All chemicals were purchased from Sigma Aldrich and used without any further purification. Solvents used were distilled and dried using the appropriate drying agents and methods prior to use. Oxidant decomposition reactions were conducted in a Radleys Carousel 12 batch reactor. Fluorescence spectroscopy was conducted on a Applied Photophysics Chirascan Circular Dichroism spectrometer with a FP.3 fluorescence polarization accessory.

5.5.2 Decomposition of hydrogen peroxide over time

Titrations were performed by employing the procedure described in Chapter 3. The catalyst precursors (**MD1** or **MD5**) concentration was kept constant (4.3×10^{-3} M metal) for these experiments. Acetonitrile was added to the reaction mixtures to yield a final

reaction volume of 6 ml. The temperature and initial oxidant concentrations were varied as indicated. Titration experiments were performed in triplicate.

5.5.3 Modelling oxidant decomposition according to the Haber-Weiss cycle

The parameters of the Arrhenius equation that will best fit the proposed reaction model was determined through the use of nonlinear regression. The regression was performed in Matlab by passing initial values for frequency factor and activation energy (of each reaction step) as well as the differential equations of the proposed model, to a nonlinear least-squares regression function (LSQNonlin).

The regression function determines the reaction rate constants for each reaction in the model at the given temperatures. This is then used to generate concentration-time data for the decomposition of the oxidant. The residual (contained within a vector) between the model and experimental oxidant concentration (per unit time) is minimized by iteratively adjusting the frequency factor and activation energy values. The goodness of fit of the model and experimental data is then assessed using the output of the LSQNonlin function.

5.5.4 Oxidation of disodium terephthalate by transition metal complexes

A solution of NaTA (0.134 M) and either **MD1** or **MD5** (20 µM metal concentration) in water was prepared and added to a quartz cuvette. The pH of the solution was adjusted to 9 using small amounts of HCl.[17] The spectrometer is equipped with both temperature control and stirring. The quartz cuvette containing the reaction mixture is placed inside the spectrometer and kept at 25°C while stirring. H_2O_2 (0.134 M) was then added to the reaction mixture and the fluorescence spectrum recorded using an excitation wavelength of 315 nm. Fluorescence spectra were recorded between 340 and 500 nm.

5.6 References

1 S. Skounas, C. Methenitis, G. Pneumatikakis and M. Morcellet, *Bioinorg. Chem. Appl.*, 2010, **2010**, 1–9.

2 E. N. Rizkalla, L. H. J. Lajunen and G. R. Choppin, *Inorganica Chim. Acta*, 1986, **119**, 93–98.

3 S. F. Vyboishchikov, M. Bühl and W. Thiel, *Chem. - A Eur. J.*, 2002, **8**, 3962–3975.

4 A. L. Casado and P. Espinet, *Organometallics*, 1998, **17**, 954–959.

5 M. D. Alexander and H. G. Hamilton, *Inorg. Chem.*, 1969, **8**, 2131–2134.

6 R. V. Prasad and N. V. Thakkar, *J. Mol. Catal.*, 1994, **92**, 9–20.

7 K. Cui, H. Yi, Z. Zhou, Q. Zhuo, Y. Bing, Q. Guo and Z. Xu, *Environ. Eng. Sci.*, 2014, **31**, 217–224.

8 L. Saussine, E. Brazi, A. Robine, H. Mimoun, J. Fischer and R. Weiss, *J. Am. Chem. Soc.*, 1985, **107**, 3534–3540.

9 A. D. Bokare and W. Choi, *J. Hazard. Mater.*, 2014, **275**, 121–135.

10 F. Haber and J. Weiss, *Naturwissenschaften*, 1932, **20**, 948–950.

11 W. H. Koppenol, *Redox Rep.*, 2001, **6**, 229–234.

12 W. G. Barb, J. H. Baxendale, P. George and K. R. Hargrave, *Trans. Faraday Soc.*, 1951, **47**, 462–500.

13 H. B. Dunford, *Coord. Chem. Rev.*, 2002, **233**–**234**, 311–318.

14 R. P. Houghton and C. R. Rice, *Polyhedron*, 1996, **15**, 1893–1897.

15 S. Goldstein, *Acc. Chem. Res.*, 1999, **32**, 547–550.

16 A. Xu, X. Li, S. Ye, G. Yin and Q. Zeng, *Appl. Catal. B Environ.*, 2011, **102**, 37–43.

17 M. Sahni and B. R. Locke, *Ind. Eng. Chem. Res.*, 2006, **45**, 5819–5825.

18 W. A. Armstrong, R. A. Facep, D. W. Grant and W. G. H. U. J. Phreys, *Can. J. Chem.*, 1963, **41**, 1575–1577.

19 L. G. Stadtherr, R. Prados and R. B. Martin, *Inorg. Chem.*, 1973, **12**, 1814–1818.

20 A. Nishinaga, H. Tomita and H. Ohara, *Chem. Lett.*, 1983, **12**, 1751–1754.

21 B. Shin, K. D. Sutherlin, T. Ohta, T. Ogura, E. I. Solomon and J. Cho, *Inorg. Chem.*, 2016, **55**, 12391–12399.

22 M. B. Kadiiska, K. R. Maples and R. P. Mason, *Arch. Biochem. Biophys.*, 1989, **275**, 98–111.

23 F. A. Chavez, J. A. Briones, M. M. Olmstead and P. K. Mascharak, *Inorg. Chem.*, 1999, **38**, 1603–1608.

24 F. A. Chavez, C. V. Nguyen, M. M. Olmstead and P. K. Mascharak, *Inorg. Chem.*, 1996, **35**, 6282–6291.

Chapter 6: Chapter Summaries, Conclusions and Future Work

6.1 Aims of this study

Hydrocarbon oxidation, under mild reaction conditions, is one of the great challenges in modern chemistry and is the subject of intensive research across the globe.[1–4] Current hydrocarbon oxidation processes suffer from a number of difficulties including poor activity, selectivity and- in the case of homogeneous catalyst systems- removal of the spent catalyst material from the product stream. With this in mind, the aims of this study as discussed in Chapter 1, were to synthesize and characterize novel mononuclear (model) and dendritic transition metal complexes by drawing inspiration from enzymatic systems and other successful catalysts systems reported in literature. A further aim was to evaluate the synthesized metal complexes as catalyst precursors in the catalytic oxidation of various hydrocarbons. In Chapter 1, the importance of the reaction mechanism by which such hydrocarbon oxidation reactions occur was discussed. Thus, the final aim of this study was to attempt to gain an understanding of the mechanism by which these complexes affect hydrocarbon oxidation.

In this chapter, an overview of this study is presented and the most important conclusions, addressing and expanding on the aims listed above, are reviewed.

6.2 Summary of content and most important conclusions Chapter 1

The difficulty in oxidizing C-H bonds is due to the extremely unreactive nature of the C-H bond.[5] In Chapter 1, the most significant challenges facing potential hydrocarbon oxidation processes were examined. These challenges included the low reactivity of the substrate and the difficulty in obtaining good product selectivity and also over-oxidation of the products.

Subsequently, the three most widely accepted mechanisms for C-H bond activation were reviewed.[4] These include C-H bond activation through the formation of a metal carbon σ-bond in the so-called organometallic oxidative addition mechanism. Oxidation can also occur through proton abstraction by free radicals generated from the oxidant. Finally, a metal-based oxidant (high valent metal-oxo species) may form in the rebound mechanism. The rebound mechanism is thought to be operative in many enzymatic hydrocarbon oxidation processes.

A number of biological enzymatic systems were also reviewed including the heme co-factor and methane mono-oxygenase.[6, 7] These biocatalysts are responsible for C-H activation and subsequent oxidation of hydrocarbons in biological organisms. The structures of these biocatalysts are of immense importance. The heme co-factor consists of a iron metal center coordinated by a porphyrin ligand.[6] The active site of soluble methane monooxygenase is believed to consist of carboxylic acid ligands coordinated to an oxo-bridged di-iron center.[7] In contrast particulate methane monooxygenase is believed to have a copper active center.[7] The structures of these biocatalysts have inspired the development of synthetic coordination complexes that attempt to mimic the catalytic properties of these biocatalysts.

Using the enzymatic systems as inspiration, various transition metal complexes have been reported in the literature as active catalysts for hydrocarbon oxidation processes. It was found that many of the active catalysts reviewed, (for hydrocarbon oxidation reactions) had various chemical moieties in common. Many of the catalyst precursors employed iron, copper, nickel or cobalt as the transition metal center, while the ligands coordinated to these transition metals typically had salicylaldimine or pyridine-imine moieties. A number of catalyst precursors also incorporated sulfur donor groups in their ligand structure.[8, 9] These observations thus inspired the synthesis of our own catalyst precursors as detailed in Chapter 2.

6.3 Summary of content and most important conclusions Chapter 2

Drawing inspiration from the highly active catalyst precursors reviewed in Chapter 1, the synthesis and characterization of several transition metal complexes were attempted. A number of salicylaldimine ligands including dendritic ligands were successfully synthesized and characterized. These salicylaldimine ligands were then employed in the synthesis of cobalt metallodendrimers (**MD1** and **MD2**) and model complexes (**C1** and **C2**). Attempts were undertaken to synthesize the corresponding Fe(II) metallodendrimer, however, only Fe(III) species could be isolated. Thus, the synthesis was modified (employing $FeCl_3$ instead of $FeCl_2$) to yield the Fe(III) metallodendrimer, **MD3**.

With the salicylaldimine complexes in hand, the synthesis of pyridine-imine iron complexes was attempted. The use of $FeCl_2$ as transition metal precursor lead to the formation of a complex mixture of products containing $FeCl_4^-$ as well as chlorides as counterions. Other authors have also reported the formation of $FeCl_4^-$ (in related systems).[10] The literature suggests that $FeCl_4^-$ might be formed via photo-oxidation of a chlorinated solvent or the metal-halide precursor.[11] However, it was determined that formation of $FeCl_4^-$ takes place in the absence of a chlorinated solvent and when excluding ambient light. The exact mechanism of $FeCl_4^-$ formation is still not understood. Optimization of the reaction was undertaken in an attempt to yield a material containing only $FeCl_4^-$ counterions (**MD4**); unfortunately this was not successful.

Reaction of the pyridine-imine ligands with the transition metal precursor $Fe(OTf)_2$, yielded the expected Fe(**L3**)$_3$$(OTf)_2$ and Fe_2(**D3**)$(OTf)_4$ products for the model (**C4**) and metallodendrimer (**MD5**) systems respectively.

Thioether-amine ligands were employed in the synthesis of dendritic and mononuclear copper (**C5**, **MD6**) and cobalt complexes (**C6**).

With the complexes in hand their reaction with peroxide oxidants such as H_2O_2 was investigated in an attempt to identify any intermediates of the reaction and, where possible, to postulate a plausible mechanism of reaction.

6.4 Summary of content and most important conclusions Chapter 3

The reaction of several pyridine-imine iron complexes (**C4**, **MD5**) and salicylaldimine cobalt complexes (**C1**, **MD1**) with various peroxide oxidants was investigated. Mass spectrometry and UV-Vis spectroscopy were used in an attempt to characterize the intermediates of the reaction between a metal complex with an oxidant. Reaction of the mononuclear iron complex **C4** with H_2O_2 resulted in the formation of intermediates possibly containing alkoxy and peroxy moieties. These are intermediates that have previously been invoked for complexes that generate free radicals from peroxides.[12]

A potential cobalt-oxo species was identified in the reaction of **MD1** with H_2O_2. It is possible that such a species is formed in an extremely low concentration or could be formed in situ during the ionization process in the mass spectrometer and not necessarily during the catalytic test reactions. In contrast, UV-Vis spectroscopy seems to indicate that a cobalt-oxide or hydroxide species is formed during reaction with H_2O_2. Spectral changes, observed during our experiments, do not match those reported for Co(IV) species in the literature.[13] The presence of Co(IV) normally indicates a possible metal-oxo, rebound mechanism in oxidation reactions. This was not apparent from our UV-Vis experiments.

Reaction of the model cobalt complex **C1** with a peroxide-based oxidant, possibly, results in the formation of oxo/ peroxo bridged complexes as indicated by the high m/z signals observed in the mass spectrum of samples taken from the oxidation reaction. Similar structures, including crystal structures, of analogous compounds have been reported in the literature.[14,15] Furthermore, vigorous gas evolution was observed upon addition of H_2O_2 to a solution of the cobalt complex (**C1**). This seemed to suggest that H_2O_2 disproportionation to H_2O and O_2 is occurring through a catalase-like process as shown in Scheme 1.

$$2H_2O_2 \xrightarrow{[TM\ Catalyst]} 2H_2O + O_2$$

Scheme 1: Disproportionation of H_2O_2 to H_2O and O_2

Titration experiments revealed that decomposition of the oxidant is extremely rapid when employing the model complexes **C1** and **C2**, while decomposition of the oxidant occurs more gradually when using either **MD1** or **MD2** (metallodendrimers) as catalyst precursors. When employing the cobalt metallodendrimers as catalyst precursors virtually no effervescence is observed in the presence of H_2O_2. Based on these results, along with the mass spectrometry, UV-Vis data and the poor catalytic activity of these complexes in hydrocarbon oxidation reactions, we propose that the reaction of H_2O_2 with the model cobalt complexes occurs, chiefly, via a pathway whereby hydrogen peroxide is disproportionated to H_2O and O_2. Homolytic cleavage of the oxidant, to form radical species, is probably in competition with this catalase-like pathway and that the rate of disproportionation is much faster than radical formation. Similar observations were made by Turrá et al. who investigated the formation of O_2 from the reaction of cobalt complexes with peroxides.[16] The authors postulated a mechanism for this reaction based on computational modelling. In their mechanism hydroxo and peroxo-bridged cobalt species are invoked as important intermediates that lead to the formation of O_2. These bridged species suggested by Turrá et al. are quite similar to the bridged intermediates proposed to form during the reaction of **C1** with H_2O_2 (as detected by mass spectrometry (Chapter 3.3.1), thus lending some credence to the hypothesis that H_2O_2 is converted to O_2 via a bridged cobalt intermediate, in the **C1** and **C2** catalysed reactions. This might also explain why the disproportionation of H_2O_2 does not occur as readily when employing the metallodendrimers (**MD1** and **MD2**) as catalyst precursors. The formation of a bridged species is probably less favourable for the metallodendrimers, due to the increased steric bulk of the dendritic species, compared to the model systems.

The application of these transition metal complexes as catalyst precursors in two different hydrocarbon oxidation processes was then investigated.

6.5 Summary of content and most important conclusions Chapter 4

The cobalt complexes **C1**, **C2**, **MD1** and **MD2** were applied as catalyst precursors in the catalytic oxidation of cyclohexene with hydrogen peroxide as the oxidant. The model cobalt complexes (**C1** and **C2**) performed poorly as catalyst precursors for the oxidation of cyclohexene when employing H_2O_2 as oxidant. In hindsight, this is not really surprising as it is most likely due to the disproportionation reaction (H_2O_2 to H_2O and O_2) being in competition with the typical oxidation reaction mechanisms i.e. generation of free radicals or the formation of a metal-oxo species. Substrate conversions lower than 10% were obtained during these reactions. Interestingly, the cobalt metallodendrimers, that exhibit a much lower degree of gas evolution in the presence of H_2O_2, also showed poor substrate conversions. Thus, other factors inhibiting the reaction must be operative in this case.

In an attempt to improve the catalytic performance of these cobalt complexes H_2O_2 was replaced with TBHP as oxidant. It was envisaged that TBHP, a more stable oxidant, might be more resistant to disproportionation by the model cobalt complexes. Indeed, using TBHP as the oxidant, substrate conversion in reactions catalysed by both the model as well as the metallodendrimers increased significantly. In addition, no effervescence was observed when employing TBHP along with the model cobalt complexes. Under the optimized reaction conditions, the model complexes achieved cyclohexene conversions up to 25%.

Reactions catalysed by the cobalt metallodendrimers yielded slightly lower conversions (< 20%). This could possibly be as a result of the higher oxidation potentials of the metallodendrimers compared to the model complexes (measured by cyclic voltammetry and described in Chapter 3). Furthermore, mass spectrometry experiments conducted on solutions containing the oxidant and either the model complexes or the metallodendrimer (Chapter 3) revealed a difference in the nature of the intermediates. The metallodendrimers seem to form intermediates with terminal alkoxyl or peroxyl ligands. A number of examples of such complexes have previously been found to be fairly stable and were found to perform poorly as oxidation catalysts.[17, 18] The relatively

high stability of such complexes could account for the lower activity of the metallodendrimers when using TBHP as oxidant.

In the reactions discussed above, relatively high selectivity towards the allylic oxidation product, 2-cyclohexen-1-one as the major product is observed. In reactions employing TBHP as oxidant along with the cobalt and copper catalyst precursors, 1-(*tert*-butylperoxy)-2-cyclohexene formed in relatively high concentrations (selectivity > 20% in some cases). This peroxide product is most likely formed during a radical chain termination process involving the combination of cyclohexenyl and *tert*-butylperoxyl radicals. Thus, the presence of this compound in the product stream strongly suggests that a free radical mechanism is operative when TBHP is employed as oxidant. The formation of this species is outlined in Scheme 2.

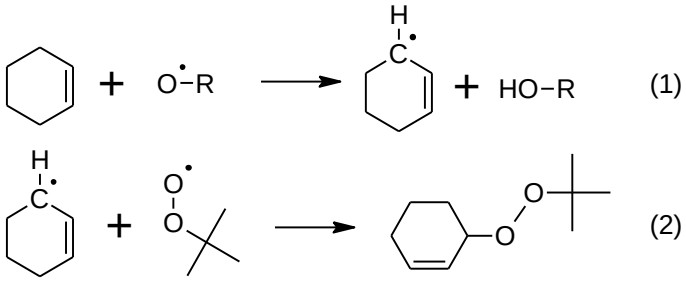

Scheme 2: Formation of 1-(*tert*-butylperoxy)-2-cyclohexene by radical termination

The cyclohexene substrate was then replaced with n-octane. As expected, based on their performance in cyclohexene oxidation, the cobalt salicylaldimine complexes were not very active as catalyst precursors in the catalytic oxidation of n-octane, achieving around 2% product yield under optimized conditions. Under these conditions, high selectivity towards the various ketone products was obtained.

The iron complexes were also employed as catalyst precursors for hydrocarbon oxidation reactions. The pyridine-imine iron complexes, **MD5** and **C4** were relatively active in the oxidation of cyclohexene, obtaining reasonable TON and TOF values, comparable to other iron catalyst systems reported in literature. Similar to the cobalt catalysed oxidation reactions, high selectivity towards the formation of 2-cyclohexen-1-

one is observed. However, in contrast to the cobalt catalysed reactions 1-(*tert*-butylperoxy)-2-cyclohexene is only observed at trace levels when TBHP is used as oxidant. Other overoxidized products are, however, present in the product stream and include 1,2-cyclohexanediol, 2-hydroxycyclohexanone and 2,3-epoxycyclohexanone. The obtained product distribution is typical of oxidation reactions, operating via free radical species generated through homolytic decomposition of the oxidant. This hypothesis was evaluated by the addition of a radical scavenger to the oxidation reactions catalysed by **C4** and **MD5**. With the addition of the radical scavenger (BHT) a sharp decrease in catalytic activity is observed. A similar observation is made for the cobalt complexes **C1** and **MD1**, thereby providing additional evidence that a free radical centered mechanism is most likely the major pathway for oxidation reactions mediated by these catalyst systems.

At first glance, the unusually high product selectivity appears at odds with a highly unselective free radical species. However, the formation of 2-cyclohexene-1-one could be explained through auto oxidation of 2-cyclohexen-1-ol and incorporation of atmospheric oxygen.[19]

Both the iron as well as the cobalt complexes evaluated, operate via a free radical centered mechanism, however, stark differences in catalytic activity was observed. To account for this observation, it was speculated that reaction of the cobalt complexes (metallodendrimers **MD1** and **MD2**) with the peroxide oxidant results in the formation of metastable Co(III)-peroxyl or Co(III)-hydroxyl adducts (as observed in the ESI-MS experiments). Oxidation of the substrate would then only occur upon the dissociation of these adducts to form radical species (reactive oxygen species) and Co(II).

The type of reactive oxygen species (ROS) formed during catalytic oxidation reactions, operating via free radicals, could also potentially affect the observed catalytic activity. For instance, hydroxyl radicals are known to be much more reactive than peroxyl and alkoxyl radicals. This should impact the overall oxidation reaction and was further investigated in Chapter 5.

6.6 Summary of content and most important conclusions Chapter 5

It was postulated that the kinetics of the reaction between the transition metal complex, either cobalt (**MD1**) or iron (**MD5**) and oxidant (H_2O_2), could possibly provide further insight into the difference in catalytic activity observed for these complexes. By elaborating on the oxidant decomposition experiments reported in Chapter 3, the effect of initial oxidant concentration as well as the temperature dependence of the reactions catalysed by **MD1** and **MD5** were evaluated by constructing oxidant decomposition curves. By employing both Arrhenius and Eyring plots, the kinetic parameters of these reactions (**MD1** or **MD5** reaction with H_2O_2) were determined.

The free energy of activation obtained for the cobalt dendrimer **MD1**, was significantly higher than that of the iron metallodendrimer **MD5**, with the former representing a significant barrier to reaction. This is in part due to the activation enthalpy obtained for **MD1** which is significantly higher than that obtained for **MD5**. Thus, formation of a transition state by **MD5** is more facile (compared to **MD1**). The entropy of activation is negative for both **MD1** and **MD5** catalyst precursors, possibly due to the formation of a transition state via an associative pathway for these catalysts. The stark difference in the observed catalytic activity for the cobalt and iron complexes is due to the significant difference in activation energy. However, the nature of the reactive oxygen species could also have an influence on the catalytic activity observed for these catalyst systems.

The nature of the reactive oxygen species was further investigated through the use of disodium terephthalate (NaTA) as chemical dosimeter. Xu et al. showed that NaTA reacts selectively with hydroxyl radicals (under the reaction conditions) to produce 2-hydroxy terephthalate (HTA).[20] The oxidation of NaTA by hydroxyl radicals could conveniently be followed by fluorescence spectroscopy.

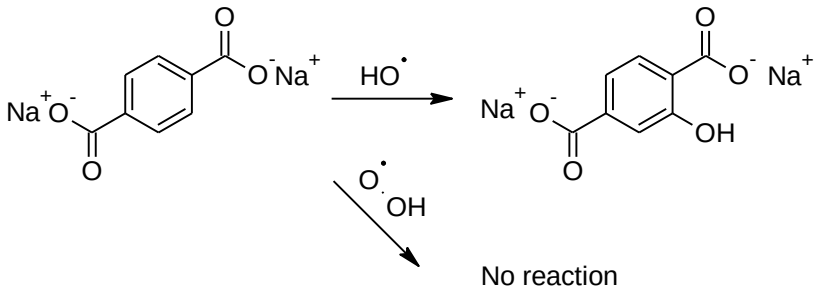

Scheme 3: Selective oxidation of disodium terephthalate by hydroxyl radicals as reported by Xu et al.[20]

A sharp increase in the 2-hydroxy terephthalate concentration is observed within the first hour of reaction when employing the iron complexes **C4** and **MD5** along with H_2O_2. In contrast, virtually no HTA formation is observed when employing cobalt metallodendrimer **MD1** as catalyst precursor (H_2O_2 as oxidant). The catalytic activity of both sets of catalyst precursors (iron and cobalt complexes) was also inhibited by the addition of a radical scavenger (as observed in Chapter 4). Additionally, the product selectivities obtained for these catalyst precursors are typical of oxidation reactions occurring via free radicals. Given that oxidant decomposition for **MD1** (measured via a titration method) still occurs at a rate comparable to those of **MD5** and **C4** and the arguments presented above, it is suggested that the nature of the radical species being formed is different. Both the cobalt and the iron complexes decompose the oxidant but in the case of the iron complexes hydroxyl radicals are formed in relatively high concentrations, while in the case of the cobalt metallodendrimers peroxyl or alkoxyl radical species are likely formed in high concentration. This could be a possible reason for the stark difference in catalytic activity observed for the iron and cobalt complexes. The high selectivity towards 1-(*tert*-butylperoxy)-2-cyclohexene as a major product in cyclohexene oxidation reactions catalysed by **MD1** and **MD2** lends further credence to this hypothesis. In contrast, 1-(*tert*-butylperoxy)-2-cyclohexene is only formed in trace levels in cyclohexene oxidation reactions catalysed by **MD5** and **C4** (Chapter 4).

6.7 Concluding remarks and recommendations for future work

In this study the synthesis and characterization of various iron, cobalt and copper complexes, including metallodendrimers, were reported. A number of these complexes are also novel. Among these were unusual products such as the iron complex, **MD4**, with $FeCl_4^-$ counterions which were isolated and characterized.

The complexes reported in Chapter 2 all showed some activity for cyclohexene oxidation, however, both the activity and selectivity of most of these complexes are lower when compared to some known literature systems as discussed in Chapter 4. Only the iron complexes showed any appreciable activity in the oxidation of n-octane and compared well with other catalyst systems reported in literature. The mechanistic studies conducted on these complexes yielded interesting results on the nature of the reactive oxygen species. However, there remains room for improvement in both the catalytic activity and product selectivity obtained during this study. The nature of the oxidant is a very important parameter to consider in these hydrocarbon oxidation reactions. In this study the use of H_2O_2, TBHP and O_2 as oxidants was investigated. Various other authors have employed PhIO as oxidant to great effect, obtaining high turnover numbers.[21, 22] The use of other oxidants such as iodosylbenzene (PhIO) should thus be investigated in the future. PhIO is, however, significantly more expensive than either H_2O_2 or TBHP and is therefore highly unattractive for use in industrial processes.[23, 24] For such a process to be economically feasible, catalyst systems capable of utilizing O_2 as oxidant need to be developed. Alternatively, in-situ generation of the oxidant from cheap and abundant resources in tandem with the oxidation reactions reported above would greatly enhance the utility of such catalyst systems.[25]

Unfortunately, high valent metal-oxo species are probably not present during our oxidation reactions. Many examples of such catalyst precursors previously reported also have N-donor ligands similar to **MD5** and **C4**.[26] Chen et al. showed that the incorporation of cis labile coordination sites and cis-α coordination of the ligand to the metal center seems to be a requirement for these types of complexes to operate via the so-called rebound mechanism.[21, 26] Thus, it is suggested that the next step in improving upon the ligand architecture of **C4** and **MD5** should aim to accommodate such

coordination modes. However, such a task is likely not trivial, especially for an octahedral complex such as **C4**, or a dendritic ligand.

Based on the results of the mechanistic studies, the catalyst systems (reported in Chapter 2) seem more to likely operate via a free radical mediated oxidation mechanism. Further investigation into the different free radical species present during the oxidation reactions yielded interesting results with regards to the nature of the reactive oxygen species present in the reaction medium. However, further mechanistic study would greatly benefit from the use of EPR spectroscopy and spin trapping experiments.[27] Quantification and positive identification of the radical species obtained through the use of these techniques will aid in confirming our hypotheses regarding the nature of the reactive oxygen species and allow for further rationalization of the obtained activity and selectivity results.

Poor product selectivity is often a problem in catalytic reactions that occur via the free radical mechanism, as described in Chapter 4. In order to enhance the utility of our catalytic systems (that operate via free radicals), methods for improving the product selectivity must be investigated. Yang et al. discussed two different approaches to this end.[28] The authors suggested that the selectivity of a radical process can be tailored by controlling the rate of radical generation. The rate of radical formation could be controlled through the use of inorganic buffers, thereby enhancing the stability of H_2O_2 and reducing the rate of radical generation. This was demonstrated by Yang et al. to lead to less overoxidation and a more selective process. Alternatively, the use of additives such as N-hydroxyphthalimide or (2,2,6,6-Tetramethylpiperidin-1-yl)oxyl (TEMPO) has shown promise.[28] Reaction of these compounds with hydroxyl or peroxyl radicals lead to the formation of less reactive but more selective radical species. However, such an approach will be of less utility in octane oxidation, where highly reactive radical species are required.

6.8 References

1 Y. Ishii, S. Sakaguchi and T. Iwahama, *Adv. Synth. Catal.*, 2001, **343**, 393–427.

2 G. B. Shul'pin, *J. Mol. Catal. A Chem.*, 2002, **189**, 39–66.

3 A. A. Shteinman, *J. Organomet. Chem.*, 2015, **793**, 34–40.

4 G. Shul'pin, *Catalysts*, 2016, **6**, 50.

5 S. J. Blanksby and G. B. Ellison, *Acc. Chem. Res.*, 2003, **36**, 255–263.

6 M. Sono, M. P. Roach, E. D. Coulter and J. H. Dawson, *Chem. Rev.*, 1996, **96**, 2841–2888.

7 M. Merkx, D. A. Kopp, M. H. Sazinsky, J. L. Blazyk, J. Muanẗller and S. J. Lippard, *Angew. Chemie - Int. Ed.*, 2001, **40**, 2782–2807.

8 R. R. Fernandes, J. Lasri, A. M. Kirillov, M. F. C. Guedes da Silva, J. A. L. da Silva, J. J. R. Fraústo da Silva and A. J. L. Pombeiro, *Eur. J. Inorg. Chem.*, 2011, 3781–3790.

9 L. Soobramoney, M. D. Bala and H. B. Friedrich, *Dalton Trans.*, 2014, **43**, 15968–15978.

10 F. Pelascini, M. Wesolek, F. Peruch, A. De Cian, N. Kyritsakas, P. J. Lutz and J. Kress, *Polyhedron*, 2004, **23**, 3193–3199.

11 M. A. Peck, G. R. Hearne, C. Obuah and J. Darkwa, *Phys. Chem. Chem. Phys.*, 2018, **20**, 11682–11691.

12 E. N. Rizkalla, L. H. J. Lajunen and G. R. Choppin, *Inorganica Chim. Acta*, 1986, **119**, 93–98.

13 S. Hong, F. F. Pfaff, E. Kwon, Y. Wang, M.-S. Seo, E. Bill, K. Ray and W. Nam, *Angew. Chemie Int. Ed.*, 2014, **53**, 10403–10407.

14 C. E. Anson, W. Klopper, J.-S. Li, L. Ponikiewski and A. Rothenberger, *Chemistry*,

2006, **12**, 2032–8.

15 L. Saussine, E. Brazi, A. Robine, H. Mimoun, J. Fischer and R. Weiss, *J. Am. Chem. Soc.*, 1985, **107**, 3534–3540.

16 N. Turrà, U. Neuenschwander, A. Baiker, J. Peeters and I. Hermans, *Chem. - A Eur. J.*, 2010, **16**, 13226–13235.

17 F. A. Chavez, C. V. Nguyen, M. M. Olmstead and P. K. Mascharak, *Inorg. Chem.*, 1996, **35**, 6282–6291.

18 F. A. Chavez and P. K. Mascharak, *Acc. Chem. Res.*, 2000, **33**, 539–545.

19 I. Hermans, P. Jacobs and J. Peeters, *Chem. - A Eur. J.*, 2007, **13**, 754–761.

20 A. Xu, X. Li, S. Ye, G. Yin and Q. Zeng, *Appl. Catal. B Environ.*, 2011, **102**, 37–43.

21 K. Chen and L. Que, *J. Am. Chem. Soc.*, 2001, **123**, 6327–6337.

22 M. Mitra, H. Nimir, D. A. Hrovat, A. A. Shteinman, M. G. Richmond, M. Costas and E. Nordlander, *J. Mol. Catal. A Chem.*, 2017, **426**, 350–356.

23 J. Brinksma, J. W. de Boer, R. Hage and B. L. Feringa, in *Modern Oxidation Methods*, ed. J. E. Bäckvall, Wiley-VCH, 2nd edn., 2005, pp. 302–321.

24 B. Royo, in *Sustainable Synthesis of Pharmaceuticals: Using Transition Metal Complexes as Catalysts*, eds. M. Pereira and M. Calvette, Royal Society of Chemistry, 2018, pp. 160–163.

25 D. I. Enache, J. K. Edwards, P. Landon, B. Solsona-espriu, A. F. Carley, A. A. Herzing, M. Watanabe, C. J. Kiely, D. W. Knight and G. J. Hutchings, *Science (80-.).*, 2006, **311**, 362–366.

26 A. C. Lindhorst, S. Haslinger and F. E. Kühn, *Chem. Commun.*, 2015, **51**, 17193–17212.

27 S. Leonard, P. M. Gannett, Y. Rojanasakul, D. Schwegler-Berry, V. Castranova,

V. Vallyathan and X. Shi, *J. Inorg. Biochem.*, 1998, **70**, 239–244.

28 G. Yang, Q. Lin, X. Hu, Y. Wu and Z. Zhang, *J. Catal.*, 2014, **2014**, 1–6.